



The
University
Of
Sheffield.

**Preventing porphyrin aggregation and controlling
microenvironments using mixed polymer micelles**

Samira M Hussein

A Thesis submitted for the Degree of Doctor of Philosophy

Department of Chemistry, University of Sheffield

Sheffield S3 7HF

August 2019

Author's Declaration

The work described in this thesis was carried out between January 2015 and 2019 in the department of chemistry at the University of Sheffield. It is the individual work of the Author. Any views expressed in this thesis are those of the author, and in no way represent those of the University of Sheffield. This thesis has not previously been submitted, in part or whole, for any other degree in this University or any other institution.

Acknowledgments

Firstly, I am grateful to Allah for everything such as good health and well-being and guidance that were necessary to complete this thesis, I would like to express my sincere gratitude to my advisor Dr. Lance Twyman for the continuous support of my Ph.D study and related research, for his patience, motivation, and immense knowledge. My sincere thanks also go to A* Star for funding my research. My thanks also goes to Lynne the head of English language teaching centre (ELTC), I would like to thank Twyman research group especially, Dr. Azra, Dr. Jawad and Dr. Fatima for their listening, sharing knowledge and company throughout the course have been encouraging and a delight. I would like to thank Miss Heather Grievson. My thanks also goes to my best friends, Dr. Layla Al-Haidari from Spain group, Najwa M El Farsi and Dr. Rukaya. M. Finally, I extremely express my thanks to my family member specially my Mother for all her praying and encouragements.

List of figures

Figure 1.1: different configurations of diblock copolymers: Linear copolymers, 2
comb graft copolymer, star copolymers and cyclic block copolymers.

Figure 1.2: the linear AB diblock copolymer, each block consists of one type of 3
monomer.

Figure 1.3: Equilibrium morphologies of A-b-B copolymer where S and S' are 5
body-centred cubic spheres, C and C' are hexagonally packed cylinders, G and G'
= bicontinuous gyroids, and L =lamellae.⁵ This figure is reused with kind
permission from references.

Figure 1.4: (Left) schematic diagram demonstrates the arrangement of block 10
copolymers in vesicles, cylindrical and spherical micelles. (Right) (A–C), cryoTEM
images of PB-b-PEO diblock copolymer assemblies.

Figure 1.5: TEM of, a, ‘hamburger’ micelles, b, helical micelles, c, bilayer tubules, 11
and d, mixtures of polymer vesicles and ‘octopi’ structures. This figure is reused
with kind permission from references

Figure 1.6: GPC spectra of the PCL-b-PEG-b-PCL tri-block copolymer (1000- 15
1000-1000), using THF as eluent.

Figure 2.1: molecular models for the LH1-Rc and LH2 light-harvesting complexes 22
in purple bacteria. B800, B850 and B875 of BCs are shown in green, red and orange
respectively BC in RC is shown as yellow. The lifetimes for energy transferring
events demonstrated by arrows, one headed arrows are indicated the lifetimes in
picoseconds (ps). Energy is passed on to adjacent BChls by antenna carotenoids.
Two-headed arrows represent the energy migrations in femtosecond (fs) between
B850 or B875 pigment rings.

Figure 2.2: a, the absorption spectra of several plant pigments, b, the energy transfer 23
of accessory pigments to the Chl a in red-algae.

Figure 2.3: self-assembly of light-harvesting structures, formed by mixing TMVP 26
monomers labelled with 1 and 3, which were assembled into rods. 105 This figure
is reused with kind permission from references105© 2007 American Chemical
Society.

Figure 2.4: chemical structures and design of the polymer–chromophore 27
nanocomposites. Chemical structures of (A), the PEO-b-PBD polymer, (B) the
BODIPY-HPC donor chromophore, (C) the BC-1 acceptor chromophore, (D) the
Schematic of the proposed chromophore arrangement in the polymer micelle (PEO,
red; PBD, blue; BC-1, purple diamond; BODIPY, green), (E) SANS showing
scattering data from a concentration range PEO-b-PBD micelles fitted to a spherical
core-shell model and (F) the absorbance spectra of three representative
polymer–chromophore preparations.

Figure 2.5: a synthetic artificial light-harvesting system based on surface cross- 28
linking micelles.

Figure 2.6: light-harvesting complex (LH cox) and the reaction centre (RC). A large 30
number of bacteriochlorophylls (purple) are precisely arranged around a pair of
different bacteriochlorophylls (red and yellow) in the reaction centre. The whole
system is contained within nano-scopic protein matrices.

Figure 2.7: schematic representation of Hui-Qing Peng artificial LH system. Where 31
D and A represent donor and acceptor molecules respectively. Donor molecules are
functionalised in way that allows them to bind at surface of cross-linked micelles
through electrostatic interaction. The single acceptor molecule is kept within the
core of the micelle, close to the surface.

Figure 2.8: representation of **a)** natural, and **b)** artificial light-harvesting systems 31
 where blue and red regions respectively represent hydrophilic and hydrophobic parts
 in diblock copolymer micelles in artificial LH system. Donor molecules (D) and
 acceptor molecules (A).

Figure 2.9: schematic representation of **a)** the random aggregation of unattached 32
 porphyrin (red ball) and phthalocyanine (green ball) molecules inside the micelle.
b) The self-assembly of mPEG-porphyrin and phthalocyanine in micelles.

Figure 2.10: overlap (black lines) of emission spectrum of donor (red curve) and 34
 absorption spectrum of acceptor (green curve) units.

Figure 2.11: ^1H NMR spectra of mPEG-b-PCL in CDCl_3 . 37

Figure 2.12: the ^1H NMR spectra of mPEG-b-PCL. All visible ^1H resonances in 38
 CDCl_3 are attributed to the protons of both blocks; mPEG-b-PCL in D_2O only ^1H
 resonances correspond to PEG protons appeared.

Figure 2.13: GPC spectra for **a,** mPEG₄₅-PCL₂₅ and **b,** mPEG₄₅-PCL₄₅. 39

Figure 2.14: GPC spectra for **a,** mPEG₄₅-PCL₄₅ and **b,** mPEG₄₅-PCL₂₅ for the 42
 second attempt.

Figure 2.15: CMC plots of ΔAbs vs $\log C$ for mPEG-PCL diblock copolymers with 46
 different PCL length. **a,** mPEG₄₅-b-PCL₁₅ and **b,** mPEG₄₅-b-PCL₂₅

Figure 2.16: **a** and **b** show the size change as a function of the logarithm 47
 concentration of the mPEG₄₅-bPCL₁₅ and mPEG₄₅-bPCL₂₅, respectively.

Figure 2.17: **a** and **b** show the size change as a function of the logarithm 48
 concentration of the mPEG₄₅-bPCL₁₅ and mPEG₄₅-bPCL₂₅, respectively.

Figure 2.18: the TEM image **a,** for mPEG₄₅-b-PCL₁₅ and **b,** for mPEG₄₅-b-PCL₂₅ 50
 diblock copolymers micelles at concentration 30 $\mu\text{g/mL}$.

- Figure 2.19:** CMC and size of mPEG₄₅-PCL_n for different degree of polymerisation 51
of PCL (n=15,25,35,45).
- Figure 2.20:** represents the ¹H NMR spectra for porphyrin **8** (porphyrin-COOCH₃) 55
in CDCL₃ at room temperature. The arrow indicates the peaks that correspond to
pyrrole and phenyl (C-H) hydrogens of **8**.
- Figure 2.21:** represents the ¹H NMR spectra for porphyrin **8** (porphyrin-COOCH₃) 56
and **9** (porphyrin-COOH) in CDCL₃ at room temperature. The blue framed
enlargement emphasises the peaks that correspond to the pyrrole and phenyl (C-H)
hydrogens of porphyrin-COOH **9**. The red circle indicates the disappearance of
methoxy protons in **9**.
- Figure 2.22:** represents the ¹H NMR of PEG-porphyrin ester **10** in CDCL₃ at room 58
temperature. The arrow refers to the peaks that correspond to pyrrole and phenyl (C-
H) hydrogens of **10**.
- Figure 2.23:** ¹H-NMR result of mPEG-Tosyl **5** and mPEG-NH₂ **6**. 59
- Figure 2.24:** ¹H-NMR spectrum of PEG-porphyrin amide **11**. The arrow indicates 61
the resonances corresponding to pyrrole and phenyl (C-H) hydrogens of **11**.
- Figure 2.25:** prediction of self-assembly of PEG-porphyrin polymers in aqueous 62
solution.
- Figure 2.26:** plot of the fluorescence intensity as function of the logarithm 62
concentration.
- Figure 2.27:** **a**, represent the DLS measurements of different concentration of PEG- 63
porphyrin **b**, the absorption of PEG-porphyrin in water (red line) and DCM (blue
line) and the figure on right side of UVvis spectra demonstrates the H-aggregation
of PEG-porphyrin.
- Figure 2.28:** H- and J- aggregation of porphyrin molecules. 63

Figure 2.29: **a**, SEM images of high concentration PEG-porphyrin, **b**, TEM images 64
of PEG-porphyrin at high concentration.

Figure 2.30: schematic illustration of the formation of PEG-porphyrin /mPEG-PCL 65
mixed micelles **13**.

Figure 2.31: the differences in the fluorescence intensity and absorption between 65
fixed concentration free PEG-porphyrin (5 $\mu\text{g/mL}$) in water (Blue line) and
incorporated PEG-porphyrin (5 $\mu\text{g/mL}$) in mPEG₄₅-PCL₁₅ diblock micelles, **a**, the
fluorescence spectra, **b**, UV-vis spectra.

Figure 2.32: the fluorescence emission intensity of the different series of logarithm 68
concentration of PEG-porphyrin **10** in the presence (red line) and without presence
diblock micelles (blue line) of **a**, mPEG₄₅-b-PCL₁₅/ PEG-porphyrin mixed micelles,
b, mPEG₄₅-b-PCL₂₅ / PEG-porphyrin mixed micelles.

Figure 2.33: the absorption of different series of concentration of PEG-porphyrin in 69
the presence (red line) and in the absence of diblock micelles (blue line) of **a**,
mPEG₄₅-b-PCL₁₅ /PEG-porphyrin mixed micelles, **b**, mPEG₄₅-b-PCL₂₅ / PEG-
porphyrin mixed micelles.

Figure 2.34: the average diameter of the different series of ratios PEG-porphyrin to 71
mPEG-b-PCL diblock polymers in mixed micelles measured by DLS, **a**, PEG-
porphyrin/mPEG₄₅-b-PCL₁₅, **b**, PEG-porphyrin/mPEG₄₅-b-PCL₂₅.

Figure 2.35: TEM images for, **a**, free mPEG₄₅-b-PCL₁₅ diblock micelles, and **b**, 72
PEG-porphyrin / mPEG₄₅-b-PCL₁₅ diblock mixed micelles. The concentrations of
diblock and mPEG-porphyrin are 30 $\mu\text{g/mL}$ and 10 $\mu\text{g/mL}$.

Figure 2.36: TEM images for, **a**, free mPEG₄₅-b-PCL₂₅ diblock micelles and **b**, 72
PEG-porphyrin / mPEG₄₅-b-PCL₂₅ diblock mixed micelles. The concentration of
diblock and mPEG-porphyrin are 30 $\mu\text{g/mL}$ and 5 $\mu\text{g/mL}$.

Figure 2.37: $^1\text{H-NMR}$ spectra of pentoxy phthalonitrile 15 and tin phthalocyanine 16	75
Figure 2.38: the four isomers of tin phthalocyanine 16 , C_s , C_{2v} , D_{2h} , C_{4h} .	76
Figure 2.39: the UV-vis spectra of tin phthalocyanine 6×10^{-6} M in DCM.	77
Figure 2.40: artificial light harvesting system, self-assembled from the PEG-porphyrin, tin phthalocyanine and mPEG-PCL diblock micelles.	78
Figure 2.41: a DLS measurements of free porphyrin tin phthalocyanine –micelles and two (PEG-Porphyrin/PEG-PCL ₂₅ /tin phthalocyanine) micelles with low and high concentration of PEG-porphyrin.	79
Figure 2.36: a, the zoom out TEM image for the tin phthalocyanine-PEG-porphyrin-mPEG ₄₅ -b-PCL ₂₅ micelles 17, b, TEM image for the tin phthalocyanine-mPEG ₄₅ -b-PCL ₂₅ micelles and TEM image for the two samples of tin phthalocyanine-PEG-porphyrin-mPEG ₄₅ -b-PCL ₂₅ micelles 17 micelles with c, low and, d, high concentration of PEG-porphyrin.	80
Figure 2.43: fluorescence spectra of artificial light harvesting using fixed concentration of PEG-porphyrin ($2 \mu\text{g/mL}$) and diblock ($20 \mu\text{g/mL}$) and different concentrations of tin phthalocyanine (from 5×10^{-8} M to 4×10^{-6} M).	81
Figure 2.44: the graph of the degree of quenching for the different ratios PEG-porphyrin to tin phthalocyanine in the light harvesting micelles, the concentration of PEG-porphyrin 10 was fixed at 7.67×10^{-7} M while the concentration of tin phthalocyanine varied from 9×10^{-8} M to 4×10^{-6} M.	81
Figure 2.45: the degree of quenching % was calculated for the different degrees of polymerisation (n) of the PCL segment in mPEG ₄₅ -b-PCL _n .	83
Figure 2.46: the fluorescence measurement of tin phthalocyanine at 1×10^{-6} M in different solvents and with micelles.	84

- Figure 2.47:** the aggregation behaviour of tin phthalocyanine in different solvents 85 and diblock micelles.
- Figure 2.48:** observed absorption of tin phthalocyanine ($1 \times 10^{-6} \text{M}$) in the presence 86 of different concentrations of porphyrins (from $0.2 \mu\text{g/mL}$ to $2 \mu\text{g/mL}$) (green dotes) and the predicted absorption of tin phthalocyanine in the absence of porphyrin (red dotes).
- Figure 2.49:** artificial light harvesting system, self-assembled from the PEG- 89 porphyrin/ mPEG-PCL diblock micelles **12** and tin phthalocyanine dendrimer.
- Figure 3.1:** the structure of Horseradish peroxidase, where, the alpha-helic protein 93 is a large protein that binds Heme as a redox cofactor.
- Figure 3.2:** the structure of hemin. 94
- Figure 3.3:** the component of catalytic oxidation reaction of orange II with m-CPB 96 in the core of PEG-PCL diblock micelle in the presence of PEG-Fe-porphyrin as a catalyst.
- Figure 3.4:** the component of catalytic oxidation reaction of red oil with m-CPB in 97 the core of PEG-PCL diblock micelle in the presence of PEG-Fe-porphyrin **12** as a catalyst.
- Figure 3.5:** the structure of different oxidants, **a**, hydrogen peroxide, **b**, t-BuOOH 97 and **c**, m-CPBA.
- Figure 3.6:** the assembly of mPEG₄₅-PCL₂₅ diblock **21** and PEG-Fe-porphyrin **12** 98 into FePorphyrin/ mPEG₄₅-PCL₂₅ mixed micelles¹⁸.
- Figure 3.7:** UV-vis absorption spectrum of free base PEG-porphyrin (red) and iron 100 inserted PEG-Fe-porphyrin (blue).
- Figure 3.8:** the difference of UV-vis absorption spectrum of PEG-Fe-porphyrin **12** 101 in the absence of micelles (red) and PEG-Fe-porphyrin **12** in the presence of micelles

(blue) when a, simply water solution of PEG-Fe-porphyrin **12** and diblock mixed, **b**, diblock micelles is prepared with the addition of PEG-porphyrin **12**.

Figure 3.9: DLS data **a** and **b**, TEM of PEG-Fe-porphyrin/ mPEG₄₅-PCL₂₅ **18** micelles. 102

Figure 3.10: the assembly of the catalytic oxidation reaction of orange II with different oxidants (H₂O₂, *t*-BuOOH, *m*-CPBA) and PEG-Fe-porphyrin/ mPEG₄₅-PCL₂₅ micelle **18** as a catalyst. 103

Figure 3.11: the kinetic study of the catalytic oxidation reaction of orange II which involves different oxidants (H₂O₂, *t*-BuOOH, *m*-CPBA) and PEG-Fe-porphyrin/ mPEG₄₅-PCL₂₅ micelle **18** as a catalyst (data point collected every 10 seconds. 104

Figure 3.12: the kinetic study of the catalytic oxidation reaction of orange II with *m*-CPBA as oxidants and Fe-porphyrin **12** with and without micelles as a catalyst (data point collected every 10 seconds. Some data points are omitted for clarity). 106

Figure 3.13: the kinetic study of the catalytic oxidation reaction of orange II in two different catalytic systems, PEG-Fe-porphyrin in micelles **18** /*m*-CPBA (blue), and PEG-Fe-porphyrin **12** /*t*-BuOOH (red). 107

Figure 3.14: the assembly of the catalytic oxidation reaction of red oil with *m*-CPBA and FePorphhyrin/ mPEG₄₅-PCL₂₅ micelle **18** as a catalyst. 109

Figure 3.15: the kinetic study of the catalytic oxidation reaction of red oil with different *m*-CPBA as oxidants and PEG-Fe-porphyrin **12** with and without micelles as a catalyst (data point collected every 10 seconds. Some data points were omitted for clarity). 110

Figure 3.16: the structures of orange II and red oil. 113

Figure 3.17: UV-vis absorption spectrum of free base TPP **12** (red) and Fe-porphyrin **19** (blue), 4 x 10⁻⁶ M in DCM. 112

Figure 3.18: the assembling of mPEG ₄₅ -PCL ₂₅ diblock 21 and Fe-TPP 19 in water.	113
Figure 3.19: the kinetic study of the catalytic oxidation reaction of red oil o with <i>m</i> -CPBA and different catalyst systems Fe-TPP (red), Fe-TPP/ mPEG ₄₅ -PCL ₂₅ micelle (grey) and ordered PEG-Fe-porphyrin/ mPEG ₄₅ -PCL ₂₅ micelle 18 (blue).	113
Figure 3.18: the assembly of mPEG ₄₅ -P4VP diblock and PEG-Fe-porphyrin 12 into FePorphyrin/ mPEG ₄₅ -P4VP mixed micelles.	118

List of tables:

Table 1.1: block copolymers and their formed delivery systems.	7
Table 2.1: basic properties of produced mPEG ₄₅ -b-PCL _n	40
Table 2.2: the basic characterisation results new synthesised diblock copolymers.	41
Table 2.3: characterisation results of mPEG ₄₅ -b-PCL _n diblock copolymers with the different repeat unit of ε-caprolactone monomer in copolymer chain and PEG-porphyrin in water	43
Table 2.4: summarised the CMC of two different ratios mPEG ₄₅ -PCL ₁₅ and mPEG ₄₅ -PCL ₂₅ using different characterisation methods.	43
Table 2.5: summary the determination of pre-quenching limit for the four diblock copolymers.	73
Table 2.6: the degree of quenching for the different degrees of polymerisation (n) for PCL in mPEG ₄₅ -b-PCL _n .	82
Table 2.7: the UV-vis measurements of tin phthalocyanine at 1 x 10 ⁻⁶ M in different solvents and within the micelle	83

Table 3.1: k_{obs} value of the orange II oxidation reaction with different oxidant and PEG-Fe-porphyrin/ mPEG ₄₅ -PCL ₂₅ . 18 micelles.	105
Table 3.2: k_{obs} value of the orange II oxidation reaction with <i>m</i> -CPBA and different catalytic systems	106
Table 3.3: k_{obs} value of the red oil oxidation reaction with <i>m</i> -CPBA and different catalytic systems	110
Table 3.4: k_{obs} value of the red oil oxidation reaction with <i>m</i> -CPBA and different catalytic systems	114
Table 3.5: the constant rate of oxidation reaction of orange II with H ₂ O ₂ and different halogenated porphyrins as catalyst (Mamoru systems) and the constant rate of reaction in our micelle system.	115

List of Scheme

Scheme 1.1: styrene-butadiene triblock (SBS) copolymers structure.	3
Scheme 1.2: the proposed reaction pathway of the ring-opening polymerisation of a cyclic ester formed by the coordination-insertion mechanism.	14
Scheme 2.1: synthesis of mPEG ₄₅ -b-PCL _n .	36
Scheme 2.2: synthesis of tetraphenyl porphyrin (TPP) 3 .	45
Scheme 2.3: the synthetic steps of ester PEG-porphyrin (compound 10), amide PEG-porphyrin (compound 11) and PEG-Feporphyrin iron (compound 12).	53
Scheme 2.4: synthesis of tin phthalocyanine 16	74
Scheme 3.1: the roles of imidazole that Form the active oxidant.	92
Scheme 3.2: the oxidation reaction of orange II in the presence of H ₂ O ₂ as an oxidant and the hemin-micelle system as a catalyst.	95
Scheme 3.3: decomposition of Orange II in the presence of oxidant and a Catalyst	99

Scheme 3.4: the insertion reaction of iron into PEG-porphyrin 10 to form PEG-Fe-porphyrin 12 .	99
Scheme 3.5: pathway of homolytic O-O bond cleavage (E) and heterolytic O-O bond cleavage (D) of hydroperoxide.	108
Scheme 3.6: the insertion reaction of iron to TPP 3 to form Fe-TPP 19.	112

Abstract

Inspired by the porphyrin-protein composites in the biological system, such as chlorophyll, peroxidase, neuroglobin, myoglobin, haemoglobin and cytochrome, the self-assembly method has proven to be a promising one for assembling biomimetic materials. In most biological systems, proteins have a unique structure that provides a distinctive isolated and hydrophobic macroenvironment for porphyrins, which stabilize them in the aqueous solution. Therefore, a protein matrix can optimise the functionality of porphyrins by incorporating and spacing many of them in close proximity, without sacrificing their activities due to aggregation. One of the aims of this project was to develop a simple synthetic system that could mimic this property of porphyrin containing biomolecules. Specifically, the development of a self-assembled system that could incorporate a number of porphyrins at precise locations without being aggregated was targeted.

The first step of this thesis involved the synthesis of an amphiphilic mPEG₄₅-PCL_n diblock copolymer using ring opening polymerisation. Four different degrees of polymerisation for the polycaprolactone component of mPEG₄₅-PCL_n were synthesised and characterised. Their aggregation in aqueous solution was also studied, determining a CMC for each polymer. The second step involved the synthesis of a PEG-porphyrin polymer that could co-assemble with the mPEG₄₅-PCL_n diblock copolymer chains in aqueous solution. The resulting micelles were able to hold a number of porphyrins in close proximity without being aggregated, as shown throughout the fluorescence quenching experiments. The size and morphology of the PEG-porphyrin/mPEG₄₅-PCL_n mixed micelles were measured by DLS and TEM. The degree of polymerisation of PCL in the mPEG₄₅-PCL_n diblock copolymer determined the amount of PEG-porphyrin that could be inserted (before quenching). Once synthesised, the micelles were tested as artificial light harvesting systems by encapsulating tin phthalocyanine as an acceptor unit. Although UV-vis experiments showed that the donor porphyrins were able to donate their energy to the phthalocyanine, no emission was observed. This was due to the uncontrolled aggregation of the phthalocyanines, which resulted in quenching – even at low concentration.

Although the micelles failed as light harvesting systems, they proved to be excellent catalytic/nanoreactors. Iron was inserted into a PEG-porphyrin system, which was then co-micellised with mPEG₄₅-PCL₂₅. The resulting micelle was utilised as an oxidation catalyst for use in water. The PEG-porphyrin/mPEG₄₅-PCL₂₅ micelle was tested against two azo dyes and showed excellent reactivity for the hydrophobic azo dye red oil when the hydrophobic oxidant m-CPBA was used. The result emphasised the importance of the micelle system that could control the porphyrin position and prevent aggregation.

Abbreviations

ABCs	Amphiphilic block copolymers
M_n	Number average molecular weight
BCPs	block copolymers
^{13}C NMR	Carbon 13 Nuclear Magnetic Resonance Spectroscopy
porphyrin-COOCH ₃	5-(4-Carbomethoxyphenyl)-10, 15, 20-triphenylporphyrin
porphyrin-COOH	5-(4-Carboxyphenyl)-10, 15, 20- triphenylporphyrin
1-CNP	1-chloronaphthalene
m-CPBA	3-Chloroperbenzoic acid
CAC	Critical aggregation concentration
CMC	Critical micelle concentration
CMT	critical micelle temperature
D_p	Degree of polymerisation
D ₂ O	Deuterium oxide
DBCPs	Diblock copolymers
DCM	dichloromethane
DCC	dicyclohexyl carbodiimide

DMAP	Dimethylaminopyridine
DHU	dicyclohexylurea
DLS	dynamic light scattering
FT-IR	Fourier transform infrared spectroscopy
GPC	Gel Permeation Chromatography
D_h	Hydrodynamic diameter
HCL	hydrochloric acid
H_2O_2	hydrogen peroxide
LH	Light harvesting
$FeCl_2$	Iron(II) chloride
mPEG-b-PCL	Methoxy poly(ethylene glycol)-block-poly(ϵ -caprolactone)
PEG-porphyrin ester	Methoxypolyethylene glycol-4-(10, 15, 20-triphenylporphyrin-5-yl)-benzoic acid ester
PEG-porphyrin amide	methoxypolyethylene glycol-4-(10, 15, 20-triphenylporphyrin-5-yl)-benzoic acid amide
PEG-Fe-porphyrin	Methoxypolyethylene glycol-4-(10, 15, 20-triphenylporphyrin-5-yl)-benzoic acid ester Iron (III) Complex

Fe-TPP	Meso-Tetraphenylporphyrin Iron (III) Complex
NBT	Nitro blue tetrazolium
PEG	Poly ethylene glycol
PCL	Poly(ϵ -caprolactone)
^1H NMR	Proton nuclear magnetic resonance
D	Poly dispersity index
P.E	petroleum ether
mPEG-Tosyl	Poly (ethylene glycol) methyl ether Tosylate
mPEG-NH ₂	Poly (ethylene glycol) methyl ether amine
ROP	Ring opening polymerisation
red oil o	red oil
Sn (Oct) ₂	Stannous-II octoate
SEM	Scanning electron microscopy
TPP	tetra phenyl porphyrin
TBD	7.9-triazabicyclo [4.4.0] dec-5-ene
TEM	Transmission Electron Microscopy
THF	Tetrahydrofuran
TMS	tetramethylsilane

Tin phthalocyanine	Tin (IV) dichlorophthalocyanine
t-BuOOH	<i>tert</i> -butyl hydroperoxide
M_w	weight-average molecular weight
UV-vis	Ultraviolet Visible Spectroscopy

Table of Contents

Chapter 1 - Review	1
1.1 A block copolymer structure and properties:.....	2
1.1.1 Block copolymers in bulk and solution.....	4
1.2 Amphiphilic block copolymers:.....	6
1.2.1 Micellization of block copolymers	7
1.2.2 The morphology of amphiphilic block copolymer and packing parameter:	9
1.2.3 Synthesis of Amphiphilic Block Copolymers:.....	13
1.2.3.1 Coordination-insertion Ring Opening polymerisation:.....	14
1.3 Important applications of Polymeric micelles	16
1.4 General objective	18
Chapter 2 - Artificial light harvesting	21
2.1 Introduction.....	21
2.1.1 Natural light harvesting.....	21
2.1.2 Artificial light harvesting	23
2.2 The aim	29
2.3 Results and discussion: Artificial light harvesting system.	35
2.3.1 Synthesis of methoxypolyethylene glycol-4-(10, 15, 20-triphenyl porphyrin-5-yl)-benzoic acid ester 5 (donor unit)	51
2.3.2 The behaviour of PEG-porphyrin 10 in aqueous solution (CAC):.....	61
2.3.3 Self-assembly of isolated (non-aggregated) porphyrin arrays in mPEG-PCL diblock micelles: 64	

2.3.4	Synthesis of dichloride (Phthalocyanato) tin (IV)(Tin phthalocyanine) (acceptor unit)	73
2.3.5	Tin phthalocyanine 16 and PEG-porphyrin 10 in polymeric micelles as an artificial photosynthesis reaction centre system:	77
2.4	Conclusion and future work.....	86
Chapter 3 - Artificial catalyst based on micelles for organic reaction.....		90
3.1	Introduction:.....	90
3.2	Aim	93
3.3	Result and discussion	98
3.3.1	The catalytic activity of PEG-Fe-porphyrin/ mPEG45-PCL25 diblock micelle 18....	102
3.4	Conclusion:	116
Chapter 4 - Experimental:		119
4.1	Chemicals and Apparatus	119
4.2	Instrumentation	119
4.3	Synthetic procedures:.....	122
4.3.1	Synthetic procedures for mPEG-b-PCL diblock copolymer	122
	Synthesis of mPEG₄₅-b-PCL₁₅ a1	122
	Synthesis of mPEG₄₅-b-PCL₂₅ b	123
	Synthesis of mPEG₄₅-b-PCL₃₅ c	123
	Synthesis of mPEG₄₅-b-PCL₄₅ d	123
4.3.2	Meso-Tetraphenylporphyrin 3	124
4.3.3	Methoxypolyethylene glycol-4-(10, 15, 20-triphenylporphyrin-5-yl)-benzoic acid ester 10 (donor unit).....	125

4.3.3.1	5-(4-Carbomethoxyphenyl)-10, 15, 20-triphenylporphyrin 8	125
4.3.3.2	5-(4-Carboxyphenyl)-10, 15, 20- triphenylporphyrin 9	126
4.3.3.3	Synthesis of Methoxypolyethylene glycol-4-(10, 15, 20-triphenylporphyrin-5-yl)-benzoic acid ester 10	127
4.3.4	Synthesis of Methoxypolyethylene glycol-4-(10, 15, 20-triphenylporphyrin-5-yl)-benzoic acid ester 11	128
4.3.4.1	Synthesis Poly (ethylene glycol) methyl ether Tosylate 2	128
4.3.4.2	Poly (ethylene glycol) methyl ether amine 3	129
4.3.4.3	Synthesis of Methoxypolyethylene glycol-4-(10, 15, 20-triphenylporphyrin-5-yl)-benzoic acid amide 11	130
4.3.5	Tin (IV)dichlorophthalocyanine (The acceptor unit)	131
4.3.5.1	3-pentyloxy-1,2-dicyanobenzene	131
4.3.5.2	Tin (IV) dichlorophthalocyanine	132
4.3.6	Methoxypolyethylene glycol-4-(10, 15, 20-triphenylporphyrin-5-yl)-benzoic acid ester Iron (III) Complex (12)	132
4.3.7	Meso-Tetraphenylporphyrin Iron (III) Complex (19)	134
4.4	Analytical procedures:	135
4.4.1	Beer-Lambert experiment for Tetraphenyl porphyrin	135
4.4.2	The Preparation of Block Copolymer Micelles and the determination of the Critical micelles concentration (CMC)	135
4.4.3	Self-assembly of porphyrin in aqueous solution:	136
4.4.4	General preparation PEG-porphyrin/mPEG ₄₅ -PCL _n 13 Block Copolymer Micelles and the determination of pre-quenching.	136

4.4.5	Beer-Lambert experiment for dichloride (Phthalocyanato)tin(IV)(Tin phthalocyanine) (acceptor unit)	137
4.4.6	The general preparation of LH polymeric micelle	137
4.4.7	Preparation of LH micelle with different ratio of PEG-porphyrin 10 to tin phthalocyanine 16	138
4.4.8	Preparation of mPEG ₄₅ -PCL ₁₅ diblock stock solution	138
4.4.9	Preparation of PEG-porphyrin 10 stock solution	139
4.4.10	Preparation of Tin phthalocyanine/micelles stock solution (solution A)	139
4.4.11	Preparation of PEG-porphyrin/micelles stock solution (solution B)	139
4.4.12	The preparation of (mPEG ₄₅ -PCL _n , PEG-porphyrin, tin phthalocyanine) LH micelles at different ratio of tin phthalocyanine to PEG-porphyrin.	139
4.4.12.1	The preparation of LH micelle (solution C) at R ₅ =5.2	140
4.4.12.2	The preparation of LH micelle (solution D) at R ₄ =2.61	140
4.4.12.3	The preparation of LH micelle (solution E) at R ₃ =1.31	140
4.4.12.4	The preparation of LH micelle (solution F) at R ₂ =0.65	140
4.4.12.5	The preparation of LH micelle (solution G) at R ₁ =0.13	140
4.4.13	General procedure for preparation of the PEG-Fe-porphyrin/ mPEG ₄₅ -PCL ₂₅ micelle 18 for catalytic study	140
4.4.14	General procedure for preparation of the Fe-TPP/ mPEG ₄₅ -PCL ₂₅ micelle 20 for catalytic study	141
4.4.15	Beer-Lambert experiment orange II.....	141
4.4.16	Beer-Lambert experiment red oil.....	141
4.4.17	General procedure of catalytic oxidation reaction of Orange II.....	142
4.4.18	General procedure of catalytic oxidation reaction of red oil.....	142

Chapter 5 - Conclusion and future work:144
Reference:148

Chapter 1 - Review

Staudinger first identified polymers in 1920 and he was awarded the Nobel Prize in 1953 for this discovery.¹ Since then, polymer science has developed to be one of the most investigated areas nowadays.¹ Polymers are defined as large molecules that are indispensable to our survival.¹ They are one of the key components of our food including types such as protein, starch, etc., of our clothes like nylons, polyester, etc., our bodies (poly (nucleic acids), proteins, etc.) and houses (alkyd paints, wood cellulose, etc.).¹ They are created from numerous small molecules linked together.¹ The polymers spontaneous assembling-disassembling process in solutions and the simplicity of their preparation made them an excellent scaffold material²⁻⁴ to assemble; they confine the functional bio-active compounds such as porphyrins within nanoscale size to form a well-defined morphology.⁵

Copolymers are a variety of polymers and they consist of two or more different monomers linked together via covalent bonds.⁶ The importance of synthesizing copolymers is that they bear the properties of both polymer chains;⁶ therefore, they can be exploited in the production of industrial products. For example, copolymers have been used as sensitive hot-melt pressure, adhesives thermoplastic elastomers, drug delivery system. Recent studies have presented the benefit of using copolymer as nano-patterning. In order to understand the physical properties of block copolymer, it is essential to control the self-assembly process.

This part of thesis mainly highlights the property, synthesis and application of amphiphilic diblock copolymers; it also focuses on the morphology of amphiphilic diblock copolymers assemblies in aqueous solution.

1.1 A block copolymer structure and properties:

The physical and chemical properties of polymers such as being light-weight, having good mechanical strength and easy processability, make polymers one of the important industrial materials in the world.⁶ However, several improvements were made to obtain the desired properties; for example, a mixture of two different homopolymers AB was prepared; this mixture was referred to as polymer alloy or polyblend.⁶ Macro-phase separation usually occurs when the two components of the homopolymer are not compatible in a mix.⁵ The chemical bonds reduce or eliminate the degree of segregation. In the block copolymers, two or more long sequence monomer subunits of various types are linked covalently to form a single macromolecule.⁵ Unlike homopolymers, individual blocks in macromolecules can be chosen to obtain the desired chemical or physical properties. The arrangement of blocks in the backbone of the macromolecule is crucial because it leads to the formation of various architectures of block copolymers.⁵ **Figure 1.1** demonstrates some of the several architectures of block copolymers, which can be organised into linear,⁵ cyclic molecular and branched (graft and star) architectures.⁸ The formation of these architectures depends on the developed synthetic routes, and on the specifically desired chemical and physical properties.⁵

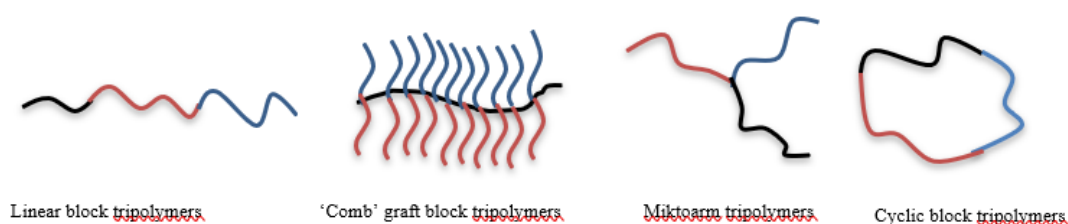


Figure 1.1: different configurations of diblock copolymers: Linear copolymers, comb graft copolymer, star copolymers and cyclic block copolymers.⁵

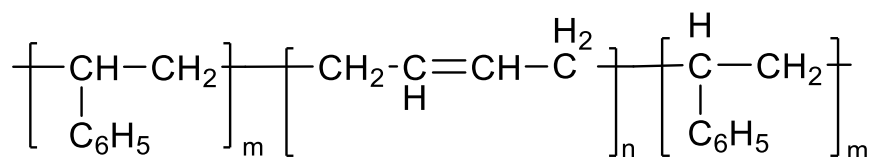
As **Figure 1.2** illustrates, the simplest and most common architecture of block copolymers is the linear AB diblock copolymer. This diblock is synthesised by adding monomers of type B repetitively to the end of an initiated homopolymer chain of type A (poly(A)).⁵ A-b-B represents a diblock sequence arrangement; where b refers to a block, and the corresponding polymers are named, polyA—block—polyB; for example, poly (isoprene-block-ethylene oxide), PI-b-PEO.



Diblock Copolymer

Figure 1.2: the linear AB diblock copolymer, each block consists of one type of monomer.

The preparation of a linear triblock (ABA) was achieved by Fong.⁹ A well-defined structure of styrene-butadiene triblock (SBS) copolymer (**Scheme 1.1**) contains polystyrene chain (PS) on both ends of polybutadiene (PB); it has attracted various world industries due to its thermoplastic elastomeric properties, such as rigidity and rubbery-like properties which are represented by polystyrene and polybutadiene blocks, respectively.⁹



Scheme 1.1: styrene-butadiene triblock (SBS) copolymers structure.

The linear ABC triblock copolymer structure can be designed by either adding a third type of monomer C. For example, N-isopropylacrylamide was sequentially added to the end of halo tailed PEG110-b-P4VP35 macroinitiator to synthesise PEG110-b-P4VP35-b-PNIPAM22 using atom transfer radical polymerization. The other possibility is that polymerisation can occur at both ends of the macro-initiator; for example, the styrene-butadiene tri-block, where the butadiene polymer could initiate from both ends the polymerisation of polystyrene to form the styrene-butadiene triblock.⁹

Whereas, the Star block copolymers can only be obtained when diblock and triblock branched out from a central core. This structure leads to the formation of star-shaped macromolecules and dendritic structures.⁶ In terms of the polydispersity index (\mathcal{D}), synthetic techniques such as a living anionic polymerisation, the formed block copolymers (BCPs) can have a quite low \mathcal{D} ($M_w/M_n < 1.1$), where M_w and M_n are average weight and number molecular weight, respectively, (more is discussed in the synthesis of amphiphilic block copolymers, **Section 2.2**).^{10, 11}

1.1.1 Block copolymers in bulk and solution.

Diblock copolymers (DBCPs) possess two distinct segments in their structure that have different chemical natures, which make them act differently in melt and solution. Therefore, these materials do not only show excellent engineering applications¹², but they can also mimic the various natural biological systems. In the bulk, the poly-blends of the two component polymers are usually subjected to separation at a macroscopic scale.⁸ This is due to the repulsive interaction between the components of a mixture of two polymers. On the other hand, such separation cannot take place in block copolymers due to the covalent bonds between the different blocks in BCPs. This covalent bond suppresses the macro-phase separation.⁶ Instead, microphase separation occurs in the melt because of immiscibility between the different parts of BCPs. Hence, BCPs can form numerous nanometer-scale structures, because the BCPs molecules are forced to rearrange themselves in small domains, typically between (10-100nm) depending on the molecular weight of the block copolymers.⁶ This situation is similar to what happens when two small molecules liquids are mixed. However, the domain becomes larger when the chains are too long; it consist of incompatible polymer blocks.⁸ Figure 1.3 displays the different morphologies of (A-b- B) diblock copolymers in the bulk.⁵

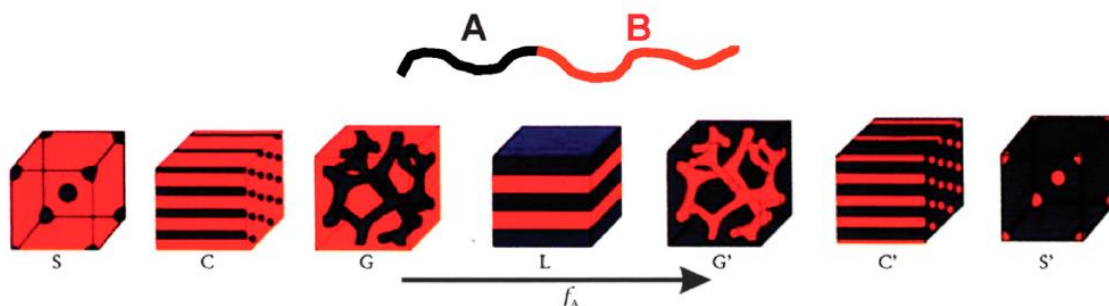


Figure 1.3: equilibrium morphologies of A-b-B copolymer where S and S' are body-centred cubic spheres, C and C' are hexagonally packed cylinders, G and G' = bicontinuous gyroids, and L = lamellae.⁵ This figure is reused with kind permission from references¹⁴³© 1995 American Chemical.

A different number of morphologies can be separated from the bulk block copolymer's micro-phase (**Figure 1.3**);⁶ this depends on the block length and interfacial tension. In general, the morphologies of copolymers revealed that the constituents of the segregated micro-phase most commonly can be spherical (S), hexagonally ordered cylinders (HEX) and lamella (LAM).⁵ The formation of these morphologies depends on parameters, such as volume fraction (f), the degree of polymerisation (N) and the Flory-Huggins interaction parameter (χ).⁵ LAM is parallelly arranged in a repeating order, whereas the cylinders and spheres organise themselves into a two-dimensional hexagonal lattice and cubic lattice, respectively.⁵

When well-defined BCPs are dissolved in a liquid or a homopolymer, they spontaneously aggregate into spherical-like structures.⁵ For simplicity, imagine a linear A-B block copolymer with two units; A is a unit of BCPs that interacts with a solvent (solvophilic), and B is a polymer which avoids any interaction with a solvent (solvophobic).⁵ In the presence of a solvent, the B segments of diblock copolymers assemble tightly toward each other to prevent or reduce any contact with a solvent to form a wide range of structures. Spheres, cylinders and hollow pockets of copolymers known as spherical micelles, worm-like micelles and vesicles, respectively are the most common of those structures (for more clarification, see **Section 1.3.1**).¹³ In this case, BCPs are called amphiphilic block copolymers. The assembly of amphiphilic block copolymer

in aqueous solution is similar to that of amphiphilic molecules which usually exists in the biological systems, for example, lipids.

1.2 Amphiphilic block copolymers:

Amphiphilic block copolymers (ABCs) are types of copolymers that are capable of self-assembly into micelles in an aqueous environment. This type of micelle is called polymeric micelles, due to the unique structure of ABCs which consists of at least two distinct chemical natures. They exhibit unique structural features, similar to those of surface-active agents as the polymeric micelles can be formed by attaching hydrophilic polymers to hydrophobic polymers. ABCs also undergo phase separation in the presence of a selective solvent which can dissolve one block and precipitate the other block.^{14,15} ABCs can also arrange themselves to form distinct morphologies e.g. aspheric, worm-like, vesical¹⁶ depending on the temperature, the solvent system, the pH of the solution, the nature of the components and the lengths of the segments.¹⁷ The hydrodynamic diameter of the micelles falls typically in a range between 10 and 100 nm.¹⁸ To date, numerous block copolymers have been synthesised (**Table 1.1**), not only with a variety of block combinations but also with varying hydrophilic and hydrophobic block lengths.¹⁸

Table 1.1: block copolymers and their formed delivery systems.¹⁸

Copolymer	Abbreviation	Delivery systems formed
mPEG-b-poly (D,L-lactic acid)	mPEG-b-PDLLA	Micelles, nanospheres, nanocapsules, polymersomes
mPEG-b-poly(caprolactone)	mPEG-b-PCL	Micelles, nanospheres, polymersomes, nanocapsules
mPEG-b-poly (lactic-co-glycolic acid)	mPEG-b-PLGA	Nanospheres, nanocapsules, micelles
PEO-poly (propylene oxide)-PEO	PEO-PPO-PEO Pluronic [®]	Micelles
PEG-poly(β -benzyl-l-aspartate)	PEG-b-PBLA	Micelles
Poly (acrylic acid)-b-polystyrene	PAA-b-PS	Micelles
PEO-b-polybutadiene	PEO-b-PBD	Polymersomes

1.2.1 Micellization of block copolymers

The polymeric micelles are formed when the hydrophobic segments coil toward each other avoiding any direct interaction with the polar solvent (water), forming the core part of micelles.¹⁹ Whereas, hydrophilic blocks extend between the core and the surrounding solvent and interact with an aqueous solvent making the shell region.¹⁹ This process is referred to as the micellization process.¹⁹ Although it is considered a reversible process,¹⁹ the assembling block copolymer chains can stabilise the insoluble compounds²⁰ which are positioned in the hydrophobic core¹⁹, they employ the hydrophilic shell to interface the region between the aqueous and the core. Hydrophobic interaction, hydrogen bonding, electrostatic and Van der Waals forces are forces that drive the di-block copolymers to self-assemble themselves in the water solution. Since they are considered weak forces, a small alteration in the environment can break the formed bonds and cause the disassembling of micelles. The interaction between

the different segments of the copolymers with the solvent influences the formation of micelles.¹⁹ It is worth mentioning that the hydrophilic part of the copolymer forms the corona (or shell) of micelles when a polar solvent is used, whereas the use of a non-polar solvent leads to the formation of reversed micelles where the hydrophilic part forms the core of micelles.¹⁹ As with the low molecular weight surfactants, ABCs form micelles at or above the critical micelle concentration (CMC).¹⁹ Below this concentration, the number of ABCs adsorbed at the interface between water and air increases with the increase in concentration.¹⁹ However, at the CMC, ABCs are saturated in the interface; they also constitute the bulk polymer solution which is fully saturated with the single diblock copolymers chains (unimers). This forces the unimer aggregation to form micelles.¹⁹ CMC can be determined by monitoring the physical and chemical properties of solution; these properties suddenly change at the CMC point.¹⁹ A number of techniques such as TEM, light scattering, surface tension and the fluorescent probe can be used to track the CMC.¹⁹

The self-assembly of ABCs is initiated not only by increasing concentration (until it reaches CMC) but also by altering the temperature (until it reaches the critical micelle temperature (CMT)).¹⁹ Several parameters such as the CMC, CMT, aggregation number, core/shell size and micelle shape are essential to characterise BCPs behaviour in solution.¹⁹

It was observed in the literature that the formation of micelles is entropically driven, which involves reordering the solvent particles. The aggregation of unimers expands the solvent volume due to the release of arranged water molecules into the bulk aqueous phase.²¹ Owing to the dilution that has occurred in the system, the overall entropy is positive.¹⁹ Even at the critical micelles temperature, the temperature and entropy resulting from micellization surpass the enthalpy of micellization, introducing negative change in the free energy (equation 1).¹⁹ Hence, several molecules are spontaneously involved in the micellization process; they

aggregate. Equation 1 represents the standard change in the free energy for the micelle formation. Equation 2 shows how change in the free energy relates to the CMC.

$$\Delta G^{\circ}_{\text{mic}} = \Delta H^{\circ}_{\text{mic}} - T\Delta S^{\circ}_{\text{mic}} \quad (\text{Equation 1})$$

Where ΔG_{mic} represents the free energy of micellization, ΔS_{mic} is the entropy of micellization ΔH_{mic} is the enthalpy of micellization and T is the temperature of the system.

$$\Delta G^{\circ}_{\text{mic}} = RT \ln(\text{CMC}) \quad (\text{Equation 2})$$

Where R is the gas constant, T is the temperature of the system and CMC is the critical micelle concentration. When compared to the CMC value of small molecular surfactants (10^{-3} – 10^{-4} M)²⁶, micelles start forming for ABCs²² at a concentration around 10^{-6} – 10^{-7} M. Consequently, micelles formed from ABCs are generally more thermodynamically stable than those formed from low molecular weight surfactants.²³ The thermodynamic stability minimises the dissociation of polymeric micelles into the free chain unimers when the system was diluted with a large amount of solvent. Such a property is fundamental, especially when micelles are used as a carrier system (scaffold for drug delivery and light harvesting system).^{24, 25}

The discussion above illustrates that the well-defined amphiphilic (A-B) block copolymers in aqueous solution self-assemble into various structures to minimize the energetically unfavourable oil-water interaction when solvent selectively solvate one block.¹⁹

1.2.2 The morphology of amphiphilic block copolymer and packing parameter:

The morphologies of the amphiphilic block copolymer aggregates mainly depend on the relative volume ratio of the different blocks and on the packing parameters, which are defined in equation 3.²⁶

$$P = \frac{V_o}{a_o l_c} \quad \text{Equation 3}$$

Where V_o and l_c are the volume and length of the hydrophobic chain and a_o is the optimal area of head group.²⁶ The packing parameter concept provides explanation and predication of the possible self-assembled morphology.²⁸ Depending on the copolymer volume fraction, the spherical micelles, worm-like micelles and vesicals are possibly to form when $P \approx 1/3$, $\approx 1/2$, ≈ 1 , respectively (**Figure 1.4**).²⁶ The head group has an influence on the amphiphilic di-block morphology. The smaller the area of the head group, the higher the value obtained from the packing parameters, which leads to the formation of large vesicles.²⁷ The chain packing also affects the morphology of the amphiphilic diblock copolymer assemblies, as it introduces a branched chain into the hydrophobic chain or allows organic molecules to penetrate the hydrophobic part of the micelles (core).²⁷ In both cases, the l_c is reduced, which leads to a high packing parameter value.²⁷ **Figure 1.4** displays the amphiphilic arrangements into different morphologies and the cryoTEM images of the PB-b-PEO diblock copolymer assemblies, A, vesicle, B, cylinder micelles and D, spherical micelles.²⁶

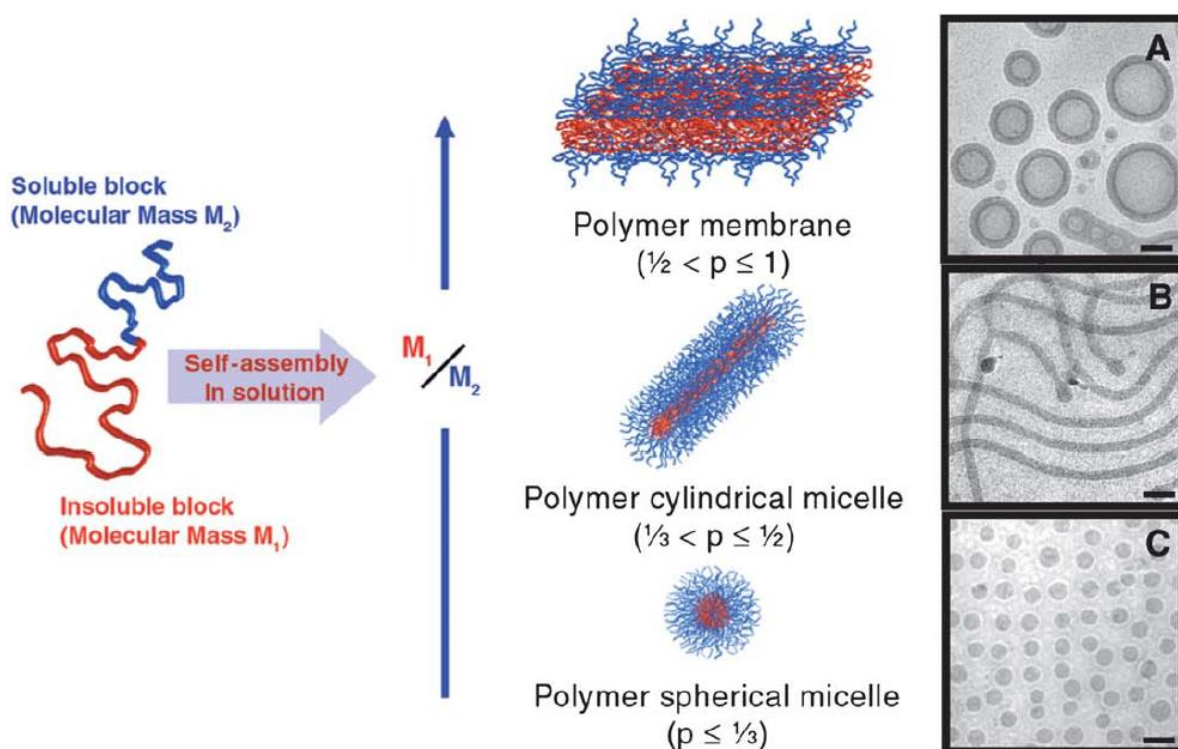


Figure 1.4: (Left) schematic diagram demonstrates the arrangement of block copolymers in vesicles, cylindrical and spherical micelles. (Right) (A–C), cryoTEM images of PB-b-PEO diblock copolymer

assemblies.^{26,140} Reused with permission from [ref. 26,140](#) ©2011 Royal society of chemistry; American association for the advancement of science.

These conventional morphologies have been extensively reported. However, other possible morphologies have recently been determined as result of the remarkable development in the copolymer architectures which is currently taking place.²⁸ Shell cross-linked²⁹ and multi compartmental ‘hamburger’ micelles²⁸ are examples of micelles that are developed from spherical micelles.²⁸ Block copolymer cylindrical micelles have also developed from simple worm-like micelles into more complex morphologies, for example giant³⁰ and short worms,³¹ Y-junction³², end cap defects and even worms like micelles networks have been reported in the literature.³³ Even additional advanced structures have been generated from a wide range of intramolecular and intermolecular interactions inside the block copolymer assemblies.²⁸ It has been reported that poly (acrylic acid)-b-poly (methyl acrylate)-b- polystyrene copolymers could self-assemble into different morphologies micelles, such as toroidal,³⁴ segmented³⁵ and helical³⁶ cylindrical micelles (**Figure 1.5**). Minimizing the end-cap energy was the driving force for the formation structure in each case.^{28, 37}

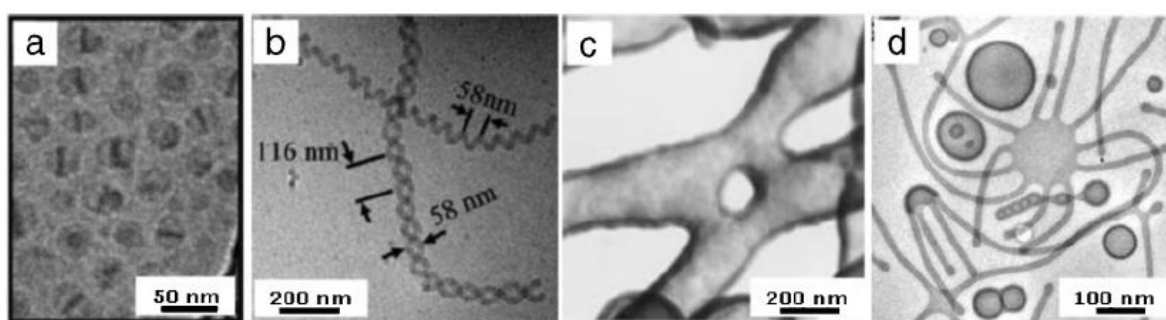


Figure 1.5: TEM of, **a**, ‘hamburger’ micelles, **b**, helical micelles, **c**, bilayer tubules, and **d**, mixtures of polymer vesicles and ‘octopi’ structures. This figure is reused with kind permission from references^{38,32,36,39} © 2006 American Chemical, 2008 Royal Society of Chemistry and 1998, 2004 American Chemical Society, respectively).

Spherical vesicles are bilayer-type structures; they are among the well-known amphiphilic diblock copolymer morphologies.²⁸ However, they are not the only potential bilayer-type structures as bilayer tubules were formed when the copolymers directly dissolved in the solvents mixture then dialysed; it was also formed in pure organic solvent.⁴⁰ However, in

aqueous solutions, copolymer bilayer energetically prefers to form spherical vesicles than tubules.²⁸ Reinecke *et al.*,⁴¹ reported that in aqueous sugar solution, poly (ethylene oxide)-poly (butadiene) (PEO-PBD) diblock copolymer went through a thermo-reversible transition between the tubes and vesicles due to the thermal effect on the membrane bending elasticity.⁴¹ The diblock copolymer that aggregates could undergo into morphological transition induced by the external stimuli including pH, temperature and CO₂ gas.⁴² The Armes group observed various morphological transitions including the sphere to worm, vesicle to worm, vesicle to spherical micelles and worm to sphere by designing a collection of diblock copolymers that consists of poly (2-hydroxypropyl methacrylate) (PHPMA) and poly (glycerol monomethacrylate) (PGMA) which served respectively as the hydrophobic and hydrophilic blocks.^{43, 44} The morphological transition that occurs in this amphiphilic diblock aggregates was induced by the ionisation of the carboxylic acid end group which occurs due to the change in the pH of the solution.⁴² In contrast to the stimulus-responsive block copolymer, the morphological transition of amphiphilic block copolymer may occur due to the delicate equilibrium between segments in the aqueous solution.⁴¹ Yoshida's research on poly (methacrylic acid)-block-poly (alkylmethacrylate-random-methacrylic acid) random block copolymers revealed that the morphological transition of the giant vesicle was due to the hydrophobicity effect and the size of the hydrophobic block determined by the morphology of the random block copolymers.⁴⁵

However, the design of a controlled macromolecular that could mimic the assemblies in nature is necessary to construct an efficient synthetic system.²⁸ Therefore, many researchers aimed to control the morphology of the amphiphilic polymers by controlling the degree of polymerisation. Many controlled polymerisation methods were utilized to control the degree of polymerisation and hence, control the morphology of micelles.²⁸

1.2.3 Synthesis of Amphiphilic Block Copolymers:

The dispersity or polydispersity (\mathcal{D}) describes the wide distribution of the polymer chains. It is an important parameter that affects the molecular weight and the morphology of micelles. For example, high polydispersity leads to the formation of a mixture of small and large polymers which can form a mixture of spherical and worm-like micelles and/or vesicles, whereas the solvated unimolecular diblock copolymer chains only form either spherical micelles or worm-like micelles or vesicles.^{46,47} Hence, different aggregated structures are the result of polydispersity, besides, controlling the dispersity plays an important role in controlling the shape of the aggregated polymers in solution.⁴⁶

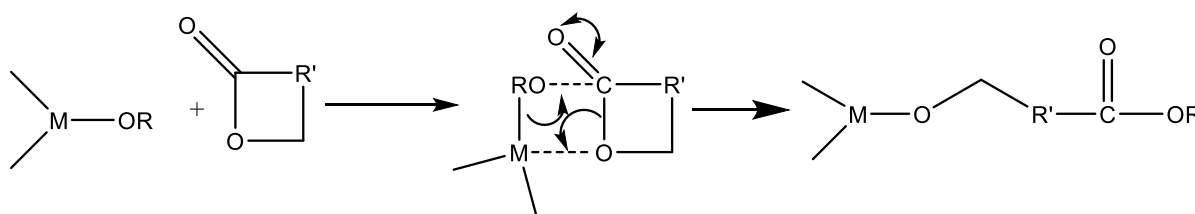
Many synthetic approaches have been developed to synthesise BCPs with the controlled molecular weight and dispersity. The synthesis of the diblock copolymers involves the addition of different monomers in a number of steps. The traditional polymerisations (non-living polymerisation) including cationic, anionic, free radical, coordination, group transfer and step growth were used to synthesise the diblock copolymers.⁴⁸ They are well-detailed and studied in many papers.⁴⁹⁻⁵³ However, the findings showed that they have less control over dispersity and molecular weight than living polymerisation,⁴⁸ which is a promising method to synthesise block copolymers with controlled dispersity and molecular weight due to the absence of termination.⁵⁴ Szwarc was the first scientist who observed the living polymerisation in 1956,⁵⁵ and that was during the anionic polymerisation of styrene with alkali metal/naphthalene.⁵⁵ He noticed that the viscosity of the reaction mixture increased with the increase in the amount of the added monomer. After the consumption of all monomers in the reaction, the viscosity remains constant.⁵⁵ However, adding more monomer into the reaction increased the viscosity.⁵⁵ This indicated that the polymer chain was not terminated.⁵⁵ The living polymerisation involves only two steps which are initiation and propagation.⁵⁴ Since the initiation step is much faster

than the propagation step, the chain grows continuously without termination.⁵⁴ This leads all chains to propagate at more constant rate compared to the non-living polymerisation. In this case, the lengths of all polymer chains are almost the same, and hence a low dispersity.⁵⁴ In addition to that, the molecular weight of polymer can be predicted in the living polymerisation due to the absence of termination, which means that each initiator is responsible for forming one polymer chain.⁵⁴ Therefore, a linear increase was observed between the number average molecular weight and conversion during the living polymerisation.⁵⁴

Living polymerisation can be mainly classified into living free radical polymerization,⁵⁷ living cationic polymerization,⁵⁸ living anionic polymerization,⁵⁴ living chain-growth polycondensations⁵⁹ and living ring-opening metathesis polymerization.⁵⁶

1.2.3.1 Coordination-insertion Ring Opening polymerisation:

Coordination-insertion Ring Opening polymerisation (CIROP) is polymerisation whereby the cyclic monomer is attached to the initiator through the coordination bond.⁵⁶ The initiator has a metal atom that is inserted into the oxygen next to the carbonyl group to form a metal-oxygen bond which stays on the propagating chain, whereas the alkoxy group in initiator associates to the carbon atom of the carbonyl to form an ester group during the chain growth (**Scheme 1.2**).⁵⁶



Scheme 1.2: the proposed reaction pathway of the ring-opening polymerisation of a cyclic ester formed by the coordination-insertion mechanism.⁵⁶

Hydrolysis of the propagated chains causes the termination of the reaction and the formation of hydroxyl end group. The CIROP has been studied extensively due to its potentiality to form distinct polyesters via living polymerisation.⁵⁶ BCPs can be efficiently prepared, if two

monomers that have similar reactivity are subsequently added to the living system. Stannous (II) 2-ethyl hexanoate ($\text{Sn}(\text{Oct})_2$) is most commonly used as a catalyst in the ROP of lactone and lactide.⁵⁶ It most likely starts from the coordination interaction between OH- functional group in the co-initiator and $\text{Sn}(\text{Oct})_2$ yielding the actual initiator (tin complex) of ROP.⁵⁶ Khodaverdi *et al.*⁶⁰ aimed to synthesise the polycaprolactone-b-polyethylene glycol-b-polycaprolactone (PCL-PEG-PCL) triblock copolymer with molecular weight (1000, 1000, 1000) using ring opening polymerisation. $\text{Sn}(\text{Oct})_2$ and PEG were used respectively as a catalyst and an initiator in the ring opening polymerisation. The result was a triblock copolymer with molecular weight (M_n) 1200-1000-1200 determined by $^1\text{H NMR}$ and low Đ 1.49 which is specified by GPC (**Figure 1.6**).⁶⁰

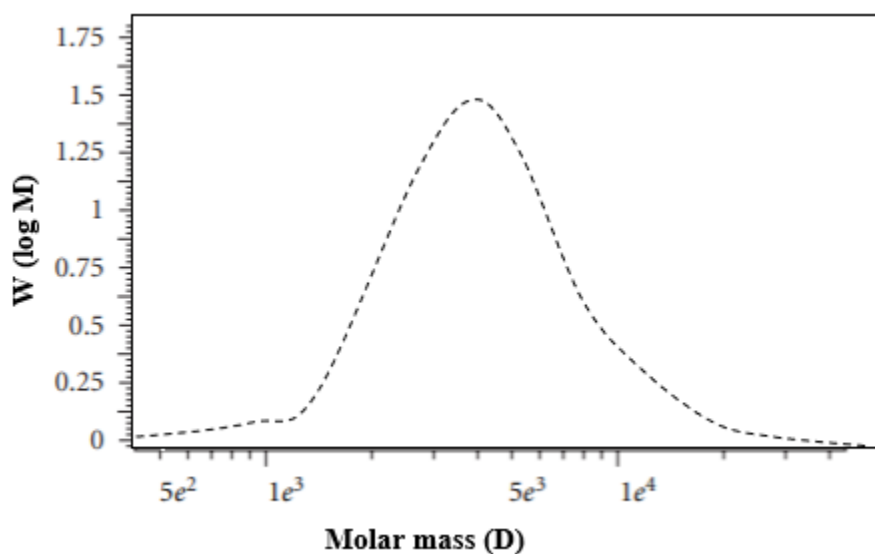


Figure 1.6: GPC spectra of the PCL-b-PEG-b-PCL tri-block copolymer (1000-1000-1000), using THF as eluent.⁶⁰

This result exhibited that the ring opening ROP is a straightforward polymerisation that can yield polymers with a reasonable Đ and a high molecular weight (MWT) when a specific catalyst initiates the ring opening of the cyclic monomers.

1.3 Important applications of Polymeric micelles

Owing to the stability of polymeric micelles during dilution, their ability to solubilise a large number of hydrophobic compounds, their low toxicity, and enhanced blood circulation time makes them one of the most versatile materials applied in various applications especially for in the medical field; for example, in the gene and drug delivery. They can also be utilized as an intelligent scaffold for encapsulating bio-active units to construct artificial light-harvesting complex and peroxidase systems.⁶¹ They also demonstrate a potential to concentrate the hydrophobic components inside the core. Therefore, they act as mini-reactors^{61, 62}, they can also be employed as a carrier of imaging agents.⁶³

The applications mentioned above are not limited to the conventional polymeric micelles (the hydrophobic part of the chain form the core of the micelles and the hydrophilic part form the shell of micelles), polyionic micelles can also serve most if not all those roles, when compared to conventional micelles, polyionic micelles are easier to prepare and they aggregate into a well-fine spherical shape in aqueous solution, besides, they have a higher drug loading. However, under specific stimuli, the compounds entrapped in the core of the micelles can efficiently be released.⁶⁴

Jeong *et al.*,⁶⁵ successfully synthesised methoxy poly (ethylene glycol)-grafted-chitosan. The formed micelles in aqueous solution managed to encapsulate all trans-retinoic acid by making electrostatic interaction between the carboxylic acid group of all-trans retinoic acid and the amine group of chitosan. These drug polyionic micelles complexes were formed to deliver the drug to the tumour in the brain; they achieved 80% efficiency in loading the drug. Polymeric micelles can be used as scaffold for many chromophore molecules, for example, Wang *et al.*,⁶⁶ formed a micelles-chromophore complex using electrostatic interaction between poly (ethylene glycol)-block-poly(L-lysine) (PEG-b-PLys), zinc tetrakis (4-sulfonatophenyl) porphyrin

(ZnTPPS) and fullerene (mC60) to mimic the antenna-reaction centres in photosynthesis. The same group⁶⁷ used PEG-PCL diblock micelles to entrap the hydrophobic electronic donor and acceptor units of porphyrins and fullerene or phthalocyanine respectively through hydrophobic interaction to build the artificial photosynthesis system. Polymeric micelles are not only used as carrier, but they can also be used as nano-reactors, for example, Bigey *et al.*,⁶⁸ used micelles as mini-reactors to produce porphyrin in an aqueous solution by making use of the micelles properties of gathering, concentrating the start materials.⁶⁸ The utilization of micelles for porphyrin formation can result in an equilibrium between the reactant and porphyrin to shift toward porphyrin production, since the resulting water molecules from the reaction are constantly removed outside the micelles core, and their hydrophobic nature increases, which facilitates the encapsulation of more porphyrin molecules.⁶⁹ However, a high concentration of surfactants is required. As mentioned before, micelles could be a promising alternative to protein and it could be further used to mimic more biological systems. For instance, Qu *et al.*,⁷⁰ succeeded in building an artificial peroxidase mainly using PEG-poly vinyl pyridine to stabilise and to carry the hemin (catalyst) in aqueous solution; they showed how different interactions between hemin and diverse diblock copolymers PEG-b-P4VP, PEG-b-PLys, PEG-b-PCL could affect the catalytic activity of the artificial catalyst system. Polymeric micelles have recently been considered a promising material for biomimicry applications and hence, a starting point for innovations. They have enhanced the efficacy of drugs and made drug delivery successful.⁷² The development of this material involves adding smart functions. As a result, many anti-cancer drugs encapsulated into polymeric micelles are now being found in clinical trials. For example, Kataoka *et al.*,⁷¹ modified the diblock copolymers by chemically attaching doxorubicin (DXR) to the PEG-b-poly (aspartic acid) copolymers to form pH-sensitive polymeric micelles of the PEG-block-P (Asp-Hyd-DXR).⁷² At pH 5, drastic release of DXR was achieved compared to the slow release of liposomes-conjugated DXR due to the limited

penetration of the later inside the multicellular tumour spheroid (MCTS) and the difficulty in drug release.⁷² Hence, polymeric micelles are a promising tumour infiltrating drug carrier and a significant material in active targeting.⁷²

Polymeric micelles could also be used as gene vectors, the method is considered sophisticated to develop medicine due to the micelles ability to treat incurable diseases and tissues engineeringly.⁷² Owing to the safe use of polycations (polyplex) in the clinic, they have been well-known as substitutional materials to viral vectors. Additionally, polycations have the potential to conceal the negative charge of plasmid DNA (PDNA). When they are entrapped into the nanoscopic particle, they can be transferred to the cell.⁷² However, free polycations in vivo can activate toxic side effects. To solve this problem, Fukushima *et al.*,⁷³ developed a smart system using triblock copolymer that consists of two different types of polycation and polyethylene glycol, Polyethylene glycol-b-poly [(3-morpholinopropyl) amide]-b-(poly (L-lysine), PEG-b-PMPA-b-PLL, where PMPA and PLL are polycations with low PKa around 6.2 and high PKa around 9.4, respectively.^{72,73} The biocompatibility that was offered by PEG prevented the aggregation of erythrocyte⁷⁴ and complemented activation.⁷⁵ Toxicity related to the artificial vectors in the bloodstream such as erythrocyte aggregation was prevented successfully by a PEG block, which provided the formed polyplex micelles with their biocompatibility.⁷² Hence, the new system with three-layered polyplex micelles has significantly reduced free polymers, achieving efficient transfection.

The current thesis describes two projects using the same materials for different applications which are artificial light harvesting and catalyst system.

1.4 General objective

The main aim of this thesis is to address the aggregation of porphyrin in water. In many biological systems such as photosynthesis, haemoglobin and enzyme systems, water is a

medium where biological processes take place. In these systems, the protein provides the controlled macro-environment and stability for the active compounds such as porphyrin in aqueous solution. The polymer-driven assembly process empowers modularity to integrate virtually any hydrophobic or amphiphilic cofactor into the same basic architecture, compared to natural porphyrin-protein complexes with high affinity binding sites unique to a given cofactor. Therefore, in the current project, the capability of the mPEG-b-PCL di-block and the copolymer di-block will be investigated as a potential alternative of protein matrix to incorporate noncovalently large arrays of porphyrins within the nanoscopic micelles in an aqueous condition. A random incorporation of unfunctionalized porphyrins will lead to the porphyrin aggregation inside micelle. This significantly reduces its functionality; hence, the synthetic systems will not be efficient. One way to form a successful system is the isolation of porphyrins within PEG-PCL micelle. This will require mono-functionalizing of the tetra phenyl pyrrole (TPP) which is then covalently attached to the mPEG. The resulting PEG-Porphyrin will be allowed to be self-assembled at hydrophobic/hydrophilic interface where porphyrin faces the core of micelle whereas mPEG faces the corona of the micelle. Owing to the high molar absorption coefficient of porphyrins which is above $10^6 \text{ L cm}^{-1}\text{mol}^{-1}$, UV-vis and fluoresce can be used to confirm whether PEG-porphyrin arrays are inserted and isolated inside micelles by comparing PEG-porphyrin in the presence and absence of micelles. Four different ratios of PEG-PCL_n di-block copolymers with a fixed repeated unit of PEG (n=45) and a varied repeated unit of PCL (n=15, n=25, n=35 and n=45) will be synthesised using ring opening polymerisation to determine the amount of PEG-porphyrin that can be inserted into the micelle before it starts quenching. The size and morphology of PEG-porphyrin/ mPEG-PCL mixed micelles can be verified by DLS measurements and TEM. Once the isolated porphyrins within micelle are successful, they will be exploited to construct artificial light harvesting system. In this artificial system, tin phthalocyanine will be inserted and employed as an acceptor unit, an

isolated PEG-porphyrin inside micelle as a donor unit. Energy is transferred between the donor and the acceptor through Förster's mechanism. Porphyrins and phthalocyanine were selected in this system because they have high molar absorption coefficient which is around 10^5 - 10^6 L cm⁻¹mol⁻¹ due to the extensive conjugated system in their structure. Additionally, the maximum absorption capacity of porphyrin is around 418 nm; it emits around 650 nm whereas, the tin phthalocyanine highest absorption capability is around 700-750 nm, emitting near infrared. Therefore, the emission of porphyrin overlaps with the absorption of tin phthalocyanine. This is consistent with one of the Förster's criteria. Observing light at 760 nm when the system operates at 418 nm gives strong evidence of the success of the artificial light harvesting system.

The isolated PEG-porphyrin/mPEG₄₅-PCL₂₅ will be also utilised as catalyst and nanoreactor. This requires the insertion of iron in PEG-porphyrin/mPEG₄₅-PCL₂₅ to form PEG-Fe-porphyrin/mPEG₄₅-PCL₂₅. Since the reaction occurs in the hydrophobic part of the micelles where the catalyst exists, different oxidants and substrates with different polarity will be tested. Orange and red oil are azo dyes and they were selected as substrates due to their absorption in visible light. This will enable the researcher to monitor the kinetic of the catalytically oxidation reaction using UV-vis spectroscopy. The catalytic activity of the PEG-Fe-porphyrin/mPEG₄₅-PCL₂₅ micelle system will be compared to the PEG-Fe-porphyrin without micelles and FeTPP/mPEG₄₅-PCL₂₅.

Chapter 2 - Artificial light harvesting

2.1 Introduction

The urgent need for renewable sources of energy has increased recently due to the drastic increase in the global demand for energy and the dependence on fossil fuel, which causes serious environmental degradation. In addition, non-renewable resources are becoming more expensive and difficult to find due to the population growth. As a result, humans look to nature and natural systems for inspiration. Therefore, many researchers have focused on the means that utilise and harness the light energy of the sun. This task becomes easier because of the hints and blueprints that have already been found in nature.⁷⁶

2.1.1 Natural light harvesting

Photosynthesis is a natural light-harvesting system where many chromophores precisely assemble in the protein matrix; a process that converts the captured photons from sunlight into the chemical energy in the reaction centre (RC).^{77,78} When compared to the light harvesting complex (LH complex) in plant and cyanobacteria, purple bacteria have the most uncomplicated design of the LH complex. They contain two chromophore-proteins LH complex named LH1 and LH2 which have similar molecular structures and consist of bacteriochlorophyll molecules (BChl_a), which are a large group of magnesium-porphyrins. They are associated with the imidazole side chain through a coordination bond, forming a ring shape. LH2 surrounds LH1 which, in turn, surrounds the RC (Figure 2.1).⁷⁶ The separation distance between the neighbouring chromophores is adequate (in the range of 10-100 Å) to transfer the excitation energy to each other and toward the RC, where the ejection of an electron occurs (Redox reaction).⁷⁶

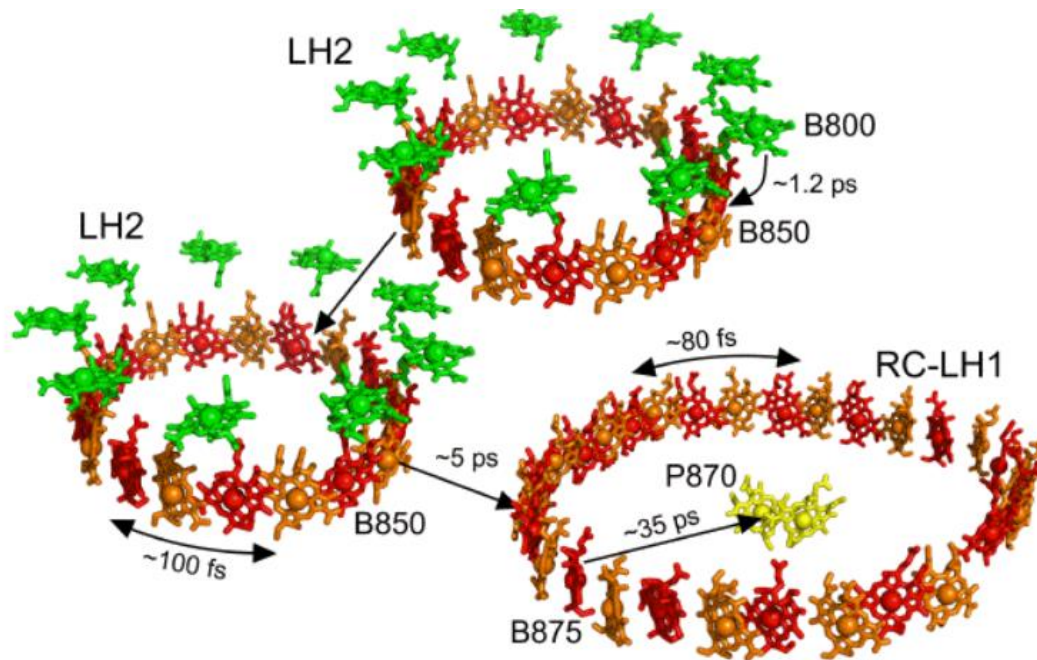


Figure 2.1: molecular models for the LH1-Rc and LH2 light-harvesting complexes in purple bacteria. B800, B850 and B875 of BCs are shown in green, red and orange respectively BC in RC is shown as yellow. The lifetimes for energy transferring events demonstrated by arrows, one headed arrows are indicated the lifetimes in picoseconds (ps). Energy is passed on to adjacent BChls by antenna carotenoids. Two-headed arrows represent the energy migrations in femtosecond (fs) between B850 or B875 pigment rings.⁷⁹

It is worth pointing out that energy transfer travels typically in one direction due to the fluorescence band of the chromophore, which has absorbed the photons at the shortest wavelength, usually overlapping with the absorption band of the another chromophore that absorbs the photon with a longer wavelength, but the process cannot happen the other way around.⁷⁶ For instance, in red-algae, energy transfer goes from pigments (with blue region absorption of spectra (carotenoid)) which are absorbed in the blue region of the spectra, to the pigments with green region absorption (phycoerythrin), and later to the molecules with orange absorption (phycocyanin), and finally to the pigments with red absorption (Q band of chlorophyll (Chla), as revealed in Figure (2.2.b)).⁸⁰ Some electronic energy is turned into vibrational energy (then wasted into the heat) in each transfer.

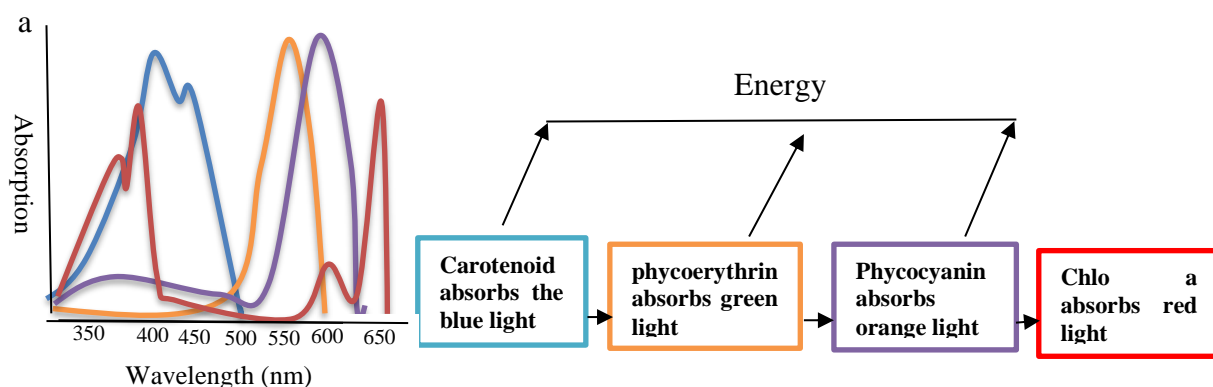


Figure 2.2: a, the absorption spectra of several plant pigments, b, the energy transfer of accessory pigments to the Chl a in red-algae.⁸¹

Förster observed that excitation energy transfer is controlled by three parameters: the distance between the two chromophore molecules, Förster's overlap integral which is the overlap of the donor fluorescence band together with the absorption band of the acceptor and finally, the orientation factor which associates the dipole's orientation of the acceptor with the donor molecules.^{83,81}

2.1.2 Artificial light harvesting

Many different artificial light-harvesting antennae systems have been constructed using various electron donor/acceptor unities, to mimic the energy transfer in the purple bacteria. The most commonly used donor/acceptor unities are porphyrin/phthalocyanine,^{84,85} porphyrin/fullerene,⁸⁵ phthalocyanine/fullerene,^{86,87} porphyrin/quinone,^{88,89} and phthalocyanine-quinone,⁹⁰ where they are covalently and/or non-covalently associated.^{66,91} However, the non-covalent interaction has drawn the most attention, as the assembly of chromophores in the biological photosynthesis system occurs through non-covalent interaction.⁶⁶ Therefore, a variety of donor/acceptor unities systems were self-assembled by using different association methods such as metal-ligand coordination, electrostatic interactions, π - π stacking and hydrogen bonding.^{66,67} Porphyrins (Ps) and phthalocyanines (PCs) are the most closely components linked to natural chromophores such as chlorophyll and

bacteriochlorophylls.⁶⁶ Additionally, being chemically stable and easily synthesised, they exhibit desired features and variable electronic and redox properties, which can be obtained by changing the chemical structure of their macrocycles and the central atom of Ps and PCs.^{91,92} Their planar structure, rigidity, and high extinction coefficients (ca. 10^5 – 10^6 cm⁻¹ M⁻¹) which are potentially capable of absorbing and emitting the light in visible and near-infrared regions (at 350 nm and 750 nm)^{91,92} make them excellent materials for constructing the artificial system of photosynthesis and the potential donor/acceptor units to investigate energy and charge the transfer processes.⁹²

Unlike porphyrins which have been widely used as donor unities, the use of PCs as an acceptor unit is limited due to their extreme aggregation behaviour.^{92,93} Different means were attempted to overcome the aggregation problem.⁹² one way is, the use of an appropriate organic solvent that yields a monomer of both dyes and shows no influence in the attraction between Ps and PCs.⁹¹

Both are hydrophobic compounds that have poor solubility in water, which is the medium where all biological processes occur.^{94,66} They often undergo high levels of aggregations in aqueous solutions due to the π - π interactions between their molecules,^{94,66} which reduce their activities and stability in aqueous solutions.⁹⁵ Many efforts have been made to overcome such disadvantages by understanding and mimicking spontaneous self-assembly processes that are naturally carried out in the living system⁹⁶⁻¹⁰⁰ inspired by the porphyrin-protein composites in the biological systems. Self-assembly has proven to be a promising method of assembling biomimetic materials, for example, the formation of cell membranes from the natural aggregation of phospholipids to vesicular.¹⁰¹ In most biological systems, proteins have a unique structure that provides the hydrophobic macroenvironment for porphyrins, stabilising them in the aqueous solution.¹⁰² Notable examples are the photosynthesis¹⁰³ and peroxidases^{99,104} where porphyrins derivatives are often self-assembled through non-covalent interactions; they are

precisely and spatially organised within nanoscopic protein matrices to form nanoscale superstructures.¹⁰⁵ Thus protein matrices can optimise the functionality of porphyrins by incorporating and spacing hundreds of them within minimal distance (porphyrins and carotenoid are confined between two proteins that are formed from two polypeptides α and β with radius 18 Å and 34 Å, respectively) from each other without sacrificing their activities due to the aggregation.¹⁰⁵ Additionally, proteins-porphyrins complexes also form excellent several functional components in the living organisms, such as chlorophyll, peroxidase, neuroglobin, myoglobin, haemoglobin and cytochrome.^{106,107} Thus, they play essential roles in many crucial biological processes including metabolism and oxygen carrying.^{108,109}

Protein-based artificial light harvesting was reported by Miller *et al.*,¹⁰⁵ associated the donor and acceptor chromophores to the cysteine residues and then to the tobacco mosaic virus coat protein (TMVP) monomers. These were able to aggregate into stacks of disks or into rods where their length reached 100 nm in the right buffer conditions.¹⁰⁵ In that system, a large number of the donor's chromophores transferred the energy to the single acceptor. Since they managed to expand the light spectra collection by using three different chromophores in their system, they achieved 90% efficiency.¹⁰⁵

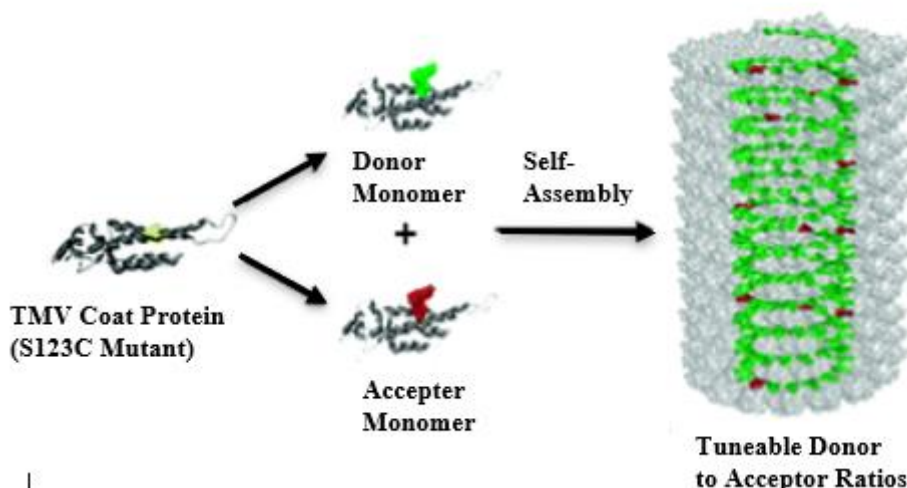


Figure 2.3: self-assembly of light-harvesting structures, formed by mixing TMVP monomers labelled with 1 and 3, which were assembled into rods.¹⁰⁵ This figure is reused with kind permission from references¹⁰⁵© 2007 American Chemical Society.

Various scaffolds have been employed; they can mimic the function of a protein in an artificial LH system. These include organogels,¹¹⁰ biopolymer assemblies,¹¹¹ organic-inorganic hybrid materials,¹¹² dendrimers¹¹³ and porphyrin arrays/assemblies.¹¹⁴ Despite their excellent outcomes, many steps are involved in synthesising the complex architectures; the process could be described as labour-intensive; it involves complex and expensive purification process. These restrain the product from maximising and being used in widespread applications.¹¹⁷

Polymers are excellent scaffold materials¹¹⁵ to assemble and confine the functional bio-active compounds such as porphyrins, within nanoscale size to form well-defined morphologies.⁶¹ This is because of being spontaneously assembled in water, which simplifies their preparation. Additionally, the biological function can often be enhanced by polymers that can efficiently mimic the structure and function of the proteins. The assembly of diblock polymers is spontaneous. They form stable, well-defined micelles in aqueous solutions allowing for the incorporation of a variety of distinct cofactors.¹¹⁶ Additionally, synthetic polymers are useful materials; they have many applications such as drug delivery and encapsulation of hydrophobic drugs, nano-reactor and potential scaffold for many artificial system, because they are

commercially available, capable of functionalising, easy to manufacture, having a tendency to self-assembly, producing tuneable responses to external stimuli (high stability) and most importantly being soluble in common solvent including water which is considered a green-friendly solvent for the environment.⁶¹

Amphiphilic diblock copolymers have previously been employed to encapsulate and highly order chromophores under specific conditions, which demonstrated the possibility to control the energy transfer processes.¹¹⁶ As a result, hydrophobic compounds such as porphyrins can be easily incorporated in the core of micelles by hydrophobic interaction. For example, Adams *et al.*,¹¹⁶ exploited poly (ethylene oxide)-block-poly (butadiene) as a holder and spacer of bacteriochlorin and boron-dipyrromethene (BODIPY) that are presented as the energy-acceptor and energy-donor chromophores of this system respectively (**Figure 2.4**). The donor molecules were placed at the centre of the micelles, whereas the acceptor molecules were assembled at the interference of the micelles to control the distance between the active units in this system.¹¹⁶ However, significant energy transfer efficiency was observed when the system was coated on solid support to form bilayer films with 90% energy transfer efficiency.¹¹⁶

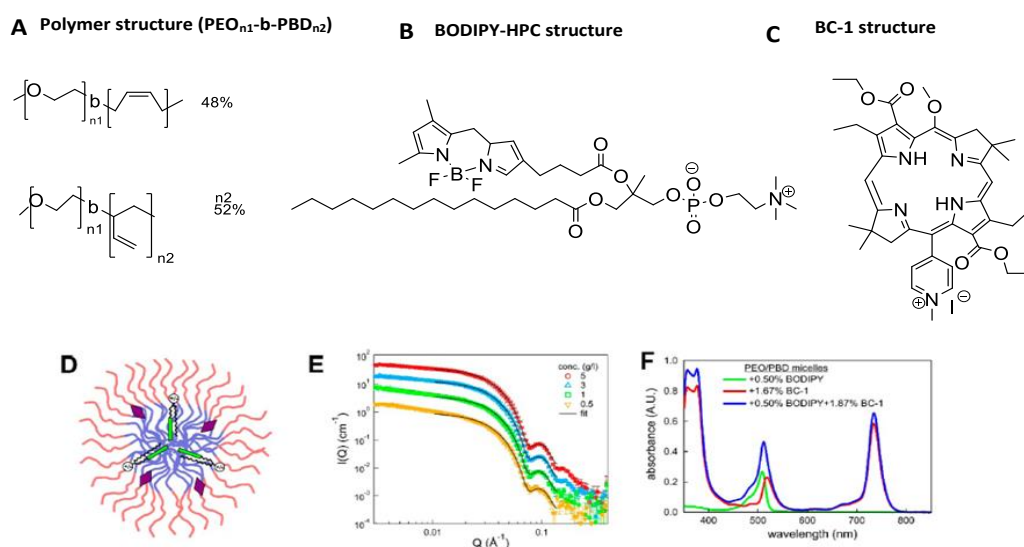


Figure 2.4: chemical structures and design of the polymer–chromophore nanocomposites. Chemical structures of (A), the PEO-b-PBD polymer, (B) the BODIPY-HPC donor chromophore, (C) the BC-1 acceptor chromophore, (D) the Schematic of the proposed chromophore arrangement in the polymer micelle (PEO, red; PBD, blue; BC-1, purple diamond; BODIPY, green), (E) SANS showing

scattering data from a concentration range PEO-b-PBD micelles fitted to a spherical core-shell model and (F) the absorbance spectra of three representative polymer–chromophore preparations.¹¹⁷ This figure is reused with kind permission from references¹¹⁷© 2015 American Chemical Society.

Peng *et al.*,¹¹⁷ built an artificial light-harvesting system based on the surface cross-linking micelles, using two self-assembling methods (electrostatic interaction and micellization), and a covalent bond utilised to build a robust, cheap and efficient artificial light harvesting system.¹¹⁷ The system afforded highly efficient energy transfer due to the absence of self-quenching. 9, 10-bis (4-methyl phenyl) anthracene (DPA) and Eosin Y disodium salt (EY) represent the energy-donor and energy-acceptor of that system, respectively. 4-(dodecyloxy) benzyl tripropargyl ammonium bromide is a cationic surfactant which can form micelles at particular concentration (above 0.14 mM in water).¹¹⁷ The surface of the micelle was covered with a dense layer of alkynyl, and it was anchored with 1, 4-diazidobutane-2, 3-diol (2) by 1, 3-dipolar cycloaddition with a Cu^I catalyst (**Figure 2.5**).¹¹⁷

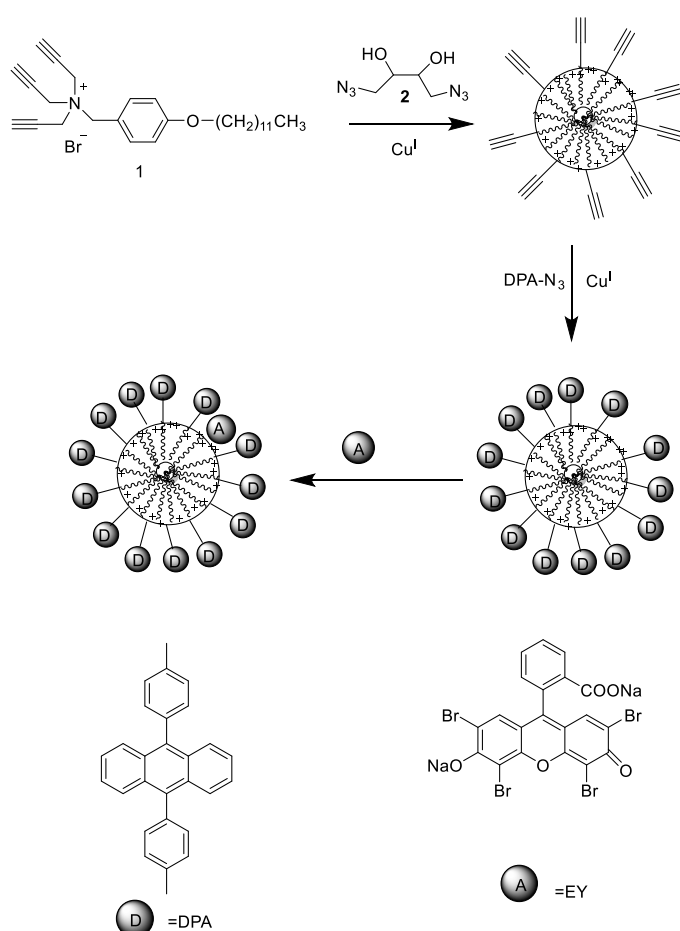


Figure 2.5: a synthetic artificial light-harvesting system based on surface cross-linking micelles.¹¹⁷

Since natural light-harvesting complexes what have been attempted to duplicate, it is preferable for polymeric light harvesting to self-assemble under more biologically relevant aqueous conditions. Therefore, in this project, the capability of mPEG-b-PCL diblock copolymer was investigated as a potential alternative protein matrix to non-covalently incorporate hundreds of modified tetraphenyl porphyrin (TPP) molecules and a single molecule of phthalocyanine tin (IV) dichloride (tin phthalocyanine) which acts as donor molecules and acceptor molecule, respectively, within the nanoscopic micelles in aqueous condition. A simple modification of the tetraphenylpyrrole (TPP) structure will be made by covalently attaching hydrophilic polymers such as mPEG to one of the meso-phenyl units, which allows for the isolation of porphyrin arrays at the edge of the core of micelles, leaving a sufficient distance between them and the tin phthalocyanine (the acceptor molecule), which will be located at the centre of micelles. Hence, there is potential for a simple and more stable donors/acceptor system that bio-mimicks the antenna complex in purple bacteria has been successfully to be assembled. The aggregation behaviour of donor and acceptor in presence and absence of micelles in aqueous solution will be studied. The importance of the hydrophobic block size to assembling a large number of porphyrins before pre-quenching occurs is also highlighted. For that purpose, four different mPEG-b-PCL diblock copolymers with a fixed length of MPEG block at different lengths of PCL block have been synthesised.

2.2 The aim

This chapter is concerned with photosynthesis, the most important reaction on planet Earth. LH assemblies in natural photosynthetic systems hold hundreds of differently organised chromophores. These chromophore arrays are precisely and spatially organised and entrapped within nanoscopic protein matrices (**Figure 2.6**), where energy and electron transfers take place efficiently via a sequence of fluorescence resonance energy transfer (FRET).

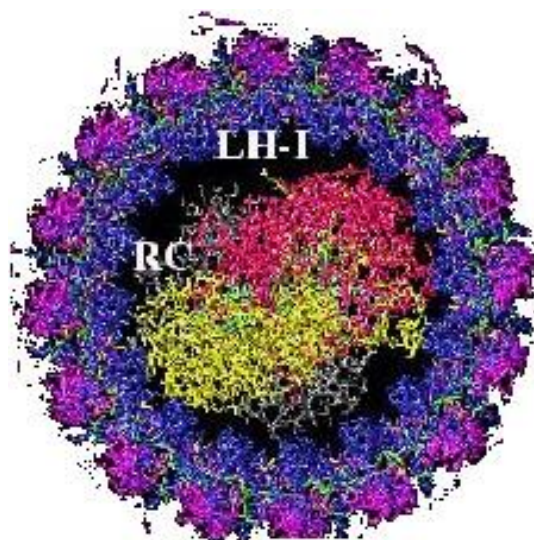


Figure 2.6: light-harvesting complex (LH cox) and the reaction centre (RC). A large number of bacteriochlorophylls (purple) are precisely arranged around a pair of different bacteriochlorophylls (red and yellow) in the reaction centre. The whole system is contained within nano-scopic protein matrices.

These highly ordered arrays function to absorb light over a wide range of the solar spectrum; this energy is funnelled into a single chromophore in the reaction centre. This dramatically enhances the rate of successive redox processes that occurs in photosynthesis. Controlling the arrangement of functional chromophores into highly organised self-assembled arrays within a nanoscopic controlled macroenvironment, has caught the attention of many research groups. Inspired by the structure of the natural photosynthesis, these research groups, have developed an artificial LH system that confines the photo-active units within a nanometre scale. This strategy can lead to an efficient energy transfer through a Förster's mechanism. Peng¹¹⁷ and Adams¹¹⁷ designed an artificial LH system that could operate successfully in aqueous solutions by employing cross-linked micelles and micelles (**Figure 2.7**). These have donor and acceptor molecules, situated at precise locations within and around the micelle structure.¹¹⁷ The process was complicated and difficult to modify.

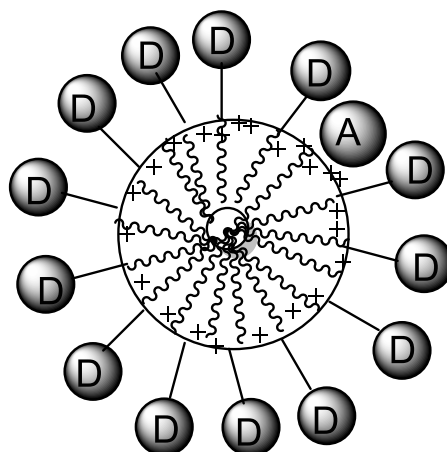


Figure 2.7: schematic representation of Hui-Qing Peng artificial LH system. Where D and A represent donor and acceptor molecules respectively. Donor molecules are functionalised in way that allows them to bind at surface of cross-linked micelles through electrostatic interaction. The single acceptor molecule is kept within the core of the micelle, close to the surface.¹¹⁷

The aim of this project is to build a simple artificial LH system that mimics the structure of the natural system. We aim to use polymeric micelles as a controlled microenvironment that is capable of supporting a number of donor molecules around a single, central acceptor molecule (Figure 2.8).

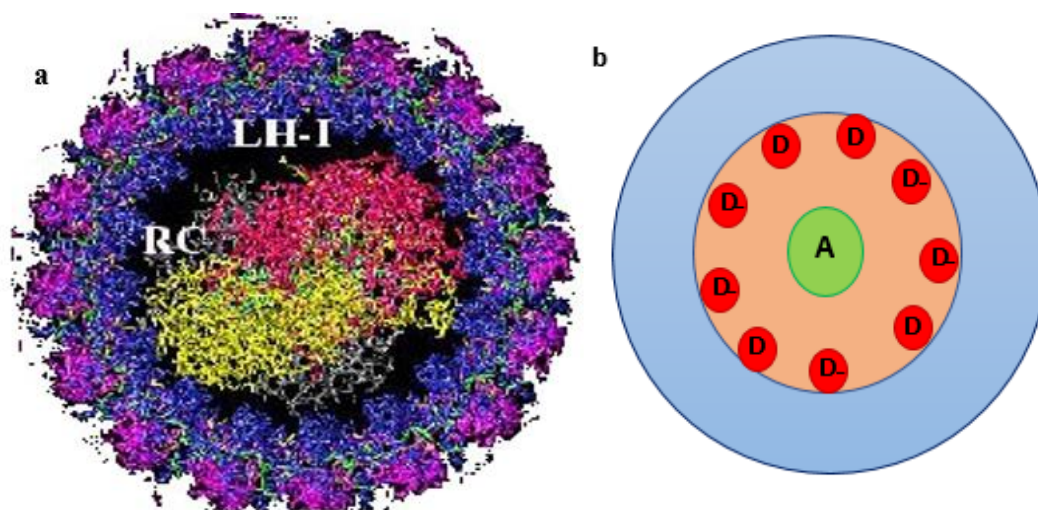


Figure 2.8: representation of *a*) natural, and *b*) artificial light-harvesting systems where blue and red regions respectively represent hydrophilic and hydrophobic parts in diblock copolymer micelles in artificial LH system. Donor molecules (D) and acceptor molecules (A).

In all LH systems, donor molecules are designed to absorb light energy at a specific wavelength and funnel it into the acceptor molecule, which will emit light at different and energetically useful wavelengths. However, simply mixing donors and acceptor molecules within a nano-scale-sized micelle will result in quenching. This is due to the hydrophobicity and mobility of

the molecules, which are present in high within the micelle core leading to aggregation (**Figure 2.9.a**).

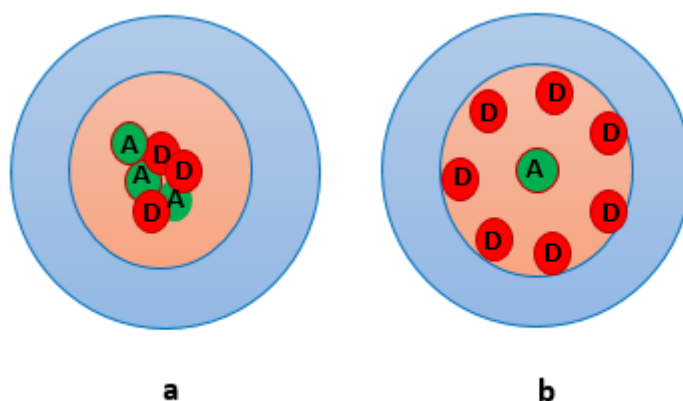


Figure 2.9: schematic representation of *a*) the random aggregation of unattached porphyrin (red ball) and phthalocyanine (green ball) molecules inside the micelle. *b*) The self-assembly of mPEG-porphyrin and phthalocyanine in micelles.

The approach selected to avoid this random aggregation involved attaching a hydrophilic polymer to the donor molecules, which will place the donors close to the hydrophilic/hydrophobic interface within the mixed micelles (**Figure 2.9.b**). The acceptor molecule will be left at the centre of a micelle's core. Polymeric micelles can thus be considered a simple alternative to a protein scaffold, as they possess high-loading capacities, they are water-soluble, and they can be produced on a large scale and are inexpensive.

Although there are many polymers that could be considered, mPEG-b-PCL diblock copolymer was chosen as the amphiphilic diblock polymer for use in this model artificial LH model. It was selected as it is one of the most widely investigated polymers used in biological applications and can be synthesised easily. Additionally, the resulting micelles can enhance the solubility of the poorly water-soluble chromophores and the flexibility of PCL block allowing the core of micelles to encapsulate a large number of donors and acceptors. Unlike some diblock copolymers such as methoxy polyethylene glycol-b-polyvinyl pyridine (mPEG-b-P4VP), mPEG-PCL does not have binding sites. This allows the incorporation of various

hydrophobic and amphiphilic chromo-phores facilitating the modulation of the whole system. MPEG-PCL micelles will not interfere with the absorption the light, harvesting the light and energy transfer process, MPEG-PCL micelles are unable to absorb or emit light in a visible and near infrared region. Therefore, the shining light only is absorbed by the donor and acceptor molecules and there is no energy loss due to the surrounding PCL chains.

Many electron donor/acceptor units have been studied extensively for the purpose of building artificial LH systems. However, teraphenyl porphyrin (TPP) and dichloride (phthalocyanato)tin(IV) (tin phthalocyanine) will be used as our donor and acceptor molecules. Porphyrins and phthalocyanines are closely related to the chromophores found in nature and are ideal components to fulfil the donor and acceptor roles in our synthetic LH system. TPP absorbs light energy around 420 nm and emits around 650nm-715 nm, whereas the maximum light absorption of tin phthalocyanine occurs round 700nm-750 nm with emission at near infrared wavelengths. Thus, most of the solar spectrum can be covered by using these as donor and acceptor units. Attaching a hydrophilic polymer such as mPEG to TPP (porphyrin), allows porphyrin to be isolated within a region of the micelles (monomeric species). This also fixes a distance between the porphyrin molecules and an acceptor molecule located at the centre of micelles. As result, maximum energy can be harvested from this system.

Since mPEG-porphyrin polymers are amphiphilic polymers, it is important to study their aggregation behaviour in aqueous solution in the absence and presence of mPEG-PCL diblock copolymer micelles. To enhance the efficiency of this model LH system, the encapsulating the maximum amount of non-aggregated mPEG-porphyrin polymers in the core of micelles is essential. Therefore, four different mPEG-PCL DBCs will be synthesised with a fixed length of mPEG block and differing lengths of the PCL block. The larger the hydrophobic block, the more mPEG-porphyrin polymers can be incorporated before quenching. Therefore, it is also

important to determine the level of porphyrin loading that can be achieved before they are close enough to quench.

Due to the extensive conjugated system, unsubstituted phthalocyanines and metallophthalocyanines (MPc) have very low solubility in most solvents, which can result in aggregation. To overcome this problem, alkyl or alkoxy groups will be introduced into the non-peripheral positions; this will increase solubility and should reduce aggregation within the core of the micelles. To avoid aggregation, it is important to insert just one molecule of tin phthalocyanine at the centre of micelles, therefore a very low concentration of tin phthalocyanine will be required. The final step in this study of the proposed artificial light-harvesting system, will be energy transfer. These energy transfer experiments, a fluorimeter machine and UV-vis spectrometer were used to determine the emission wavelength of the donor and the absorption wavelength of the acceptor units. In order to observe energy transfer within our system, the emission spectrum of the donor units should overlap with the absorption spectrum of the acceptor unit as shown in **Figure 2.10**.

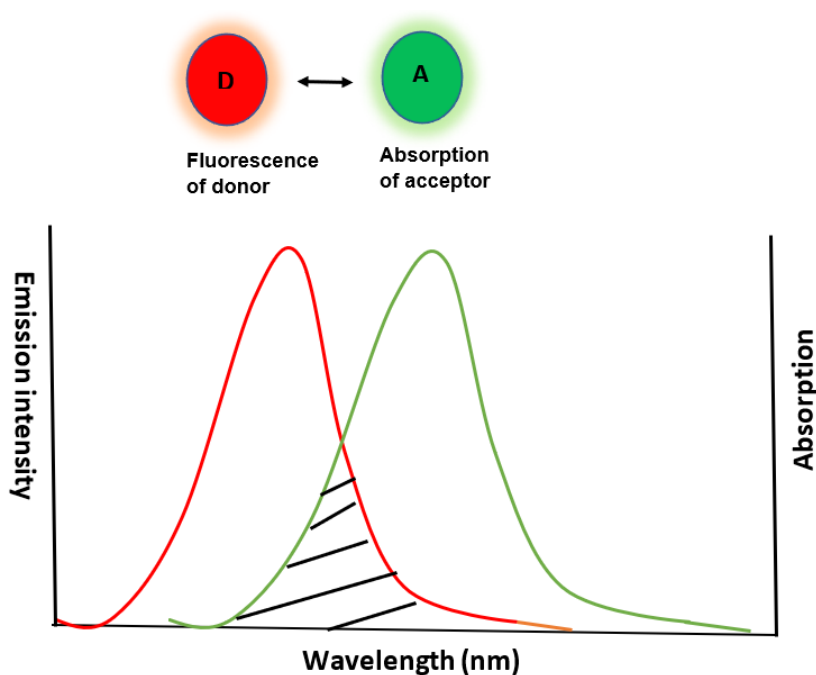


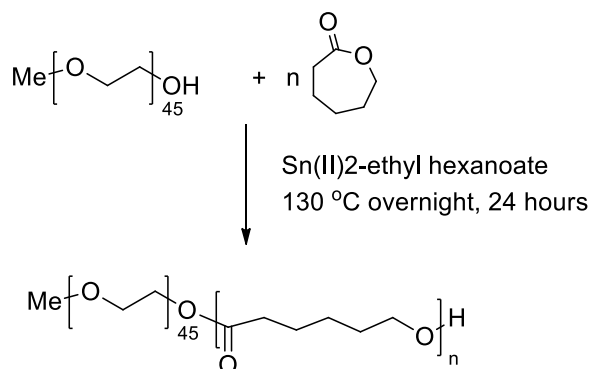
Figure 2.10: overlap (black lines) of emission spectrum of donor (red curve) and absorption spectrum of acceptor (green curve) units.

2.3 Results and discussion: Artificial light harvesting system.

To construct an artificial antenna complex, one needs to prepare amphiphilic diblock copolymers that form well-defined polymeric micelles in an aqueous solution. These nanoscopic micelles provide a space that can hold and organise a number of PEG-porphyrin polymers precisely, as well as a single tin phthalocyanine; these will be used as donor and acceptor molecules, respectively. Polymeric micelles can also reduce the aggregation level of the chromophoric acceptors and donors, leading to an efficient energy/electron transfer in these fluorescence compounds. To exploit the properties of porphyrin in this work, a simple modification of tetra phenyl porphyrin (TPP) structure was made, whereby mPEG is covalently attached through one of the meso-phenyl positions. A substituted tin phthalocyanine was chosen as it possessed high extension coefficient near infrared region (600 nm-750 nm) and emitted light with a high quantum yield.

Poly ethylene glycol (PEG) is the most common block used in amphiphilic diblock copolymers. It has many advantages; it is atoxic, cheap, easy to functionalise and capable of forming a dense, brush-like shell, which increases the stability of the formed system. Additionally, it is approved by the Food and Drug Administration.¹¹⁸ PEG is mostly employed as a hydrophilic block, not only in hydrophobic/hydrophilic diblock or hydrophilic /hydrophobic/hydrophilic tri block, but also in hydrophilic/ionic copolymers whereas ϵ -caprolactone was the selected hydrophobic part as it is a biodegradable material that has been investigated extensively due to its low toxicity, commercial availability and low cost.¹¹⁸ For this reason, the mPEG-b-PCL diblock copolymer, and its aggregated structure were chosen as an alternative to the protein matrix in the LH systems. This design allows many porphyrins to be incorporated within nanoscopic micelles in aqueous conditions, using noncovalent chemistry.

The following copolymers were synthesised by the use of ring opening polymerisation: poly (ethylene glycol) methyl ether-*block*-poly (ϵ -caprolactone) (mPEG-PCL) diblock copolymers with different ratios of polycaprolactone (PCL) block and a monomethoxy poly (ethylene glycol) (mPEG with a fixed degree of polymerisation ($n=45$)). mPEG was used as a micro-initiator and Sn (2-ethyl-hexanoate) as a catalyst (**Scheme 2.1**).



Scheme 2.1: synthesis of mPEG₄₅-b-PCL_n.

To obtain a high conversion of a diblock, and to prevent any trace of homopolymers in the final product, molecules that trigger the termination step of ROP (such as water, oxygen, some solvents) were eliminated prior to starting the reaction. Therefore, all traces of moisture in the mPEG were removed by azeotropic distillation in dry toluene. Moreover, the polymerisation proceeded in bulk at a temperature above the melting point of polyethylene glycol (130 °C), which avoids the use of added solvents in reaction. The reactants' mixture was placed in flasks, which were subjected to a vacuum and then they were degassed, before adding the catalyst and monomer (ϵ caprolactone). The mixture was stirred under nitrogen then the completed reaction was left to cool to room temperature. Small amount of DCM was added, and the product was precipitated with petroleum ether. Finally, the petroleum ether was decanted, and the precipitant was dried under vacuum.

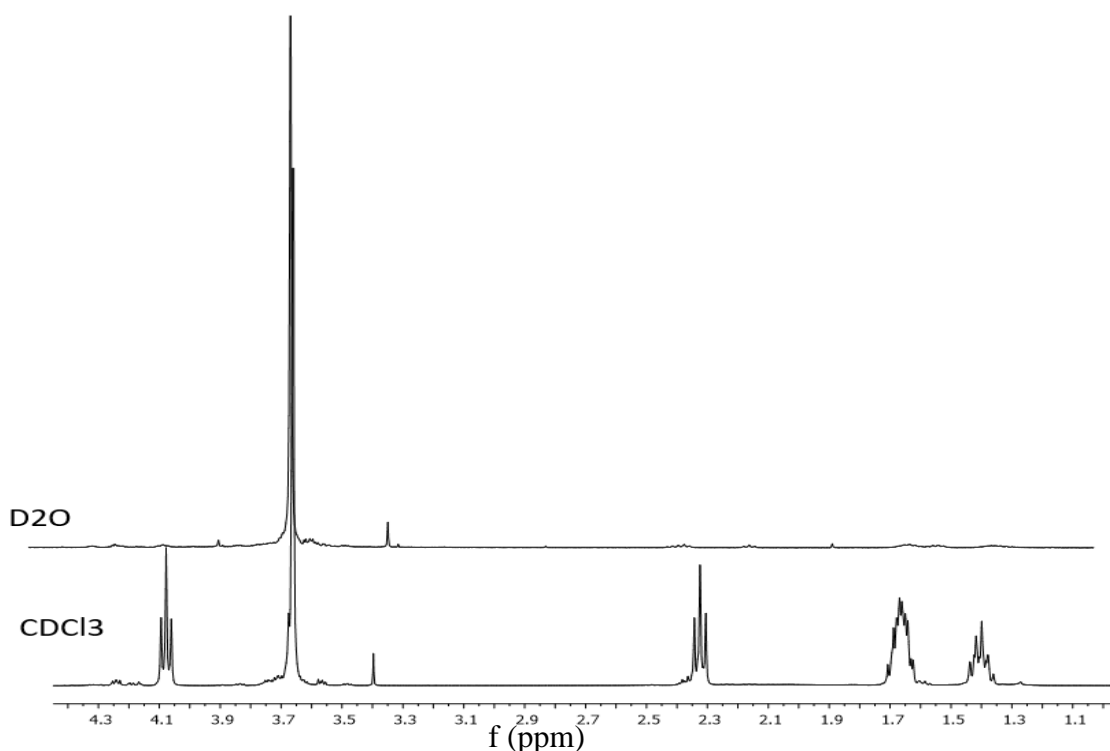


Figure 2.12: the ^1H NMR spectra of mPEG-b-PCL. All visible ^1H resonances in CDCl_3 are attributed to the protons of both blocks; mPEG-b-PCL in D_2O only ^1H resonances correspond to PEG protons appeared.

The molecular weight observed by GPC was much higher than that calculated theoretically and by ^1H -NMR.¹¹⁸ This is due to calibration of the GPC column with polystyrene beads which may interact with mPEG in the diblock copolymer. Therefore, even average number molecular weight (M_n) of mPEG ($M_n=2000$ g/mol) alone resulted in a molecular weight above 3000 g/mol. A more plausible reason for the observed molecular weights could be the presence of impurities and other polymers in the final product (presence in GPC spectra as shoulder or another peak) (**Figure 2.13**). The data from GPC indicated that these impurities were homopolymers (of either PCL or mPEG); they were formed during the ring opening polymerisation due to the presence of another initiator such as water. These impurities were clear from the GPC result for the mPEG₄₅-b-PCL₄₅ which yielded two obvious peaks (**Figure 2.13 a**).

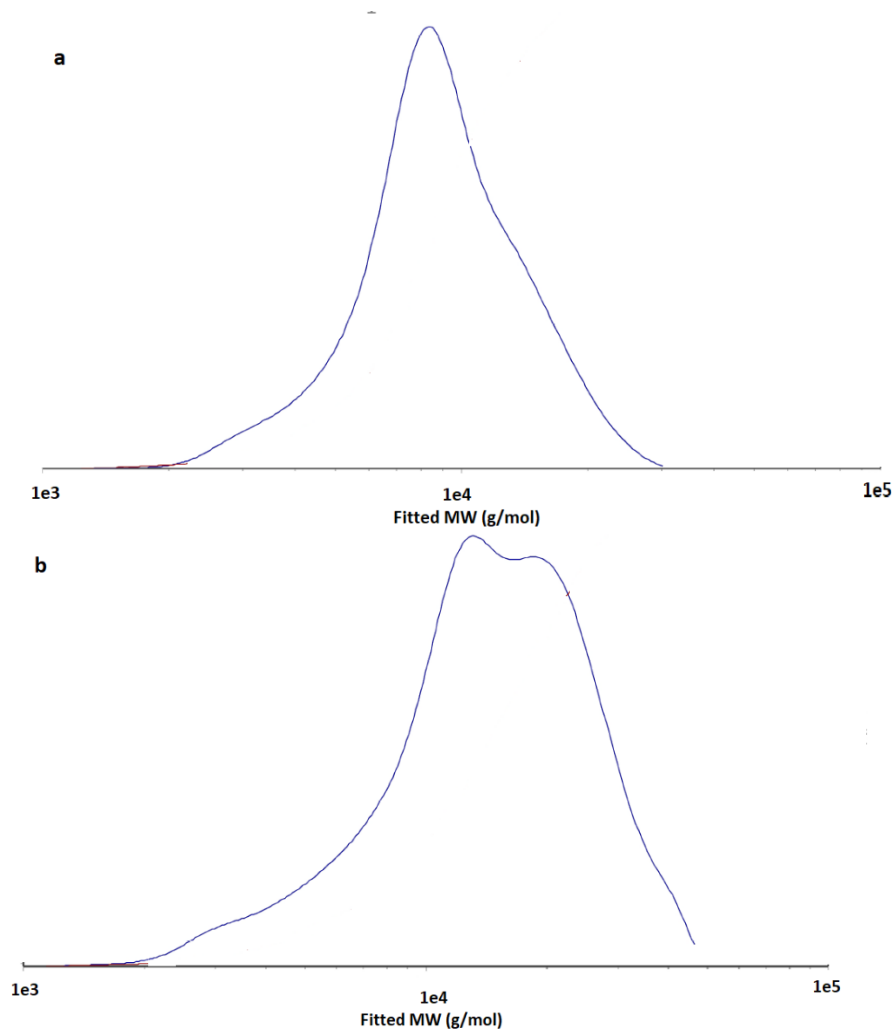


Figure 2.13: GPC spectra for a, mPEG₄₅-PCL₂₅ and b, mPEG₄₅-PCL₄₅.

Additionally, ROP showed poor control over dispersity; high \bar{D} was observed (above 1.4 for most ratios). Since the ¹H NMR spectroscopy technique requires attaching every mPEG block to PCL block, it is only valid when the product is pure. **Table 2.1** shows the estimated M_n calculated from ¹H NMR spectroscopy and GPC and theoretically for four diblock copolymers, (the first attempt of ROP polymerisation).

Table 2.1: basic properties of produced mPEG₄₅-b-PCL_n

Copolymers Targeted n ^a	Observed n ^b	M _n /g mol ⁻¹			Đ
		Theoretical	¹ H NMR	GPC	
1a n=15	14	3722	3722	3764	1.44
1b n=25	28	4862	5192	7538	1.28
1c n=35	33	6002	5762	7848	1.48
1d n=45	47	7142	7472	10994	1.47

Note: n in subscripts represents the number of repeat ϵ -caprolactone monomer in copolymer chain. All the copolymers have contained fixed mPEG₄₅

a. A series compositions of PCL designed before the experiment

b. As determined by integration (methoxy ¹H resonances) of ¹H NMR spectroscopy in CDCl₃

The results were not satisfactory in terms of purity as the GPC trace indicated the presence of homopolymers. Therefore, it was decided to resynthesise the polymers, taking more care with the purity/quality of the stored materials. A much better result in terms of purity of mPEG₄₅-PCL_n diblock copolymers was obtained when ϵ -caprolactone was also purified by azeotropic distillation in the presence of calcium hydride; this removed any moisture present in the ϵ -caprolactone. Moreover, a better result has been obtained when 1,5,7-triazabicyclo [4.4.0] dec-5-ene (TBD) was used as a catalyst. For ROP polymerisation to occur, a lower temperature was required (110°C) and the polymerisation was completed in 10 minutes. The result was achieving a better control over molecular weights and polydispersity (lower Đ, 1.18 for mPEG₄₅-PCL₂₅). The average molecular weight (M_n) was calculated using ¹H NMR spectroscopy of four diblock copolymers, and these were close to the M_n value which was calculated theoretically. **Table 2.2** displays the basic characterisation results of the newly synthesised diblock copolymers.

All of the mPEG protons re-observed at 3.40 and 3.67 ppm and the protons of the ϵ -caprolactone were also observed at 2.35, 1.65, 1.41 ppm and the protons α to the ester bond

were observed at 4.08 ppm. The methoxy peak was used to determine the integration of the rest protons which helped to determine the degree of polymerisation of PCL.

Table 2.2: the basic characterisation results new synthesised diblock copolymers.

Copolymers Targeted n ^a	Actual n ^b	Mn/g mol ⁻¹			Đ
		Theoretical	¹ H NMR	GPC	
1a n=15	12	3722	3400	4700	1.22
1b n=25	19	4862	4200	5600	1.18
1c n=35	37	6002	6200	7800	1.21
1d n=45	47	7142	7500	9300	1.47

The GPC results for four diblock copolymers yielded a single peak (**Figure 2.14**), which is attributed to the pure diblock copolymers and the absence of any impurities.

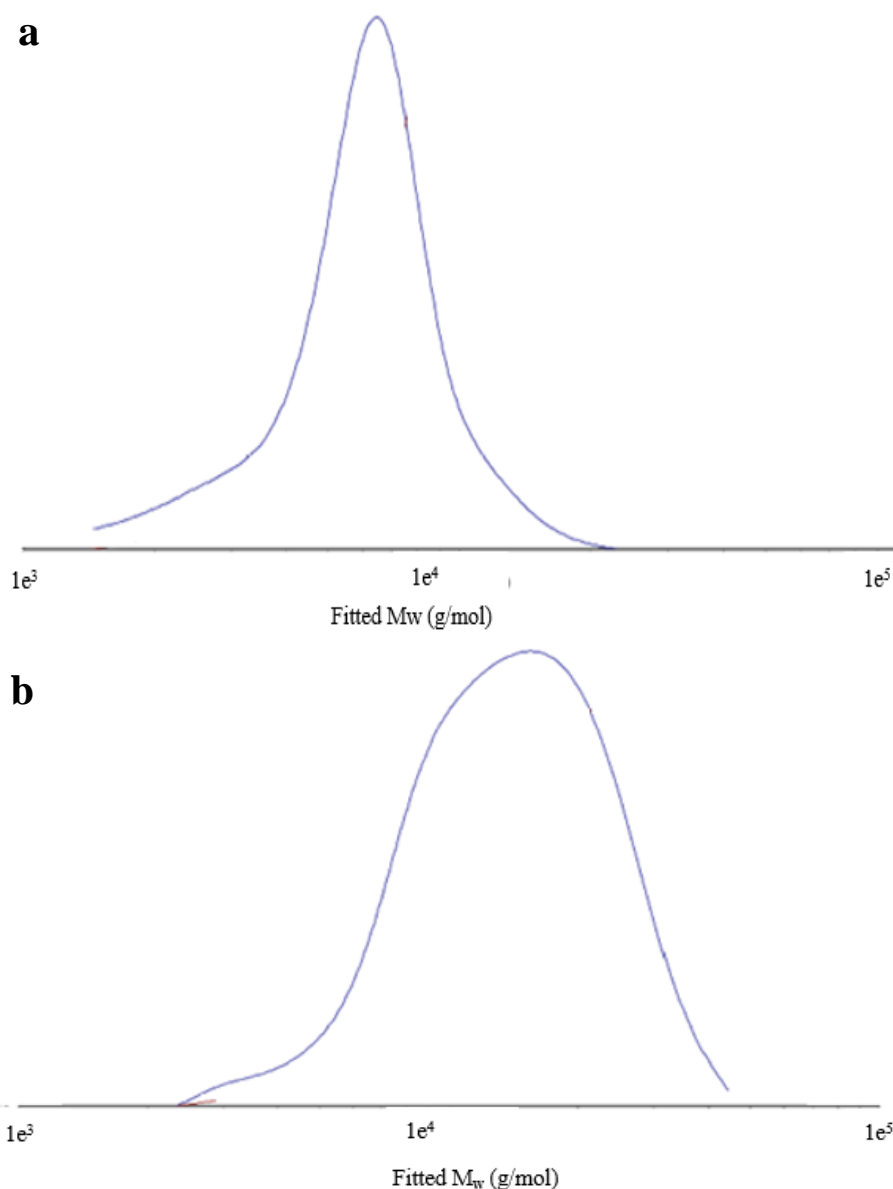


Figure 2.14: GPC spectra for **a**, mPEG₄₅-PCL₄₅ and **b**, mPEG₄₅-PCL₂₅ for the second attempt.

The hydrophobic property of PCL of any aggregates allows hydrophobic compounds to be encapsulated in aqueous solution. TPP and tin phthalocyanine, which respectively act as the donor and acceptor in our LH system, are very hydrophobic. They are going to be encapsulated in diblock copolymeric micelles to form complexed micelles. Therefore, the successful synthesis of pure mPEG-b-PCL_n diblock was essential to form highly stable polymeric micelles in aqueous solution. The self-assembly of the first four ratios of diblock copolymers (mPEG₄₅-b-PCL₁₅, mPEG₄₅-b-PCL₂₅, mPEG₄₅-b-PCL₃₅, mPEG₄₅-b-PCL₄₅) was studied (**Table 2.3**), and the critical micelle concentration (CMC) was estimated using many different measurements.

Table 2.3: Characterisation results of mPEG45-b-PCL_n diblock copolymers with the different repeat unit of ϵ -caprolactone monomer in copolymer chain and PEG-porphyrin in water.

Type of characterisation	mPEG ₄₅ -b-PCL ₁₅	mPEG ₄₅ -b-PCL ₂₅	mPEG ₄₅ -b-PCL ₃₅	mPEG ₄₅ -b-PCL ₄₅	PEG-porphyrin
Number molecular weight calculated theoretically (g mol ⁻¹)	3700	4900	6000	7100	2658
Number molecular weight calculated by ¹ H-NMR spectroscopy (g mol ⁻¹)	3400	4200	5800	7500	2658
Number molecular weight calculated by GPC (g mol ⁻¹)	4700	5600	7800	1100	3881
\bar{D}	1.22	1.18	1.17	1.3	1.05
Critical micelles concentration(μ g/mL)	5	1	0.5	0.3	16
Diameter of micelles at critical micelles concentration(nm)	134	143	261	280	20

These included UV-vis, fluorescence and dynamic light scattering (DLS). **Table 2.4** the CMC of two different ratios mPEG₄₅-PCL₁₅ and mPEG₄₅-PCL₂₅ using different characterisation methods and their size using DLS.

Table 2.4 Summarised the CMC of two different ratios mPEG₄₅-PCL₁₅ and mPEG₄₅-PCL₂₅ using different characterisation methods.

n ^a	CMC (μ g. mL)		
	UV-vis ^b	Fluorescence ^c	DLS ^d
15	10	5-10	10
25	1	2-5	2

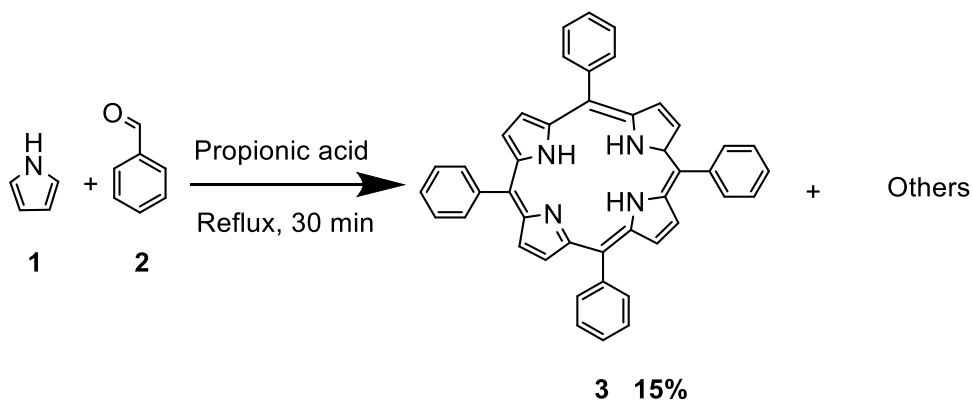
- n in subscripts represents the number of repeat ϵ -caprolactone monomer in copolymer chain. All the copolymers have contained fixed mPEG₄₅.
- The determination of CMC through UV-vis (using porphyrin as probe).
- The determination of CMC through fluorescence (pyrene experiment).
- The determination of CMC through Dynamic light scattering (DLS).

Different concentrations of diblock copolymers in aqueous solution were prepared. Although diblock (mPEG-b-PCL) copolymer usually dissolves in water, our polymers were only partially

dissolved. Therefore, two methods were tried to dissolve the diblock copolymers. Firstly, a small amount of THF was used to dissolve the copolymers and then diluted with water. After stirring for 12 hours, the THF evaporated leaving a homogenous copolymer solution. Dialysis is a common method to prepare micelles, as it allows all impurities and organic solvent to pass through the dialysis bag, leaving the pure copolymers within the bag. This method formed well-dispersed polymeric micelles. The hydrophobicity and high molecular weight of poly (ϵ -caprolactone) were the main reasons for being unable to prepare polymeric micelles directly or via THF. Different concentrations of diblock, ranging from 0.5 $\mu\text{g/mL}$ to 500 $\mu\text{g/mL}$, were prepared from a stock solution with 1000 $\mu\text{g/mL}$ concentration.

At the beginning of this project, meso-tetraphenylporphyrin **6** (TPP) was chosen as a UV-vis probe to determine the CMC of diblock copolymers. TPP **6** is aromatic and has a very high molar extinction coefficient within a λ_{max} value at 418.5 nm. Also, due to the high hydrophobicity of TPP **6**, it was thought to be a convenient method, as its solubility will be dramatically increased when encapsulated inside the micelles (UV detects porphyrin at $\lambda_{\text{max}}=418.5$ nm).

Propionic acid was used in the synthesis of TPP **3** (**Scheme 2.2**) to dissolve and catalyse the condensation of four molecules of benzaldehyde **2** and pyrrole **1**. The solution was heated under reflux before the addition of the starting materials. This avoided pyrrole polymerisation and directed the reaction towards TPP **3** formation. The mixture solution was cooled to room temperature, this induced the formation of dark black crystal in propionic solution. The crystal was filtered and the solid on filter paper was washed with hot methanol and water. Finally, the product was dried in oven. The product obtained was a bright purple solid, with a yield of 15%.



Scheme 2.2: synthesis of tetraphenyl porphyrin (TPP) **3**.

^1H NMR of TPP **3** showed strong de-shielded resonance at 8.91 ppm, 8.25 ppm and 7.81 ppm, which corresponded to the protons directly connected to the pyrrole and phenyl groups, respectively. An extremely shielded resonance at -2.73 ppm was attributed to the amine hydrogens inside the porphyrin ring. Electrospray mass spectrum (ES) indicated a molecular ion at 615 m/z. The UV-vis spectra had a strong Soret band at 418.5 nm, and four much weaker Q absorptions between 510 and 650 nm.

To determine the CMC for each polymer, a stock solution of TPP **3** 1×10^{-4} M was made, and 1 mL of this solution was added to the polymer solutions ranged in concentration from 0.5 $\mu\text{g/mL}$ to 500 $\mu\text{g/mL}$; the solutions were left stirring overnight. The logarithm of concentrations of diblock was plotted against absorption (ΔAbs); the TPP **3** graph is shown in **Figure 2.15**. ΔAbs was used to reduce the influence of baseline drift.

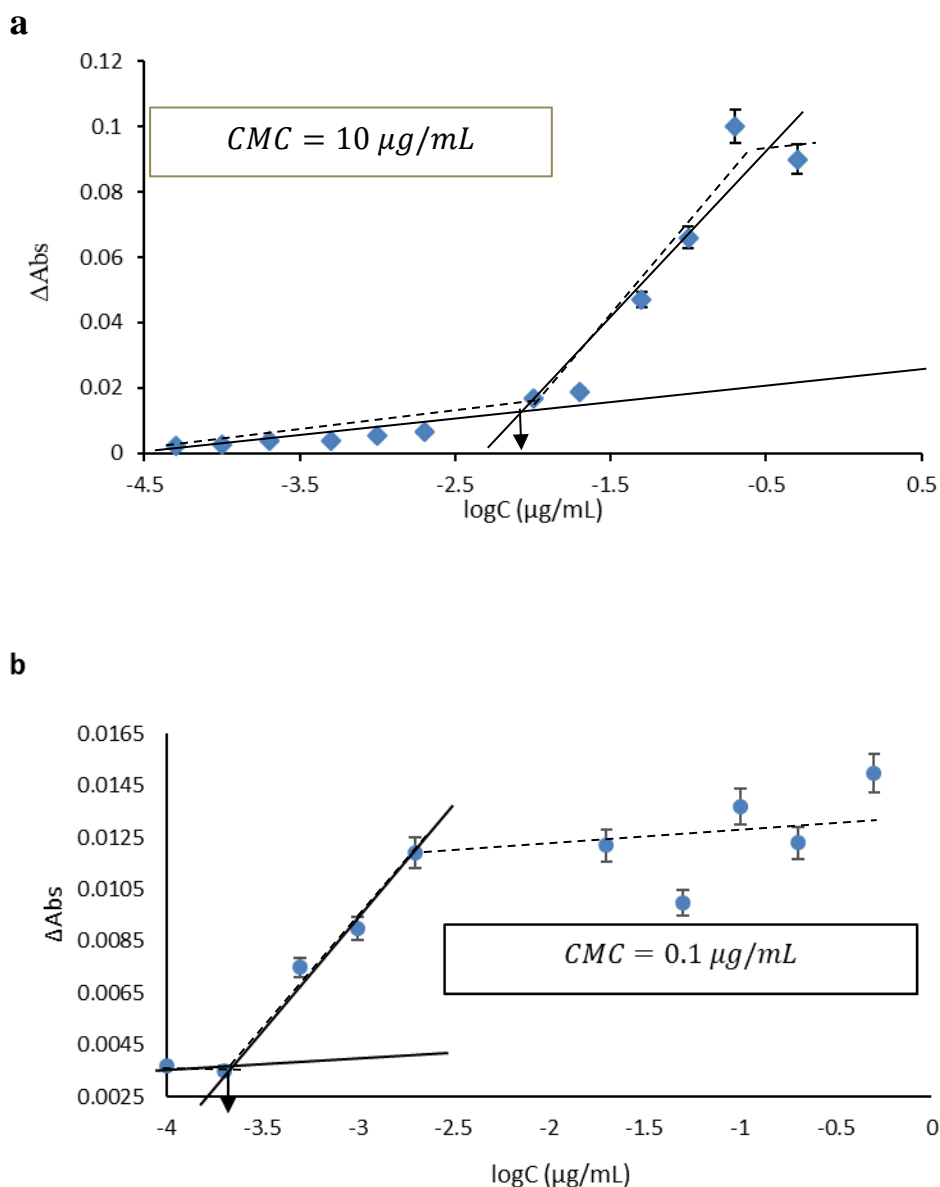


Figure 2.15: CMC plots of ΔAbs vs $\log C$ for mPEG-PCL diblock copolymers with different PCL length. **a**, mPEG₄₅-b-PCL₁₅ and **b**, mPEG₄₅-b-PCL₂₅.

The CMC for mPEG₄₅-b-PCL₁₅ was higher than mPEG₄₅-b-PCL₂₅; this is due to the hydrophobic block (PCL) in mPEG₄₅-b-PCL₁₅ being shorter than that found in mPEG₄₅-b-PCL₂₅. Therefore, mPEG₄₅-b-PCL₁₅ expected to form micelles at higher concentration. In comparison to the CMC values published in the literature (around 5 $\mu\text{g/mL}$),¹¹⁹ the CMC of mPEG₄₅-b-PCL₂₅ was very low (0.35 $\mu\text{g/mL}$). This may be due to the TPP, which very hydrophobic and could enhance the aggregation by assembling polymers around it in aqueous solution at a lower concentration. The CMC was also measured by fluorescence spectroscopy

using pyrene as the probe. This experiment is a common method to determine CMC in aqueous solution. Unlike porphyrin, pyrene has some solubility in water, and the fluorescence properties of pyrene change when it is transferred from an aqueous environment into the hydrophobic microenvironment of the micelles. Specifically, the intensities of emission peaks at 373 nm and 383 nm, respectively, denoted as I_1 and I_3 , change. Therefore, the logarithm of different concentrations has been plotted against the I_3/I_1 ratio (**Figure 2.16**).

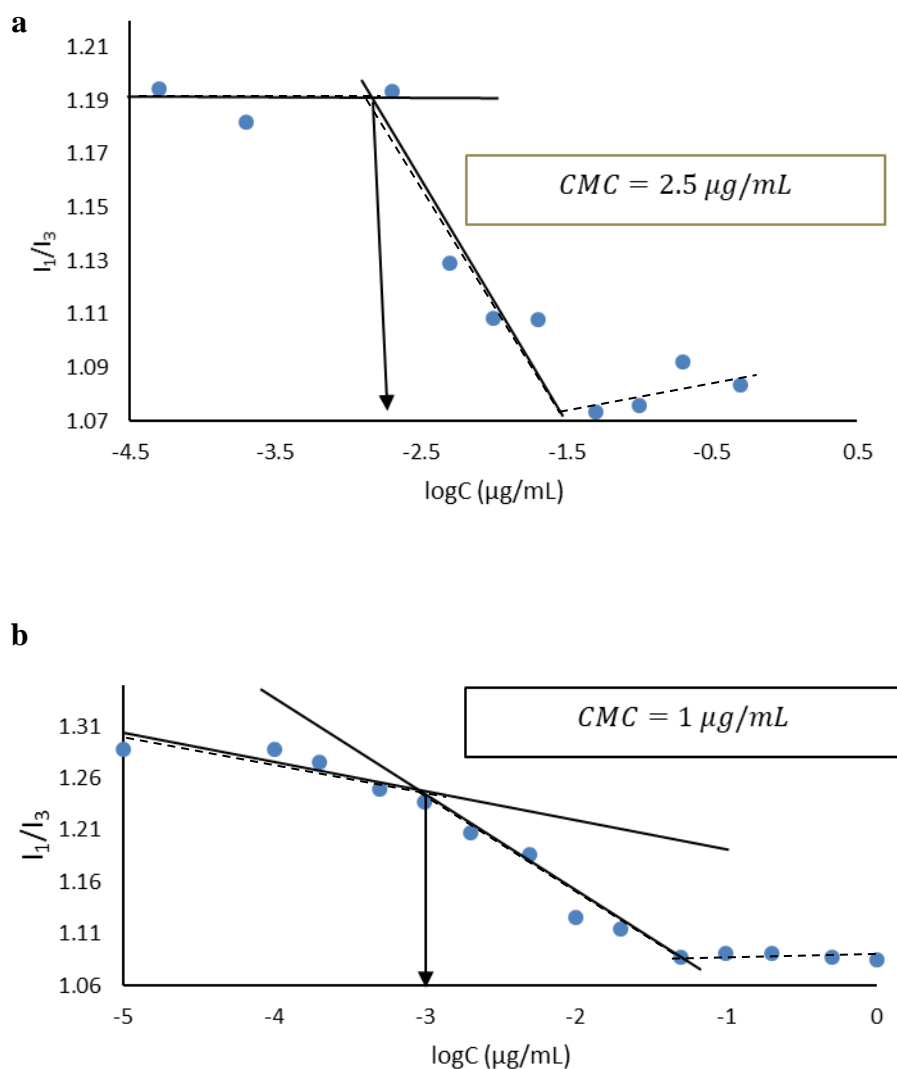


Figure 2.12: **a** and **b** show the size change as a function of the logarithm concentration of the mPEG₄₅-bPCL₁₅ and mPEG₄₅-bPCL₂₅, respectively.

For further confirmation, the CMC of mPEG₄₅-bPCL₁₅ and mPEG₄₅-bPCL₂₅ copolymer micelles were also determined by DLS, which cannot detect the presence of unimers. However, as micelles form, there was a significant increase in hydrodynamic diameter (D_h). This increase then slows down at higher concentration (above the CMC). **Figures 2.17.a** and **b** show the size change as a function of the logarithm concentration of mPEG₄₅-bPCL₁₅ and mPEG₄₅-bPCL₂₅.

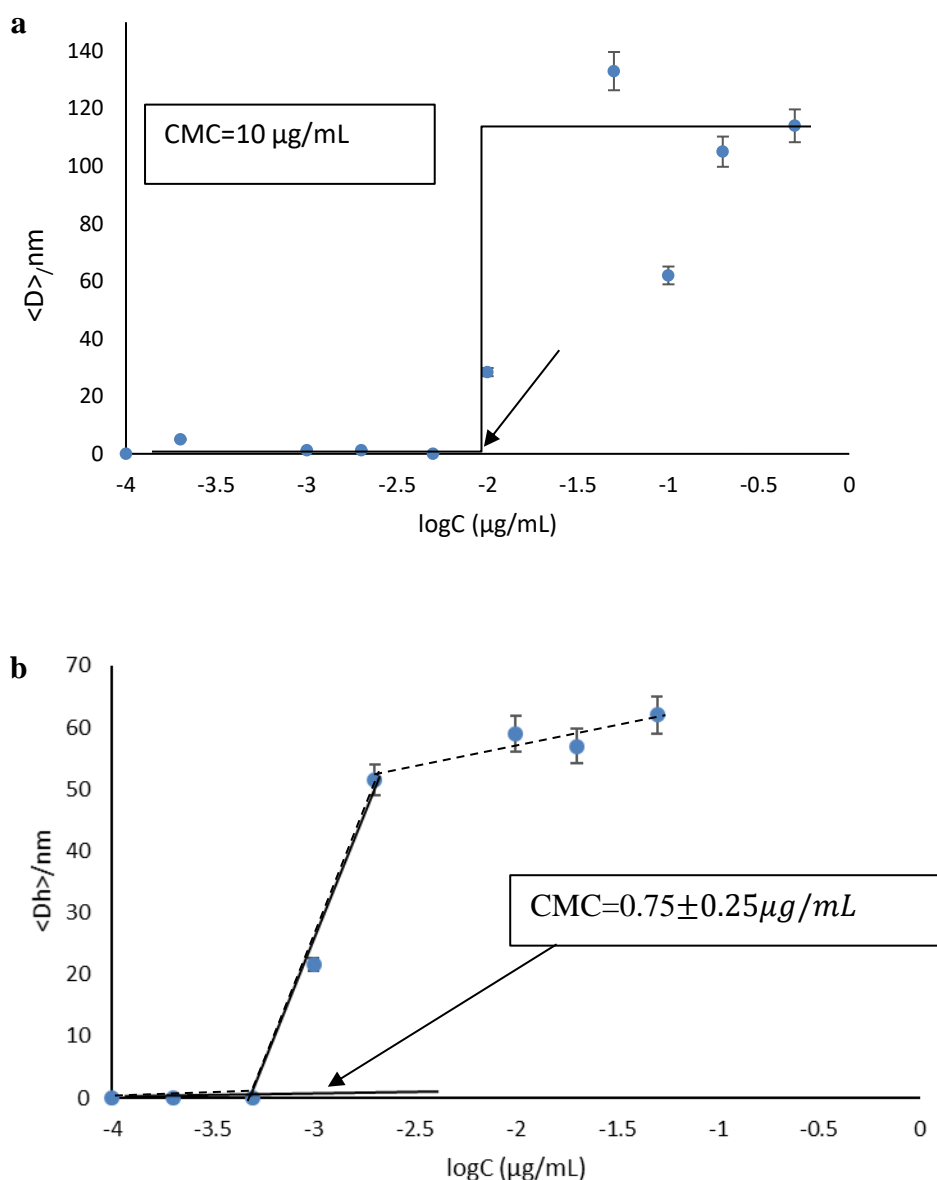


Figure 2.17. a and **b** show the size change as a function of the logarithm concentration of the mPEG₄₅-bPCL₁₅ and mPEG₄₅-bPCL₂₅, respectively.

It is evident that CMC values were different for each di-block copolymers when diverse methodologies were used. In contrast to UV-vis and fluorescence methods whereby the use of

hydrophobic probe is required, DLS determines the formation of empty micelles. The CMC value that is determined by UV-vis and fluorescence might sometimes be different because of the various sensitivities of the two devices. The CMC value for mPEG₄₅-b-PCL₂₅ that was determined by UV-vis method (0.1 µg/mL) was 10-fold smaller than CMC values determined by the fluorescence and the DLS methods which involved 1 µg/mL and 0.75 µg/mL, respectively. This is due to the high hydrophobicity of porphyrin that influenced the micelles formation at lower concentrations. Unlike mPEG₄₅-b-PCL₂₅, the obtained CMC values for mPEG₄₅-b-PCL₂₅ by UV-vis and DLS method were same, 10 µg/mL. This result indicates that porphyrin has no effect on the micelle formation. This might be due to the majority of mPEG₄₅-b-PCL₁₅ copolymer chains with longer PEG chain than PCL chain. The estimated CMC value of mPEG₄₅-b-PCL₁₅ by the fluorescence method was smaller (2.5 µg/mL) than the estimated values by UV-vis and the DLS methods whereas, the estimated CMC of mPEG₄₅-b-PCL₂₅ by fluorescence method was very close to the estimated value by DLS. This is due to the Đ of mPEG₄₅-b-PCL₁₅ which was higher than the Đ of mPEG₄₅-b-PCL₂₅. This means that mPEG₄₅-b-PCL₁₅ contains more of the mixture of short and long chains. This gives an entropic advantage for the self-organising process. It was found that Đ influences the self-assembly of di-block copolymer and the previous theoretical studies of micelle solution indicated that CMC decreases with polydispersity. Based on these studies, the long chains of mPEG₄₅-b-PCL₁₅ form micelles at lower concentration (2.5 µg/mL, were only detected by fluorescence method), whereas the shorter chains remain in the solution until a higher concentration is reached (10 µg/mL, detected by DLS and UV-vis). Since fluorescence is a more sensitive tool than UV-vis and its measurements are more accurate, micelles that were formed by long chains was detected at concentration 2.5 µg/mL. The Transmission Electron Microscopy (TEM) of mPEG₄₅-b-PCL₁₅ provides strong evidence for the dispersity micelles (**Figure 2.18, a**) where very big micelles, around 114 nm were formed by long chains whereas, small micelles as a majority were formed

by short micelles. The TEM of mPEG₄₅-b-PCL₂₅ agree with the fluorescence and the DLS results; they confirmed that the formed micelles are less dispersive (**Figure 2.18, b**).

On close inspection, it was noticed that the average size of mPEG₄₅-b-PCL₁₅ was bigger than mPEG₄₅-b-PCL₂₅ above the CMC. These unlikely, as the longer diblocks should result in bigger size. This result is due to the high poly dispersity of mPEG₄₅-b-PCL₁₅ which is broader than mPEG₄₅-b-PCL₂₅ (DLS is also sensitive to large particles). Therefore, TEM was used to explore the morphology of the diblock copolymer micelles, where it was noticed that mPEG₄₅-b-PCL₁₅ has a range of different sized micelles. Although mPEG₄₅-b-PCL₂₅ also has a range of sizes, and the range of sizes appears less (**Figures 2.18**).

For the preparation of TEM samples, firstly, mPEG₄₅-b-PCL₂₅ and mPEG₄₅-b-PCL₁₅ diblock copolymers micelles (30 µg/mL) were prepared by taking 0.6 ml from 1 mg/mL stock solution which was then diluted with 1.4 ml distilled water. After that, the micelles solution was sonicated and one drop from this solution was placed on the TEM grids. Finally, the grids were allowed to dry overnight inside the fume-hood before taking the TEM images.

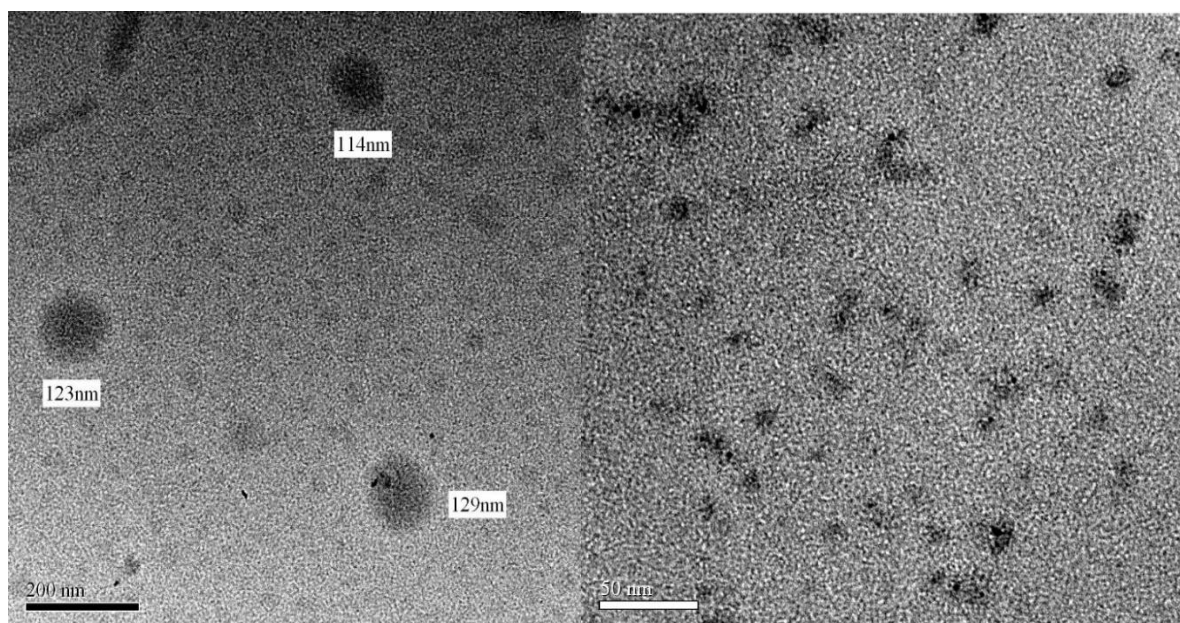


Figure 2.18: the TEM image **a**, for mPEG₄₅-b-PCL₁₅ and **b**, for mPEG₄₅-b-PCL₂₅ diblock copolymers micelles at concentration 30 µg/mL.

The CMCs' for four diblock copolymers, mPEG₄₅-b-PCL₁₅, mPEG₄₅-b-PCL₂₅, mPEG₄₅-b-PCL₃₅ and mPEG₄₅-b-PCL₄₅ were 10 μg/mL, 1 μg/mL, 0.5 μg/mL and 0.3 μg/mL respectively (see **Table 2.3**). At low concentration, the polymers exist as unimers, but their size suddenly increases once the CMC is reached and micelles form in the solution. The balance between hydrophobicity and hydrophilicity in the diblock copolymers is an important factor with respect to aggregation. The longer the hydrophobic block, leads to micelle formation at lower concentration (**Figure 2.19**). The data for all CMC measurements is shown in **Table 2.3**.

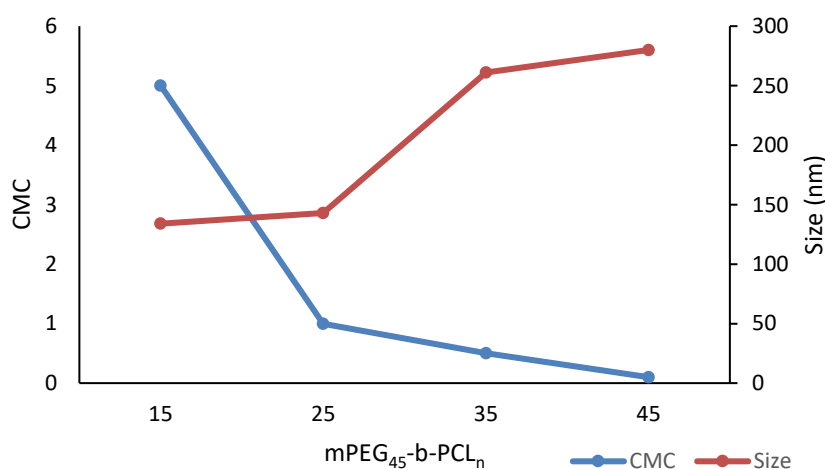
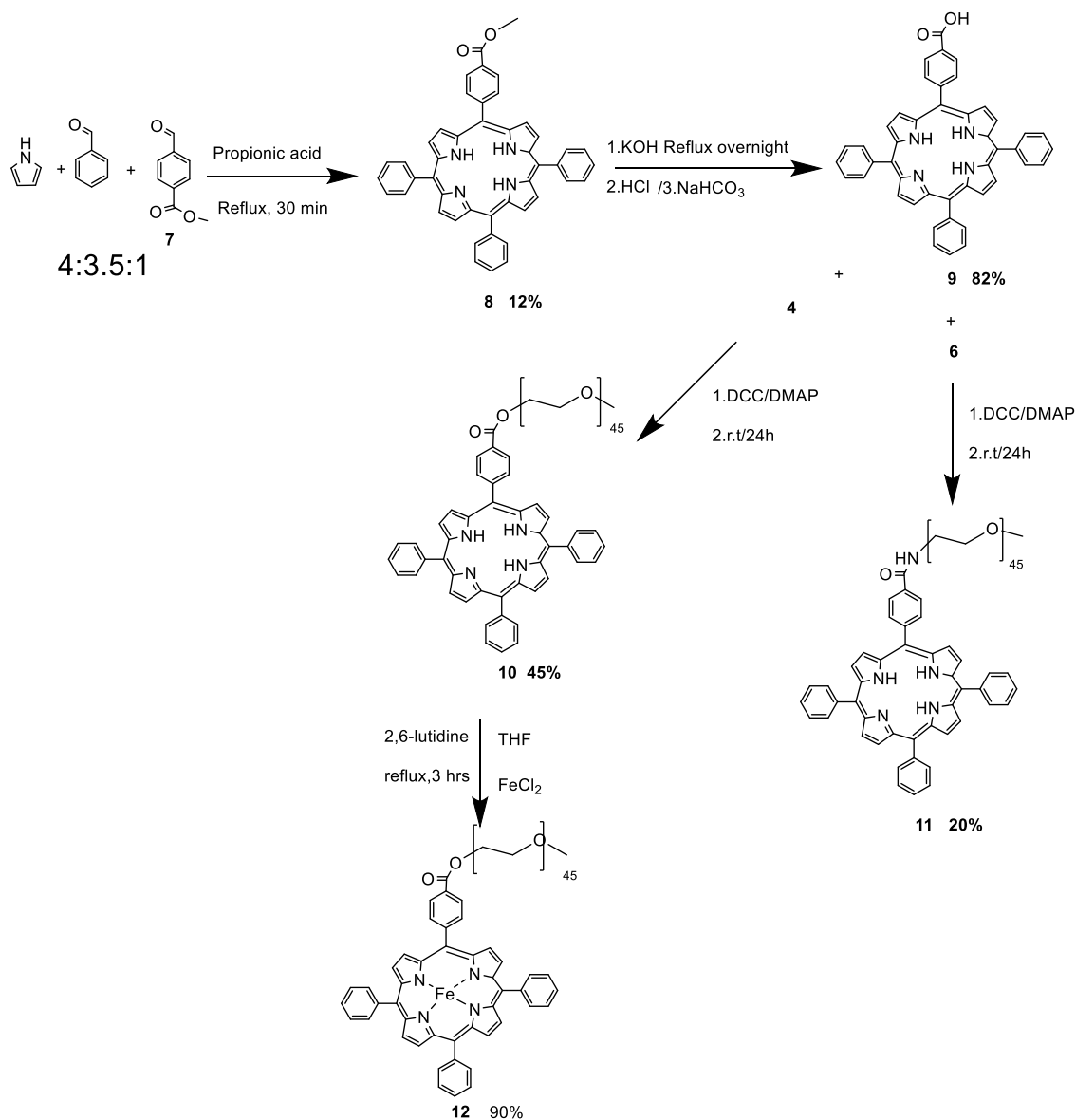
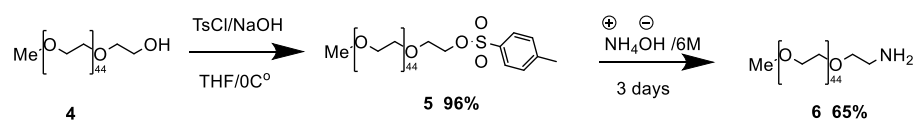


Figure 2.19: CMC and size of mPEG₄₅-PCL_n for different degree of polymerisation of PCL (n=15,25,35,45).

2.3.1 Synthesis of methoxypolyethylene glycol-4-(10, 15, 20-triphenyl porphyrin-5-yl)-benzoic acid ester 5 (donor unit)

TPP **3**, was chosen as the donor unit for our LH system. However, TPP **3** is a very hydrophobic compound and it tends to aggregate, which means it can quench the emitted energy instead of transferring it to an acceptor. Therefore, good separation between the molecules is an essential requirement to harness the transferred energy. To achieve this, the aggregation of porphyrin should be prevented. This can be done by keeping the porphyrin molecules at the edge of micelles and away from each other. The main proposal was to tether the porphyrin to PEG with a diblock polymer to form a mixed micelle. To achieve this, a porphyrin was needed that could

be functionalised. For example, a porphyrin with a carboxylic acid that could be reacted with the hydroxyl group on the end of mPEG to give PEG-porphyrin ester **10** (**scheme 2.3**). The reaction involved three steps. Firstly, 5-(4-carbomethoxyphenyl)-10, 15, 20-triphenylporphyrin (porphyrin-COOCH₃ **8**) was prepared from pyrrole **1**, benzaldehyde² and methyl 4-formyl benzoate **7** at ratios of 4: 3.5 :1, respectively. The starting materials were held under reflux in propionic acid, which served as solvent and catalyst in this reaction.



Scheme 2.3. The synthetic steps of ester PEG-porphyrin (compound **10**), amide PEG-porphyrin (compound **11**) and PEG-Feporphyrin iron (compound **12**).

The reactants involved in the preparation of porphyrin-COOCH₃ **8** include those in TPP.

Therefore, there was a certain amount of TPP **3** in the final product, which was equivalent to the amount of porphyrin-COOCH₃ **8**. Furthermore, the addition of methyl 4-formyl benzoate **7** in the reaction did not only form the mono-carbomethoxy porphyrin **8**, but it also created a small amount of the di-, tri-, and tetra- carbomethoxy porphyrin (indicated by TLC), which

complicated the purification steps. The desired product **8** was obtained by subjecting the reaction mixture to the following purification process. Firstly, two-thirds of the propionic acid was removed by distillation, and then the crude product was precipitated using methanol. The solid was then further purified using column chromatography, eluting with 10% petroleum ether in DCM. TPP **3** and porphyrin-COOCH₃ **8** eluted together, but they were successfully separated from the rest of the impurities. Another column was used to separate the two porphyrins using the same eluent to give a 6% yield of pure, purple solid porphyrin **8**.

¹H NMR spectroscopy confirmed the structure of porphyrin-COOH₃ **8** (**Figure 2.20**), showing a resonance at 4.14 ppm, which corresponded to the protons of the methyl ester; meanwhile, a shielded resonance at -2.75 ppm indicated amine hydrogens (H₁) inside the porphyrin ring. The pyrrole C-H hydrogen resonance of the porphyrin ring were observed between 8.82 and 8.88 ppm. The pyrrole hydrogens' signal appeared at 8.88-8.82 ppm as a multiplet due to the proximal phenyl group (H₃) and the pyrrole hydrogens (H₂). The de-shielded protons located at 8.47 ppm and 8.34 ppm are doublet of doublets and correspond to the phenyl hydrogens of substituted phenyl - H₄ and H₅ respectively. The resonance at 8.24 ppm is assigned to the hydrogens of the unsubstituted phenyl units at the ortho position (H₆), which appear as a doublet of doublet. The peak that appears at 7.80-7.76 ppm is a multiplet; it corresponds to hydrogens in the meta and para positions in the unsubstituted rings. Mass spectra showed a molecular ion at 673 m/z, and the UV-vis had the solet peak at 418 nm with four Q bands at 516, 549, 590 and 647 nm.

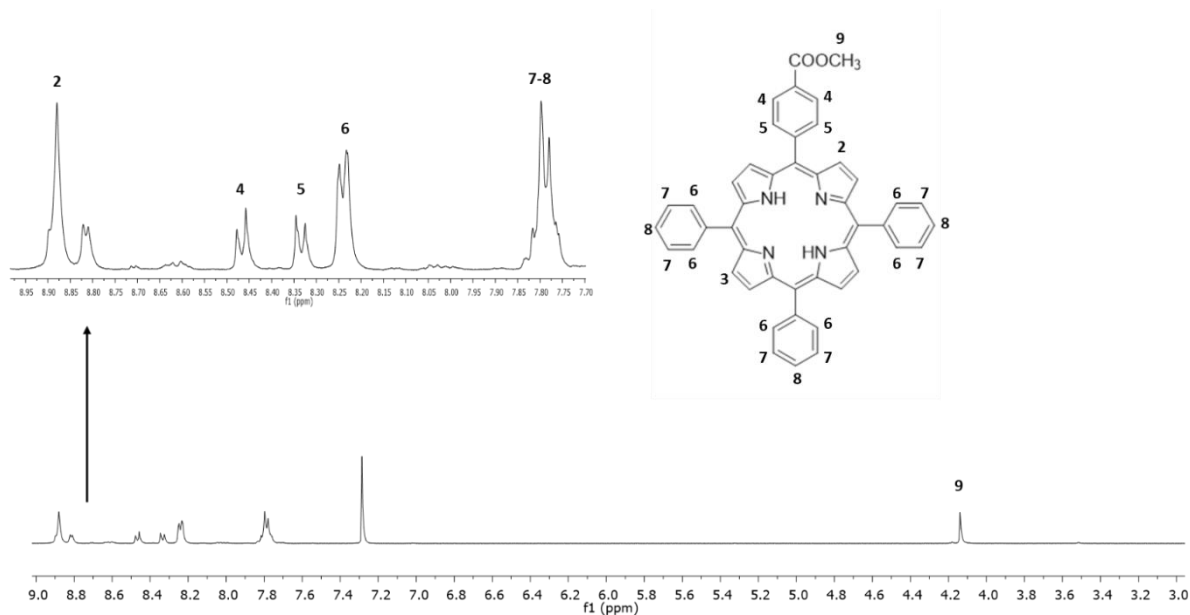


Figure 2.20: represents the ¹H NMR spectra for porphyrin **8** (porphyrin-COOCH₃) in CDCl₃ at room temperature. The arrow indicates the peaks that correspond to pyrrole and phenyl (C-H) hydrogens of **8**.

The second step was the conversion of the ester group in porphyrin **8** to the carboxyl group. The resultant porphyrin **8** was dissolved in THF; then potassium hydroxide solution was added into the solution and it was held under reflux overnight. The ester group was subsequently hydrolysed under the basic environment to give carboxylate **9**. The THF was removed by azeotropic distillation, and a solution of hydrochloric acid (HCl) was added until pH 2 was achieved and the mixture turned from purple to green. Mass spectra confirmed the molecular mass of carboxylate **9** (659 g/mol). ¹H NMR indicated the shielded porphyrin N-H resonance at -2.76 ppm (**Figure 2.21**). The resonances at 8.89-8.83 ppm corresponded to pyrrole hydrogens on the edge of the porphyrin ring, which splits to yield a multiplets. The resonances at 7.82-7.76 ppm, 8.25 ppm, 8.37 ppm, 8.52 ppm correspond to the phenyl hydrogens; their pattern of splitting was similar to the phenyl protons in **8**. However, the resonance of the ester group in porphyrin **8** is no longer visible, which proves the conversion of porphyrin **8** to porphyrin **9** (**Figure 2.21**).

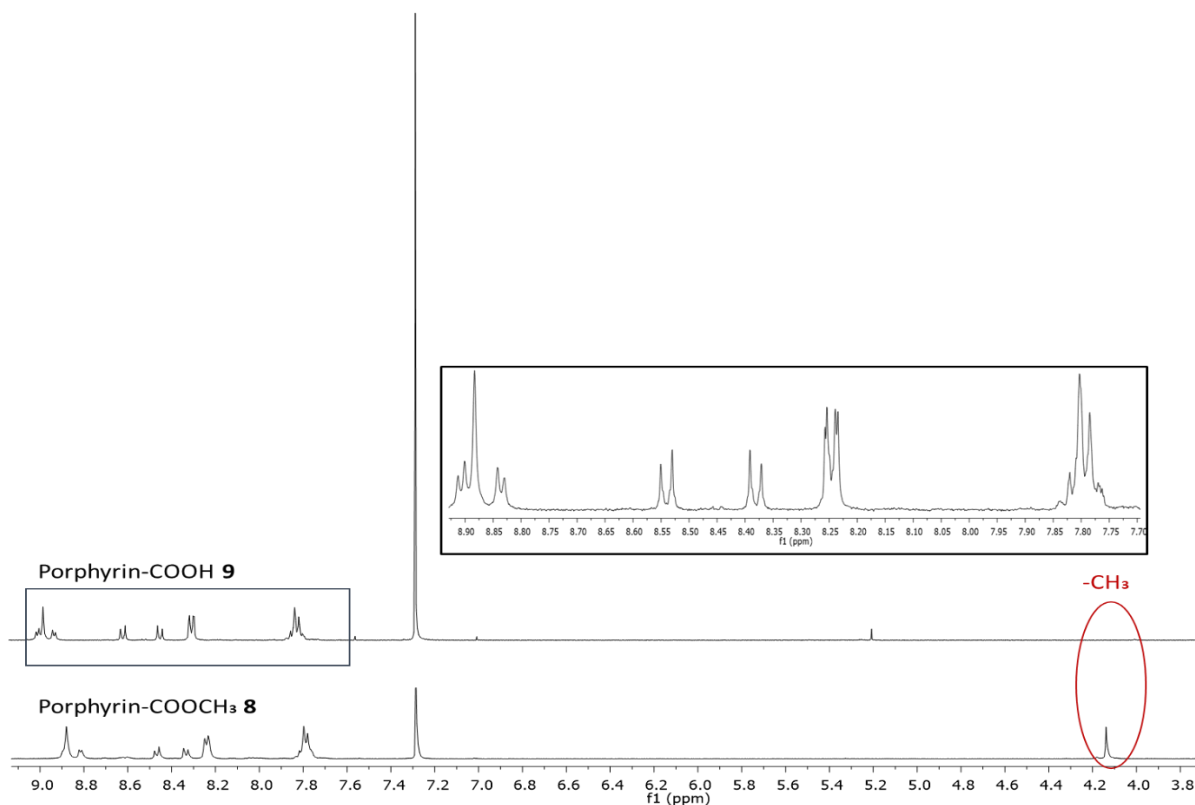


Figure 2.21: represents the ^1H NMR spectra for porphyrin **8** (porphyrin- COOCH_3) and **9** (porphyrin- COOH) in CDCl_3 at room temperature. The blue framed enlargement emphasises the peaks that correspond to the pyrrole and phenyl (C-H) hydrogens of porphyrin- COOH **9**. The red circle indicates the disappearance of methoxy protons in **9**.

The next step involved coupling the porphyrin- COOH **9** to the mPEG **4**. However, the acid on porphyrin- COOH **9** is not sufficiently reactive to react with the hydroxyl group in mPEG **4**. Therefore, it was activated by using DCC (dicyclohexylcarbodiimide), which formed an intermediate carboxylic acid anhydride that reacted with the OH on the mPEG **4**. The addition of 4-Dimethylaminopyridine (DMAP) 5 mol-% was essential for esters to form efficiently. A side product of dicyclohexylurea (DHU) also formed and was removed by filtration. After the reaction, the DCM was removed completely, and the residual dark purple material was dissolved in methanol. since porphyrin- COOH **9** does not dissolve in methanol, it could be collected by filtration. The methanol was removed and the product was dissolved in a minimal amount of DCM and loaded onto a pre-prepared Bio-Bead size-exclusion column. It was eluted with DCM to give a dark red oil of pure PEG-porphyrin **10** in 45% yield (**Scheme 2.3**). Its structure was confirmed by ^1H NMR (**Figure 2.22**). The porphyrin resonances were observed

at -2.76, 8.87, 8.81, 8.49, 8.29, 8.02, 7.79 ppm, which corresponded to H₁, H₂, H₃, H₄, H₅, H₆, H₇ and H₈, respectively. A strong resonance of mPEG was observed at $\delta = 3.41$ ppm, corresponding to CH_3 and 3.65 ppm for $\text{OCH}_2\text{CH}_2\text{O}$.

The PEG-porphyrin polymer **10** has both hydrophilic and hydrophobic parts, and the potential to self-assemble into micelles. Assembly was implicated by the presence of very broad resonances for PEG-porphyrin **10** in the ¹H NMR spectrum, in which a sample was analyzed in D₂O. This also confirmed that porphyrin had been attached to the mPEG successfully, appearing as strong resonance on the spectra. The hydrogen in porphyrin was observed as weak resonance in the ¹H NMR spectrum; this is attributed to the formation of mPEG-porphyrin **10** micelles in water (D₂O) solution. The porphyrin is within the hydrophobic core of the micelles, where there is no D₂O, meaning only a few porphyrins were fully solvated. In contrast, the mPEG segment forming the shell of the micelles is fully solvated by D₂O to give a strong signal. Using RI and UV detectors, GPC also was carried out for the PEG-porphyrin polymers **10**. The mPEG was detected by the RI detector, and the porphyrin was detected by UV at 420 nm. Both signals were superimposable and sharp, providing strong evidence for the formation of PEG-porphyrin polymers **10**.

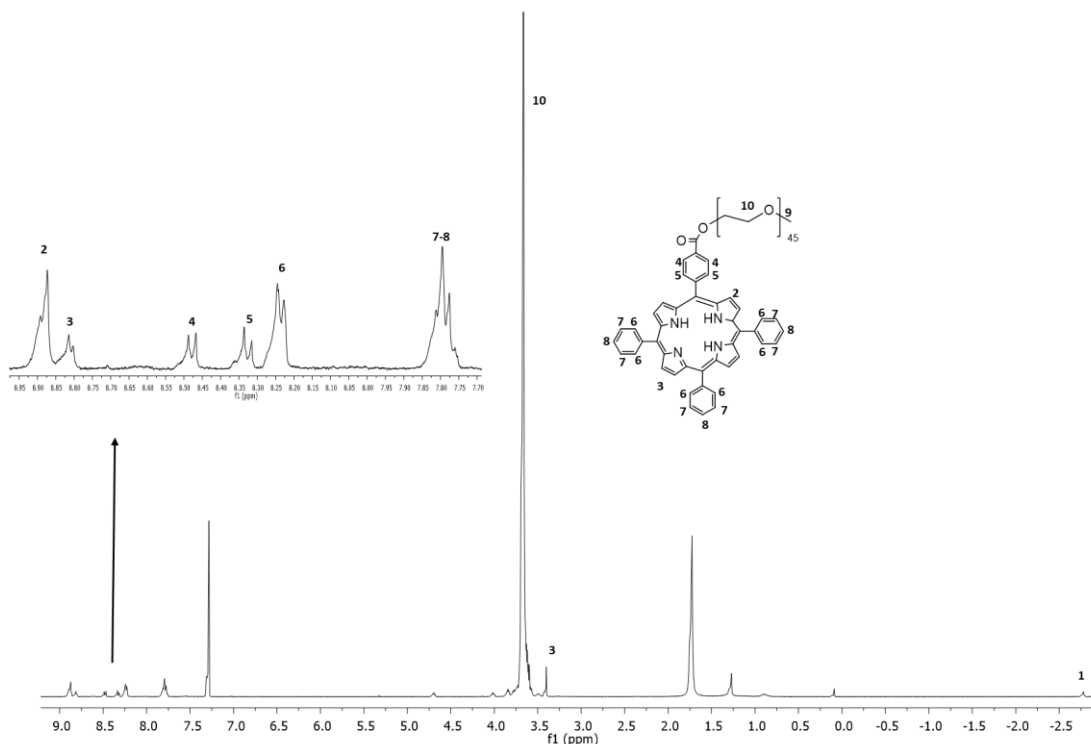


Figure 2.22: represents the ^1H NMR of PEG-porphyrin ester **10** in CDCl_3 at room temperature. The arrow refers to the peaks that correspond to pyrrole and phenyl (C-H) hydrogens of **10**.

Another way to attach the porphyrin to the mPEG is to convert the hydroxyl group of mPEG into an amine functional group, which is more reactive and generates a more stable amide group. A nucleophilic substitution cannot occur on the alcohol, as it is poor leaving group; instead, the hydroxyl group was converted into tosyl. A stirred solution of mPEG in THF was cooled to 0°C , and then a sodium hydroxide solution was added. This was followed by the addition of tosyl chloride in THF under N_2 . The mixture was allowed to warm to room temperature and then stirred for an hour. To remove the unreacted tosyl chloride, the crude product was dissolved in DCM and washed with aqueous solution of sodium hydroxide. A pure, colourless liquid was obtained, and the structure of tosylate **2** was confirmed by ^1H -NMR spectroscopy and GPC analysis.

The tosylate ester **5** was reacted with an excess of ammonia (6 M) to give mPEG-NH₂ **6**; a ^1H and ^{13}C NMR spectrometer was used to confirm its structure. From the ^1H NMR spectrum of the mPEG, mPEG-Tosyl and mPEG-NH₂ samples (**Figure 2.23**), two strong peaks were

detected at 3.41 ppm for methoxy hydrogens (-OCH₃) and 3.65 ppm for methylene in ethylene glycol (-O-CH₂-CH₂-O-). However, the presence of a tosyl functional group in mPEG-Tosyl **2** led to the appearance of a de-shielded doublet and a triplet peak at 7.70 ppm and 7.27 ppm respectively; these correspond to the phenyl hydrogens in tosyl. Additionally, peak was observed at 3.60 ppm, which corresponded to the methylene hydrogens (-CH₂) adjacent to polyethylene glycol (-O-CH₂-CH₂-). Whereas, the -CH₂ adjacent to tosyl (-O-CH₂-CH₂-O-SO₂-), appeared as peak with triplet splitting at 4.06 ppm. The singlet peak at 2.36 ppm corresponded to the methyl hydrogen (-CH₃) that was attached to phenyl in mPEG-Tosyl **2**. The conversion of mPEG-Tosyl **2** to mPEG-NH₂ **3** was accompanied by some changes in the ¹H-NMR spectrum. The peaks corresponding to the phenyl and methyl moieties of the tosyl function group disappeared in a mPEG-NH₂ **3** ¹H-NMR spectrum. Additionally, the peak corresponding to methylene (-O-CH₂-CH₂-NH₂) adjacent to the amine functional group was chemically shifted to 2.79 ppm.

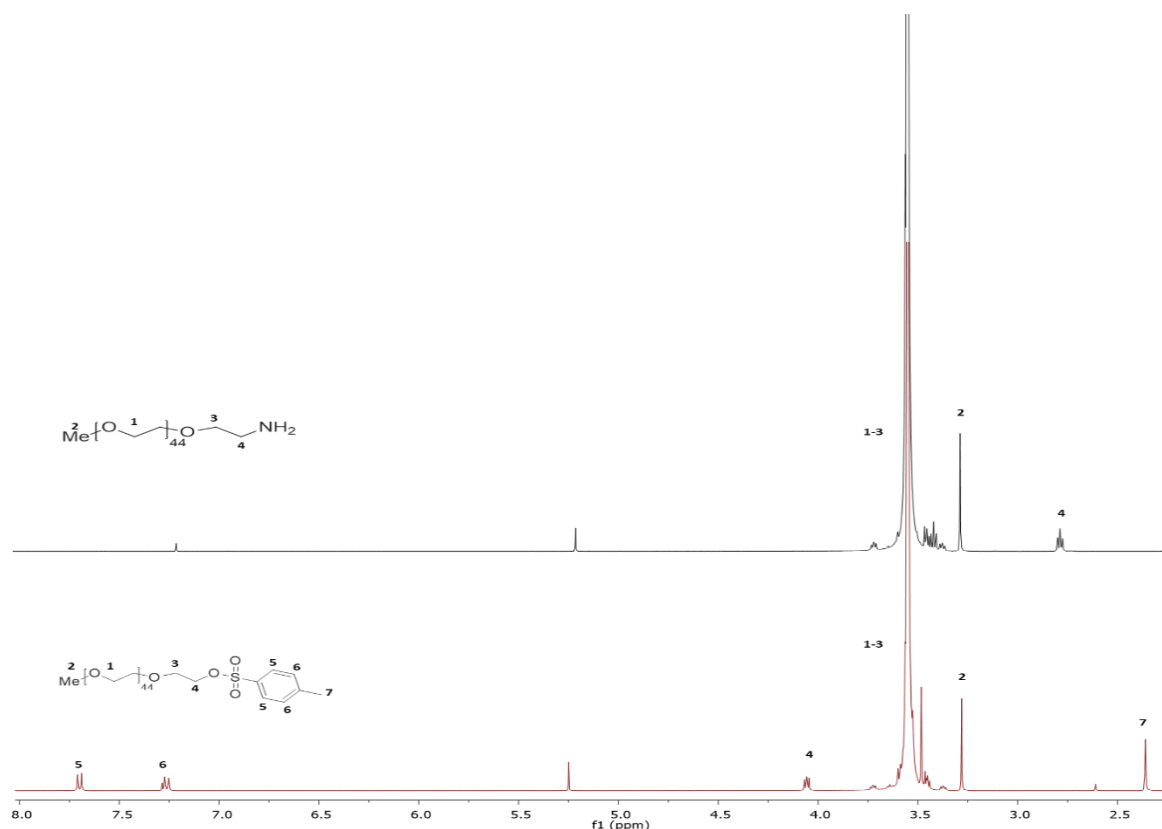


Figure 2.23: ¹H-NMR result of mPEG-Tosyl **5** and mPEG-NH₂ **6**.

The reaction and purification steps that were used to produce an ester PEG-porphyrin polymer **10** were repeated in this step to obtain methoxypolyethylene glycol-4-(10, 15, 20-triphenylporphyrin-5-yl)-benzoic amide (amide PEG-porphyrin) or porphyrin **11**. However, PEG-NH₂ **3** reacted instead with porphyrin **8**, to form amide PEG-porphyrin (**11**). The dark purple residue was dissolved in a minimum amount of DCM and loaded onto a pre-prepared Bio-Bead size-exclusion column and eluted with DCM to give a red oil of PEG-porphyrin **11** in 20% yield, **Scheme 2.3**. The ¹H NMR spectrum showed resonances for the porphyrin ring at -2.76 ppm, which corresponded to the N-H pyrrole hydrogens inside the porphyrin ring. Resonances at 8.87- 8.81 ppm, corresponded to C-H pyrrole hydrogens and resonances at 8.29- 7.79 ppm corresponded to the phenyl hydrogens. A strong resonance for the CH₃ protons of mPEG was observed at δ= 3.41 ppm, with the CH₂ protons resonating at 3.65 ppm (**Figure 2.24**). However, the resonances for porphyrin hydrogens were broad. This was due to a few unreacted polymers, indicating that only some of the porphyrins had reacted with the amine on the mPEG-NH₂ **6**. The unreacted porphyrin could be removed using Bio-Beads, but as the molecular weights for both mPEG and PEG-porphyrin polymer **11** were close, it was difficult to separate them using the Bio-Bead size-exclusion column. As a result, the yield of PEG-porphyrin amide polymer **11** (20%) was lower than PEG-porphyrin ester polymer **10** (45%). The ¹H-NMR spectrum of PEG-porphyrin polymer **11** was also obtained in D₂O, where the resonances for porphyrin were no longer visible, confirming they were inside the unsolvated core region. Strong evidence for the formation of PEG-porphyrin amide polymer **11** was provided by GPC, as the peaks were observed from the RI and UV detectors were superimposable and sharp.

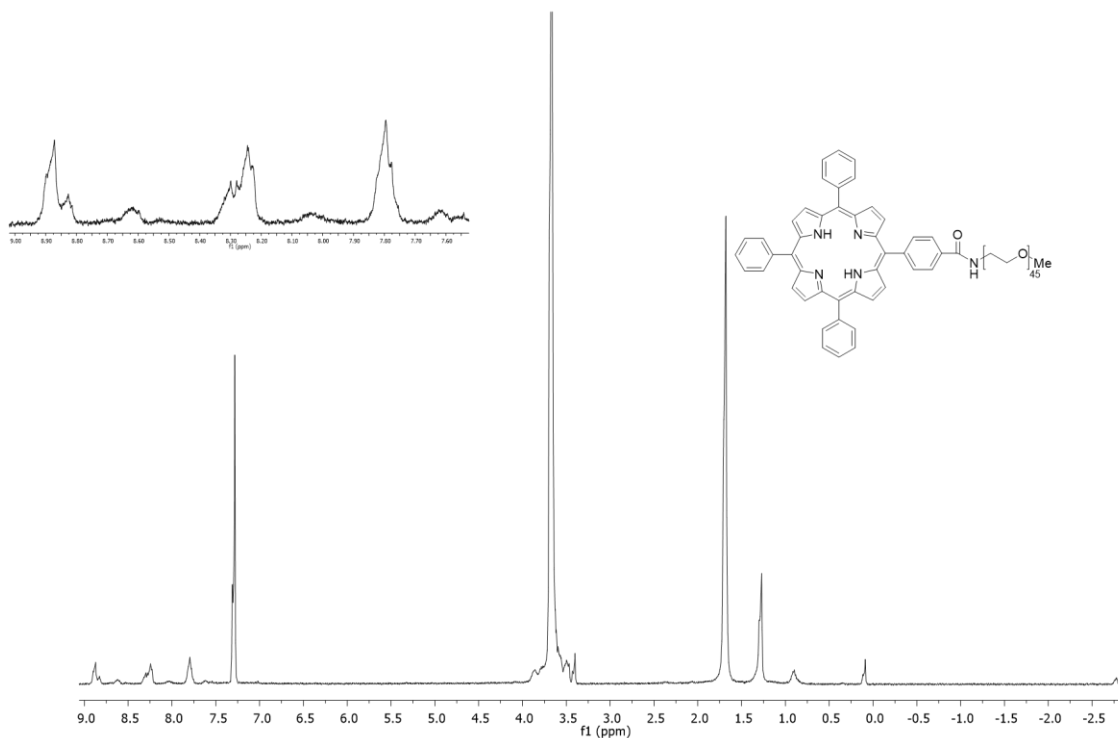


Figure 2.24: $^1\text{H-NMR}$ spectrum of 1 PEG-porphyrin amide **11**. The arrow indicates the resonances corresponding to pyrrole and phenyl (C-H) hydrogens of **11**.

2.3.2 The behaviour of PEG-porphyrin **10** in aqueous solution (CAC):

Attaching the hydrophilic polymer to hydrophobic porphyrin endowed the compound with amphiphilic properties; hence, a small amount of PEG-porphyrin **10** (low concentration) was added to an aqueous solution. This led to the mPEG component coiling around the porphyrin, protecting it from water (state one and two of **Figure 2.25**). These behaviour of porphyrin arrays in water were investigated using UV-vis and fluoresce spectroscopy and DLS. There was an expectation that the intensity of the fluorescence of porphyrin would increase as the concentration rises. However, fluorescence could also drop as the concentration of PEG-porphyrin **10** in solution increased. This is due to the increase in collisions at higher concentrations (state 3, **Figure 2.25**). There was also the possibility that the PEG-porphyrin **10** would aggregate into micelles (homo-aggregate). Had this occurred, there would have been a reduction in the fluorescence emission intensity (state 3' of **Figure 2.25**).

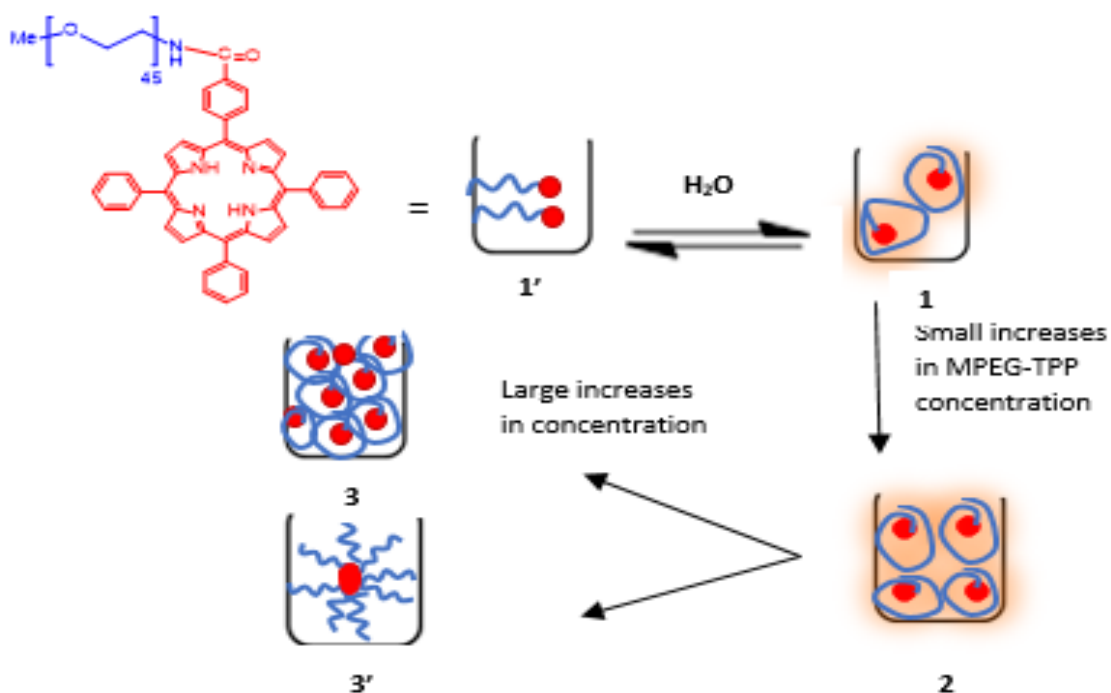


Figure 2.25: prediction of self-assembly of PEG-porphyrin polymers in aqueous solution.

To investigate the above predictions, fluorescence measurements were performed for different concentrations of PEG-porphyrin **10**, ranging from 1.56 $\mu\text{g/mL}$ to 200 $\mu\text{g/mL}$ in water. The intensity of fluorescence increased as the concentration of PEG-porphyrin **10** increased but started dropping as the concentration exceeded 12.5 $\mu\text{g/mL}$ (**Figure 2.26**).

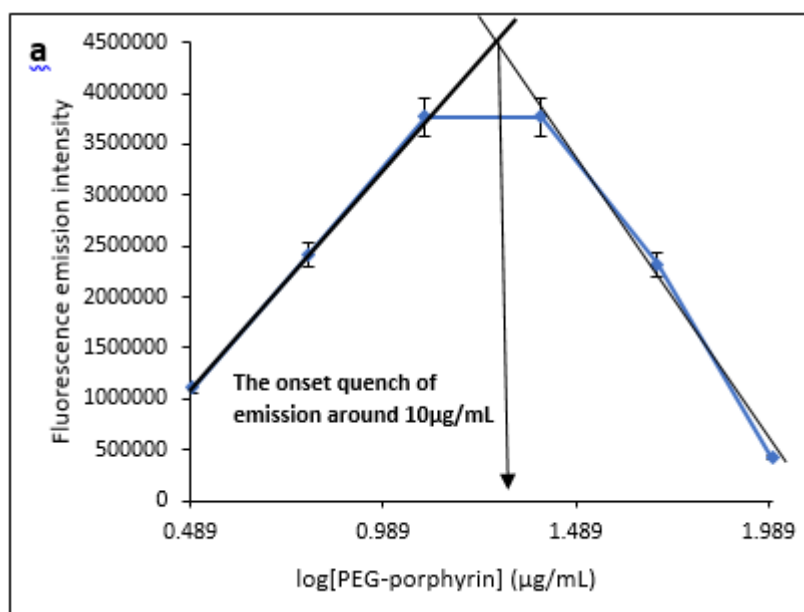


Figure 2.26: plot of the fluorescence intensity as function of the logarithm concentration.

The question that arises from this phenomenon is does the emission intensity drop due to the high concentration, or it is due to micelle formation. To answer this question, the size of any PEG-porphyrin **10** aggregates at different concentrations was measured by DLS. There was no evidence for any large aggregates at concentrations between 2 $\mu\text{g/mL}$ and 10 $\mu\text{g/mL}$. However, when the concentration reached 16 $\mu\text{g/mL}$, aggregates of ~ 20 nm were visible (**Figure 2.27.a**).

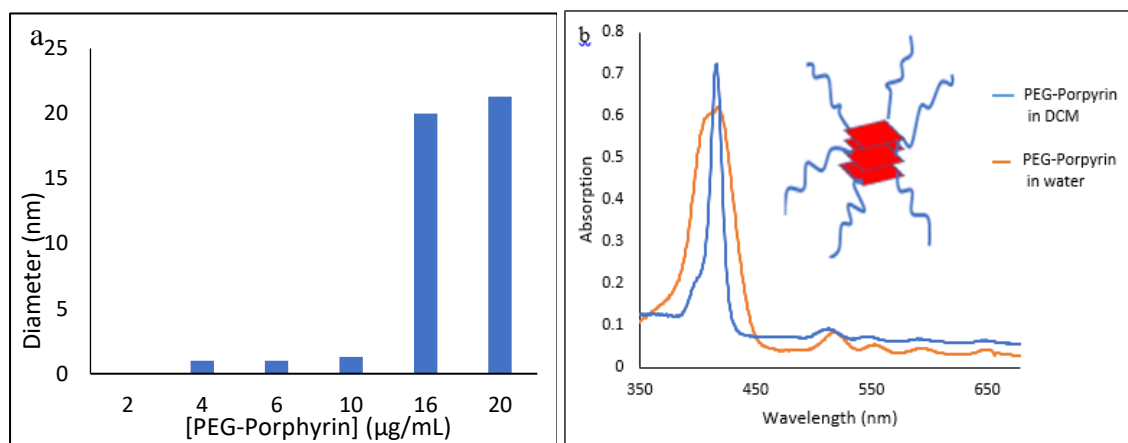


Figure 2.27: a, represent the DLS measurements of different concentration of PEG-porphyrin b, the absorption of PEG-porphyrin in water (red line) and DCM (blue line) and the figure on right side of UVvis spectra demonstrates the H-aggregation of PEG-porphyrin.

Porphyrins can aggregate to form oligomers or a higher aggregation order through H- or J- interaction (**Figure 2.28**), which can be detected using UV-vis spectroscopy.¹²⁰

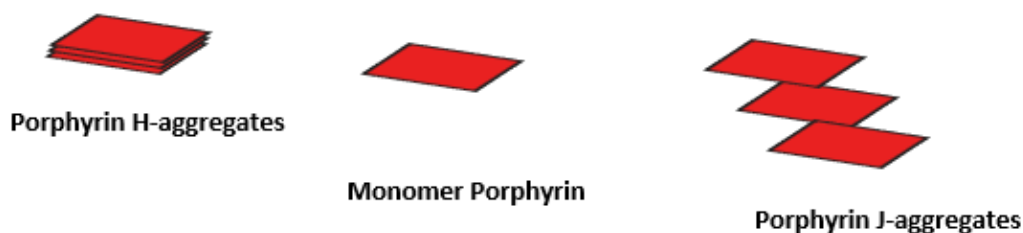


Figure 2.28: H- and J- aggregation of porphyrin molecules. Monomeric porphyrin absorbs energy at a wavelength of 418.5 nm. If it forms J- or H-aggregates, the absorption band broadens and shifts to the red (lower energy) and blue (higher energy), respectively.

The UV-vis spectra of PEG-porphyrin (4 $\mu\text{g/mL}$) in DCM show a single narrow peak at 418.5 nm (**Figure 2.27.b**). However, a mixture of monomeric and H-aggregated porphyrin is observed in an aqueous solution of polymeric micelles (at concentrations above the CMC). Scanning electron microscopy (SEM) and TEM images provided further evidence for high concentration PEG-porphyrin to self-assemble into micelles (**Figures 2.29.a and b**).

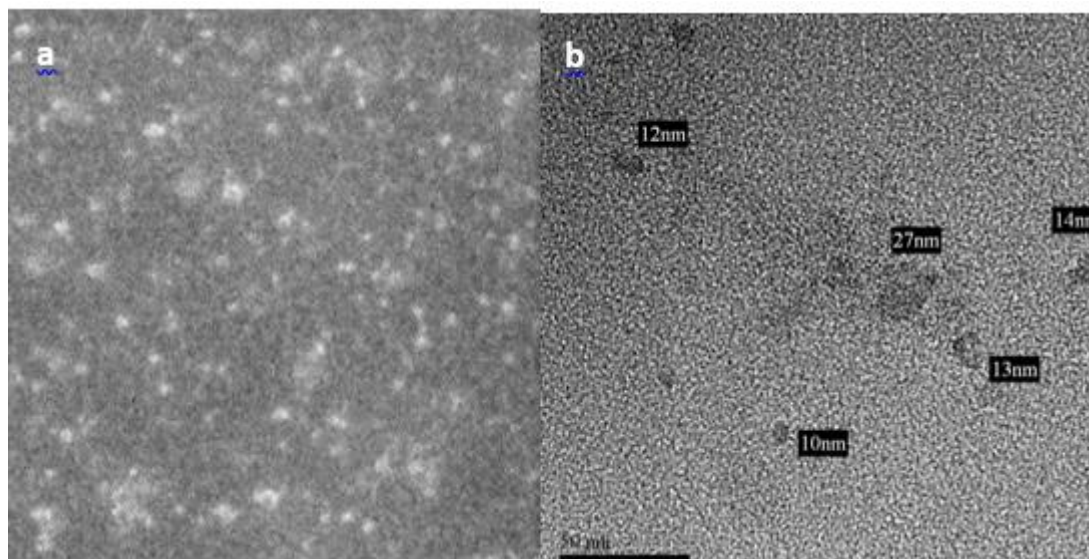


Figure 2.29: **a**, SEM images of high concentration PEG-porphyrin, **b**, TEM images of PEG-porphyrin at high concentration.

2.3.3 Self-assembly of isolated (non-aggregated) porphyrin arrays in mPEG-PCL diblock micelles:

Four diblock copolymers with a fixed length of the mPEG block and different lengths of the Poly (ϵ -caprolactone) block were successfully synthesised by ring opening polymerisation. Their synthetic steps and analysis were discussed at the beginning of this chapter (**section 2.3**). A summary of the characterisation data is shown in **Table 2.3**.

This indicated the strong interaction between porphyrin and polycaprolactone. Although mPEG₄₅-PCL_n diblock copolymer can incorporate porphyrin in core of micelles, large aggregation of porphyrin in the small hydrophobic part of micelle reduces the functionality of the porphyrins, additionally not all added porphyrin will be inserted inside the micelles (poor

loading). PEG is hydrophilic block in mPEG₄₅-PCL_n diblock copolymer and hydrophilic chain in PEG-Porphyrin, which makes it an amphiphilic compound. The amphiphilicity of PEG-porphyrin makes it to adopt a similar behaviour of small molecular surfactant. The mixture of two amphiphilic systems in aqueous solution leads the formation of mixed micelle. The formation of mixed micelle is induced by the strong interaction between porphyrin and polycaprolactone in mPEG-PCL micelles, this was observed when TPP **3** was used previously as prob to determine the CMC and the hydrophobicity of porphyrin was enough high to significantly lower the CMC of mPEG₄₅-PCL₂₅ diblock copolymer. This means that porphyrin in =PEG-porphyrin is rather to be inserted inside micelle than remain in water phase. In order to obtain isolated porphyrins within micelles, the mixed micelle should be prepared at concentration of PEG-porphyrin below its aggregation concentration and at the concentration of mPEG₄₅-PCL_n diblock copolymer above its CMC.

The proposed structure of the mixed micelle **13** has the PEG-porphyrin polymer **10** in the external mPEG layer. Due to the very hydrophobic nature of porphyrin, the proposed structure has the porphyrins ends away from water and pointing towards the hydrophobic PCL core as shown in **Figure 2.30**. The structure has a well-organised array of porphyrins surrounding the core of the micelle. In this respect, it resembles natural light harvesting systems.

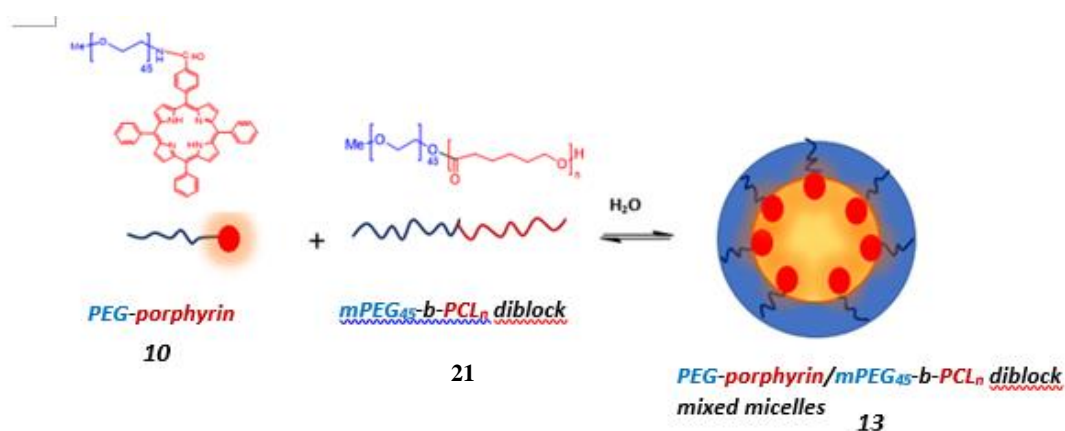


Figure 2.30: schematic illustration of the formation of PEG-porphyrin /mPEG-PCL mixed micelles **13**.

To verify the self-assembly of PEG-porphyrin **10** arrays in the presence of mPEG₄₅-b-PCL_{n **21**, the micelles were studied using fluorescence, UV-vis and DLS; the results were compared against the PEG-porphyrin **10** results. The mixture of mPEG-PCL diblock copolymer **21** and PEG-porphyrin **10** micelles in aqueous solution showed a higher fluorescence intensity and stronger UV absorption (**Figures 2.31 a and b**). This is due to the local environment of the porphyrin within the mPEG₄₅-b-PCL_{n **21** micelles.}}

When the PEG-porphyrin **10** is incorporated into the micelles, the porphyrin is no longer in contact with water and does not aggregate. As such, quenching due to porphyrin-porphyrin interactions is no longer visible. At higher ratios of PEG-porphyrin **10** (to mPEG-PCL diblock copolymer **21**) some quenching can be seen. Therefore, there is an optimum ratio.

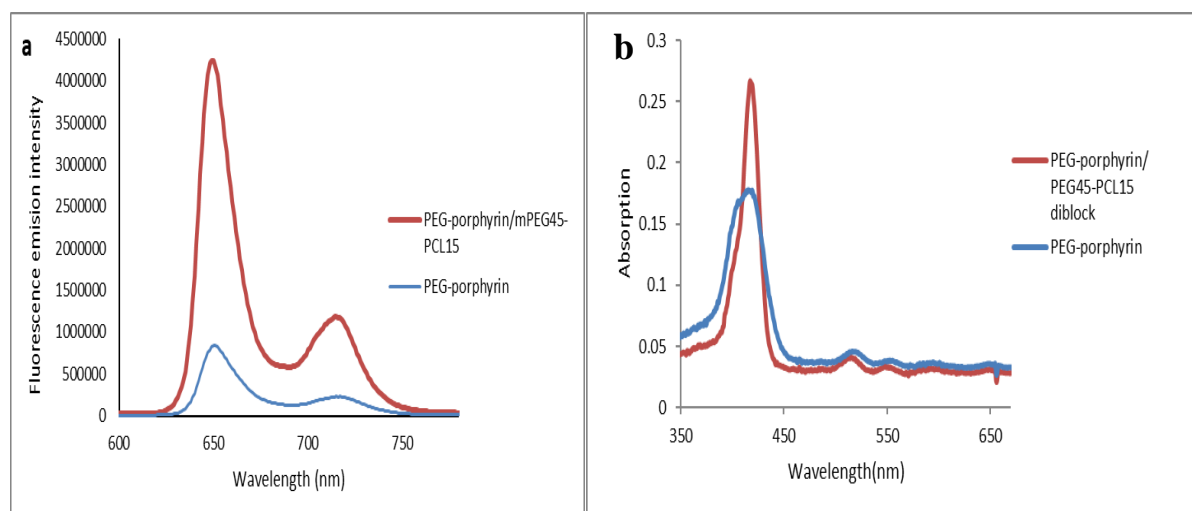
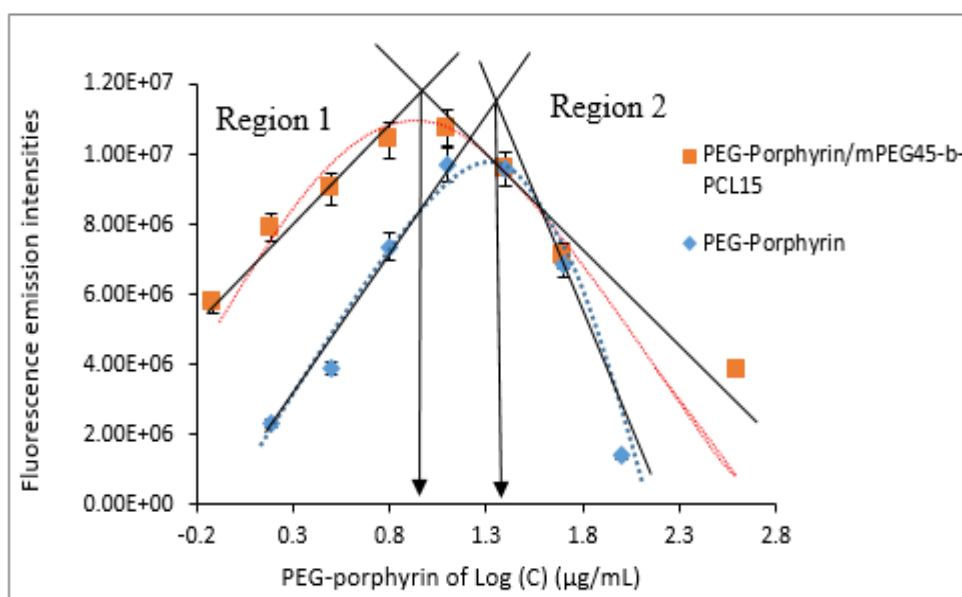


Figure 2.31: the differences in the fluorescence intensity and absorption between fixed concentration free PEG-porphyrin (5 $\mu\text{g/mL}$) in water (Blue line) and incorporated PEG-porphyrin (5 $\mu\text{g/mL}$) in mPEG₄₅-PCL₁₅ diblock micelles, **a**, the fluorescence spectra, **b**, UV-vis spectra.

Spectroscopy studies were carried out on the mixture (PEG-porphyrin/mPEG-b-PCL diblock micelles) by preparing a series of mixed solutions that were made at a fixed concentration of mPEG₄₅-b-PCL_n (almost twice above the CMC value), with different concentrations of PEG-porphyrin **10** ranging from 0.78 $\mu\text{g/mL}$ to 200 $\mu\text{g/mL}$. The final ratio of mPEG₄₅-b-PCL_n to PEG-porphyrin ranged from 1:0.15 to 1:20. The mixed micelles were compared to free PEG-porphyrin with the same concentration (0.78 $\mu\text{g/mL}$ to 200 $\mu\text{g/mL}$) in the presence and absence

of diblock micelles. It was clear from the fluorescence of PEG-porphyrin **10** that the emission intensity in mixed PEG-porphyrin/mPEG-b-PCL diblock micelles initially increased with the increase in the concentration of PEG-porphyrin **10**. The intensity then dropped at a concentration above 6.25 $\mu\text{g/mL}$ and 10 $\mu\text{g/mL}$ for mPEG₄₅-b-PCL₂₅ and mPEG₄₅-b-PCL₁₅, respectively (**Figure 2.32 a and b**). This difference is due to the small interior space of the diblock micelle. However, as mentioned earlier, the decrease in the emission intensity for the free PEG-porphyrin **10** polymer in water appeared between 12.5 $\mu\text{g/mL}$ and 25 $\mu\text{g/mL}$ due to its self- aggregation. The different behaviour of PEG-porphyrin **10** in the mixed micelles strongly proved their assembling inside the micelles (region1 of **Figure 2.32**). However, quenching is also observed at very high concentration of PEG-porphyrin **10** in the mixed micelles **13** (region 2 of **Figure 2.32**). Therefore, the additional PEG-porphyrin polymers either aggregate inside the micelles forming H-type aggregations or exist outside the diblock micelles to form their own aggregates.



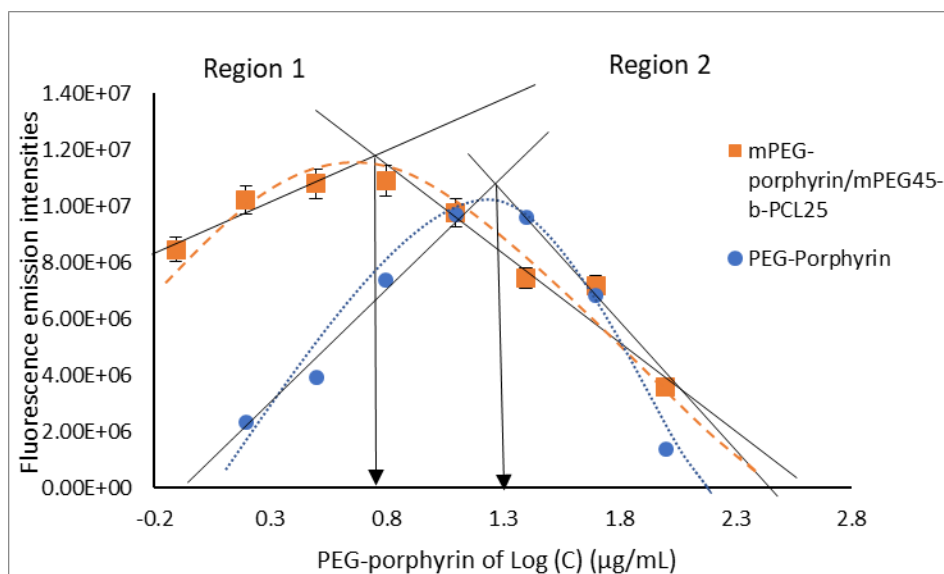


Figure 2.32: the fluorescence emission intensity of the different series of logarithm concentration of PEG-porphyrin **10** in the presence (red line) and without presence diblock micelles (blue line) of **a**, mPEG₄₅-b-PCL₁₅/ PEG-porphyrin mixed micelles, **b**, mPEG₄₅-b-PCL₂₅ / PEG-porphyrin mixed micelles.

If we examine a plot of the data, we observe that the quenching behaviour is very different for the mixed micelles **13**. Quenching especially occurs at lower concentration for mixed micelles **13**; this confirms that PEG-porphyrin **10** does not behave independently and that it does not form its own homo aggregates. As such, the data clearly indicates the formation of the mixed micelle **13** as predicted. Although the emission intensity of PEG-porphyrin/mPEG₄₅-b-PCL₂₅ mixed micelles is reduced at a concentration lower than the PEG-porphyrin/mPEG₄₅-b-PCL₁₅ mixed micelles, the fluorescence emission intensity and absorption are higher. In terms of the PEG-porphyrin to mPEG₄₅-b-PCL_n ratio, the quenching was not observed for the mPEG₄₅-b-PCL₁₅ and mPEG₄₅-b-PCL₂₅ micelles at ratios below 1:0.5 and 1:1, respectively. Therefore, the highest PEG-porphyrin loadings were observed for mPEG₄₅-b-PCL₂₅. UV-vis studies produced data that supported the fluorescence study. UV-Vis spectroscopy is less sensitive than fluorimeter analysis; however, both mPEG₄₅-b-PCL₁₅/PEG-porphyrin and mPEG₄₅-b-PCL₂₅/PEG-porphyrin mixed micelles exhibited deviation from the Beer-Lambert law as there was a clear break at the concentration of PEG-porphyrin around 7 µg/mL and 5 µg/mL, respectively

(Figure 2.33). This deviation in the beer-lambert law occurred due to the aggregation of PEG-porphyrin in micelle.

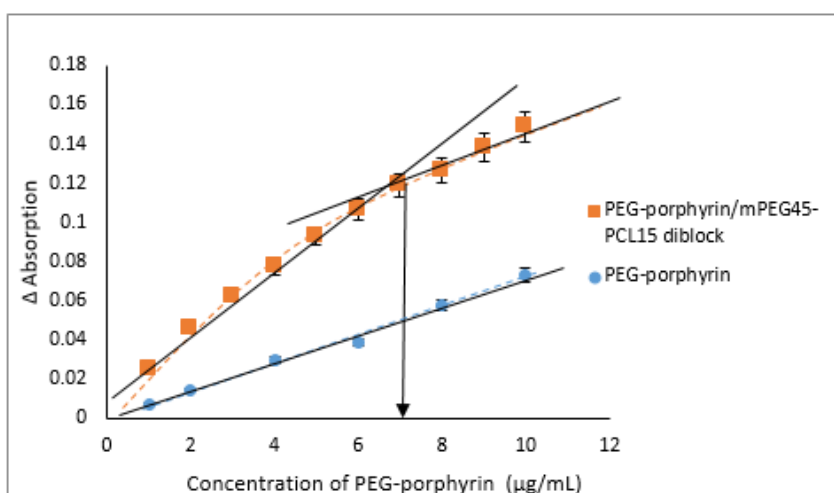
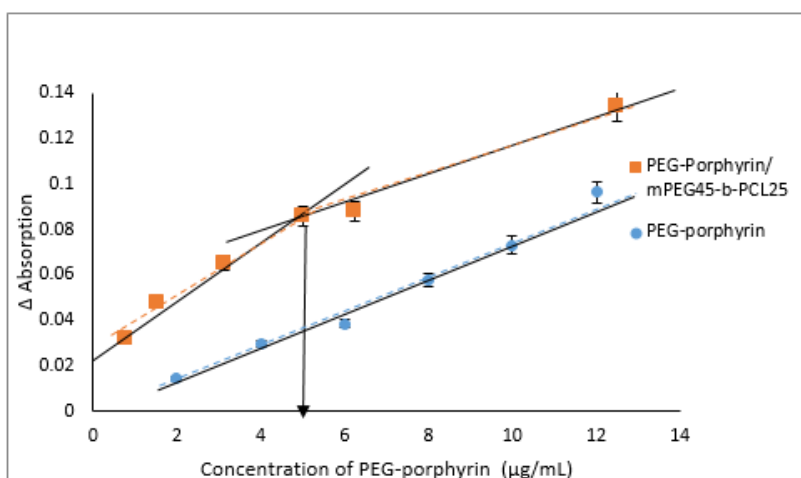


Figure 2.33: the absorption of different series of concentration of PEG-porphyrin in the presence (red line) and in the absence of diblock micelles (blue line) of a, mPEG₄₅-b-PCL₁₅ /PEG-porphyrin mixed micelles, b, mPEG₄₅-b-PCL₂₅ / PEG-porphyrin mixed micelles.

Additionally, the size and shape of the diblock micelles were studied for the mixed micelle systems. mPEG₄₅-b-PCL_n copolymers have been extensively investigated in the literature.^{118,119} They form different morphologies, including micelles, worms and vesicles depending on the length and shape of their hydrophobic block.²⁹ The morphology of the aggregates is mainly determined by the critical packing parameter which can in turn be determined by equation 1.

$$\text{critical packing parameter} = \frac{V}{a_o l_c} \quad \text{equation 1}$$

V is the volume of the hydrocarbon chains, a_o is the optimal area of the hydrophilic group, and l_c is the critical chain length of the hydrophobic group.²⁹ Hence, any change in the hydrophobic length can lead to the formation of non-micelles. In addition, the incorporation of the PEG-porphyrin within mPEG₄₅-b-PCL_n micelle can cause elongation in the hydrophobic chains, resulting in a morphological transition. Therefore, the size of the mixed micelles depends on the length of the PCL segment of the mPEG₄₅-b-PCL_n polymer and the amount of the PEG-porphyrin incorporated within the diblock micelles. DLS measurements were recorded at different ratios of PEG-porphyrin to diblock, ranging from 0:1 to 4:1; the results are revealed in **Figure 2.34**. The size of the mixed micelles is maintained around 60 nm up to a ratio of 1:1; however, it starts to increase at a ratio of 2:1 for the PEG-porphyrin /mPEG₄₅-b-PCL₁₅ mixed micelle. At a 2:1 ratio, it is likely that a phase change from micelle (around 100 nm) to vesicle (above 200 nm) has occurred, due to the influence of PEG-porphyrin on the packing parameter. However, PEG-porphyrin/mPEG₄₅-b-PCL₂₅ mixed micelles demonstrated a different behaviour, with sizes remaining constant as the ratio increases. Since the sizes of all micelles are above 200nm, it is possible they are all vesicles (vesicle sizes range from 100 to 1000 nm).¹⁴⁶

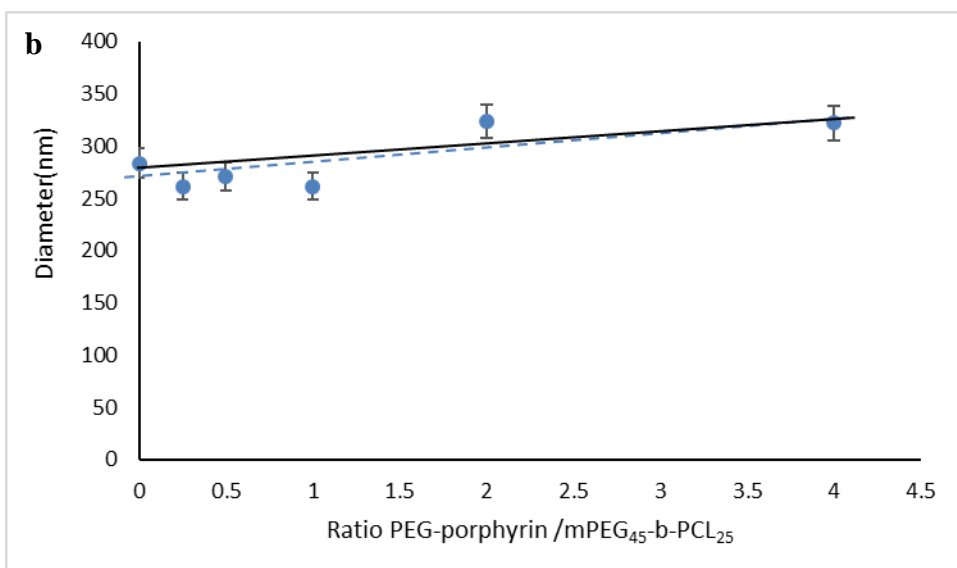
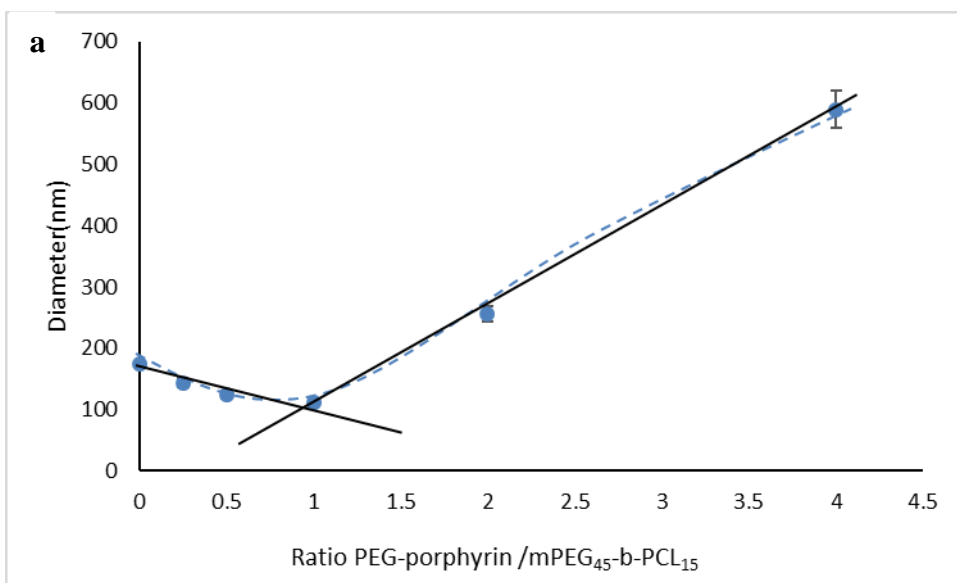


Figure 2.34: the average diameter of the different series of ratios PEG-porphyrin to mPEG-b-PCL diblock polymers in mixed micelles measured by DLS, **a**, PEG-porphyrin/mPEG₄₅-b-PCL₁₅, **b**, PEG-porphyrin/mPEG₄₅-b-PCL₂₅.

TEM has further supported the DLS results which indicate the size of the empty diblock micelles around 30nm for mPEG₄₅-b-PCL₁₅ diblock (**Figure 2.35, a**), and around 40 nm for mPEG₄₅-b-PCL₂₅ (**Figure 2.36, a**). The sizes start getting bigger after the incorporation of PEG-porphyrin diblock using the PEG-porphyrin/mPEG₄₅-b-PCL₁₅ and PEG-porphyrin/PEG₄₅-b-PCL₂₅ mixed micelles, which are around 60 nm (**Figure 2.35, b**), and 90 nm (**Figure 2.36, b**), respectively.

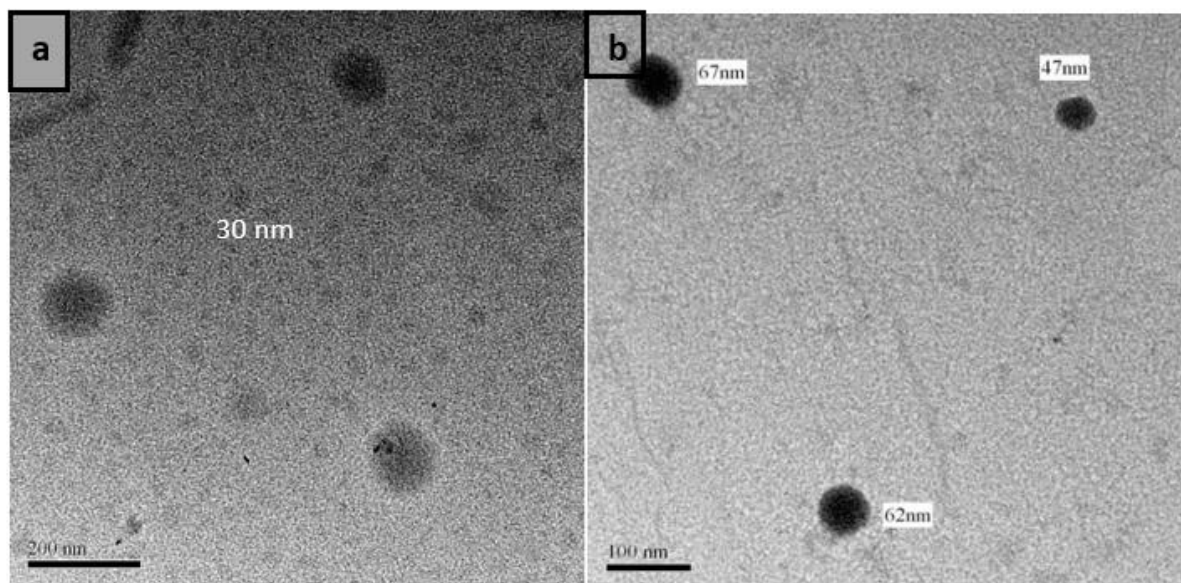


Figure 2.35: TEM images for, **a**, free mPEG₄₅-b-PCL₁₅ diblock micelles, and **b**, PEG-porphyrin / mPEG₄₅-b-PCL₁₅ diblock mixed micelles. The concentrations of diblock and mPEG-porphyrin are 30 $\mu\text{g/mL}$ and 10 $\mu\text{g/mL}$.

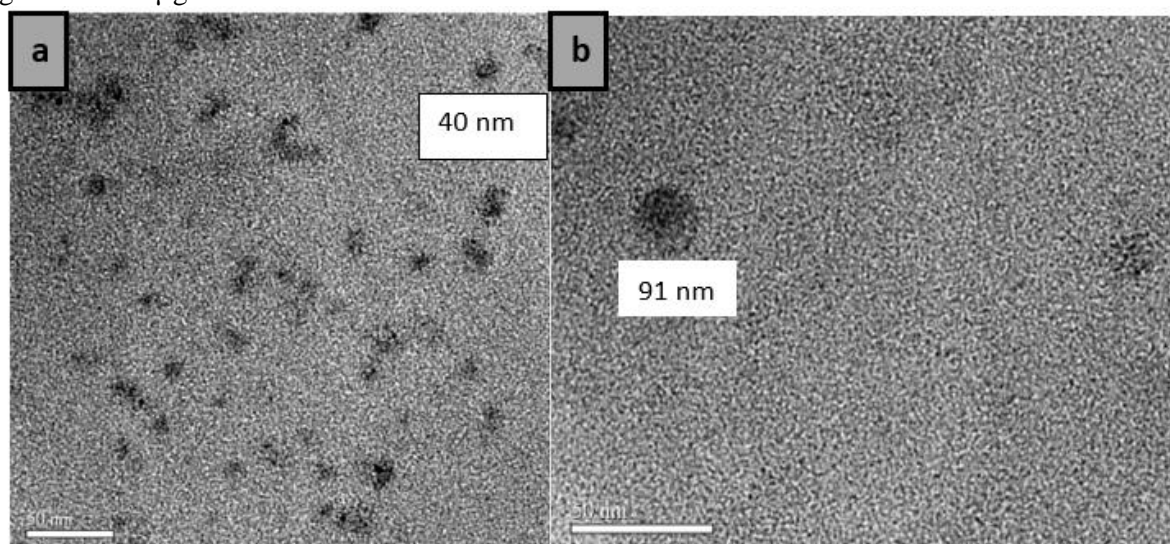


Figure 2.36: TEM images for, **a**, free mPEG₄₅-b-PCL₂₅ diblock micelles and **b**, PEG-porphyrin / mPEG₄₅-b-PCL₂₅ diblock mixed micelles. The concentration of diblock and mPEG-porphyrin are 30 $\mu\text{g/mL}$ and 5 $\mu\text{g/mL}$.

Increasing the PCL length in mPEG₄₅-b-PCL_n diblock will increase the diameter of the micelles; hence, more PEG-porphyrin can be incorporated within the diblock before being quenched. mPEG₄₅-b-PCL₃₅ and mPEG₄₅-b-PCL₄₅ micelles were also studied as shown in **Table 2.5**. As the length of PCL increased, the CMC is reduced and the size of the micelle increases.

The onset quenching for the different polymers was dependent on the diblock concentration; it was not constant across all levels of the degree of polymerisation. The ratio of the polymer to porphyrin at which quenching was observed, was also dependent on the ratio of the polymer to porphyrin at which higher amounts of the PEG-porphyrin **10** are required at lower diblock concentrations. The results were not as expected and the experiments were repeated; nonetheless, the same results were obtained. The diameter of mixed micelles increased with the increase in the length of PCL, confirming the prediction that the larger the hydrophobic block, the more porphyrins can be incorporated, resulting in a morphology change. It is possible that this morphology change is the cause of the quenching observed above (quenching is dependent on the polymer concentration and ratio).

Table 2.5. Summary the determination of pre-quenching limit for the four diblock copolymers.

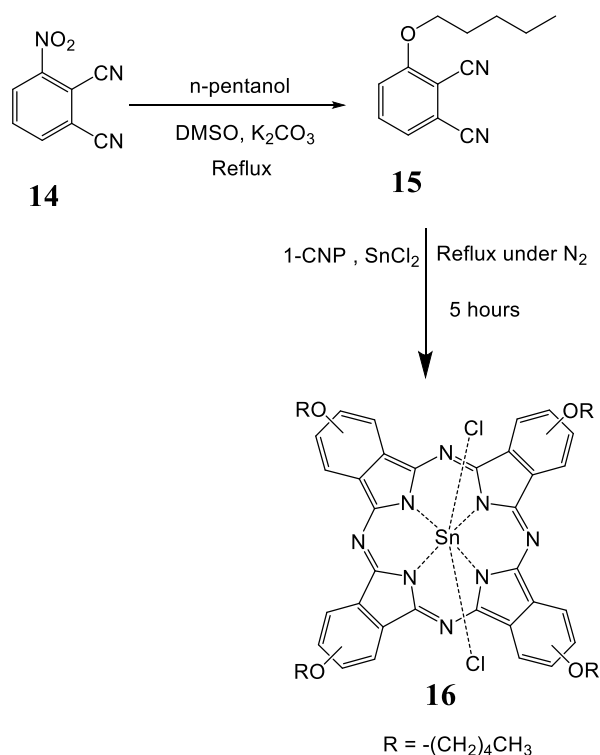
Different diblock ^a	mPEG ₄₅ -b-PCL ₁₅	mPEG ₄₅ -b-PCL ₂₅	mPEG ₄₅ -b-PCL ₃₅	mPEG ₄₅ -b-PCL ₄₅
Concentration of diblock ^b ($\mu\text{g/mL}$)	20	5	4	2
Onset of quench (ratio of diblock to PEG-porphyrin)	2:1	1:1	1:5	1:10
Diameter of mixed micelles (DLS) ^c (nm)	125	261	387	595

- Diblock refer to mPEG₄₅-b-PCL_n where n (repeat unit of caprolactone) = 15, 25, 35, 45.
- The concentration of diblocks was used to construct the mixed micelles was above the CMC.
- The size of mixed micelles at onset quench measured using DLS.

2.3.4 Synthesis of dichloride (Phthalocyanato) tin (IV)(Tin phthalocyanine) (acceptor unit)

Phthalocyanine and metallophthalocyanines (MPc) possess a highly conjugated electron system; they have been chosen as the acceptor units for this project. Unsubstituted phthalocyanines have very low solubility in organic solvents, and alkyl or alkoxy groups must be introduced to improve solubility. In addition, substituents at the non-peripheral position or axial ligands on the central metal are thought to prevent phthalocyanine self-aggregation. Functionalisation, therefore, affords the chance to maximise their photo activities.

Dichloride (phthalocyanine) tin (IV) (tin phthalocyanine **16**) was selected and synthesised from 3-pentyloxy phthalonitrile **15** as shown in **Scheme 2.4**.



Scheme 2.4: synthesis of tin phthalocyanine **16**

For the synthesis of tin phthalocyanine **16**, the first step involves the synthesis of pentyloxy phthalonitrile **15** via a base-catalysed nucleophilic substitution of 3-nitroththalonitrile **14** with n-pentanol in the presence of anhydrous potassium carbonate. The reaction mixture was refluxed for 4 hours at 90 °C and then cooled to room temperature. After the addition of water, the reaction mixture was stirred vigorously for another 10 minutes and the resulting precipitates were collected and washed with water. Purification of the pentyloxy phthalonitrile **15** was carried using chromatography with the DCM as eluent. The structure of the desired product was confirmed by ^1H NMR spectroscopy, which showed it multiple at 7.66-7.62 ppm, doublet - doublet at 7.35 ppm and doublet at 7.24 ppm corresponding to phenyl ring protons. Multiplets at 1.89-1.92 ppm and 1.54-1.35 ppm and triplets at 4.14 ppm and 0.96 ppm corresponded to the phenoxy protons. Further confirmation was carried out using mass spectroscopy, which displayed a molecular ion peak at $215(\text{M}+\text{H})^+$.

After the successful synthesis of pentoxy phthalonitrile **15**, tin phthalocyanine **16** was synthesised by dissolving phthalonitrile **15** in 1-chloronaphthalene. Tin (II) chloride was added and the mixture was refluxed for 5 hours. The reaction mixture was then cooled to room temperature and the solution was allowed to pass through a short column of silica to remove 1-chloronaphthalene, with the product remaining on the column. The column was then eluted with 4/1 dichloromethane and methanol. The solvent evaporated, and the final product was obtained after washing it with hot methanol. The analysis of the ^1H NMR spectrum exhibited three sets of multiplets at 9.35-9.17 ppm, 8.32-8.24 ppm and 7.90-7.76 ppm for the tin phthalocyanine **16** aromatic protons. The n-pentyl protons resonated as multiplets at 4.99-4.92, 4.79-4.72 ppm, 2.57-2.35, and 1.88-1.54 ppm and 1.24-1.03 ppm (**Figure 2.37**). The mass spectroscopy indicated a molecular ion at 1008 $[\text{M}-\text{Cl}]^+$.

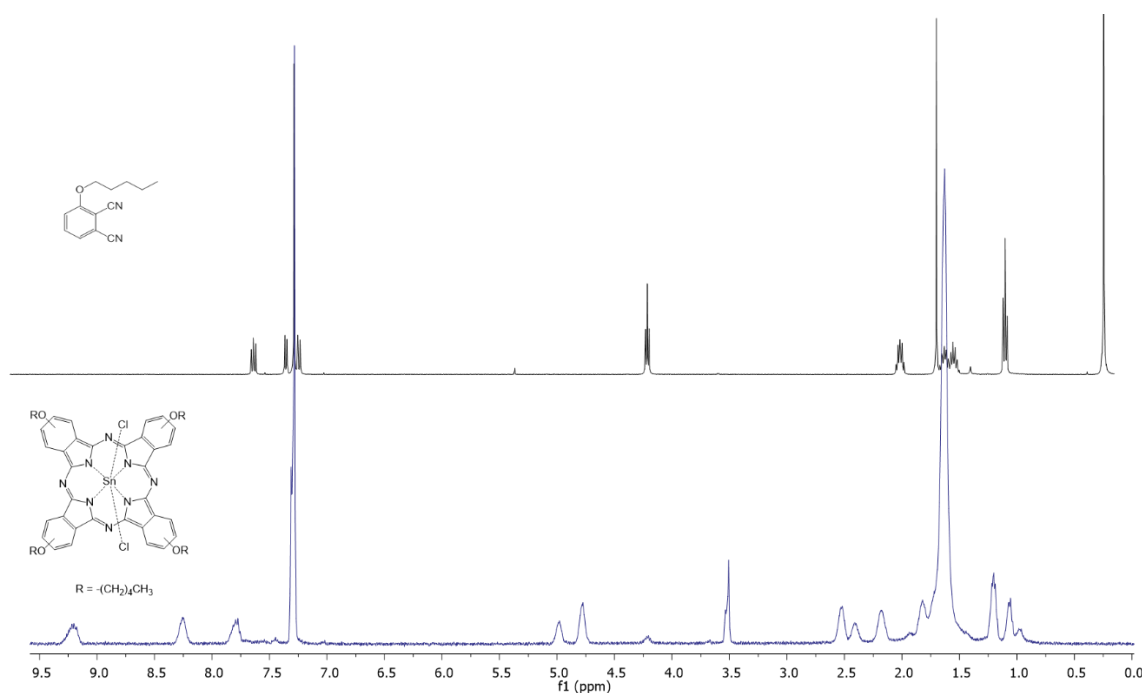


Figure 2.37: ^1H -NMR spectra of pentoxy phthalonitrile **15** and tin phthalocyanine **16**

It is evident that cyclotrimerization can lead to the formation of four constructional isomers which are C_s , C_{2v} , D_{2h} , C_{4h} (**Figure 2.38**),¹²¹ therefore, a low yield of the required tin phthalocyanine **16** (33%) was obtained.

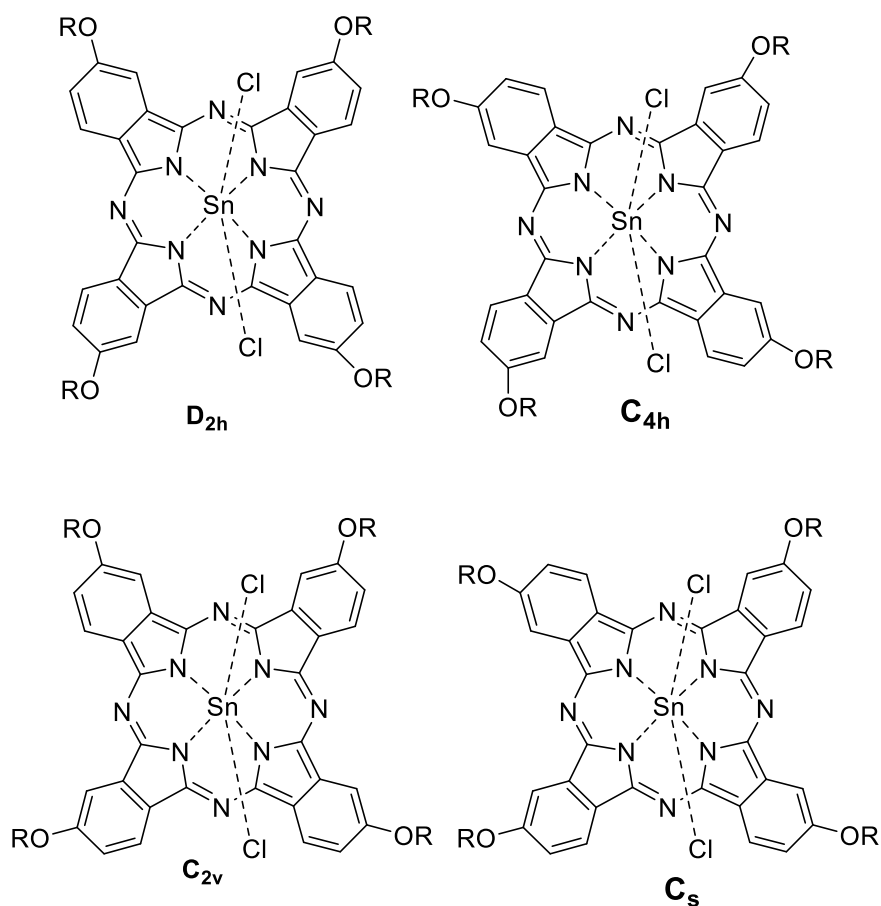


Figure 2.38: the four isomers of tin phthalocyanine **16**, C_s , C_{2v} , D_{2h} , C_{4h} .

The UV-vis spectra of the phthalocyanine complexes (**Figure 2.39**) exhibited characteristic Q band at 600 nm-750 nm; it was attributed to the π - π^* transition. A second peak at 300 nm-400 nm (B-band), corresponds to deeper π - π^* transitions.¹²²

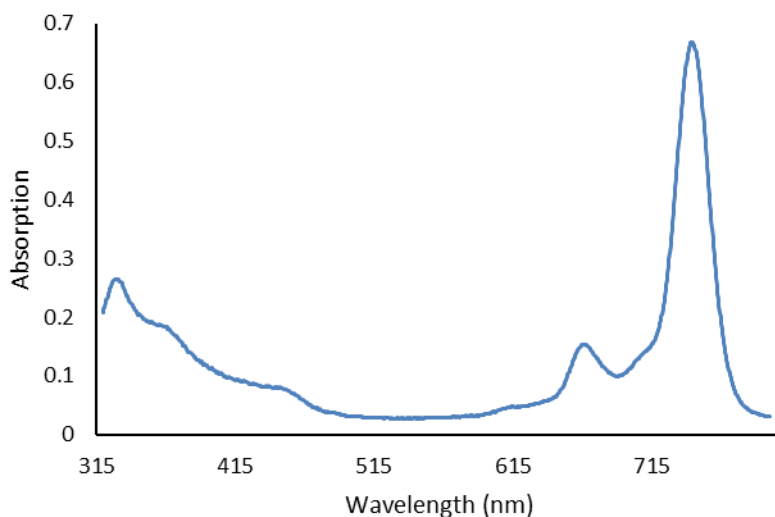


Figure 2.39: the UV-vis spectra of tin phthalocyanine 6×10^{-6} M in DCM.

In the natural system, the photoactive units are accommodated within a protein matrix. The proteins organise the relative position and geometry of the chromophores, ensuring that energy is transferred efficiently to the reaction centre. Polymeric micelles are seen as simple and effective alternatives to the protein while chromophores can be confined within the hydrophobic core of the micelles and their periphery.

2.3.5 Tin phthalocyanine 16 and PEG-porphyrin 10 in polymeric micelles as an artificial photosynthesis reaction centre system:

The novel donor-acceptor system is constructed from tin phthalocyanine **16** and PEG-porphyrin **10**, which are the acceptor and donor units, respectively and which are trapped in the core of micelles through hydrophobic interaction (**Figure 2.40**).

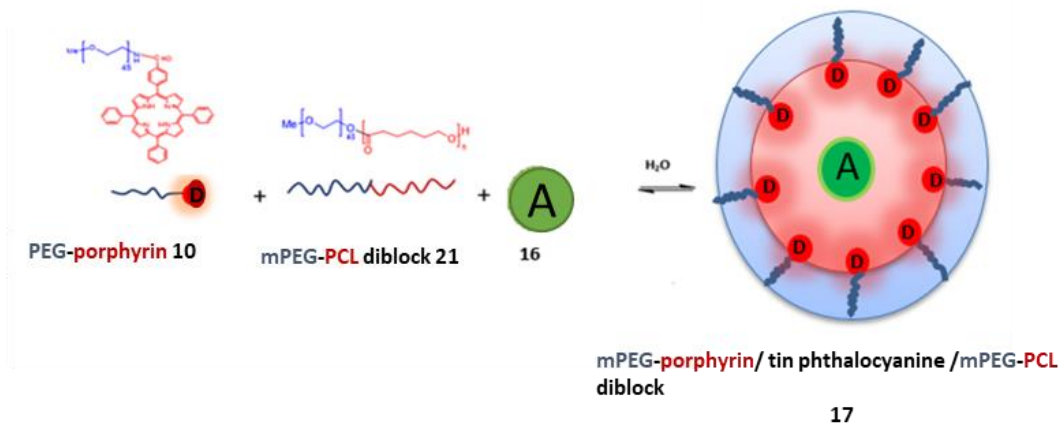


Figure 2.40: artificial light harvesting system, self-assembled from the PEG-porphyrin, tin phthalocyanine and mPEG-PCL diblock micelles.

The mPEG-PCL diblock polymer plays a double role in this artificial system. Firstly, it improves the solubility of the hydrophobic chromophores and secondly, it helps to organize the chromophores within the micelles. To perform the second role, the donor units (porphyrin) are functionalised with a hydrophilic polymer (mPEG). This is to ensure that the donor porphyrins assemble at the hydrophobic/hydrophilic interfaces within the micelles leaving some distance between them and the acceptor molecule within the centre of the hydrophobic region of the micelles. Although the structure of the tin phthalocyanine **16** molecules is modified by the adding alkanes to the α -periphery, a high level of aggregation was observed, even at a very low concentration (to be discussed later). Previously, it was noticed that the diameter of mPEG₄₅-b-PCL₂₅ diblock increased from 40 nm to 90 nm (**Figure 2.36**), after the addition of PEG-porphyrin. However, the diameter of mPEG₄₅-b-PCL₂₅ diblock micelles remained constant with respect to the concentration of PEG-porphyrin; this was verified by DLS measurements of the different ratios of mPEG₄₅-b-PCL₂₅ to PEG-porphyrin (**Figure 2.34, b**). The question is, “Does the diblock micelle maintain its ability to control its structure and properties after the addition of tin phthalocyanine?” The answer is that tin phthalocyanine was encapsulated inside the micelles and its size was measured using TEM and DLS (**Figures 2.41 and 2.42 b**); it was around 200 nm. This is compared to a size of 50 nm for the diblock alone. This big change in the morphology of micelles after the addition of tin phthalocyanine is

attributed to the access of too many of aggregated tin phthalocyanine molecules to one micelle. This was followed by measuring the morphology of the self-assembled artificial system using DLS and TEM (PEG-Porphyrin/PEG-PCL₂₅/tin phthalocyanine). The DLS data for tin phthalocyanine-PEG-porphyrin-diblock complex micelles, **17** at low and high concentration of PEG-porphyrins, are found to have similar diameter (**Figure 2.41**). TEM measurements (**Figure 2.42**) are consistent with the DLS results. Overall, this indicates that the self-assembly process is efficient and that is not affected by the presence or the amount of inserted PEG-porphyrin.

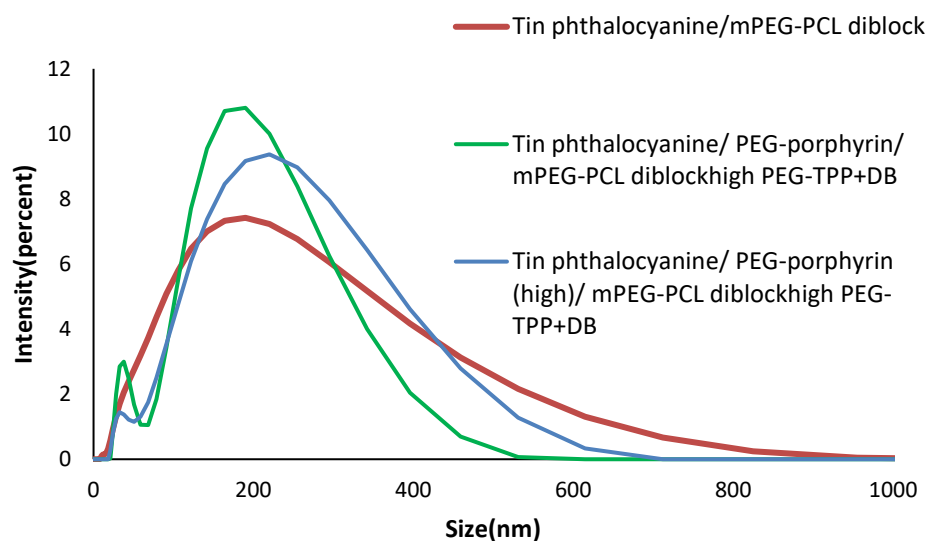


Figure 2.41: a DLS measurements of free porphyrin tin phthalocyanine –micelles and two (PEG-Porphyrin/PEG-PCL₂₅/tin phthalocyanine) micelles with low and high concentration of PEG-porphyrin.

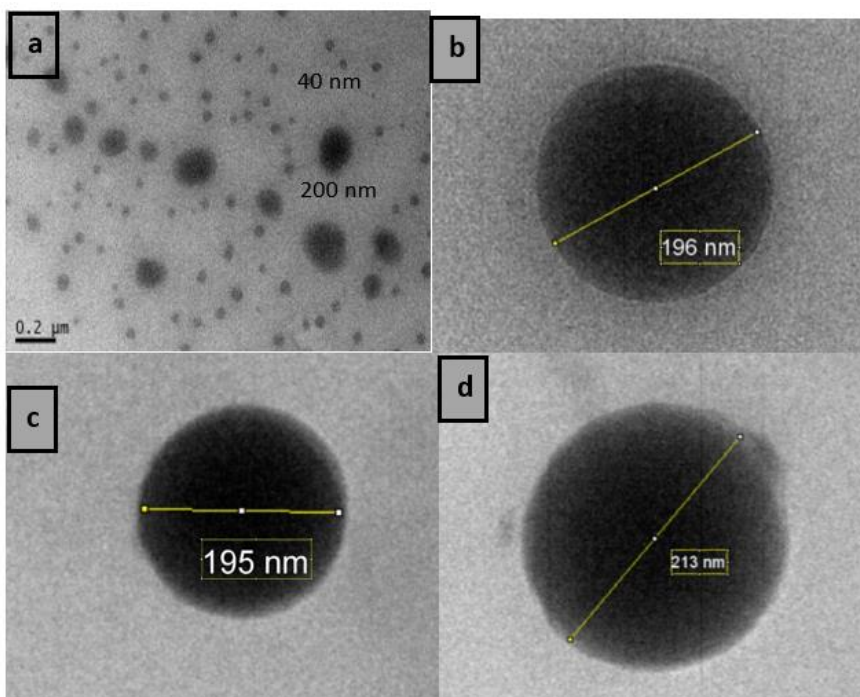


Figure 2.36: **a**, the zoom out TEM image for the tin phthalocyanine-PEG-porphyrin-mPEG₄₅-b-PCL₂₅ micelles17, **b**, TEM image for the tin phthalocyanine-mPEG₄₅-b-PCL₂₅ micelles and TEM image for the two samples of tin phthalocyanine-PEG-porphyrin-mPEG₄₅-b-PCL₂₅ micelles17 micelles with **c**, low and, **d**, high concentration of PEG-porphyrin.

Fluorescence and UV-vis techniques were used to observe and verify any photo-induced energy transfer processes. A series of samples with different concentrations of tin phthalocyanine, ranging from 5×10^{-8} M to 4×10^{-6} M, and fixed concentration of PEG-porphyrin ($2 \mu\text{g/mL}$) and diblock micelles ($20 \mu\text{g/mL}$) was prepared. The samples were excited at the porphyrin maximum absorption (418.5 nm); besides, any emission from the tin phthalocyanine at 750 nm was monitored; nevertheless, no emission was observed (**Figure 2.43**). However, a decrease in the fluorescence emission intensity of the porphyrin with an increase in the tin phthalocyanine concentration was observed; it served as an evidence of energy transfer.

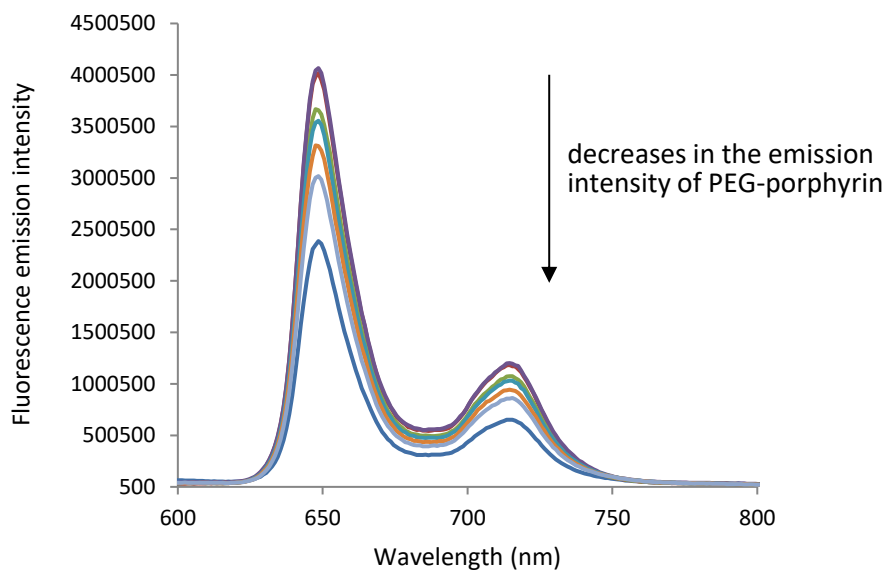


Figure 2.43: fluorescence spectra of artificial light harvesting using fixed concentration of PEG-porphyrin (2 µg/mL) and diblock (20 µg/mL) and different concentrations of tin phthalocyanine (from 5×10^{-8} M to 4×10^{-6} M).

The degree of the quenching of light harvesting micelles (PEG-porphyrin/tin phthalocyanine/diblock) based on the emission intensity of PEG-porphyrin (donor) at 650 nm was calculated using **equation 1**⁶⁶ (**Figure 2.44**), where, F_0 represented the emission intensity of PEG-porphyrin/diblock mixed micelles and F represented the emission intensity of light harvesting micelles in the presence of tin phthalocyanine in the core.

$$\text{Degree of quenching} = 1 - \frac{F}{F_0} \quad (1)$$

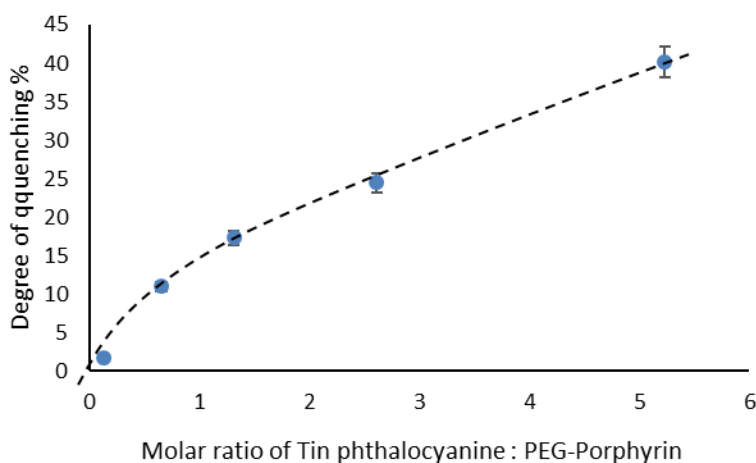


Figure 2.44: the graph of the degree of quenching for the different ratios PEG-porphyrin to tin phthalocyanine in the light harvesting micelles, the concentration of PEG-porphyrin **10** was fixed at 7.67×10^{-7} M while the concentration of tin phthalocyanine varied from 9×10^{-8} M to 4×10^{-6} M.

The amount of quenching was also determined for micelles with different lengths of the hydrophobic PCL component which is related to the size of the hydrophobic core. Experiments were carried out for PEG-porphyrin/tin phthalocyanine/diblock light harvesting micelles at diblock concentrations around twice the CMC and 4 $\mu\text{g/mL}$, 1 $\mu\text{g/mL}$, 0.8 $\mu\text{g/mL}$ and 0.4 $\mu\text{g/mL}$ for the PEG-porphyrins. The concentration of phthalocyanine was 1×10^{-6} M in all systems (**Table 2.6**). The data is shown in **Figure 2.45** and the results indicate that the size of the hydrophobic PCL segment is related to the level of quenching. That is, the longer the PCL unit, the higher the level of quenching.

Table 2.6: the degree of quenching for the different degrees of polymerisation (n) for PCL in mPEG₄₅-b-PCL_n.

Different mPEG ₄₅ -b-PCL _n	mPEG ₄₅ -b-PCL ₁₅	mPEG ₄₅ -b-PCL ₂₅	mPEG ₄₅ -b-PCL ₃₅	mPEG ₄₅ -b-PCL ₄₅
Concentration of diblock ^a ($\mu\text{g/mL}$)	20	10	4	2
Concentration of PEG-porphyrin ($\mu\text{g/mL}$)	1.5×10^{-6}	3.8×10^{-7}	3×10^{-7}	1.5×10^{-7}
Concentration of tin phthalocyanine (M)	1×10^{-6}	1×10^{-6}	1×10^{-6}	1×10^{-6}
Degree of quenching %	68	83	86	91

a. concentration selected based on CMC of the diblock polymer

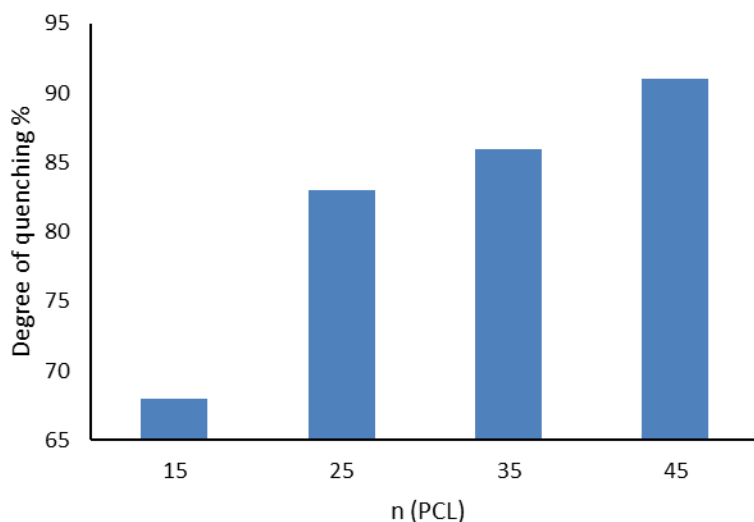


Figure 2.45: the degree of quenching % was calculated for the different degrees polymerisation (n) of the PCL segment in mPEG₄₅-b-PCL_n.

The lack of emission from the tin phthalocyanine core was thought to be due to the aggregation of tin phthalocyanine in the core of LH micelles. To estimate the level of aggregation within the mPEG-b-PCL polymeric micelles, the UV-vis spectra of tin phthalocyanine in different organic solutions were measured and compared to the spectrum obtained within the micelle (**Table 2.7**).

Table 2.7: the UV-vis measurements of tin phthalocyanine at 1×10^{-6} M in different solvents and within the micelle

Solvent used to dissolve tin phthalocyanine	λ_{\max} for tin phthalocyanine (nm)
Dichloromethane (DCM)	747
Methanol	738
Ethyl acetate	736
micelles	744

For the solvents studied, the data showed that the methanol has the highest absorption. The λ_{\max} 744 nm for tin phthalocyanine in the micelles was similar to that observed for DCM and ethyl acetate. The fluorescence data in **Figure 2.46** was obtained by exciting the tin phthalocyanine

in different solvents at 610 nm. It revealed very intense emission for methanol, with much weaker emission for the other solvents. Almost no emission was observed for the micelle.

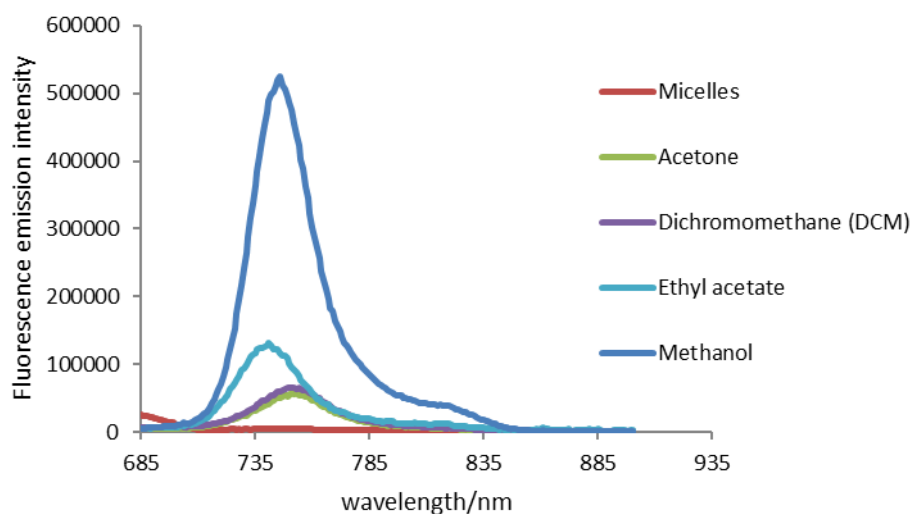


Figure 2.46: the fluorescence measurement of tin phthalocyanine at 1×10^{-6} M in different solvents and with micelles.

The lone pair on methanol can coordinate to the tin and displace the ligand. For other solvents, it is the lone pair on the alkoxy side chain at one tin phthalocyanine coordinating to tin in another tin phthalocyanine (displacing chloride) (**Figure 2.47**). This intermolecular ligation results in aggregation. Similar spectroscopic properties are observed for tin phthalocyanine in the micelle. It is thus concluded that the tin phthalocyanine is aggregating. In addition, π - π interactions will occur at high concentration. To distinguish between ligation and π - π interactions, a series of dilution experiments was carried out. If non-covalent π - π interactions were the cause of aggregation, then the fluorescence intensity should increase with dilution. The solution was diluted to 1×10^{-9} M and no increase in intensity was observed. Therefore, it was concluded that the principle mechanism for aggregation is ligation (intermolecular interactions). This is supported by the literature review research studies¹⁹.

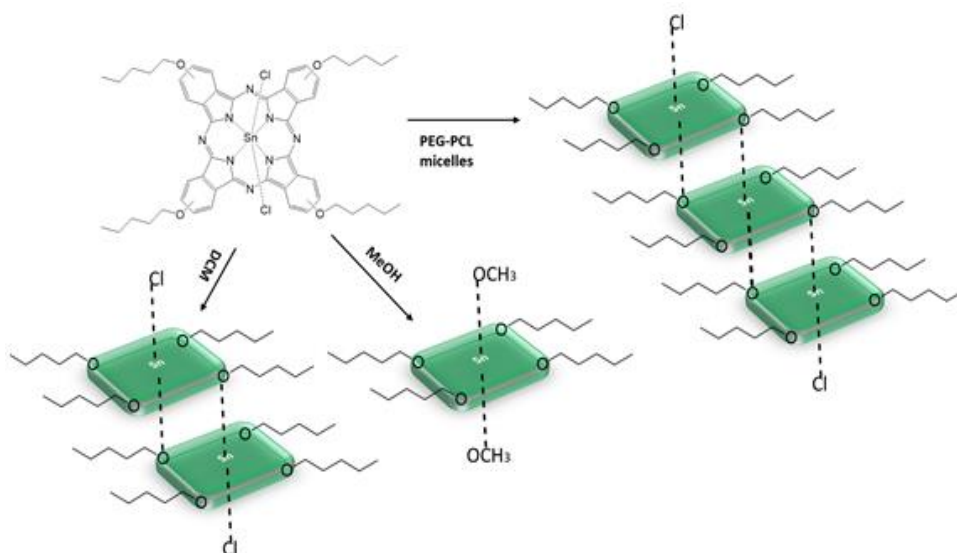


Figure 2.47: the aggregation behaviour of tin phthalocyanine in different solvents and diblock micelles.

The above results indicated that it was impossible to detect fluorescence emission from the tin phthalocyanine within the diblock micelles both in the presence and the absence of PEG-porphyrin (donors), due to the aggregation of tin phthalocyanine within the micelles even at very low concentration of tin phthalocyanine in the micelles solution. Therefore, the absorption properties of the micelles were investigated using UV-vis spectroscopy. Light harvesting micelles containing a fixed concentration of tin phthalocyanine (1×10^{-6} M) together with diblock (20 $\mu\text{g/mL}$) and different concentrations of PEG-porphyrin, ranging from 0.2 $\mu\text{g/mL}$ to 2 $\mu\text{g/mL}$ were studied. The absorption with respect to PEG-porphyrin concentration was plotted and displayed in **Figure 2.48**. The graph shows an increase in phthalocyanine absorption, despite the fact that its concentration within the micelles was fixed and did not change. If energy transfer had not occurred, then the increase in absorption should not have been observed.

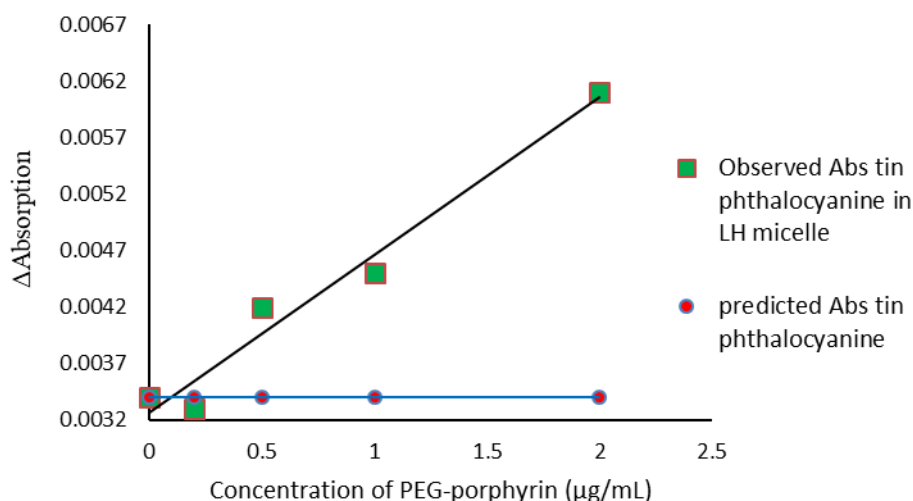


Figure 2.48: observed absorption of tin phthalocyanine ($1 \times 10^{-6} \text{M}$) in the presence of different concentrations of porphyrins (from $0.2 \mu\text{g/mL}$ to $2 \mu\text{g/mL}$) (green dots) and the predicted absorption of tin phthalocyanine in the absence of porphyrin (red dots).

Besides absorbing the constant energy that emanated from UV-vis spectroscopy, the tin phthalocyanine received an extra energy from the surrounding porphyrins since PEG-porphyrin emits light at tin phthalocyanine absorption range (650 nm -720 nm).

These results demonstrated that the non-interacted chromophores in our artificial light harvesting system based on micelles have the ability to transfer energy. However, due to aggregation of the phthalocyanine within the micelles, the energy could not be harvested, and the system did not fulfil the light harvesting requirement.

2.4 Conclusion and future work

The first aim of the project was to design and make an artificial light harvesting model based on polymeric micelles using self-assembly. This model has a simplified antenna system that possesses a number of donor molecules in an organised manner. These molecules can absorb and then emit light to single acceptor molecule in the centre of the micelles. The role of the micelle in the present artificial light harvesting complex was to spatially organise and stabilise donor and acceptor molecules in water. The second aim was to measure any light harvesting

process. This involved four steps, which were light absorption by the donor molecules, light emission from the donor molecules, absorption by an acceptor molecule and finally, emission of light from the acceptor molecule. The proposed artificial light harvesting system was constructed by assembling the PEG-porphyrin **10** (donor molecule), tin phthalocyanine **16** (acceptor molecule) and mPEG₄₅-b-PCL_n diblock in an aqueous solution. Attaching PEG chain to the porphyrin structure made a significant difference, as PEG-porphyrin **10** was isolated successfully at the hydrophobic interface of the micelle core. Experiments confirmed that the ordered array of PEG-porphyrin within the mPEG₄₅-b-PCL_n micelles was addressed from the self-quenching of the PEG-porphyrin. The most obvious finding that emerged from the study of PEG-Porphyrin/mPEG₄₅-b-PCL_n micelles was that the longer the PCL block, the more PEG-porphyrin **10** could be inserted within micelle before the quenching concentration. Investigating the morphology of the PEG-Porphyrin/mPEG₄₅-b-PCL_n micelles **13** showed that the diblock micelle underwent a phase change from micelle (less than 100 nm) to vesicle (above 200 nm) due to the addition of PEG-porphyrin **10**. However, the PEG-Porphyrin/mPEG₄₅-b-PCL₂₅ diblock micelles maintained their size, even after the insertion of high amounts of PEG-porphyrin **10**. Throughout the light harvesting experiments, no direct emission from the tin phthalocyanine (acceptor unit) was observed. However, the transfer of energy from the PEG-porphyrin (donor unit) to the tin phthalocyanine (acceptor unit) was identified through the quenching of the PEG-porphyrin (donors) emission in our model systems. The degree of quenching within light harvesting micelles increased with the amount of the inserted PEG-porphyrin **10**. The research has also shown that the degree of the quenching of light harvesting micelles increased with the increased length of PCL block in mPEG₄₅-b-PCL_n diblock. UV-vis spectroscopy was used to study the light harvesting properties of our system. A certain amount of light was given to the tin phthalocyanine micelle solutions, in the presence and absence of PEG-Porphyrin. The results showed increased absorption for the tin phthalocyanine when

PEG-porphyrin was used. Therefore, tin phthalocyanine received extra energy from donors (porphyrins) but it could not emit the energy as light. This confirms that the energy transfer from PEG-porphyrin to tin phthalocyanine took place. Additionally, the degree of quenching increased with the increased size of diblock micelles. This suggested that more active units (donor and acceptor molecules) could be incorporated within the larger hydrophobic core of the micelles and that they could generate antenna amplification through the porphyrins mPEG₄₅-b-PCL_n diblock which was synthesised via ring opening polymerisation. Four mPEG₄₅-b-PCL_n diblocks with different degrees of polymerisation were synthesised. These were mPEG₄₅-b-PCL₁₅, mPEG₄₅-b-PCL₂₅, mPEG₄₅-b-PCL₃₅ and mPEG₄₅-b-PCL₄₅. Steglich Esterification was employed to synthesis the PEG-porphyrin **10** through alcohol terminal group on (mPEG-OH) using the carboxylic porphyrin (porphyrin-COOH **9**). Tin phthalocyanine **16** was synthesised from pentoxy phthalonitrile **15** and tin (II) chloride, which aggregated within the core of the diblock micelles; no emission of tin phthalocyanine could not detected.

Aggregation is probably the reason for the lack of observed light harvesting. Therefore, it is important to find a new method where only one phthalocyanine can be loaded into the core of the micelle. This can be achieved by functionalising phthalocyanine with polymer arms, by using phthalocyanine cored hyperbranched polymer or by employing a dendrimer. For example, Taratula *et al.*,¹²⁴ successfully preserved the photophysical properties of phthalocyanine by loading phthalocyanine into a PEG modified dendrimer.¹²⁴ Jang *et al.*, (year) also addressed the aggregation behaviour of phthalocyanine by synthesising a 2nd generation phthalocyanine cored dendrimer where the aggregation is effectively prevented by large dendritic wedges.¹²⁵ The researchers also functionalised the dendrimer peripheries with a polar functional group, which increased the solubility of the dendrimer in aqueous solution. However, these low generation phthalocyanine loaded dendrimers aggregated inside the polyionic micelle. A higher generation may prevent the aggregation within the micelles.¹²⁵

Expanding this idea to our system (**Figure 2.49**), tin phthalocyanine modified to tin phthalocyanine cored dendrimer. The hydrophobicity of PEG-PCL core allows to host single molecule of tin phthalocyanine/dendrimer at the centre of the core and many PEG-porphyrin **10** polymers at the interface of micelle. In this promising system, both donor and acceptor will be isolated. Therefore, it may give an expected high efficiency light harvesting.

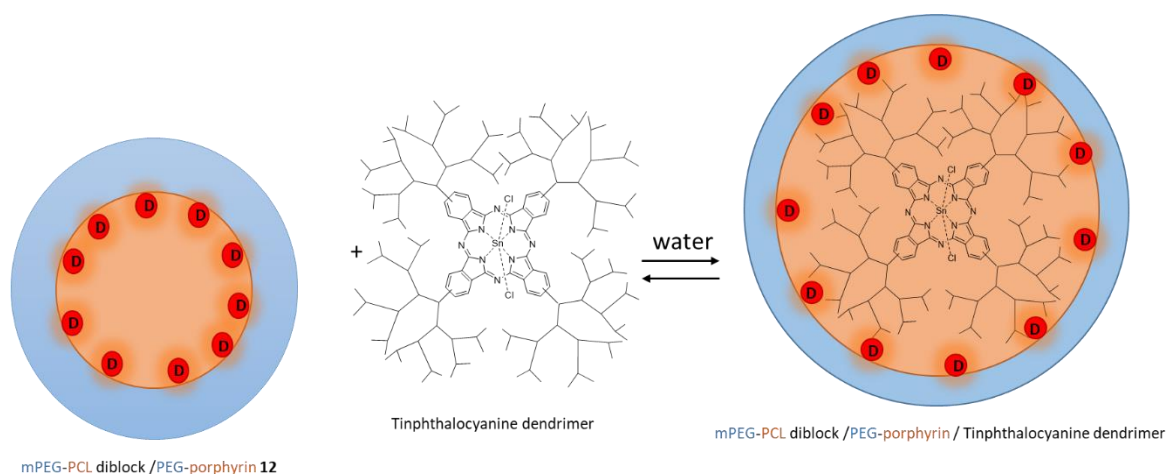


Figure 2.49: artificial light harvesting system, self-assembled from the PEG-porphyrin/ mPEG-PCL diblock micelles **12** and tin phthalocyanine dendrimer.

Another reason for not being able to detect emission from tin phthalocyanine could be attributed to the excitation energy that was transferred differently.¹²⁶ It is possible that electron transfer occurred to another appropriate acceptor molecule, such as oxygen. Different methods can be used to detect this including iodide and nitro blue tetrazolium (NBT) methods.⁶⁶ An artificial light harvesting system with high energy transfer efficiency, flexible structure and simple preparation is still required and the appropriate scaffolding for active units should be further studied.

Chapter 3 - Artificial catalyst based on micelles for organic reaction

3.1 Introduction:

Recently, researchers have demonstrated an increased interest in using water as a solvent for many organic reactions, as water is safe, abundant and inexpensive.¹²⁷ Conducting organic reactions in aqueous solutions can have many advantages, such as rate acceleration and selectivity.¹²⁷ However, many organic reactions involve hydrophobic species this limiting the use of water in synthetic organic chemistry.¹²⁷ Rideout *et al.*,¹²⁸ reported that performing organic reactions in water could increase the reaction rate. During the reaction, hydrophobic reactants form small droplets when stirred vigorously. This method resulted in significant increases in the rate of many organic reactions (when compared to those conducted in an organic solvent).¹²⁸

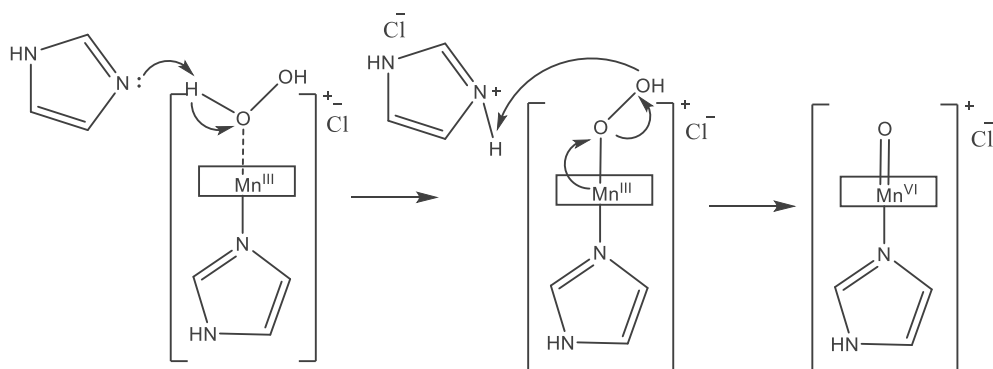
Common issues restricting the use of most catalysts are toxicity and cost.¹²⁷ Therefore, it can be an advantage to immobilize the catalysts to simplify the workup, separate and recover the catalyst.¹²⁷ Natural enzymes have unique structures that provide hydrophobic pockets for their catalytic active units, which protect and stabilize them in aqueous solution.¹²⁷ The isolation of a catalyst within a hydrophobic pocket improves its efficiency and selectivity.¹²⁷ Inspired by these natural systems, researchers have constructed a broad variety of artificial catalysts that have the same physical properties as enzymes.¹²⁷ These include dendrimers and star polymers, where the catalytic active unit is isolated from the external environment in exactly the same way as the enzyme.¹²⁷⁻¹³⁰ As a simpler system, micelles formed from surfactants can also provide a hydrophobic macroenvironment for a catalyst in water.¹²⁷ One of the advantages of

using a micelle is that it acts as nano-rector, concentrating the hydrophobic reactants inside the core of micelle, which can increase the rate and selectivity of the reaction.¹²⁷ An example of a micelle catalyst is a system designed for oxidation and epoxidation reactions. Specific catalysts include salen complexes methyltrioxorhenium based catalysts and metallated porphyrins.¹²⁸

The benefit of using a porphyrin as a catalyst for epoxidation reactions is its ability to easily modify the structure allowing for reactivity, stability and selectivity to be easily tuned. In addition, the nitrogen within the core of the macrocycles enables many transition metals, with different oxidation states to be included.^{69,131} One example that has been widely studied is the system that mimics the enzyme P450^{132,133} and its ability to catalyse the oxidation reaction of azo dyes.¹³⁴ However, few have investigated the potential of water-soluble iron and manganese porphyrins as catalysts for this oxidation reaction. This is because these porphyrins tend to form oxo dimers in water (even at trace levels), which leads to the autocatalytic degradation of the porphyrins by the oxidant. This can be reduced using porphyrins with electron-withdrawing substituents or steric groups, which prevent dimerisation.⁶⁹ The addition of an oxidant is required to these artificial systems. These can be any compounds that provide a source of oxygen [O]; for example, Iodosylbenzenes,¹³⁶ peracids,¹³⁵ or hydroperoxides⁶⁹

Iodosylbenzenes is an organoiodine compound; and due to low stability, it is only prepared in laboratory and used as an oxo transfer reagent as it can form metal oxo from metal complex and then epoxidizes alkenes. So, it is commonly employed as the source of [O]; nonetheless, its poor solubility in common organic solvents and water, low oxygen content and production of iodine benzene as a by-product, have limited its use as an oxidant.¹³⁶ H₂O₂ is produced on a large scale; it is the most popular oxidizing agent. It is water soluble with a high oxygen content; it only produces water as a by-product.⁶⁹ However, H₂O₂ is a relatively poor oxidising agent, as it can generate free radicals that interfere with the reaction and lower the yield of epoxidation.⁶⁹

Alkyl peroxides are hydroperoxides; nevertheless, they are classified as organic peroxides, as they have the ROOH functional group where R is alkyl. Similar to inorganic peroxide, organic peroxides are strong oxidising agent. The main issue of using an alkyl hydroperoxide in porphyrin catalysed oxidation reactions, is that it tends to homolytically cleave the peroxide bond on metalloporphyrin to form RO* radical that significantly reduces the epoxidation yield.⁶⁹ According to Gunathilagan,⁶⁹ the solution to this issue is to add a strong donor ligand, such as imidazole, which serves two important roles.⁶⁹ Firstly, it acts as Lewis base, by accepting a proton and secondly, it can also contribute electron density to the M^V=O species (scheme 3.1).⁶⁹



Scheme 3.1: the roles of imidazole that Form the active oxidant.⁶⁹

Barros *et al.*,¹³⁶ successfully oxidized different azo dyes, Disperse Black 3, Disperse Orange 3 and Methyl Yellow with different oxidants such as iodosylbenzene, *tert*-butyl hydroperoxide and hydrogen peroxide. In this oxidation reaction, different irons were used as the catalyst to investigate the potential of the catalyst system applied to mimic cytochrome P450; these include porphyrins, tetra carboxyphenyl porphyrin iron(III) chloride, 5,10,15,20-tetrakis-(N-methyl-4-pyridyl) porphyrin iron(III) pentachloride and 5,10,15,20-tetrakis-(2,3,4,5,6-pentafluorophenyl) porphyrin iron(III) chloride. The organic reaction was conducted in a mixture of acetonitrile and water solution (with ratio 2:1). The oxidation reaction of azo dyes was monitored using UV-vis absorption spectroscopy. Higher conversion of azo dyes was

obtained when iodosylbenzene and *tert*-butyl hydroperoxide were used as an oxidant instead of hydrogen peroxide.¹³⁴

In this chapter, the catalytic activity of the ordered array of PEG-porphyrin **10** in mPEG₄₅-PCL₂₅ diblock micelles which was previously used as a donor in the artificial light harvesting system (Chapter 2) will be tested after the insertion of iron ion in PEG-porphyrin to catalyse the oxidation reaction of orange II (azo dye) in aqueous solution. *Tert*-butyl peroxide and hydrogen peroxide, *meta*-Chloroperoxybenzoic acid, will be tested as oxidants, too. Pyridine will be employed as a co-catalyst for the orange II oxidation reaction.

3.2 Aim

The aim of the work described in this chapter is to design and study a system that can catalyse an organic reaction in water. The work is inspired by the porphyrin-protein composition in Horseradish (HR) peroxidase (**Figure 3.1**), whereby the protein structure provides a hydrophobic microenvironment that can bind heme (iron porphyrin), at the catalytic active centre of HR.¹³⁷



Figure 3.1: the structure of Horseradish peroxidase, where, the alpha-helic protein is a large protein that binds Heme as a redox cofactor.¹³⁷

In this chapter, the catalytic activity of the ordered mPEG-porphyrin **10** in mPEG₄₅-b-PCL₂₅ diblock micelle will be investigated. In these experiments, the iron will be inserted into the porphyrin to give PEG-Fe-Porphyrin **12**. The catalytic activity of iron porphyrin in micelles has been extensively studied and reported in many literature reviews. However, the location of the catalyst and its aggregation are important parameters.¹³⁸ Iron porphyrins are very hydrophobic catalysts that tends to aggregate in water. This reduces the stability and the catalytic activity of the iron porphyrin.¹³⁸ Maldott *et al.*,¹³⁹ constructed an iron porphyrin-micelle system that catalysed the epoxidation of cyclohexene and cyclooctene with a 90% selectivity in the case of cyclooctane.¹³⁹ Qu *et al.*,¹³⁷ constructed a model system using mPEG-P4VP diblock micelles and hemin (**Figure 3.2**) that could catalyse the oxidation of orange II (azo dye) (**Scheme 3.2**).

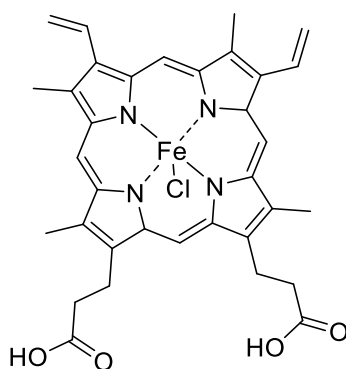


Figure 3.2: the structure of hemin.

The aggregation of Iron porphyrins in the micelles in that system was prevented by coordination of the iron in hemin to the pyridine in mPEG-P4VP.¹³⁷ As a result, the Hemin-micelle catalyst increased the rate of reaction compared to that of Horseradish peroxidase.



Scheme 3.2: the oxidation reaction of orange II in the presence of H₂O₂ as an oxidant and the hemin-micelle system as a catalyst.

Although the aggregation of Fe-porphyrin was reduced by the micelle, it was not eliminated.¹³⁸

In PEG-Fe-porphyrin **10**, the PEG chain changes the polarity of Fe-porphyrin which possibly leads the PEG-Fe-porphyrin **12** to be located at the water-micelle interface. As stated in Chapter two, PEG-porphyrin **10** has been isolated successfully inside mPEG₄₅-b-PCL₂₅ polymer micelle below the photo quenching point. The Iron porphyrin in PEG-Fe-porphyrin **12**, could also be dissolved in water, with the PEG component coiling around the Fe-porphyrin to provide an isolated macro-environment. Therefore, the catalytic activity of PEG-Fe-porphyrin **12** in the absence of micelles will be tested as a control (**Figure 3.3**). As another control, the hydrophobic catalyst, iron tetraphenylporphyrin (Fe-TPP) **19** will be incorporated into the mPEG₄₅-b-PCL₂₅ micelles and its catalytic activity compared to the results obtained for the PEG-Fe-porphyrin/mPEG₄₅-b-PCL₂₅ micelles **18**. In order to develop this methodology, there is the need to optimise the system with respect to oxidant and substrate.

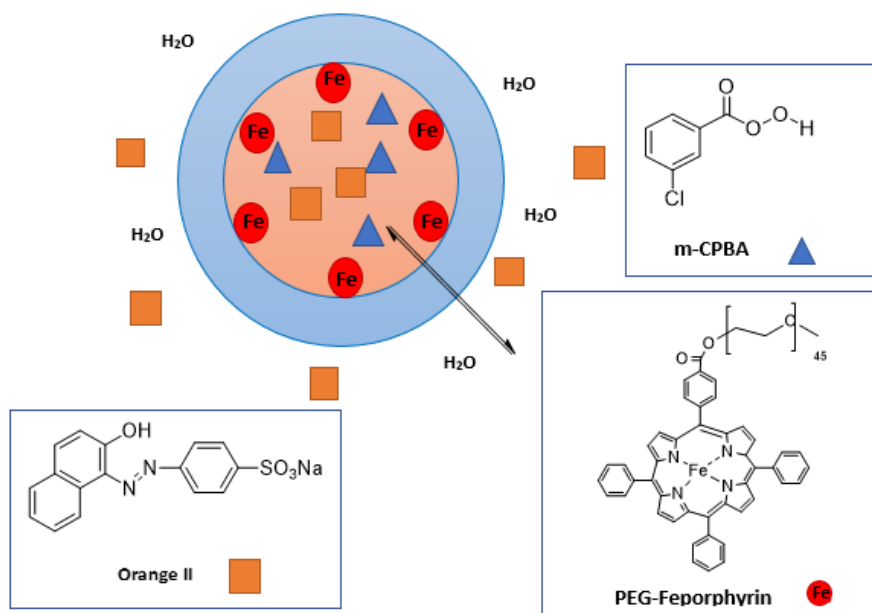


Figure 3.3: the component of catalytic oxidation reaction of orange II with *m*-CPB in the core of PEG-PCL diblock micelle in the presence of PEG-Fe-porphyrin as a catalyst.

A simple way to monitor the catalytic potential is to use a chromogenic substrate. In this study orange II and red oil were selected; these are commercially available azo dyes that absorb at 484 nm and 513 nm, respectively and possess slightly different polarities. For example, orange II is an amphiphilic and can easily go inside a micelle, but it can also be oxidised in the water phase. The precise location for the catalytic reaction (micelle or bulk water) will therefore depend on the location of the oxidant, as shown in **Figure 3.3**. On the other hand, red oil is more hydrophobic and has little water solubility. As such, it prefers the hydrophobic interior of the micelle and seems an ideal substrate for our catalytic studies due to its high hydrophobicity, as it is demonstrated in **Figure 3.4**.

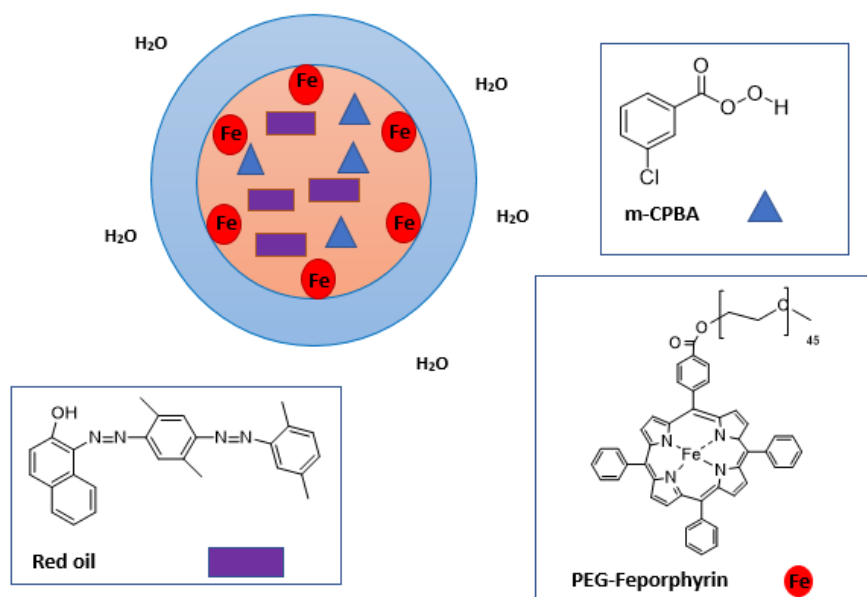


Figure 3.4: the component of catalytic oxidation reaction of red oil with *m*-CPBA in the core of PEG-PCL diblock micelle in the presence of PEG-Fe-porphyrin **12** as a catalyst.

Hydrogen peroxide (H_2O_2), *tert*-butyl hydroperoxide (*t*-BuOOH) and *meta*-chloroperoxybenzoic acid (*m*-CPBA) will be studied as oxidants for our catalytic reactions. H_2O_2 is a water-soluble oxidant that is cheap and can decompose into clean byproducts (water and oxygen). However, it is less stable compared to other oxidants. *t*-BuOOH is less soluble than H_2O_2 , but it is more a stable and an active oxidant, particularly in the presence of a coordinating species (such as pyridine), which acts as a cocatalyst. In addition, as *t*-BuOOH is more hydrophobic than H_2O_2 , it may have a greater propensity to reside within the micelle. This can be further optimised if the organic oxidant *m*-CPBA is used, which is the most hydrophobic oxidant under test. **Figure 3.5** shows the structure of different oxidants.

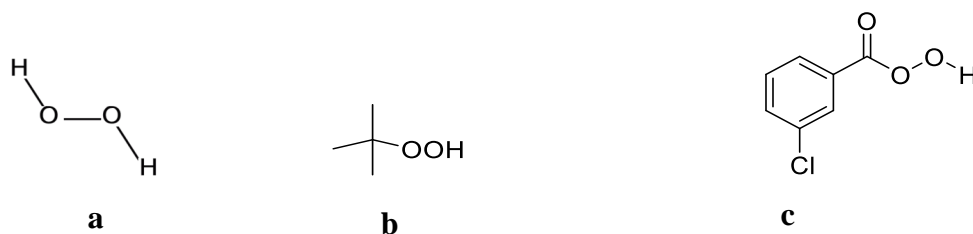


Figure 3.5: the structure of different oxidants, **a**, hydrogen peroxide, **b**, *t*-BuOOH and **c**, *m*-CPBA.

Finally, the catalytic activity of PEG-Fe-porphyrin/mPEG₄₅-PCL₂₅ systems will be compared to the catalytic activity of FeTPP/mPEG₄₅-PCL₂₅ system, to investigate the effect of the unaggregated iron porphyrin on the rate of reaction.

3.3 Result and discussion

In order to study and construct an efficient system that can catalyse organic reactions in water, it is first necessary to modify PEG-porphyrin **10** by inserting iron into the porphyrin. mPEG₄₅-PCL₂₅ diblock **21** micelle which provides an ideal environment for hydrophobic substances; thus, it can be employed as a nano-reactor to test an oxidation organic reaction in water. **Figure 3.6** demonstrates the self-assembly of PEG-Fe-porphyrin **12** and mPEG₄₅-PCL₂₅ diblock **21** into PEG-Fe-porphyrin/mPEG₄₅-PCL₂₅ micelles **18**.

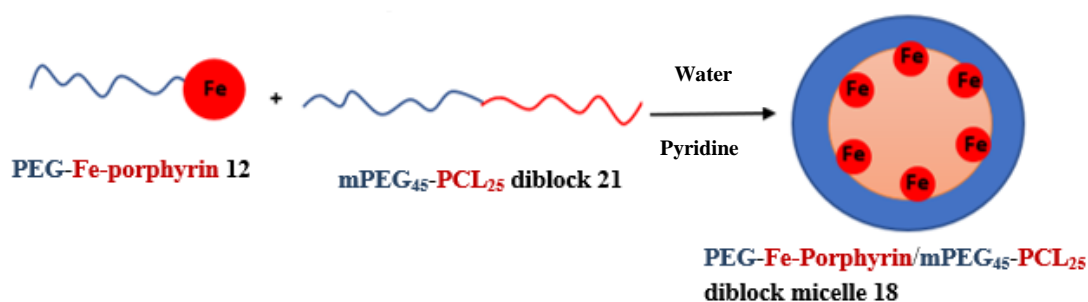
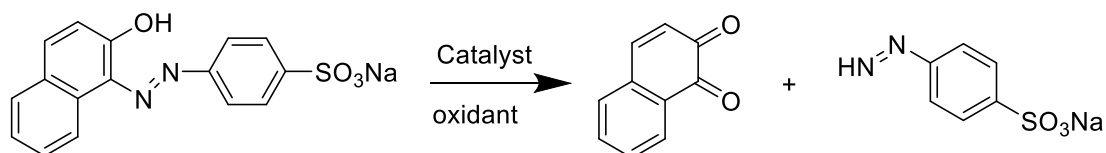


Figure 3.6: the assembly of mPEG₄₅-PCL₂₅ diblock **21** and PEG-Fe-porphyrin **12** into FePorphyrin/mPEG₄₅-PCL₂₅ mixed micelles **18**.

The specific organic reaction in this work is the catalytic oxidation of azo dyes using Fe porphyrins. There are two substrates with different hydrophobicity to choose from: orange II and red oil. Both compounds are simple azo dyes that are commonly used to test many biological and chemical treatments. They are coloured compounds, due to the presence of an azo bond in their structures, which makes the analysis of rates easy via UV-vis spectroscopy.

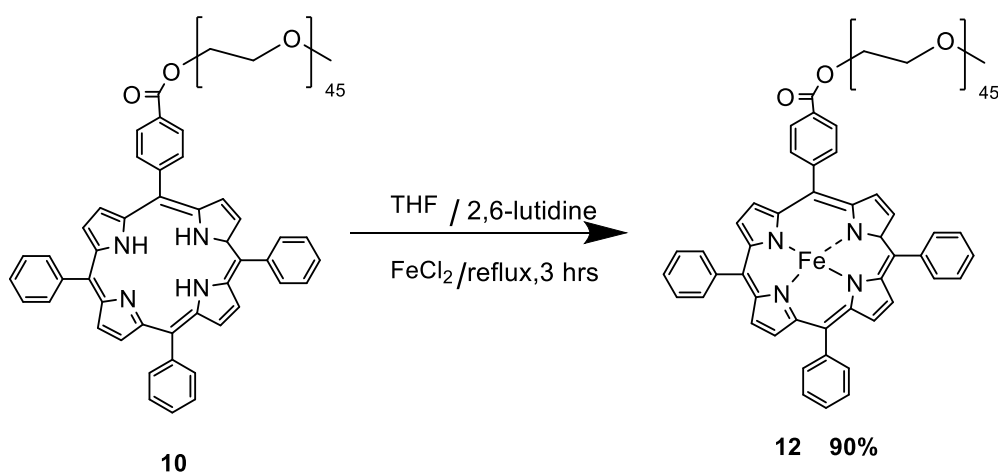
The catalytic oxidation of an azo dye will destroy the azo bond, which leads to the degradation of the compound and loss of colour, as shown in **Scheme 3.3**. This can be followed by an oxidation reaction; a kinetic analysis is then obtained by monitoring the decrease in the orange II and red oil absorption at 486 nm and 513 nm, respectively.



Scheme 3.3: decomposition of Orange II in the presence of oxidant and a Catalyst.

In terms of optimisation, different oxidants, H_2O_2 , *t*-BuOOH and *m*-CPBA, will also be tested. PEG-Fe-porphyrin **12** fully dissolves in water, allowing its catalytic activity to be compared in the presence and absence of diblock micelles.

Fe-TPP **19** is a hydrophobic compound; hence, its catalytic activity may be reduced due to poor solubility and/or aggregation. The catalytic activity of the two catalytic systems, which are Fe-TPP and PEG-Fe-porphyrin **12** in $\text{mPEG}_{45}\text{-PCL}_{25}$ micelles, will be investigated. In addition, the activity of PEG-Fe-porphyrin **12** will also be studied as an aqueous control. The insertion of iron into the free base porphyrins requires the addition of a large amount of iron (II) chloride (**Scheme 3.4**).



Scheme 3.4: the insertion reaction of iron into PEG-porphyrin **10** to form PEG-Fe-porphyrin **12**.

Porphyrin and 2,6 lutidine were added to anhydrous tetrahydrofuran; after refluxing for 15 minutes under nitrogen, iron (II) chloride was added. The mixture was maintained under reflux under nitrogen for 3 hours. Iron (II) was oxidised to iron (III) by exposing the mixture to air and stirring it at room temperature overnight. The purification of PEG-Fe-porphyrin **12** involves the filtration of the crude product to remove the excess iron; THF is then removed by rota-evaporation. This was followed by the addition of dichloromethane (DCM), which was washed with 1 M HCL. The wash was repeated until the aqueous layer became colourless. The organic layer was dried, and the DCM was removed by the rotary evaporation. Purification was carried out using preparative size exclusion to yield the PEG-Fe-porphyrin **12** in 88%. UV-vis indicated a reduction in the number of Q bands, from 4 to 2 (at 509 nm and 654 nm), which confirmed insertion (**Figure 3.7**).

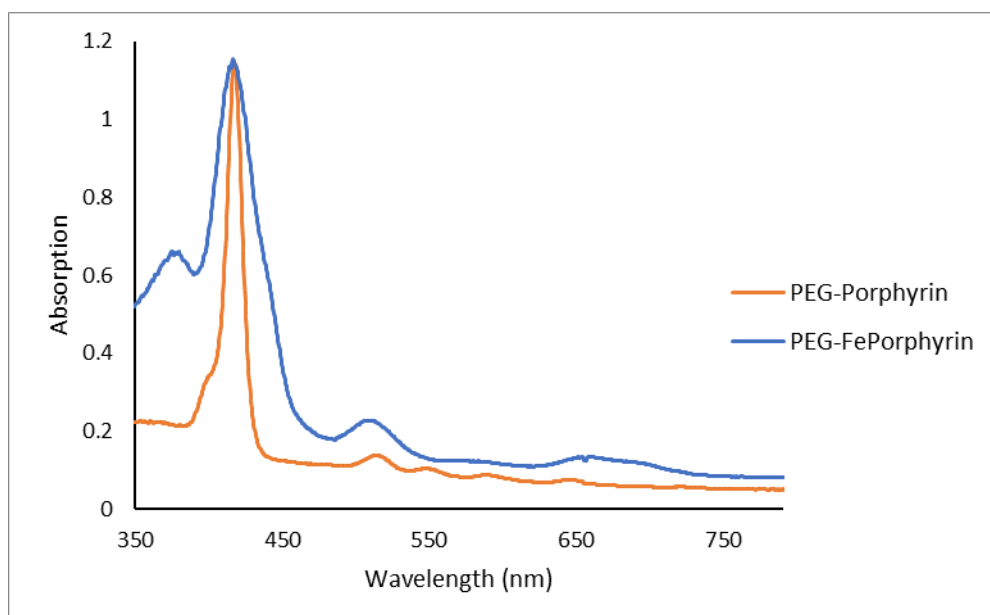


Figure 3.7: UV-vis absorption spectrum of free base PEG-porphyrin (red) and iron inserted PEG-Fe-porphyrin (blue).

In the ^1H NMR spectrum, the porphyrin peaks were significantly broadened, due to the paramagnetic effects of the inserted iron. GPC analysis was used to confirm that PEG was still attached to the iron porphyrin. During analysis, both the UV-vis and RI traces were superimposable and sharp, indicating that PEG-Fe-porphyrin **12** was intact.

Previously, it was demonstrated that the mPEG₄₅-PCL₂₅ diblock micelles could successfully be isolated to protect PEG-porphyrin **10**; it is also expected that it could function similarly for the metallated PEG-Fe-porphyrin **12**. This is important, as it is essential that the catalyst does not aggregate; it is intended to be located in the hydrophobic part of micelles, where the catalytic oxidation reaction is expected to occur. PEG-Fe-porphyrin **12** is more soluble in water than the non-metallized PEG-porphyrin **10**, due to the presence of iron in PEG-Fe-porphyrin **12**. Therefore, simply mixing **12** and mPEG₄₅-PCL₂₅ in water failed to produce the mixed micelle as most of the PEG-Fe-porphyrin **12** remained in water (**Figure 3.8. a**). Therefore, micelles were prepared by dissolving the mPEG₄₅-PCL₂₅ and PEG-Fe-porphyrin **12** in THF containing a small amount of pyridine. Small amounts of this solution were then added to a phosphate buffer (pH=7.4) solution, which was then stirred for two days to evaporate the THF. Specifically, samples were prepared at a diblock concentration of 0.05 mg/mL and PEG-Fe-porphyrin **12** concentration of 0.05 mg/mL, corresponding to a diblock, to PEG-Fe-porphyrin ratio of 1:1. UV-Vis spectroscopy used to confirm that the absorption intensity of PEG-Fe-Porphyrin **12** in micelles was higher than that of a solution in water at the same concentration (**Figure 3.8.b**).

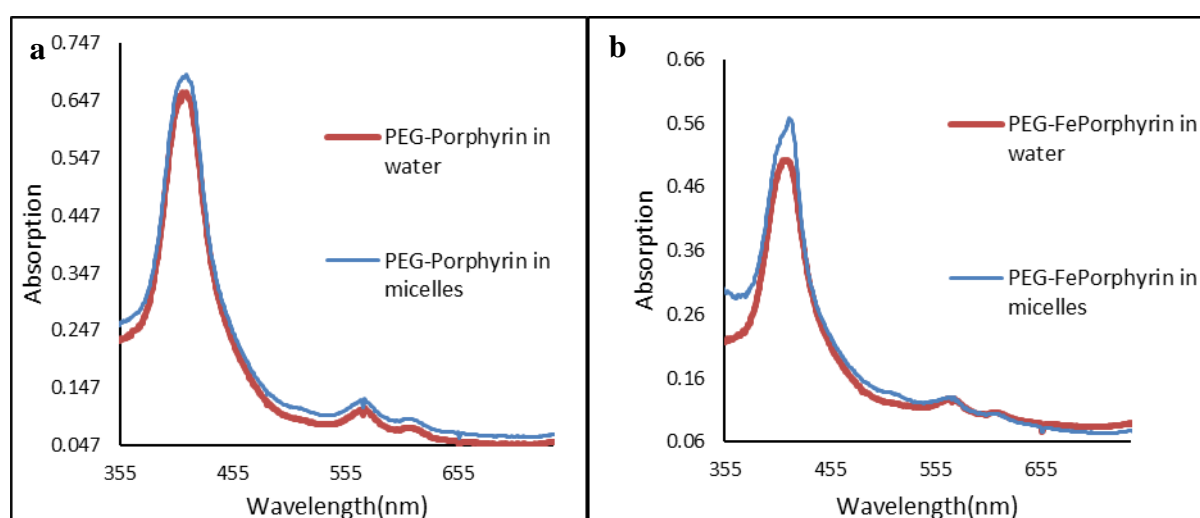


Figure 3.8: the difference of UV-vis absorption spectrum of PEG-Fe-porphyrin **12** in the absence of micelles (red) and PEG-Fe-porphyrin **12** in the presence of micelles (blue) when **a**, simply water

solution of PEG-Fe-porphyrin **12** and diblock mixed, **b**, diblock micelles is prepared with the addition of PEG-porphyrin **12**.

DLS and TEM analysis provided further evidence for the incorporation of PEG-Fe-porphyrin **12** in mPEG₄₅-PCL₂₅ diblock micelles **18**. As evident from **Figure 3.9 a** and **b**, the micelles are almost monodispersed in nature and the size of PEG-Fe-porphyrin/ mPEG₄₅-PCL₂₅ micelle **18** was around 200 nm. TEM shows a spherical particle of micelle with a diameter of almost 100 nm. Almost an identical result was obtained from PEG-porphyrin/ mPEG₄₅-PCL₂₅ micelles **13**. TEM measures the size of micelle in the dry sample whereas DLS analysis measures the swollen and solvated micelles (swollen due to the water). As a result, the sizes of micelles that are observed by TEM are smaller than those measured by DLS analysis.

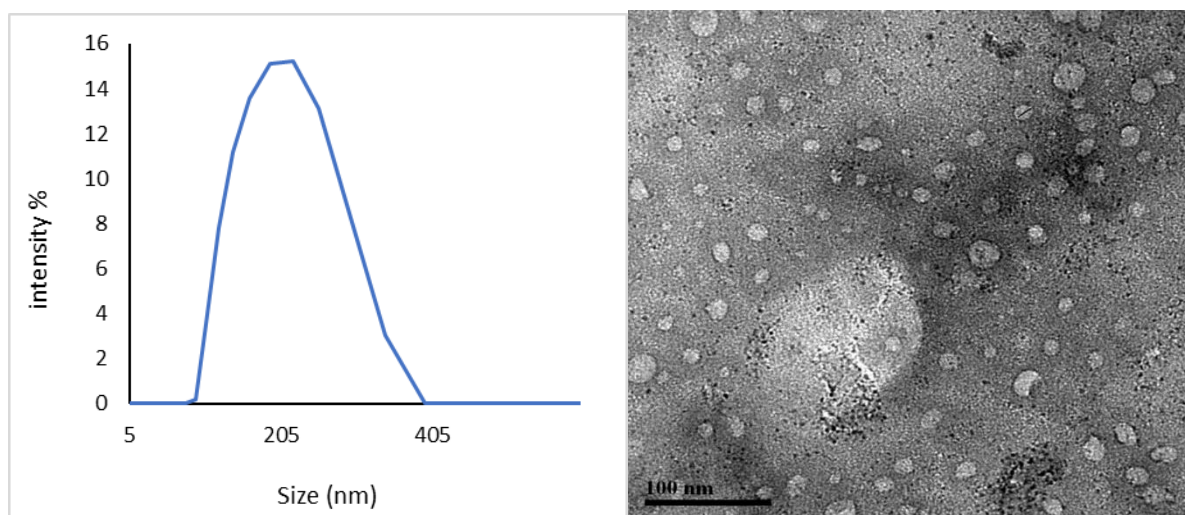


Figure 3.9: DLS data **a** and **b**, TEM of PEG-Fe-porphyrin/ mPEG₄₅-PCL₂₅ **18** micelles.

Overall, the results confirm the formation of micelles and verify that the insertion of iron does not change their morphology. The catalytic activity of this designed system is discussed in the next section.

3.3.1 The catalytic activity of PEG-Fe-porphyrin/ mPEG₄₅-PCL₂₅ diblock micelle **18**

The degradation of orange II was detected by monitoring the decrease in orange II absorption rates at 486 nm. Apparently, no changes were observed when PEG-Fe-porphyrin **12** (catalyst)

was absent from the orange II micelles solution. However, a rapid decrease in absorption was detected for the orange II solution that contained PEG-Fe-porphyrin/ mPEG₄₅-PCL₂₅ micelles **18** and, oxidant (**Figure 3.10**). To investigate the importance of our ordered PEG-Fe-porphyrin/ mPEG₄₅-PCL₂₅ micelles **18** as a catalyst for oxidation reaction, one should first carefully select the reactants. There are three different oxidants with diverse hydrophobicity: *m*-CPBA, H₂O₂ and *t*-BuOOH; they were tested to oxidize orange II in the presence of PEG-Fe-porphyrin/ mPEG₄₅-PCL₂₅ micelles **18** as a catalyst (**Figure 3.11**). Among the three oxidants, *m*-CPBA was expected to give the highest oxidation rate. This is due to the hydrophobicity of *m*-CPBA (not being dissolved in water), which allowed this compound to access the hydrophobic part of the micelles and to react with iron porphyrin to form the active intermediate (Fe^V = O) that can oxidise orange II whereas H₂O₂ and *t*-BuOOH are water-soluble, so they remained in the solution, unable to react with PEG-Fe-porphyrin **12**.

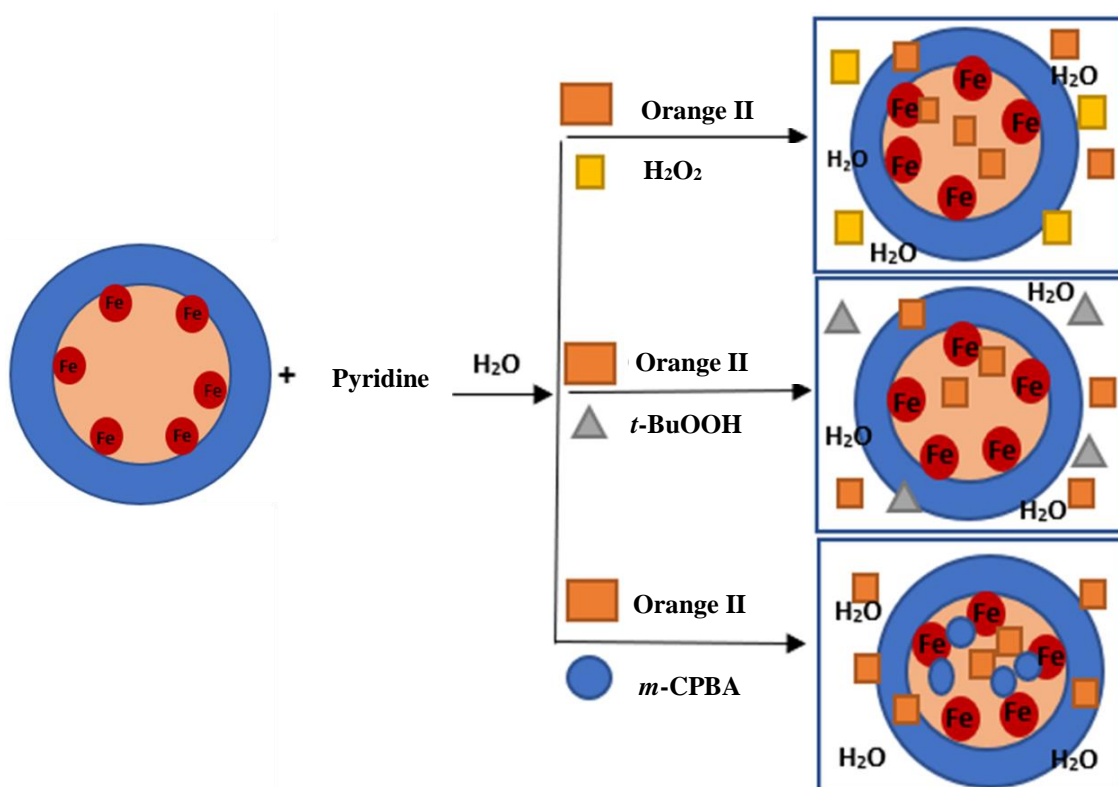


Figure 3.10: the assembly of the catalytic oxidation reaction of orange II with different oxidants (H₂O₂, *t*-BuOOH, *m*-CPBA) and PEG-Fe-porphyrin/ mPEG₄₅-PCL₂₅ micelle **18** as a catalyst.

The kinetics of the oxidation reaction was examined using UV-vis spectroscopy. The reaction was studied in a glass cuvette containing a stirring bar, the 0.025 mg/mL PEG-Fe-porphyrin/mPEG₄₅-PCL₂₅ **18** micelles (the ratio of PEG-Fe-porphyrin **12** to mPEG₄₅-PCL₂₅ diblock was 1: 1), 0.035 mM of the orange II substrate, 0.14 mM and 2.5 mM of the oxidant (0.01 M) (H₂O₂, *t*-BuOOH, *m*-CPBA). The absorption of orange II at 486 nm was measured every 10 seconds for 60 minutes. The calculated molar absorption coefficient of orange II at 484 nm was 29000 M⁻¹cm⁻¹. The natural logarithm of the (C_o/C_t) where C_o and C_t are the concentrations of orange II at time zero (C_o) and time t (C_t), was plotted vs time. **Table 3.1** shows rate constant (K_{obs}) value that was calculated from plot, the straight-line part (based on the first-order kinetics). Following equation 1

$$\ln \left(\frac{C_o}{C} \right) = k_{obs} t \quad (1)$$

As shown in **Figure 3.11**, the rate of oxidation catalysed by PEG-Fe-porphyrin/ mPEG₄₅-PCL₂₅ **18** micelles was significantly faster when *m*-CPBA was used (0.068 min⁻¹), with no significant change absorption when H₂O₂ and *t*-BuOOH were employed as oxidants, and their constant rates were 0.0008 min⁻¹ and 0.0018 min⁻¹, respectively.

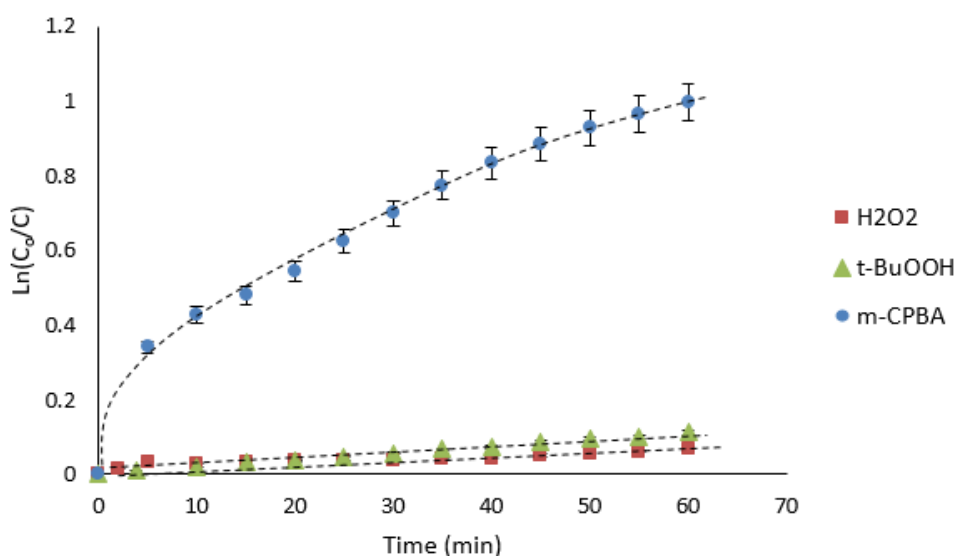


Figure 3.11: the kinetic study of the catalytic oxidation reaction of orange II which involves different oxidants (H_2O_2 , $t\text{-BuOOH}$, $m\text{-CPBA}$) and PEG-Fe-porphyrin/ mPEG₄₅-PCL₂₅ micelle **18** as a catalyst (data point collected every 10 seconds. Some data points are omitted for clarity).

Despite the fact that $t\text{-BuOOH}$ is more stable and less soluble in water than H_2O_2 , the rate of reaction was almost similar. Unlike $m\text{-CPBA}$, the activity of $t\text{-BuOOH}$ as an oxidant increases in the presence of a co-catalyst, such as pyridine. However, the role of pyridine as co-catalyst is only effective in water since it is water soluble. Therefore, the catalytic activity of PEG-Fe-porphyrin/ mPEG₄₅-PCL₂₅ **18** micelles was higher 88% when $m\text{-CPBA}$ was used as oxidant than $t\text{-BuOOH}$.

Table 3.1: k_{obs} value of the orange II oxidation reaction with different oxidant and PEG-Fe-porphyrin/ mPEG₄₅-PCL₂₅ **18** micelles.

Oxidant	k_{obs} (min^{-1})
H_2O_2	0.0008
$t\text{-BuOOH}$	0.0018
$m\text{-CPBA}$	0.068

The PEG-Fe-porphyrin component **12** is water-soluble in the absence of the micelle. To study the effect of the micelle environment on the rate of oxidation, a control reaction was performed using PEG-Fe-porphyrin **12** as a catalyst. The results would be compared to oxidations using mPEG₄₅-PCL₂₅ micelles without a catalyst, and PEG-Fe-porphyrin **12** in mPEG₄₅-PCL₂₅ micelles. For all of these reactions, $m\text{-CPBA}$ was used as the oxidant and 5% of pyridine was also added as a co-catalyst. For some of these experiments, a small amount of baseline drift was observed (between readings). To overcome this, the change in the absorption between 498.5 nm and 503.5 nm was used, where the calculated molar Δ absorption coefficient of orange II was $331.43 \text{ M}^{-1} \text{ cm}^{-1}$. As it is apparent from the graph in **Figure 3.12**, the oxidation reaction did not occur in the absence of a catalyst.

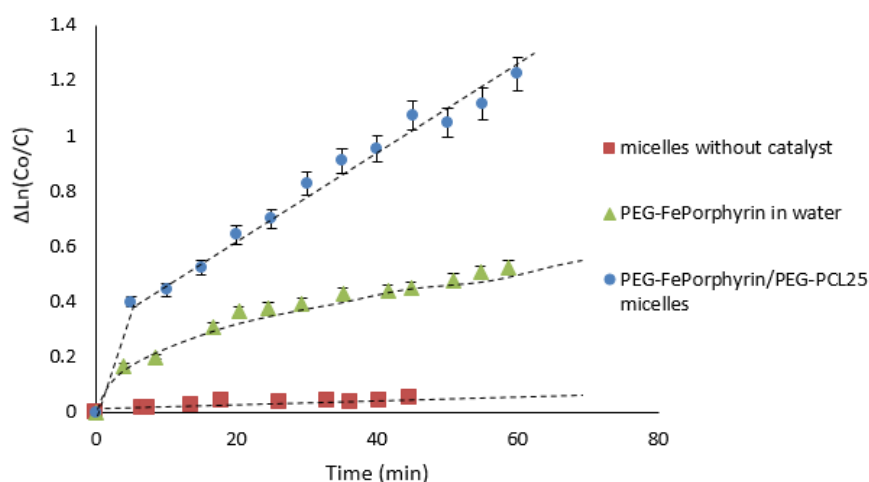


Figure 3.12: the kinetic study of the catalytic oxidation reaction of orange II with *m*-CPBA as oxidants and Fe-porphyrin **12** with and without micelles as a catalyst (data point collected every 10 seconds. Some data points are omitted for clarity).

Table 3.2: k_{obs} value of the orange II oxidation reaction with *m*-CPBA and different catalytic systems

Catalyst	k_{obs} (min^{-1})
Micelles without catalyst	0.0009
PEG-Fe-Porphyrin in water	0.00175
PEG-Fe-Porphyrin/mPEG-PCL25 micelle	0.079

The best system was the micelle containing the PEG-Fe-porphyrin **12** catalyst as the constant rate was significantly higher, 0.079 min^{-1} , compared to other two systems (**Table 3.2**). The catalytic activity of PEG-Fe-porphyrin/ mPEG45-PCL25. 18 micelles increased with 58% more than the catalytic activity of PEG-Fe-porphyrin without micelles. However, some oxidation was observed for the control reaction using PEG-Fe-porphyrin **12** as the catalyst (0.00175 min^{-1}). Therefore, PEG-Fe-porphyrin **12** is a reasonable catalyst, despite the use of a hydrophobic oxidant. This is due to the PEG chain which can coil around the Fe-porphyrin to form a hydrophobic microenvironment (nano-reactor) that allows *m*-CPBA and orange II to

interact with the Fe-porphyrin. This is also due to the amphiphilic property of orange II, which is soluble in water in any hydrophobic environment (such as the one provided by PEG-Fe-porphyrin **12**). Afterwards, it would be interesting to study the same PEG-Fe-porphyrin **12** system, but with a water-soluble oxidant. As such, the reaction was repeated using *t*-BuOOH as the oxidant and the result is presented in **Figure 3.13**, with the result of the micelle catalyst (using *m*-CPBA as oxidant) for comparison.

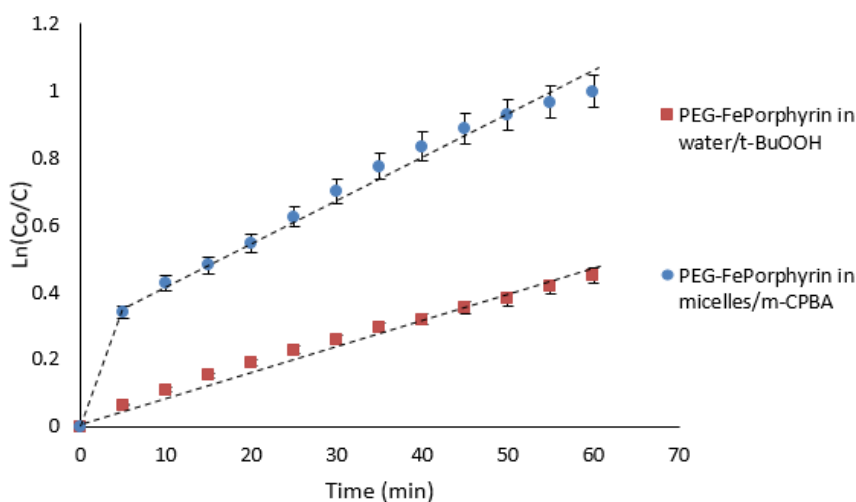
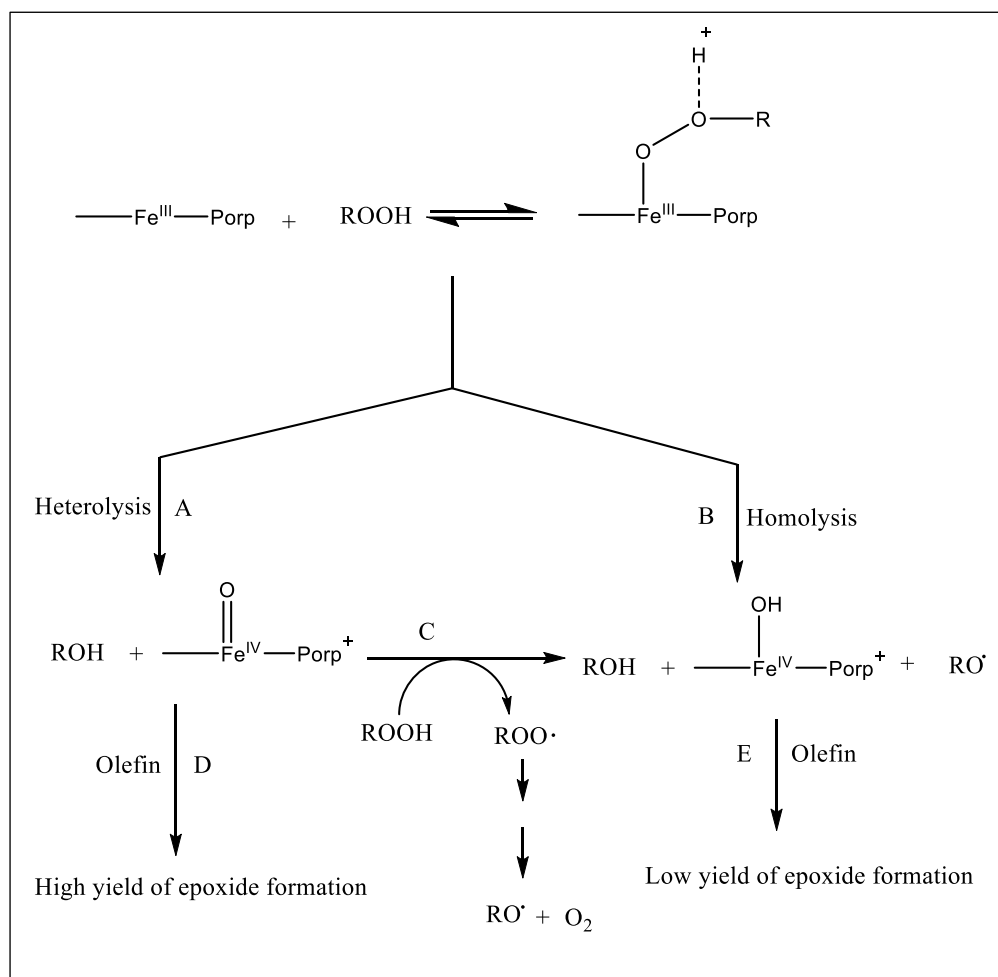


Figure 3.13: the kinetic study of the catalytic oxidation reaction of orange II in two different catalytic systems, PEG-Fe-porphyrin in micelles **18** /*m*-CPBA (blue), and PEG-Fe-porphyrin **12** /*t*-BuOOH (red).

The results clearly display that this micelle system **18** (0.068 min^{-1}), outperforms the PEG-Fe-porphyrin **12** without micelles (0.007 min^{-1}), and it increased with 55%. Therefore, it is in fact the best catalyst studied so far. The main reason was that the catalyst in the micelles was completely isolated from water which may compete with oxidant for coordination with iron whereas the hydrophobic microenvironment is formed by only PEG-Fe-porphyrin **12** which is unstable and it may be exposed to water. Unlike *t*-BuOOH, *m*-CPBA does not need pyridine to be activated (some of the pyridine was protonated in the water phase). This result further confirms that *m*-CPBA is an ideal oxidant for this reaction. This result is consistent with Nam *et al.*¹⁴⁰ found out that different oxidations (H_2O_2 , *t*-BuOOH, *m*-CPBA and 2-methyl-1-phenyl-2-propyl hydroperoxide (MPPH)), different porphyrin complexes of iron(III) and ligands that contained the electron

withdrawal and donation substituents were used to determine the heterolytic mechanisms against homolytic O-O bond cleavage of the oxidant through Fe-porphyrin and to highlight how the type of cleavage affects the yield of the catalytic peroxidation reaction of alkene. They concluded that the low yield of the epoxidation product is an evidence of the homolytic O-O bond cleavage, due to the fact that the resulting (OH) radical destroys the Fe-porphyrin (**Scheme 3.5, pathway D**) whereas, the high yield of peroxide is an evidence of the heterolytic O-O bond cleavage (**Scheme 3.5, pathway E**). Among the different oxidants, *m*-CPBA achieved the highest yield as the acyl substitution is an electron withdrawing group that facilitated the heterolytic O-O bond cleavage. On the other hand, the electron donating substitution in *t*-BuOOH and MPPH facilitated the homolytic O-O bond cleavage. The addition of ligand changes the electronic nature of iron complex.



Scheme 3.5: pathway of homolytic O-O bond cleavage (E) and heterolytic O-O bond cleavage (D) of hydroperoxide.

In their investigation of the axial ligand effect, the researcher found that the yield of the epoxidation reaction was high when *m*-CPBA was used, and that the axial ligand had no influence on the yield; besides, the

epoxide yield was independent of the electronic nature of Fe-porphyrin in *m*-CPBA reaction. In contrast to the H₂O₂, *t*-BuOOH and MPPH reaction, the amount of product was considerably influenced by the nature of imidazole binding the Fe-porphyrin. This means that the yield depended on the electronic nature of the Fe-porphyrin.

Orange II is not a completely hydrophobic substrate; however, its amphiphilic nature allows it to penetrate the micelles. To ensure that the catalytic reaction can only occur inside the micelles, a more hydrophobic dye was studied. Red oil is an azo dye that is very hydrophobic; it is absorbed at 513 nm, which makes it ideal as a test substrate, as it can only be solubilised by entering the micelle, where all the other reaction components are located, as displayed in

Figure 3.14.

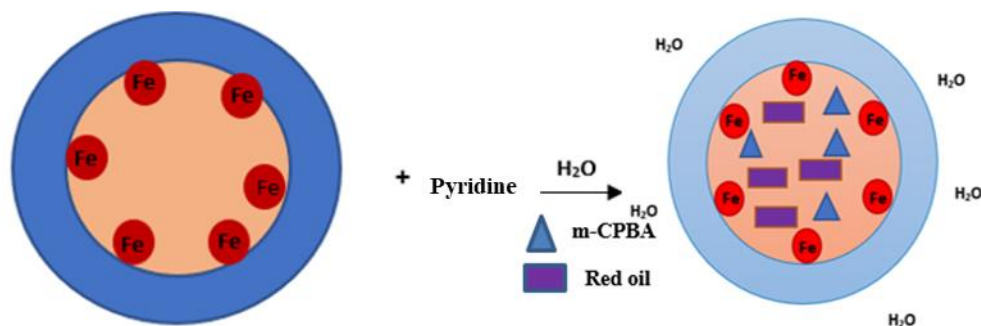


Figure 3.14: the assembly of the catalytic oxidation reaction of red oil with *m*-CPBA and FePorphyrin/ mPEG₄₅-PCL₂₅ micelle **18** as a catalyst.

The catalytic oxidation reaction of red oil was carried out in the same way as that described for orange II. Three experiments were carried out: the PEG-Fe-Porphyrin/mPEG₄₅-PCL₂₅ micelles **18**, the PEG-FePorphyrin**12** and mPEG₄₅-PCL₂₅ diblock micelles without the catalyst. The change in red oil absorption between 519 nm and 524 nm for three experiments occurred due to base line drift. The calculated molar absorption coefficient of oil red using this difference in absorption was 290.38 M⁻¹ cm⁻¹. For the control reaction, using the PEG-Fe-porphyrin **12**, the solution was colourless, with no absorption band at 513 nm. This indicated that the hydrophobic red oil was not dissolved and that the PEG chain could not provide a suitable environment to solubilise the substrate. On the other hand, the solutions were red for both the

PEG-Fe-porphyrin/mPEG₄₅-PCL₂₅ micelle solution **18** and the mPEG₄₅-PCL₂₅ diblock micelle solution. This confirmed that the substrate was dissolved and that a micelle was required to solubilise the hydrophobic oil red. The catalytic activity of these two micelle solutions was monitored by plotting $\Delta \ln(C_0/C)$ as a function of time. Although no changes in absorption were observed for the micelle that did not contain the PEG-Fe-porphyrin **12**, there was a significant change when the porphyrin containing micelle **18** was used (**Figure 3.15**).

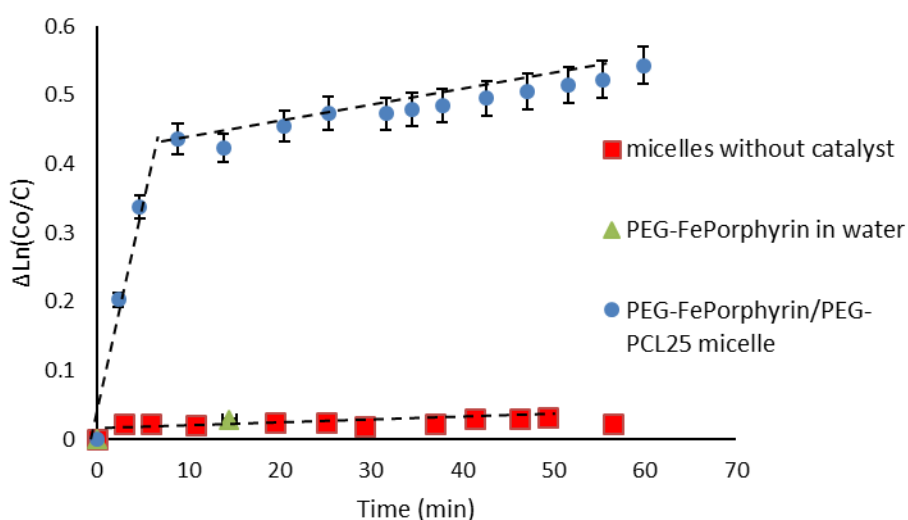


Figure 3.15: the kinetic study of the catalytic oxidation reaction of red oil with different *m*-CPBA as oxidants and PEG-Fe-porphyrin **12** with and without micelles as a catalyst (data point collected every 10 seconds. Some data points were omitted for clarity).

Table 3.3: k_{obs} value of the red oil oxidation reaction with *m*-CPBA and different catalytic systems

Catalyst	k_{obs} (min^{-1})
Micelles without catalyst	0.0003
PEG-Fe-Porphyrin in water	-
PEG-Fe-Porphyrin/mPEG-PCL25 micelle	0.072

The constant rate of the oxidation reaction with PEG-Fe-porphyrin/ mPEG₄₅-PCL₂₅. **18** as catalyst was drastically higher (0.072 min^{-1}) than the constant rate of micelles without catalyst

(0.0003 min^{-1}) (**Table 3.3**). This result confirms that the uncontrolled microenvironment provided by the PEG chain in PEG-Fe-porphyrin structure does not serve as a suitable host for both red oil and *m*-CPBA. However, as all reactants are hydrophobic, the PEG-Fe-porphyrin/mPEG₄₅-PCL₂₅ **18** micelles could provide a perfect environment and high catalytic activity for this reaction, and the catalytic reaction was 95% higher than non-catalytic reaction. It was noticed that the constant rate of oxidation reaction of orange II and red oil with *m*-CPBA, when the reaction were catalysed by PEG-Fe-porphyrin/PEG-PCL₂₅ micelle **18** almost same ($\text{Ca } 0.07 \text{ min}^{-1}$). However, if both substrates are compared, it can be observed that the catalytic decolourisation of orange II was almost twice as high as red oil. Although this was initially interesting, it was realised that it was probably due to simple stoichiometry, as there are two azo bonds in red oil structure, but only one in orange II (**Figure 3.16**).

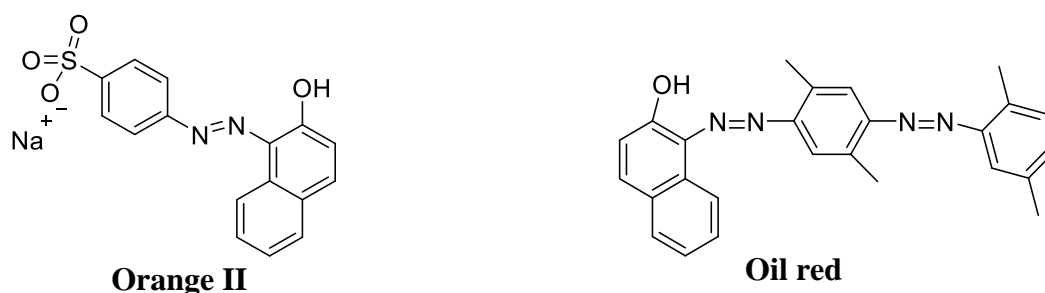
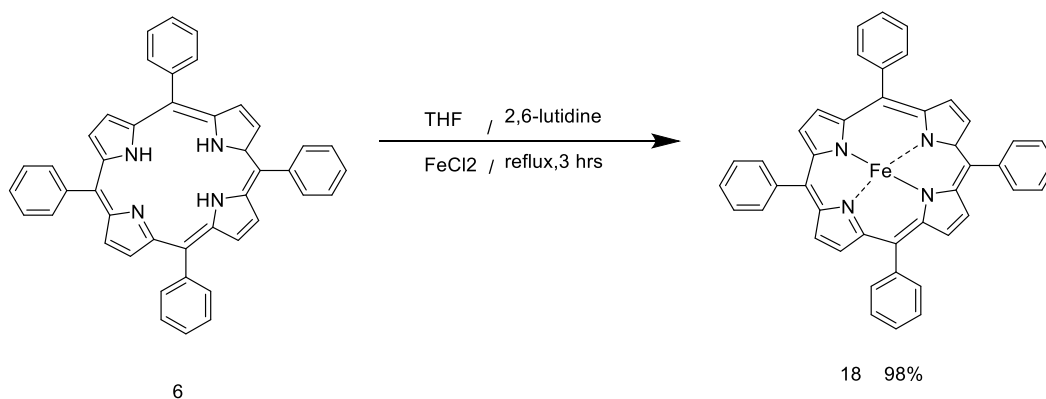


Figure 3.16: the structures of orange II and red oil.

At this stage, the confirmation of the hypothesis regarding the use of the PEG tether as an important step to prevent porphyrin from aggregation, and it was actually superior to a simpler micelle system that just encapsulated free Fe-TPP. To investigate this further, the catalytic activity of a Fe-porphyrin/mPEG₄₅-PCL₂₅ micelles system was studied. porphyrin (Fe-TPP) **19** was selected as a catalyst. This was synthesised from TPP **6** using the same method described for PEG-Fe-porphyrin **12** (**Scheme 3.6**).



Scheme 3.6. The insertion reaction of iron to TPP **3** to form Fe-TPP **19**.

The UV-vis spectrum of Fe-TPP **19** (**Figure 3.17**) was broader than that of TPP **3**; this mainly indicated the insertion of iron into TPP.

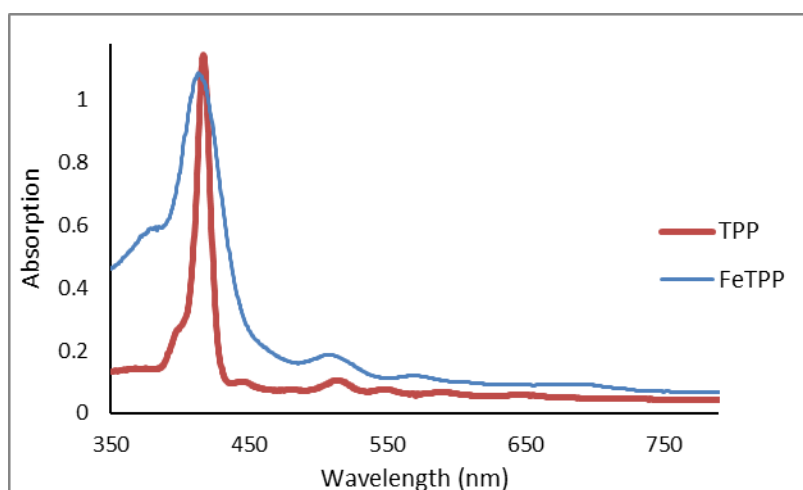


Figure 3.17: UV-vis absorption spectrum of free base TPP **12** (red) and Fe-porphyrin **19** (blue), 4×10^{-6} M in DCM.

The Fe-TPP/mPEG₄₅-PCL₂₅ **20** micelle catalytic system (**Figure 3.18**) was prepared using the same procedure described for the PEG-Fe-porphyrin/mPEG₄₅-PCL₂₅ diblock micelles **18**. Encapsulation of Fe-TPP **19** was confirmed by UV-vis spectroscopy, which indicated a sharp peak at 418 nm (Fe-TPP is completely insoluble in water and no signal was observed). DLS indicated that Fe-TPP/mPEG₄₅-PCL₂₅ micelles **20** had a diameter around 235 nm.

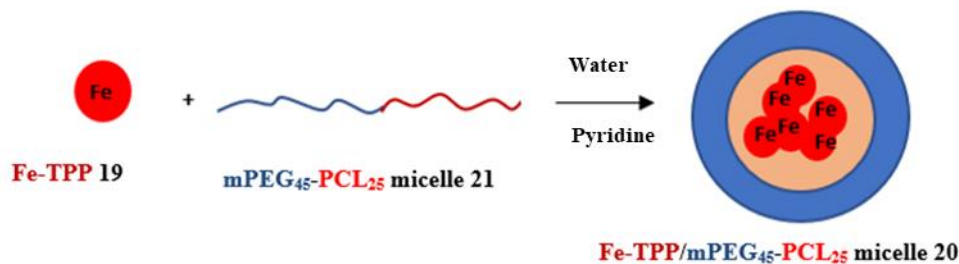


Figure 3.18: the assembling of mPEG₄₅-PCL₂₅ diblock **21** and Fe-TPP **19** in water.

The catalytic activity of the PEG-Fe-Porphyrin/mPEG₄₅-PCL₂₅ diblock micelle **18** compared to the Fe-TPP/mPEG₄₅-PCL₂₅ **20** diblock micelle was investigated by studying the oxidation reaction of red oil with *m*-CPBA as the oxidant. A control reaction using just the Fe-TPP **19** (no micelles) was also carried out. For all experiments, the same procedure that was previously used to oxidise red oil with *m*-CPBA was applied. For all reactions, $\Delta\ln(\text{Co}/\text{C})$ was plotted against time and the results are exhibited in **Figure 3.19**.

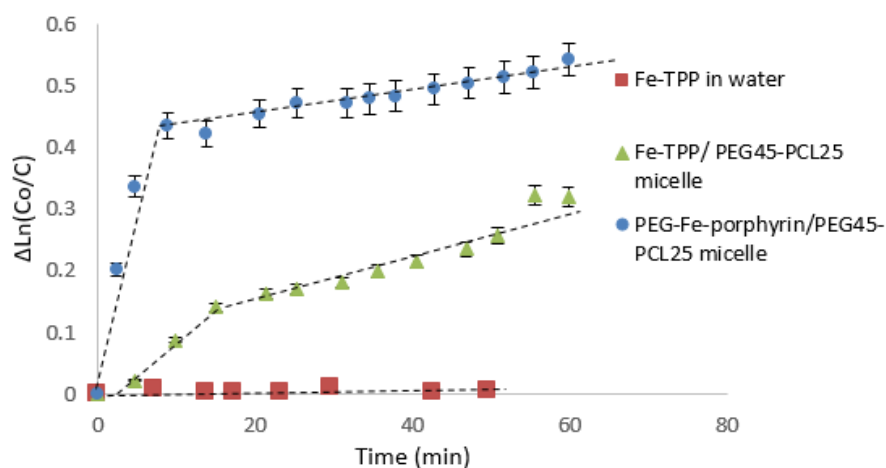


Figure 3.19: the kinetic study of the catalytic oxidation reaction of red oil o with *m*-CPBA and different catalyst systems Fe-TPP (red), Fe-TPP/ mPEG₄₅-PCL₂₅ micelle (grey) and ordered PEG-Fe-porphyrin/ mPEG₄₅-PCL₂₅ micelle **18** (blue).

Table 3.4: k_{obs} value of the red oil oxidation reaction with *m*-CPBA and different catalytic systems

Catalyst	k_{obs} (min^{-1})
FeTPP in water	0.00004
FeTPP/ mPEG-PCL25 micelle	0.0098
PEG-Fe-Porphyrin/mPEG-PCL25 micelle	0.072

The results indicate that the oxidation reaction of the red oil did not occur for the control purpose due to a lack of solubility (and aggregation). However, it occurred when the reaction was catalysed by both micelle systems, **18** and **20**. Nonetheless, there was a significant difference (40%) between the catalytic activities of the two micelle systems, with the rate of oxidation being faster when the ordered PEG-Fe-porphyrin/mPEG₄₅-PCL₂₅ system **18** was used, 0.072 min^{-1} . The rate was 0.0098 min^{-1} for the reaction in FeTPP/ mPEG-PCL₂₅ micelle **20** system (**Table 3.4**). This outcome was attributed to the high aggregation tendency of iron porphyrin, which reduced the catalytic activity of the porphyrin. Therefore, the diblock micelle **20** reduced the aggregation, but it did not eliminate it. The non-aggregated PEG-porphyrins inside mPEG₄₅-PCL₂₅ micelle **18** were able to catalyse the reaction in an optimised way. If they were aggregated, then the rate would have been similar for the two micelle systems **18** and **20**.

This was inspired by Heijnen *et al.*¹³⁸ system using micelles as a nano-reactor to perform the reaction where all reactants are hydrophobic. They incorporated separately 5,10,15,20-tetrakis (phenyl) porphyrin manganese (III) chloride (Mn (TPP)Cl) and 5,10,15,20-tetrakis (2,6-dichlorophenyl) porphyrin manganese (III) chloride (Mn (TDCPP)Cl) into micelles to catalyse the epoxidation reaction of propene and 1-octene with H₂O₂. Their results displayed that the catalytic activity of Mn (TDCPP) Cl/micelles was higher than the catalytic activity of Mn (TPP) Cl/micelles. This was due to the fact that Mn (TPP) Cl had higher tendency to aggregate

compared to Mn (TDCPP) Cl. Additionally, the chloride substitution in Mn (TDCPP) Cl structure which is an electron withdrawing group was another reason for the increased activity in Mn (TDCPP) Cl/micelles. However, the epoxide yield was low; this was caused by H₂O₂ and imidazole (axial ligand) that were hydrophilic compounds. Therefore, only few amounts were diffused inside micelles and they reacted with the catalyst and substrate. In the proposed system, not only the aggregation problem was addressed by isolating Fe-Porphyrin within micelles by attaching PEG but also the reactants were carefully selected (all are nonpolar compounds). Nango *et al.*¹⁴¹ attached the PEG chain to manganese halogenated porphyrins and employed them as a catalyst in the oxidation reaction of orange II with H₂O₂. All the selected reactants were water soluble. **Table 3.5** illustrates the constant rate of oxidation reaction using different halogenated porphyrins as catalysts (Mamoru systems) and the constant rate of reaction in the developed micelle system.

Table 3.5: the constant rate of oxidation reaction of orange II with H₂O₂ and different halogenated porphyrins as catalyst (Mamoru systems) and the constant rate of reaction in our micelle system.¹⁴¹

k _{obs} (10 ² min ⁻¹)		
catalyst	none	ligand
none	0.05	0.05
PEG-MnDCPPBr ₈	0.05	0.05
PEG-MnDCPP	0.13	14
PEG-MnPFPP	0.26	0.34
PEG-MnPFPPBr ₈	0.05	0.05
PEG-FePorphyrin/micelle ^a	6.8	-

a: The oxidation of orange II with *m*-CPBA and PEG-FePorphyrin/micelle as catalyst.

Although the halogen substitution group increases the catalytic activity and stability, the results indicate that the suggested system (PEG-Fe-Porphyrin/PEG-PCL₂₅ micelle) has extremely

higher constant rate than the Mamoru systems when the ligand was absent from the systems. However, in the presence of ligand, PEG-MnDCPP was twice higher than the micelles system. In contrast to the proposed system, Mamoru systems contain no micelles; therefore, they will be less selective when the all reactant are non-polar.

3.4 Conclusion:

The aim of the current research was two-fold; firstly, to design and study a system that could efficiently catalyse an organic reaction in water and secondly to highlight the advantages of the PEG chain for preventing catalyst aggregation. The study also aimed illustrated the benefits of using a polymeric micelle as a nano-reactor for an organic reaction. To realize these aims, experimental methodologies were developed and applied to optimise the oxidizing agent, substrate and reaction conditions.

We initially tested three oxidants and identified *m*-CPBA as the best, by virtue of its higher hydrophobicity (when compared to H₂O₂ and *t*-BuOOH). The first substrate studied was orange II, which has an amphiphilic structure. When *m*-CPBA was used, the Fe-porphyrin/mPEG₄₅-PCL₂₅ micelle **18** proved to be a good catalyst. However, when the PEG-Fe-porphyrin chain **12** was employed without micelles, appreciable catalysis was also observed. This was due in part to the amphiphilic properties of the substrate, but also the PEG chain, which could coil around the porphyrin and provide a “loose” hydrophobic environment that was good enough to encapsulate some of the hydrophobic *m*-CPBA oxidant. In fact, a very fast reaction was observed when *m*-CPBA was replaced with the more hydrophilic oxidant *t*-BuOOH. In this case all species were water soluble, leading to a fast reaction. As well as helping solubilise the porphyrin, the PEG chain was also able to provide a steric barrier that prevented the porphyrins from aggregating in water. In an effort to optimise the system, the hydrophobic substrate

known as red oil was then studied. For this substrate, the only effective system was the PEG-Fe-porphyrin/mPEG₄₅-PCL₂₅ micelle **18**, with no reaction being observed for the simple PEG-Fe-porphyrin **12**. Furthermore, the PEG-Fe-porphyrin/mPEG₄₅-PCL₂₅ micelle **18** had higher reactivity towards red oil than it did to orange II.

To confirm the importance of the micelle and the use of the PEG chains to isolate the porphyrins within the structure, control reactions were carried out using a simple porphyrin system (without the PEG chain), specifically, Fe-TPP **19** and the same porphyrin encapsulated within a diblock micelle (Fe-TPP/mPEG₄₅-PCL₂₅ micelle **20**.) The results showed that the Fe-TPP **19** without micelle completely failed to catalyse the oxidation reaction, due to its poor solubility and propensity to aggregate in water. Although there was some oxidation when the Fe-TPP/mPEG₄₅-PCL₂₅ micelle **20**, was used, the reaction was slower than the more ordered PEG system (PEG-Fe-porphyrin micelle system **18**). This was due to the very high localised concentration of Fe-TPP **19** within the micelle, resulting in internal aggregation within the micelles core.

Overall, these results highlight the importance of using micelles as nano-reactors for organic reactions in water. The data also emphasised the significant contribution of the PEG chain (in the PEG-Fe-porphyrin **12** structure), which locks the porphyrin within the micelle matrix and prevents aggregation. Although many have studied the potential of the metalloporphyrin micelles as catalyst, this new PEG based systems represent one of the simplest methods for solving the problem of porphyrin aggregation. There are number important changes which need to be made to improve the system. One way is to add halogen substitutions on the phenyl at meso position of PEG-Fe-porphyrin. This will increase the stability of catalyst against oxidation. Another approach is, the use of diblock copolymer that its formed micelles serves not only as nanoreactor, but also as axial ligands. For example, poly (ethylene glycol)-block-poly (4-vinylpyridine) (mPEG-b-P4VP). **Figure 3.18** showed how PEG-Feporphyrin **12** co-

assembles with mPEG-b-P4VP. It is hoped, these and similar systems could be employed as an artificial peroxidase that could compete with the natural peroxidase enzymes.

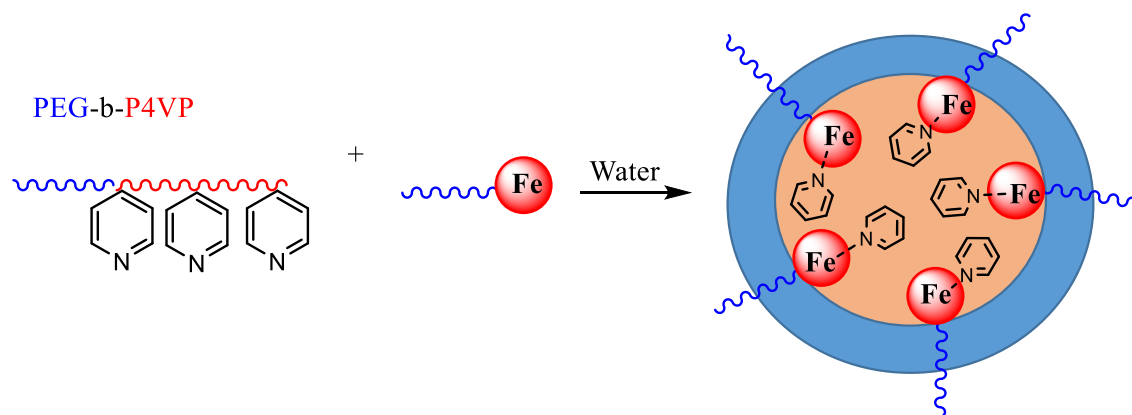


Figure 3.18. The assembly of mPEG45-P4VP diblock and PEG-Fe-porphyrin 12 into FePorphyrin/mPEG45-P4VP mixed micelles.

Chapter 4 - Experimental:

4.1 Chemicals and Apparatus

Methoxypoly (ethylene glycol) (mPEG, $M_n=2000$ g/ml) was purchased from Sigma-Aldrich and purified by azeotropic distillation with dry toluene and dried to constant weight under vacuum at 30 °C before use ϵ -caprolactone (ϵ -CL) ($M_w=114.14$) was purchased from Sigma-Aldrich and calcium hydride was added to ϵ -CL and left for two days and then was dried by azeotropic distillation. Pyrene was purchased from Sigma-Aldrich, pyrrole was purchased from Sigma-Aldrich and purified by distillation under reduced pressure. The following were purchased from Sigma-Aldrich and directly used without further purification: Stannous-II octoate ($\text{Sn}(\text{Oct})_2$); benzaldehyde; methyl 4-formyl benzoate; propionic acid; methanol; petroleum ether; dichloromethane; hexane; tetrahydrofuran; potassium hydroxide; sodium hydrogen carbonate; hydrochloric acid; magnesium sulfate; anhydrous dichloromethane; grained dicyclohexyl carbodiimide (DCC); 4-dimethylaminopyridine (DMAP); sodium hydroxide; 3-nitrophthalonitrile; 1-pentanol; 1-chloronaphthalene (1-CNP); tin(II)chloride, tosyl chloride; hydroxylammonium (NH_4OH); red oil o; orange II; hydrogen peroxide (H_2O_2) and 3-Chloroperbenzoic acid (*m*-CPBA). 1,5,7-triazabicyclo[4.4.0]dec-5-ene (TBD) was provided from the Spain group. Distilled-deionized water was prepared with Milli-Q plus System (Elix 10, Millipore Corp. India).

4.2 Instrumentation

^1H NMR spectra were measured on a Bruker BioSpin ADVANCED 400 MHz spectrometer (from Bruker BioSpin Billerica, MA, USA) at room temperature. Characterisation by ^1H and ^{13}C were recorded at 400 MHz and 100 MHz respectively at room temperature with tetramethylsilane (TMS) as an internal standard. All the chemical shifts were quoted in ppm

and referenced internal solvent signal calibrations. Residual solvent peaks were assigned according to Gottlieb *et al.*, *J. Org. Chem.*, 1997, 62, 7512. NMR spectra were recorded using Chemical shifts are quoted in parts per million (ppm). MestReNova version 6.0.2-5475 was used to analyse the NMR spectroscopy data generated.

A Perkin-Elmer Paragon 100 FT-IR machine with the universal ATR Accessory was used to record all infra-red absorption spectra. All absorption peaks were recorded to the nearest wavenumber in cm^{-1} . All data were analysed using the Perkin-Elmer spectrum application.

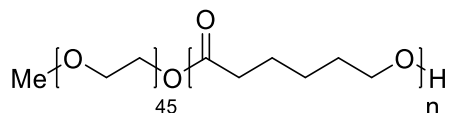
The polydispersity ($\text{Đ} = M_w/M_n$) and number average molecular weight (M_n) and weight-average molecular weight (M_w) were determined from gel permeation chromatography (GPC) and they reported relative to calibrations made using polystyrene standards (M_n 220-1, 1,000,000 Da) at 25 °C. THF was used as the eluent solvent for all GPC measurements with a flow rate of 1.0 mL/min. GPC grade tetrahydrofuran (THF) was used as both the solvent and the eluent. The characterisation was done using software released by Polymer Laboratories, Varian, Inc. (Amherst, MA, USA); PL DataStream Monitor version 1.2 and Cirrus GPC Online GPC/SEC Software version 3.0 were used to monitor the sample travelling through the columns and the data was analysed using Cirrus GPC Offline GPC/SEC Software version 3.0. Fluorescence measurements were performed with a HORIBA Scientific Fluoromax-4 spectrofluorometer using its attached software (Fluor Essence V3) using a quartz cell. Two UV-vis spectra were recorded using solutions in quartz cuvettes, recorded using Perkin-Elmer Lambda 35 dual-beam equipment. Upon a reference reading, absorbance measurements was carried out for each solution. WinASPECT software were used for analysis the spectra. Two UV-vis spectrophotometers were used to record UV-vis absorption spectra which are a UV-2550 UV-vis spectrophotometer (Shimadzu, Japan) and SPECORD® S 600 spectrometer where all recorded spectra was analysed using WinASPECT version 2.2.1.0 both from Analytik

Jena AG (Jena, Germany). Mass-to-charge ratio of the products was determined by electrospray spectrometry (ES) using Waters LCT Premier XE (Milford, MA, U.S.A).

Dynamic laser scattering (DLS) measurements were performed using the Brookhaven instrument 90Plus Particle Size Analyzer (Holtsville, NY, USA) 35mW solid state standard laser was used to determine hydrodynamic diameter of nanoparticles. Particle Sizing Software 9kpsdw32.exe.ver.3.80 was used for characterisation. Light was scattered at an angle of 173° and samples were analysed using 3 runs, each lasting 2 minutes at 25 °C. Samples were filtered using Whatman® GD/X syringe filters (Kent, UK) with a pore size of 0.45 µm prior to analysis. Results reported are based upon volume distribution. Z-average hydrodynamic diameters were calculated using the Stokes–Einstein equation. The aggregation presence in high concentration of PEG-porphyrin were obtained using a Hitachi S-3400 scanning electron microscope (Tokyo, Japan) at an acceleration voltage of 15 keV and probe current of 25 mA. Scanning electron microscopy (SEM) samples with water content were placed in silicon wafer and then dehydrated by leaving over three days in fume-hood, then coated with gold. A Jenway 210 pH Meter instrument was used for pH measurements. Calibration was carried out using pH 7 and pH 10 standard solutions (Sigma-Aldrich).

4.3 Synthetic procedures:

4.3.1 Synthetic procedures for mPEG-b-PCL diblock copolymer



A two-neck round-bottom flask was charged with mPEG-2000 (3.02 g, 1.51 mmol) and a small amount of tetrahydrofuran (THF). The THF was removed via vacuum and the mPEG was kept under vacuum at 130 °C for 120 minutes before nitrogen gas was allowed to fill the flask. ϵ -caprolactone and 5 % mol of TBD (0.1 mg/mL in dry acetone) were added. The mixture was stirred at 110 °C for 10 minutes under nitrogen. After that, the reaction was left to cool to room temperature. The crude product was dissolved in a small amount of DCM and precipitated from cold petroleum ether (P.E). The mixture was left to rest overnight, after which the P.E was decanted and the white solid left to dry in fume-hood vacuum.

Synthesis of mPEG₄₅-b-PCL₁₅ *al*

mPEG (3.02 g, 1.51 mmol) was reacted with ϵ -caprolactone (2.50 mL, 22.65 mmol) to yield mPEG-b-PCL₁₅ (6.5 g, 72 %); ¹H NMR (400 MHz; CDCl₃; ppm) 1.46-1.35 (m, 31H, γ -CH₂), 1.58- 1.72 (m, 63H, β and δ - CH₂), 2.34 (t, 30H, α - CH₂, J=7.5 Hz), 3.39 (s, 3H, CH₃O-), 3.66 (s, 181H, -OCH₂CH₂O-), 4.08 (t, 27H, -CH₂OH, J=6.7 Hz), 4.22-4.27 (m, 2H, -OCH₂CH₂OCO-); ¹³C NMR (100 MHz; CDCl₃; ppm); δ_c 24.6, 25.5, 28.3, 34.1, 59.0, 64.1, 70.5, 173.6; GPC (LMW; THF) M_n = 4700 g/mol, M_w=5800 g/mol, $\bar{D} = M_n/M_w = 1.22$, D_p=15 (the degree of polymerisation of ϵ -caprolactone as determined by ¹H-NMR).

Synthesis of mPEG₄₅-b-PCL₂₅ b

mPEG (3.02 g, 1.51 mmol) was reacted with ϵ -caprolactone (4.15 mL, 37.75 mmol) to yield mPEG₄₅-b-PCL₂₅ (6.47 g, 83 %); ¹H NMR (400 MHz; CDCl₃; ppm) 1.33-1.47 (m, 36H, γ -CH₂), 1.56-1.74 (m, 99H, β and δ -CH₂), 2.33 (t, 46H, α -CH₂, J=7.5 Hz), 3.39 (s, 3H, CH₃O-), 3.66 (s, 164H, -OCH₂CH₂O-), 4.08 (t, 40H, -CH₂OH, J=6.7 Hz), 4.16-4.26 (m, 2H, -OCH₂CH₂OCO-); ¹³C NMR (100 MHz; CDCl₃; ppm); δ_c 24.6, 25.5, 28.3, 34.1, 59.0, 64.1, 70.5, 173.6; GPC (LMW; THF) M_n = 5600 g/mol, M_w = 6600 g/mol, $D = M_n/M_w$ = 1.18, D_p = 23 (by ¹H-NMR).

Synthesis of mPEG₄₅-b-PCL₃₅ c

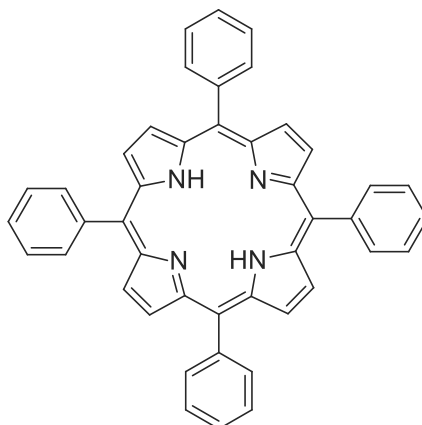
mPEG (3.02 g, 1.51 mmol) was reacted with ϵ -caprolactone (6.0 mL, 52.85 mmol) to yield mPEG₄₅-b-PCL₃₅ (7 g, 80%); ¹H NMR (400 MHz; CDCl₃; ppm) 1.34-1.46 (m, 56H, γ -CH₂), 1.58-1.74 (m, 139H, β and δ -CH₂), 2.34 (t, 70H, α -CH₂, J=7.5 Hz), 3.39 (s, 3H, CH₃O-), 3.66 (s, 173H, -OCH₂CH₂O-), 4.08 (t, 67H, -CH₂OH, J=6.7 Hz), 4.27-4.21 (m, 2H, -OCH₂CH₂OCO-); ¹³C NMR (100 MHz; CDCl₃; ppm); δ_c 24.6, 25.5, 28.3, 34.1, 59.0, 64.1, 70.5, 173.6; GPC (LMW; THF) M_n = 7800 g/mol, M_w = 9600 g/mol, $D = M_n/M_w$ = 1.2, D_p = 35 (by ¹H-NMR).

Synthesis of mPEG₄₅-b-PCL₄₅ d

mPEG (3.021 g, 1.51 mmol) was reacted with ϵ -caprolactone (7.5 mL, 67.95 mmol) to yield mPEG₄₅-b-PCL₄₅ (10 g, 88 %); ¹H NMR (400 MHz; CDCl₃; ppm) 1.34-1.47 (m, 95H, γ -CH₂), 1.60-1.75 (m, 211H, β and δ -CH₂), 2.32 (t, 92H, α -CH₂, J=7.5 Hz), 3.39 (s, 3H, CH₃O-), 3.65 (s, 164H, -OCH₂CH₂O-), 4.08 (t, 91H, -CH₂OH, J=6.7 Hz), 4.22-4.27 (m, 2H, -OCH₂CH₂OCO-); ¹³C NMR (100 MHz; CDCl₃; ppm); δ_c 24.6, 25.5, 28.3, 34.1, 59.0, 64.1,

70.5, 173.6; GPC (LMW; THF) $M_n = 9300$ g/mol, $M_w = 1400$ g/mol, $D = M_n/M_w = 1.47$, $D_p = 49$
(by $^1\text{H-NMR}$)

4.3.2 Meso-Tetraphenylporphyrin **3**

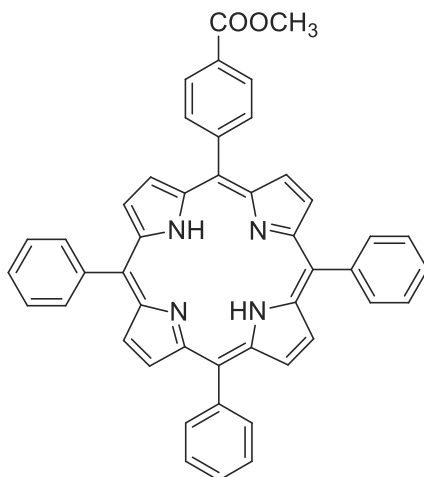


3

Propionic acid (300 mL) was heated to reflux before the addition of benzaldehyde **2** (8.15 mL, 80 mmol) and freshly distilled pyrrole **1** (5.54 mL, 80 mmol). The refluxing solution was stirred for 0.5 hour. The reaction mixture was cooled to room temperature, and the solution filtered under reduced pressure to give a purple solid that was subsequently washed with methanol and hot distilled water to give porphyrin **3** (2.1 g, 15%) as a purple solid, m.p. >360; $^1\text{H NMR}$ (400MHz; CDCl_3 ; ppm) δ -2.77 (s, 2H, NH), 7.74-7.83 (m, 12H phenolic m, p-CH), 8.12 (dd, $J = 7.3, 1.7$ Hz, 8H, phenolic o-CH), 8.87 (s, 8H, pyrrole- β H); $^{13}\text{C NMR}$ (100 MHz; CDCl_3 ; ppm) δ_c 120.2, 126.7, 127.8, 132.0, 134.6, 137.0, 142.2; FTIR (cm^{-1}) 3319 (amine N -H stretch), 3013 (aromatic and alkene, C-H stretch), 1675, 1224, 748, 695; ES-MS : 615 ($\text{M}+\text{H}^+$); UV-vis (DCM) λ (nm) = 417, 513.5, 548.5, 588, 645.5.

4.3.3 Methoxypolyethylene glycol-4-(10, 15, 20-triphenylporphyrin-5-yl)-benzoic acid ester **10** (donor unit)

4.3.3.1 5-(4-Carbomethoxyphenyl)-10, 15, 20-triphenylporphyrin **8**

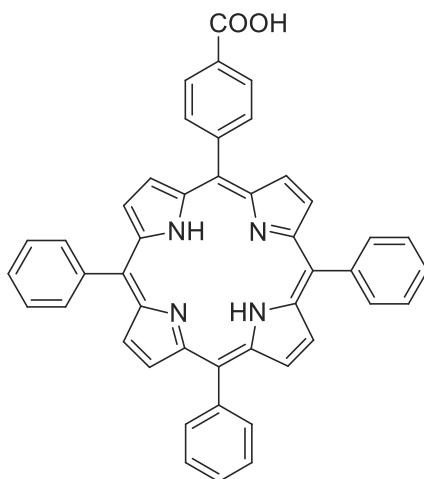


8

Propionic acid (300 mL) was heated to reflux before the addition of benzaldehyde **2** (7.1 mL, 70 mmol), freshly distilled pyrrole **1** (5.54 mL, 80 mmol) and methyl 4-formyl benzoate **7** (3.28 g, 20 mmol). The refluxing solution was stirred for two hours. This was followed the removal of three-quarter of propionic by distillation. The black solution was cooled down to room temperature, after that, methanol was added, and the solution was kept in freezer for 24 hours. The solution was filtered and the remaining solid on the filter paper was washed with cold methanol to yield a black purple solid. A small amount of 10% petroleum ether in DCM was used to dissolve the crude product and charged onto the silica column. The same ratio was used as eluting to recover firstly pure porphyrin **6** and then porphyrin **8** with impurities. The product **8** was further purified by column chromatography eluting with 10% petroleum ether on DCM to yield product **8** as a purple solid (1.6 g, 12%), m.p=225 °C; ¹H NMR(400 MHz,

CDCl₃) δ 8.88-8.82 (m, 8H), 8.57 (dd, J = 8.1, 1.8 Hz, 2H), 8.46 (dd, J = 8.1, 1.8 Hz, 2H), 8.24(dd, J =5.56, 2 Hz, 6H), 7.82-7.76 (m, 9H), 4.14(s, 3H), -2.75(s, 2H); ¹³C NMR (100.6 MHz, CDCl₃) δ_c 167.4, 147.1, 142.1 (x 2), 134.6 (x 2), 131.3, 129.6, 128.0, 127.8, 126.8, 120.6, 120.4, 118.6, 52.4; FTIR (cm⁻¹) 3307 (N -H, stretch); 2843 (C-H, stretch, alkane); 1718 (C=O, stretch); 1272 (C-O 75, stretch); 699; ES-MS: m/z expected for C₄₆H₃₂N₄O₂: 673, found: 673; UV absorbance (DCM) λ (nm): 418 (Soret), 515, 548, 589, 645 (Q bands).

4.3.3.2 5-(4-Carboxyphenyl)-10, 15, 20- triphenylporphyrin **9**

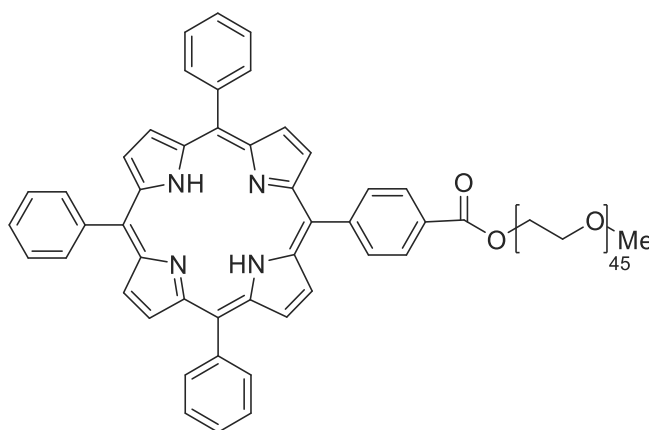


9

Porphyrin **8** was dissolved in THF, to which a solution of potassium hydroxide (2 M, 100 mL) was added and the reaction mixture stirred under reflux for 16 hours. THF was removed and the aqueous solution acidified with concentrated HCl until pH2. DCM was then added, and the organic layer extracted and neutralised with saturated sodium hydrogen carbonate. The organic layer was recovered, dried over magnesium sulfate and filtered to give porphyrin **9** as a purple solid (0.8 g, 82%), m.p>360; ¹H NMR(400 MHz, CDCl₃) δ 8.89 –8.83 (m, 8H), 8.52 (dd, J = 7.48, 0.86 Hz, 2H), 8.37 (dd, J = 7.8, 0.83 Hz, 2H), 8.25 (dd, J = 7.6, 1.6 Hz, 6H), 7.82-7.76

(m, 9H), -2.75(s, 2H); ^{13}C NMR (100.6 MHz, CDCl_3) δ_c 179.8, 146.6, 141.2, 134.6, 130.6, 128.0, 127.7, 126.5, 120.4, 120.2, 118.8; FTIR (cm^{-1}) 3312 (N-H, stretch); 2916 (O-H, stretch, alcohol); 1739 (C=O, stretch, ester); 1217 (C-O, stretch, ester); 699; ES-MS(MH $^+$): m/z[MH $^+$] expected for $\text{C}_{45}\text{H}_{30}\text{N}_4\text{O}_2$: 659, found: 659; UV absorbance (DCM) λ (nm): 418 (Soret), 515, 548, 589, 645 (Q bands).

4.3.3.3 Synthesis of Methoxypolyethylene glycol-4-(10, 15, 20-triphenylporphyrin-5-yl)-benzoic acid ester **10**



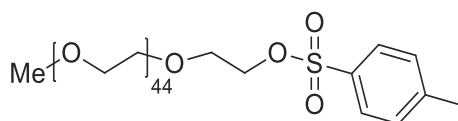
10

Porphyrin **9** (0.5 g, 0.76 mmol) was placed in two neck round bottomed flask fitted with condenser, dry DCM (40 mL) was added. The solution was stirred under nitrogen. The solution was cooled down to zero degree. The mPEG (1 g, 0.5 mmol) was dried and dissolved in a dry DCM and added into a stirring solution of under nitrogen. Well grained dicyclohexyl carbodiimide (DCC) (0.156, 7.6mmol) was added into mixture for 30 minutes. Then 5 mol-% of dimethylaminopyridine (DMAP) (4.6 mg/ 0.038 mol) was added to the mixture. After that the mixture was left stirring 24 hours at room temperature. DCM was removed and the resulting oily mixture was dissolved in methanol then filtered by vacuum filtration. The filtered solution was recovered, and methanol was removed under reduced pressure. For purification, the

product was dissolved in the minimum amount of DCM and loaded onto pre-prepared Bio-beads column eluting with DCM to yield porphyrin **10** as a dark red oil (0.59 g, 45%); ^1H NMR (400 MHz, CDCl_3) δ 8.9-8.80 (m, 8H), 8.42 (dd, $J = 8.31, 1.71$ Hz, 2H), 8.33 (dd, $J = 8.07, 1.71$ Hz, 2H), 8.24 (dd, $J=7.28, 0.98$ Hz, 6H), 7.82-7.76 (m, 9H), 3.39 (s, 3H, $\text{CH}_3\text{O}-$), 3.65 (s, 174H, $-\text{OCH}_2\text{CH}_2\text{O}-$), -2.75(s, 2H); ^{13}C NMR (100.6 MHz, CDCl_3) δ_c 167.4, 147.1, 142.1 (x 2), 134.6 (x 2), 131.3, 129.6, 128.0, 127.8, 126.8, 120.6, 120.4, 118.6, 52.4; FTIR (cm^{-1}), 3309, 2881, 1714, 1279, 1108, 963, 841 ; UV absorbance (DCM) λ (nm): 418 (Soret), 515, 548, 589, 645 (Q bands); GPC (LMW; THF) $M_n = 2300$ g/mol, $M_n = 3100$ g/mol , $D = M_n/M_w = 1.035$.

4.3.4 Synthesis of Methoxypolyethylene glycol-4-(10, 15, 20-triphenylporphyrin-5-yl)-benzoic acid ester **11**

4.3.4.1 Synthesis Poly (ethylene glycol) methyl ether Tosylate **2**



5

In a round-bottomed flask, mPEG **4** (25 g, 0.0125 mol) was dissolved in 65 mL of tetrahydrofuran. Upon vigorous stirring at 0 °C, 65 mL of 6 M sodium hydroxide solution was added. Tosyl chloride (12.39, 0.065 mol) dissolved in 70 mL of THF was added drop-wisely added into the stirred solution under N_2 . After 1h, the mixture was allowed to warm to room temperature and then stirred for another 24 hours. Finally, 500 mL of DCM was added, and the organic layer was washed with 1 M aqueous sodium hydroxide and water, sequentially. After drying over MgSO_4 , the organic solution was filtered and evaporated to yield colourless liquid **2**, Yield 25.9 g, 96%. ^1H NMR (400 MHz, CDCl_3): δ 7.73 (dd, $J = 8.2, 1.74$ Hz, 2H, (Ar)- $\text{C}=\text{CH}-\text{CH}$), 7.27 (d, $J = 8.0$ Hz, 2H, (Ar)- $\text{C}=\text{CH}-\text{CH}$), 4.06 (t, $J = 4.0$ Hz, 2H, $\text{CH}_2-\text{CH}_2-\text{O}-$

Ts), 3.62-3.50 (s, 185 H, -OCH₂CH₂O-, 3.36 (s, 3H, O-CH₃), 2,36 (s, 3H, C-CH₃). ¹³C NMR (100.6 MHz, CDCl₃) δ_c 129.9 , 128.2 ,72.1 ,69.2, 58.8 ,53.3,25.8,21.6; FTIR (cm⁻¹), 3519, 2960, 1410, 1374, 1113, 946, 841; GPC (LMW; THF) M_n= 2800 g/mol, M_n= 2800 g/mol , M_w= 2900 g/mol Đ =M_n/M_w= 1.032.

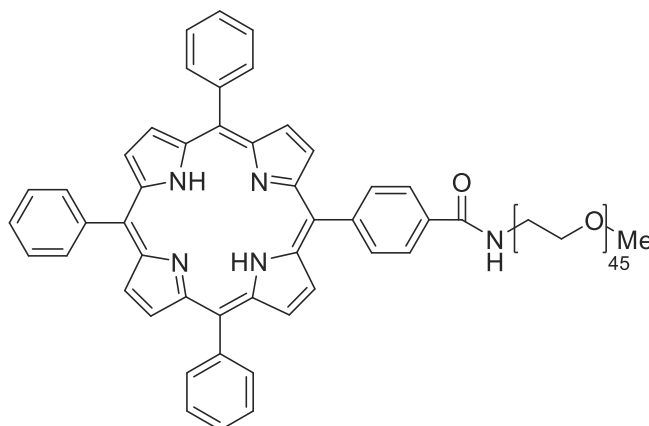
4.3.4.2 Poly (ethylene glycol) methyl ether amine **3**



6

Poly (ethylene glycol) methyl ether tosylate **5** (5 g, 0.0023 mol) was placed in 100 mL round-bottomed flask containing 50 mL of 6 M hydroxylammonium (NH₄OH). After that, the round-bottomed flask was sealed and the reaction was stirred overnight. Finally, 50 mL of DCM was added, and the organic layer was washed with 1 M aqueous solution of potassium carbonate and water, sequentially. Free amine was obtained. Yield 65%, ¹H NMR (400 MHz, CDCl₃): δ 3.66 (s, 193 H), 3.39 (s, 3H), 2.57 (t, J=5.2 Hz, 2H), ¹³C NMR (100.6 MHz, CDCl₃) δ_c 41.7, 61.6, 70.5, 72.6, 73.4; FTIR λ_{max}(cm)⁻¹: 3536, 2881, 1411, 1325, 1278, 1107, 945, 840; GPC (LMW; THF) M_n= 2200 g/mol, M_w= 2400 g/mol, Đ =M_n/M_w= 1.096.

4.3.4.3 Synthesis of Methoxypolyethylene glycol-4-(10, 15, 20-triphenylporphyrin-5-yl)-benzoic acid amide **11**

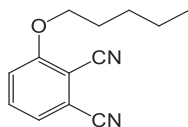


11

Dried poly (ethylene glycol) methyl ether amine **6** (1g, 0.5 mmol) was dissolved in a dry DCM and the solution was added into a stirring solution of porphyrin **9** (0.5g, 0.76 mmol) in dry DCM at 0 °C under nitrogen. Well grained dicyclohexyl carbodiimide (DCC) (0.156, 7.6mmol) was added in batches into mixture for 30 minutes. Then 5 mol% of dimethylaminopyridine (DMAP) was added to the mixture, which was left stirring 24 hours at room temperature. DCM was removed in vacuo and the resulting oily mixture dissolved in methanol then filtered by vacuum filtration. The methanol was then removed under reduced pressure. For purification, the product was dissolved in the minimum amount of DCM and then loaded onto pre-prepared Bio-beads column eluting with DCM to yield 20% of porphyrin **11** as a dark red oil. ^1H NMR (400 MHz, CDCl_3) δ 8.88-8.83(br m, 8H), 8.52 (br dd, 2H), 8.37 (br dd, , 2H), 8.24 (br dd, 6H), 7.82-7.76 (m, 9H), 3.39 (s, 3H, CH_3O -), 3.65 (s, 174H, $-\text{OCH}_2\text{CH}_2\text{O}-$), -2.75 (s, 2H); ^{13}C NMR (100.6 MHz, CDCl_3) δ_c 167.4, 147.1, 142.1 (x 2), 134.6 (x 2), 131.3, 129.6, 128.0, 127.8, 126.8, 120.6, 120.4, 118.6, 52.4; FTIR $\lambda_{\text{max}}(\text{cm})^{-1}$: 3325, 2883, 1969, 1651, 1543, 1341, 1279, 1146, 961, 731, UV absorbance (DCM) λ (nm): 418 (Soret), 515, 548, 589, 645 (Q bands). GPC (LMW; THF) $M_n = 3500$ g/mol, $M_w = 4400$ g/mol, $D = M_w/M_n = 1.11$.

4.3.5 Tin (IV)dichlorophthalocyanine (The acceptor unit)

4.3.5.1 3-pentyloxy-1,2-dicyanobenzene

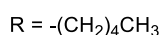
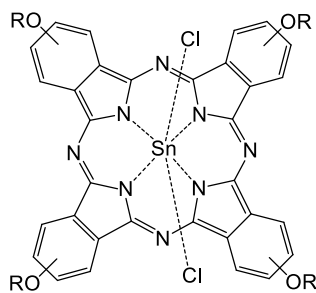


15

3-Nitrophthalonitrile 14 (1 g, 5.77 mmol) and 1-pentanol (1.25 mL, 11.54 mmol) were added to 12 mL of DMSO contained in the dry round-bottomed flask under nitrogen. After 5 minutes of stirring potassium carbonate (1.6 g, 11.54 mmol) was added and reaction mixture maintained under reflux for 4 hours at 90 °C. After 4 hours the reaction mixture was cooled at room temperature and water (150 mL) was added, the mixture was stirred vigorously for 15 minutes at room temperature. The resulting precipitate was filtered by vacuum and washed with water. The crude product was recrystallised with ethanol.

Yield 0.330 g, 33% , m.p=130 °C, $^1\text{H NMR}$ (CDCl_3 , 400MHz) δ 7.64(dd, $J = 8.6, 7.8$ Hz, 1H), 7.37 – 7.34 (m, 1H), 7.24 (d, $J = 8.7$ Hz, 1H), 4.14(t, $J = 6.5$ Hz, 2H, OCH₂), 1.89-1.92(m, 2H, OCH₂CH₂), 1.54-1.35(m, 3H, CH₂CH₂CH₃), 0.96(t, $J = 7.2$ Hz, 2H, CH₂CH₃); $^{13}\text{C-NMR}$ (CDCl_3 , 100MHz) δ_c 161.5, 134.4, 130.0, 124.8, 117.5, 115.3, 113.0, 104.9, 69.9, 28.4, 27.8, 22.2, 13.9; FTIR $\lambda_{\text{max}}(\text{cm})^{-1}$: 3088, 2959, 2934(alkyl H-C-H stretch), 2237, 2226(-CN- stretch), 1579, 1398, 1472(alkane bend), 1072(ester stretch), 795(aromatic bend); ES-MS: 215(M+H⁺).

4.3.5.2 Tin (IV) dichlorophthalocyanine

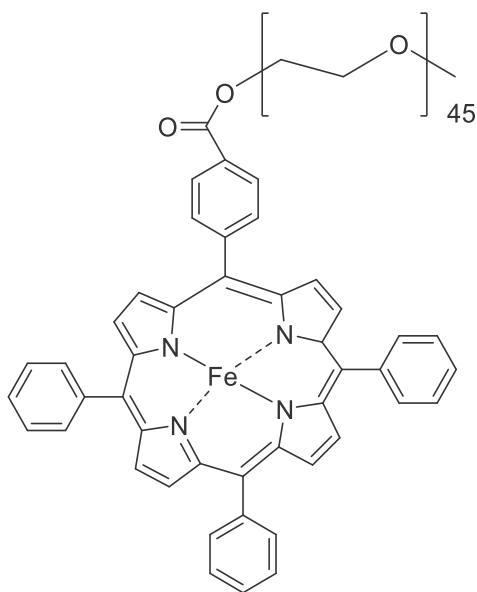


16

5 mL 1-chloronaphthalene (1-CNP) was added into 3-Pentyloxy-1,2-dicyanobenzene **15** (428.5 mg 4mmol). The solution was stirred for 5 min. after the addition of tin (II)chloride (189.62 mg 1 mmol). The reaction mixture was maintained under reflux for 5 hours under nitrogen. The solution was cooled down and it was loaded into column chromatography and eluted with hexane to remove 1-CNP. The column was then eluted with 4/1 dichloromethane and methanol. The solvent was evaporated off and crude product was obtained and washed with hot methanol to give 0.20 g (25%) of the product as a green solid **16**, $^1\text{H NMR}(\text{CDCl}_3, 400\text{MHz}) \delta$ 9.35-9.17(m, 4H), 8.32-8.24 (m, 4H), 7.90-7.76(m, 4H), 4.99-4.72(dm, 8H), 2.57-2.35(m, 8H), 1.88-1.54(m, 16H), 1.24-1.03(dm, 12H); $^{13}\text{C-NMR}(\text{d- CDCl}_3, 400\text{MHz}) \delta$ 157.9, 157.7, 149.6, 132.6, 116.6, 115.9, 114.4, 70.9, 69.5, 53.4, 29.8, 29.0, 28.9, 28.2, 23.0, 22.7, 14.3, 14.2; FTIR λ_{max} (cm^{-1}) 2858(w), 2119(s), 1582(s), 1488, 1463, 1335, 1265, 1228, 1115, 1075, 872; UV/Vis Spectroscopy(nm); 347, 749, 760; ESI-MS: 1044 (M-Cl)+,1008 (obtained).

4.3.6 Methoxypolyethylene glycol-4-(10, 15, 20-triphenylporphyrin-5-yl)-benzoic acid

ester Iron (III) Complex (**12**)



12

In dry two neck round-bottomed flask, PEG-Porphyrin **10** (0.3 g, 0.1 mmol) was added. The flask was fitted with condenser and stirring bar. The air was removed by vacuum then flushed with nitrogen. Anhydrous tetrahydrofuran (40 mL) and 2,6-lutidine (0.08 mL, 0.7 mmol) was added. The mixture solution was refluxed under nitrogen for 15 minutes. FeCl₂ (0.195 g, 1.5 mmol) was added to the reaction mixture. After that the reaction was maintained under reflux under nitrogen for three hours. The solution was exposed to air and left stirring overnight at room temperature. The solution was filtered to remove unreacted FeCl₂. Tetrahydrofuran was removed under reduced pressure and dichloromethane (50 mL) was added to dissolve the crude and washed with 1 M hydrochloric acid (50 mL) and then distilled water (50 mL). The organic layer was dried with MgSO₄ and filtered. The solution was concentrated before loading into the bio-beads column, DCM was used as eluent to yield red oil of PEG-Fe-porphyrin **12** (270mg, 90%); ¹H NMR (CDCl₃) δ 3.65 (br s, 148H, [Polymer] CH₂-CH₂); 3.40 (br s, 3H, [Polymer] CH₃); ¹³C NMR (CHCl₃) δ_c 70.5; UV-vis (DCM) λ_{max} nm = 417(Soret), 509, 654(Q bands). GPC (LMW; THF) M_n = 3400, M_w = 3800, Đ = M_w/M_n = 1.126.

4.4 Analytical procedures:

4.4.1 Beer-Lambert experiment for Tetraphenyl porphyrin

A series of DCM solutions of tetraphenyl porphyrin with different concentrations was prepared. UV-vis spectroscopy was used to measure the absorbance of TPP **3**, the Δ absorptions values were used at wavelength from 420 nm to 425 nm. A Beer-Lambert plot was shown the relationship between absorbance and concentrations of TPP **3**.

4.4.2 The Preparation of Block Copolymer Micelles and the determination of the Critical micelles concentration (CMC)

The diblock copolymers micelles were prepared by weighting 10 mg of the diblock copolymer powder then dissolved it in 1 mL THF. After obtaining a homogeneous solution, a desired volume of this solution was drop-wisely added into the 10 mL purified water with rapid stirring. The polymer solution was then dialysed using a dialysis membrane with around 3.5 kDa size pores cut-off for two days. Followed by lyophilizing to remove all residual solvents, followed by re-suspension in 10 mL water and sonication for 1 hour.

Critical micelles concentration (CMC) of mPEG₄₅-b-PCL_n copolymers in aqueous solution was determined using pyrene as fluorescence probe at 25±1 °C. The stock solution of pyrene was first prepared by weighting the right amount of pyrene and dissolving in acetone to give a concentration of 1x10⁻⁴ M then it was diluted to 1x10⁻⁵ M. That was followed by adding 0.5 mL of pyrene solution (1x10⁻⁵ M) in each of the series empty vials. Once acetone completely evaporated, 5 mL of different concentration of mPEG-PCL diblock copolymers solution ranging from 0.5 µg/mL to 500 µg/mL was added in each pyrene containing vials to give a final pyrene concentration of 1x10⁻⁶ M, after that, the vials left to equilibrate overnight in the dark.

Fluorescence measurements were performed with a HORIBA Scientific Fluoromax-4 spectrofluorometer using its attached software (Fluor Essence V3) using a quartz cell. Pyrene excited at 340 nm and the fluorescence spectra was measured from 355 nm to 480 nm, for excitation and emission fluorescence spectra, the slit width was set at 3 nm. The intensities of peaks at 373 nm and 383 nm were measured as I_1 and I_3 , respectively. The values of CMC can be determined from the best fit lines intersection that is form when the ratio of the two peaks(I_3/I_1) was plotted against the diblock copolymers concentration.

4.4.3 Self-assembly of porphyrin in aqueous solution:

The aggregation behaviour of PEG-porphyrin **10** (CMC) in aqueous solution was determined by preparing different concentration of PEG-porphyrin **10** solutions ranging from 0.5 $\mu\text{g/mL}$ to 800 $\mu\text{g/mL}$. After taking the fluorescence emission intensity of PEG-porphyrin **10** at 650 nm and the absorption at 418.5 nm for each solution, the measured intensities and changed absorption were plotted as function of the logarithm concentration and concentration of PEG-porphyrin **10**, respectively. DLS measurements were directly conducted in the same day of the fluorescence and UV measurements.

4.4.4 General preparation PEG-porphyrin/mPEG₄₅-PCL_n 13 Block Copolymer Micelles and the determination of pre-quenching.

For the incorporation of PEG-porphyrin **10** in mPEG₄₅-b-PCL_n diblock copolymers and the determination of the pre-quenching values of PEG-porphyrin **10** in different size of diblock copolymers. UV-vis, fluorescence and DLS measurements were performed for series of vials containing fixed concentration of mPEG₄₅-PCL_n diblock copolymers (double above the CMC of mPEG₄₅-b-PCL_n) and various concentration of PEG-porphyrin **10** polymers were prepared. Firstly, two stock solution of mPEG₄₅-PCL_n diblock copolymers were prepared. The concentration of first stock solution was 40 $\mu\text{g/mL}$ (four time above the CMC), this solution

was called a solution A, the second stock solution concentration was 20 $\mu\text{g/mL}$ (double above the CMC and it was made from the dilution of first stock solution to half) it was called solution A'. Secondly, a 400 $\mu\text{g/mL}$ of PEG-porphyrin **10** were prepared separately, after that 2 mL of solution A was mixed with 2 mL of solution B, to give solution C with the half concentration of B (200 $\mu\text{g/mL}$) and A (20 $\mu\text{g/mL}$). From solution C, 2 mL was taken and poured into the second empty vial, then 2 mL of solution A' was added to the same vial to half the concentration of PEG-porphyrin **10** (100 $\mu\text{g/mL}$) while the concentration of the diblock copolymer remain the same (20 $\mu\text{g/mL}$). The similar procedure was followed to prepare the mixture of diblock copolymers and PEG-porphyrin **10** in rest of vials. For each solution, the fluorescence emission intensity of PEG-porphyrin **10** at 650 nm and the absorption at 418.5 nm were measured then they were plotted as function of the logarithm concentration and concentration of PEG-porphyrin **10**, respectively. DLS measurements were directly conducted in the same day of the fluorescence and UV-vis measurements.

4.4.5 Beer-Lambert experiment for dichloride (Phthalocyanato)tin(IV)(Tin phthalocyanine) (acceptor unit)

A series of DCM solutions of tin phthalocyanine with concentrations between $1 \times 10^{-6}\text{M}$ and $1 \times 10^{-5}\text{M}$ were prepared. UV-vis spectroscopy was used to measure the absorbance of tin phthalocyanine at 740 nm. A Beer-Lambert plot was obtained by plotting the absorbance vs concentration of the tin phthalocyanine solutions.

4.4.6 The general preparation of LH polymeric micelle

The light harvesting system was assembled by adding 0.8 mL of mPEG₄₅-PCL_n diblock stock solution (1 mg/mL in THF) into 2 mL of a tin phthalocyanine 16 solution ($1 \times 10^{-4}\text{M}$ in DCM). The new solution was sonicated then left to dry. A small amount of acetone was added, and the solution sonicated before adding drop-wisely added into 20 mL of distilled water. The

solution was vigorously stirred for 24 hours at room temperature. 2 mL of this solution was mixed with 2 mL of a PEG-porphyrin **10** solution (4 $\mu\text{g/mL}$) and this final solution was left overnight in the dark, before UV and fluorescence measurements were recorded.

4.4.7 Preparation of LH micelle with different ratio of PEG-porphyrin **10** to tin phthalocyanine **16**

A stock solution of mPEG₄₅-PCL₁₅ diblock, PEG-porphyrin **10** and tin phthalocyanine/micelles was prepared separately. The table below shows the final concentration of various solutions containing different ratios of tin phthalocyanine to PEG-porphyrin **10**

Table 4.1: final concentrations of stock solutions and different ratio of PEG-porphyrin 10 to tin phthalocyanine 16 in LH micelles solutions

Solution	mPEG ₄₅ -PCL ₁₅ diblock ($\mu\text{g/mL}$)	PEG-porphyrin 10 ($\mu\text{g/mL}$)	Tin phthalocyanine 16 $\times 10^{-6}$ (M)
mPEG ₄₅ -PCL ₁₅ stock solution	40	-	-
mPEG-porphyrin stock solution	-	4	-
A	40	-	8
B	20	2	-
C	20	2	4
D	20	2	2
E	20	2	1
F	20	2	0.5
G	20	2	0.1

4.4.8 Preparation of mPEG₄₅-PCL₁₅ diblock stock solution

mPEG₄₅-PCL₁₅ diblock (20 mg) was dissolved in a very small amount of THF and added dropwisely added into 20 mL of distilled water and then with vigorously stirred for two days. From this micelle solution (1 mg/mL), 0.8 mL was diluted with 20 mL distilled water to give final concentration of 40 $\mu\text{g/mL}$ (table 4.1).

4.4.9 Preparation of PEG-porphyrin 10 stock solution

PEG-porphyrin **10** (20 mg) was dissolved in 20 mL of distilled water. The solution was then sonicated to yield a homogeneous solution of PEG-porphyrin with a concentration of 1 mg/mL. 0.2 mL was then diluted into 10 mL of distilled water. Finally, 2 mL of this solution was diluted with 10 mL distilled water to give a final concentration of 4 $\mu\text{g/mL}$ (table 4.1).

4.4.10 Preparation of Tin phthalocyanine/micelles stock solution (solution A)

mPEG₄₅-PCL_n diblock solution (0.8 mL of 1 mg/mL in THF) was added into 2 mL of tin phthalocyanine solution (1×10^{-4} M in DCM). The mixed solution was sonicated then it was left to dry. Small amount of acetone was added into the formed film. The solution was sonicated and drop-wisely added into distilled water 20 mL under vigorously stirring for overnight at room temperature. From this solution 4 mL was taken and diluted with 1 ml of mPEG₄₅-PCL₁₅ stock solution (40 $\mu\text{g/mL}$) to prepare solution A. Final concentration can be seen in **table 4.1**.

4.4.11 Preparation of PEG-porphyrin/micelles stock solution (solution B)

Solution B was prepared by mixing 10 mL of mPEG₄₅-PCL₁₅ stock solution (40 $\mu\text{g/mL}$) with 10 mL of PEG-porphyrin **10** stock solution (4 $\mu\text{g/mL}$), then the solution was left overnight in dark prior the use. Final concentration can be seen in **table 4.1**.

4.4.12 The preparation of (mPEG₄₅-PCL_n, PEG-porphyrin, tin phthalocyanine) LH micelles at different ratio of tin phthalocyanine to PEG-porphyrin.

Different ratios of tin phthalocyanine to PEG-porphyrin which are $R_1=0.13$, $R_2=0.65$, $R_3=1.31$, $R_4=2.61$, $R_5=5.23$ were prepared. Varying the concentration of tin phthalocyanine and fixing the concentration of both diblock and PEG-porphyrin which are 20 $\mu\text{g/mL}$ and 2 $\mu\text{g/mL}$

respectively. All solution was in kept in the dark for overnight before taking any measurements.

The final concentration for each solution can be seen in **table 4.1**.

4.4.12.1 The preparation of LH micelle (solution C) at $R_5=5.2$

Solution C was prepared by mixing 2 mL of solution A with 2 mL of PEG-Porphyrin diblock stock solution (4 μ /mL).

4.4.12.2 The preparation of LH micelle (solution D) at $R_4=2.61$

Solution D was prepared by mixing 2 mL of solution C with 2mL of solution B.

4.4.12.3 The preparation of LH micelle (solution E) at $R_3=1.31$

Solution E was prepared by mixing 2 mL of solution D with 2mL of solution B.

4.4.12.4 The preparation of LH micelle (solution F) at $R_2=0.65$

Solution F was prepared by mixing 2 mL of solution E with 2mL of solution B.

4.4.12.5 The preparation of LH micelle (solution G) at $R_1=0.13$

Solution G was prepared by mixing 0.5 mL of solution F with 4.5 mL of solution B.

4.4.13 General procedure for preparation of the PEG-Fe-porphyrin/ mPEG45-PCL25 micelle 18 for catalytic study

Firstly, mPEG₄₅-PCL₂₅ (1 mg/mL) stock solution was prepared from dissolving 10 mg of mPEG₄₅-PCL₂₅ in 10 mL THF, then, 1 mg of PEG-Fe-porphyrin **12** was dissolved in 1 mL anhydrous pyridine, from this solution 0.5 mL was taken and diluted with 0.5 mL pyridine. 0.5 mL was taken from PEG₄₅-PCL₂₅ solution and then mixed with PEG-Fe-Porphyrin **12** pyridine

solution. The mixed solution was slowly drop-wisely added into 10 mL stirring solution of phosphate buffer (pH=7.4). Finally, the solution was stirred for two days to remove the THF.

4.4.14 General procedure for preparation of the Fe-TPP/ mPEG₄₅-PCL₂₅ micelle 20 for catalytic study

Fe-TPP **19** (1 mg) was dissolved in 1 mL anhydrous pyridine, from this solution 0.5 mL was taken and diluted with 0.5 mL pyridine. 0.5 mL was taken from mEG₄₅-PCL₂₅ stock solution (1 mg/mL in THF) and then mixed with Fe-TPP **19** pyridine solution. The mixed solution was slowly drop-wisely added into 10 mL stirring solution of phosphate buffer (pH=7.4). Finally, the solution was stirred for two days.

4.4.15 Beer-Lambert experiment orange II

A series of phosphate buffer solutions of orange II with different concentrations between 1×10^{-6} M and 1×10^{-5} M were prepared. UV-Vis spectroscopy was employed to measure the absorbance of orange II, the Δ Absorption was calculated by subtracting the absorptions at 498.5 nm and 503.5 nm. The calculated molar absorption coefficient of orange II is $29200 \text{ M}^{-1} \text{ cm}^{-1}$. Whereas the calculated molar Δ absorption coefficient of orange II is $331.43 \text{ M}^{-1} \text{ cm}^{-1}$. A Beer-Lambert Plot was shown the relationship between absorbance and concentrations.

4.4.16 Beer-Lambert experiment red oil

A series of DCM solutions of red oil with different concentrations between 1×10^{-6} M and 1×10^{-5} M were prepared. UV-vis spectroscopy was employed to measure the absorbance of red oil, however, due to the draft shifting in the baseline in the three solutions, Δ Absorption was calculated by subtracting the absorptions at 519 nm and 524 nm. The calculated molar absorption coefficient of oil red is $53479 \text{ M}^{-1} \text{ cm}^{-1}$ and the calculated molar Δ absorption coefficient of oil red is $290.38 \text{ M}^{-1} \text{ cm}^{-1}$.

4.4.17 General procedure of catalytic oxidation reaction of Orange II

In a glass cuvette that contains a stirring bar, 1 mL of catalyst/ mPEG₄₅-PCL₂₅ micelles (the ratio of catalyst to mPEG₄₅-PCL₂₅ diblock was 1: 1), orange II (0.5 mL, 0.14 M in buffer solution) and oxidant (0.5 mL, 0.01 M), in UV-vis. The stock solution of oxidants was prepared in water solution, except m-CPBA was prepared in DCM. The absorption of orange II at 486 nm was taken every 10 seconds for an hour. Firstly, the change of orange absorption was converted into the change of concentration by substitution the equation 1, where Abs is the intensity of the absorption peak, ϵ is the molar absorption coefficient, b is the optical path (the light transmittance thickness of cuvette), C is the concentration of the substrate, t is time. Following the first-order equation 2, the Orange II degradation time was plotted against the natural logarithm of the (C_0/C) where C_0 and C are the concentration of orange II at time zero (C_0) and at the time t (C) respectively. k_{obs} is the rate constant.

$$\Delta C = \frac{\Delta Abs}{\epsilon b} \quad (1)$$

$$\ln \left(\frac{C_0}{C} \right) = k_{obs} t \quad (2)$$

4.4.18 General procedure of catalytic oxidation reaction of red oil

Oil red (1 mL, 0.1 mM in DCM) was drop-wisely added into catalyst solution. After four hours of stirring, all the DCM evaporated from solution. 1 mL of this solution was placed in a cuvette with a stirring bar. 0.5 mL of m-CPBA (0.01 M in DCM) was then added into the solution. The change in oil red absorption at 513 nm supposed to be taken every 10 seconds for an hour. However, due to the draft shifting in the baseline in reaction solutions, Δ Absorption was calculated by subtracting the absorptions at 519 nm and 524 nm. The calculated molar

absorption coefficient of oil red is $53479 \text{ M}^{-1} \text{ cm}^{-1}$. Whereas the calculated molar Δ absorption coefficient of oil red is $290.38 \text{ M}^{-1} \text{ cm}^{-1}$. Finally, $\Delta \ln (C_0/C)$ was plotted as a function of time.

Chapter 5 - Conclusion and future work:

The self-assembly process of isolated (non-aggregated) porphyrin in aqueous solution was finally realized by using polymeric micelle system to construct a novel design of macrostructure. MPEG-PCL di-block copolymer was chosen due to straightforward synthesis and stability concerning different environmental conditions. It was synthesised by using ring opening polymerisation. Due to the hydrophobic block of PCL and the hydrophilic block of mPEG, mPEG-PCL di-block, copolymer forms a stable micelle above the CMC in the water solution. Therefore, the hydrophobic part of micelles provides a suitable macroenvironment to incorporate a large amount of the active materials. The formation of micelles was confirmed using UV-vis, fluorescence and DLS. The incorporation of unfunctionalized porphyrin molecules within the micelle system cannot eliminate the aggregation of porphyrin core of micelles. Therefore, in this project, porphyrin was functionalised by covalently attaching mPEG to the porphyrin; this process involved different synthetic steps. First, the mono-functionalized Porphyrin-COOCH₃ **8** was synthesised, and hydrolysed into Porphyrin-COOH **9**. Finally, Porphyrin-COOH **9** reacted with the hydroxide functional group in mPEG to form PEG-Porphyrin ester **10** and with amine functionalized PEG to form PEG-Porphyrin amide **11**. Their structures were confirmed by ¹H and ¹³C NMR, IR and GPC. After that, PEG-Porphyrin ester was assembled alongside mPEG-PCL di-block copolymers chains in aqueous solution to form new PEG-porphyrin/mPEG-PCL mixed micelles **13**, which successfully isolated porphyrins and incredibly increased their functionality. Fluorescence and UV-vis experiments confirmed that PEG-porphyrins were part of micelle structure. The size of PEG-porphyrin/mPEG-PCL mixed micelles was measured by DLS and their structure was further confirmed by the TEM. For comparison sake, four different mPEG-PCL di-block copolymers were synthesised using the ring opening polymerisation with fixed length of mPEG block and

different length of PCL block. The CMC of the four di-blocks which are mPEG₄₅-PCL₁₅, mPEG₄₅-PCL₂₅, mPEG₄₅-PCL₃₅ and mPEG₄₅-PCL₄₅ was 1, 0.5, 0.3 and 0.1 $\mu\text{g/mL}$, respectively. The spectroscopy results revealed that the larger the hydrophobic block, the more mPEG-porphyrin polymers incorporate before the quenching occurs. For mPEG₄₅-PCL₁₅, mPEG₄₅-PCL₂₅, mPEG₄₅-PCL₃₅ and mPEG₄₅-PCL₄₅ the ratio of PEG-PCL di-block to the PEG-porphyrin were 2:1, 1:1, 1:5 and 1:10, respectively. The size of the mixed micelles for the different ratios of PEG-porphyrin **10** to mPEG-PCL DBC was also measured by DLS. However, among the four di-blocks, mPEG₄₅-PCL₂₅ micelles demonstrated the highest ability to control the size of the mixed micelles even after incorporating a large number of PEG-Porphyrins. These isolated porphyrins within the mPEG₄₅-b-PCL_n micelles will prove useful in many applications. Therefore, they were initially used to duplicate the natural antenna complexes. In this artificial system, the arrays of PEG-porphyrin polymers that are assembled at the hydrophobic/hydrophilic interface of PEG-PCL micelles were used as donor units whereas, the tin phthalocyanine which is located at the core of micelles was employed as an acceptor unit. Although light harvesting was not productive, there was evidence for energy transfer. That was confirmed by observing successive quenching of the donor molecules with an increase in the concentration of tin phthalocyanine **16** (acceptor units) for micelles (artificial light harvesting system) compared to mPEG-TPP-micelles (control experiment).

The investigation of the degree of quenching displayed that the quenching of light harvesting micelles increased with the increase in the length of PCL block in mPEG₄₅-b-PCL_n di-block. The UV-vis spectroscopy results provided a further evidence for the energy transfer from porphyrin arrays to tin phthalocyanine as the absorption of tin phthalocyanine increased with the increase in the concentration of PEG-Porphyrin; however, this extra energy could not be harvested due to the aggregation of tin phthalocyanine. That was confirmed when no emission was observed after exciting the tin phthalocyanine inside micelles at 610 nm. Consequently,

addressing the aggregation of tin phthalocyanine in the proposed system is an essential step for optimising the artificial light harvesting system.

Catalysis is another area where isolated porphyrin within micelles can be exploited. The catalytic activity of the micelle system was tested after the insertion of iron into PEG-porphyrin/mPEG₄₅-PCL₂₅. The DLS and TEM results disclosed that the insertion of iron did not change the size of the PEG-porphyrin/mPEG₄₅-PCL₂₅ micelle **13** and that the resulting PEG-Fe-porphyrin/mPEG₄₅-PCL₂₅ micelle **18** kept its morphology. The investigation revealed that the PEG-Fe-porphyrin/mPEG₄₅-PCL₂₅ micelle was an excellent catalyst and that it was a suitable nano-reactor for the oxidation reaction in water. The methodology of catalytic oxidation reaction was optimised by selecting the suitable oxidation agent and substrate for the system. Those experiments indicated that among the tested oxidants and substrates, m-CPBA and red oil proved to be the best oxidant and substrate respectively. In addition, PEG-Fe-Porphyrin/ PEG-PCL catalytic activity surpassed both PEG-Fe-porphyrin in absence of micelles and FeTPP/micelles to catalyse the oxidation reaction of the red oil with m-CPBA. Overall, it was demonstrated that porphyrin was successfully isolated in water.

Although the system was successful in its role as a catalyst and nano-reactor, it failed as a light harvesting system. The non-aggregated PEG-Porphyrins within the micelles successfully fulfilled their role as donors and they transferred their energy to the acceptor. However, the aggregation of tin phthalocyanine was the reason for making the system less successful as light harvesting. Therefore, it is necessary to address the aggregation of tin phthalocyanine in the core of the micelles. One way to solve this problem is to functionalise tin phthalocyanine with the hydrophobic component; for example, making the tin phthalocyanine the core of the hydrophobic dendrimer and to incorporate this within micelles. This ensures that the single molecule of the tin phthalocyanine will be inserted in the core of the micelle.

In general, the isolated PEG-porphyrin within micelle was achieved by attaching PEG to porphyrin and incorporating them within micelle. This method can be used to isolate other hydrophobic compounds that have the tendency to aggregate and to use them for different applications that require water presence. For instance, this method can be used to prevent the aggregation of isophthalamides, using the micelles system as receptors that bind anions. Non aggregated ordered array of porphyrins can also be employed for the molecular recognition application.

Reference:

- 1- Harris, F. (1981). Introduction to polymer chemistry. *Journal of Chemical Education*, 58(11), p.837.
- 2- Cabral, H., Nishiyama, N. and Kataoka, K. (2011). Supramolecular Nanodevices: From Design Validation to Theranostic Nanomedicine. *Accounts of Chemical Research*, 44(10), pp.999-1008.
- 3- Zhao, Y., Sakai, F., Su, L., Liu, Y., Wei, K., Chen, G. and Jiang, M. (2013). Progressive Macromolecular Self-Assembly: From Biomimetic Chemistry to Bio-Inspired Materials. *Advanced Materials*, 25(37), pp.5215-5256.
- 4- Mongwaketsi, N., Kotsedi, L., Nuru, Z., Sparrow, R., Garab, G. and Maaza, M. (2014). Porphyrin nanorods-polymer composites for solar radiation harvesting applications. *Journal of Porphyrins and Phthalocyanines*, 18(12), pp.1145-1156.
- 5- Feng, H., Lu, X., Wang, W., Kang, N. and Mays, J. (2017). Block Copolymers: Synthesis, Self-Assembly, and Applications. *Polymers*, 9(12), p.494.
- 6- Choksi, R. and Ren, X. (2005). Diblock copolymer/homopolymer blends: Derivation of a density functional theory. *Physica D: Nonlinear Phenomena*, 203(1-2), pp.100-119.
- 7- Su WF. (2013) Structure Morphology Flow of Polymer. In: Principles of Polymer Design and Synthesis. Lecture Notes in Chemistry, Springer, Berlin, Heidelberg, 82, pp.27-59
- 8- Gao, C. and Yan, D. (2004). Hyperbranched polymers: from synthesis to applications. *Progress in Polymer Science*, 29(3), pp.183-275.
- 9- Fong, H. and Reneker, D. (1999). Elastomeric nanofibers of styrene-butadiene-styrene triblock copolymer. *Journal of Polymer Science Part B: Polymer Physics*, 37(24), pp.3488-3493.

- 10- Jacquin, M., Muller, P., Talingting-Pabalan, R., Cottet, H., Berret, J., Futterer, T. and Théodoly, O. (2007). Chemical analysis and aqueous solution properties of charged amphiphilic block copolymers PBA-b-PAA synthesized by MADIX®. *Journal of Colloid and Interface Science*, 316(2), pp.897-911.
- 11- Pochan, D., Gido, S., Pispas, S., Mays, J., Ryan, A., Fairclough, J., Hamley, I. and Terrill, N. (1996). Morphologies of Microphase-Separated A2B Simple Graft Copolymers. *Macromolecules*, 29(15), pp.5091-5098.
- 12- Jin, Q., Luy, C., Ji, J. and Agarwal, S. (2011). Design and proof of reversible micelle-to-vesicle multistimuli-responsive morphological regulations. *Journal of Polymer Science Part A: Polymer Chemistry*, 50(3), pp.451-457.
- 13- Lele, B. and Leroux, J. (2002). Synthesis and Micellar Characterization of Novel Amphiphilic A-B-A Triblock Copolymers of N-(2-Hydroxypropyl)methacrylamide or N-Vinyl-2-pyrrolidone with Poly(ϵ -caprolactone). *Macromolecules*, 35(17), pp.6714-6723.
- 14- Letchford, K., Zastre, J., Liggins, R. and Burt, H. (2004). Synthesis and micellar characterization of short block length methoxy poly (ethylene glycol)-block-poly (caprolactone) diblock copolymers. *Colloids and Surfaces B: Biointerfaces*, 35(2), pp.81-91.
- 15- Yoo, H. and Park, T. (2001). Biodegradable polymeric micelles composed of doxorubicin conjugated PLGA-PEG block copolymer. *Journal of Controlled Release*, 70(1-2), pp.63-70.
- 16- Riess, G. (2003). Micellization of block copolymers. *Progress in Polymer Science*, 28(7), pp.1107-1170.

- 17- Bahadur, P. (2001). Block copolymers-Their microdomain formation (in solid state) and surfactant behaviour (in solution). *Current science-Bangalore*, 80(8), pp. 1002-1007.
- 18- Letchford, K. and Burt, H. (2007). A review of the formation and classification of amphiphilic block copolymer nanoparticulate structures: micelles, nanospheres, nanocapsules and polymersomes. *European Journal of Pharmaceutics and Biopharmaceutics*, 65(3), pp.259–269.
- 19- Nagarajan, R. (1996). Solubilization of Hydrophobic Substances by Block Copolymer Micelles in Aqueous Solutions. *Solvents and Self-Organization of Polymers* 327, pp. 121-165.
- 20- Fiscaro, E., Compari, C., Duce, E., Biemmi, M., Peroni, M. and Braibanti, A. (2008). Thermodynamics of micelle formation in water, hydrophobic processes and surfactant self-assemblies. *Physical Chemistry Chemical Physics*, 10(26), p.3903.
- 21- Nishiyama, N. and Kataoka, K. (2006). Current state, achievements, and future prospects of polymeric micelles as nanocarriers for drug and gene delivery. *Pharmacology & Therapeutics*, 112(3), pp.630-648.
- 22- Li, F., Danquah, M. and Mahato, R. (2010). Synthesis and Characterization of Amphiphilic Lipopolymers for Micellar Drug Delivery. *Biomacromolecules*, 11(10), pp.2610-2620.
- 23- Xu, W., Ling, P. and Zhang, T. (2013). Polymeric Micelles, a Promising Drug Delivery System to Enhance Bioavailability of Poorly Water-Soluble Drugs. *Journal of Drug Delivery*, 2013, pp.1-15.
- 24- Mishra, M. (2016). *Handbook of encapsulation and controlled release*. Boca Raton, CRC Press/Taylor & Francis Group.

- 25- Rapoport, N. (2007). Physical stimuli-responsive polymeric micelles for anti-cancer drug delivery. *Progress in Polymer Science*, 32(8-9), pp.962-990.
- 26- Holder, S. and Sommerdijk, N. (2011). New micellar morphologies from amphiphilic block copolymers: disks, toroids and bicontinuous micelles. *Polymer Chemistry*, 2(5), p.1018.
- 27- Israelachvili, J. (2011). *Intermolecular and Surface Forces*. Burlington: Elsevier Science.
- 28- Blanazs, A., Armes, S. and Ryan, A. (2009). Self-Assembled Block Copolymer Aggregates: From Micelles to Vesicles and their Biological Applications. *Macromolecular Rapid Communications*, 30(4-5), pp.267-277.
- 29- Read, E. and Armes, S. (2007). Recent Advances in Shell Cross-Linked Micelles. *ChemInform*, 38(42).
- 30- Won, Y., Davis, H. and Bates, F. (1999). Giant Wormlike Rubber Micelles. *Science*, 283(5404), pp.960-963.
- 31- Won, Y., Brannan, A., Davis, H. and Bates, F. (2002). Cryogenic Transmission Electron Microscopy (Cryo-TEM) of Micelles and Vesicles Formed in Water by Poly (ethylene oxide)-Based Block Copolymers. *The Journal of Physical Chemistry B*, 106(13), pp.3354-3364.
- 32- Jain, S. and Bates, F. (2004). Consequences of Nonergodicity in Aqueous Binary PEO–PB Micellar Dispersions. *Macromolecules*, 37(4), pp.1511-1523.
- 33- Jain, S., Gong, X., Scriven, L. and Bates, F. (2006). Disordered Network State in Hydrated Block-Copolymer Surfactants. *Physical Review Letters*, 96(13).
- 34- Pochan, D. (2004). Toroidal Triblock Copolymer Assemblies. *Science*, 306(5693), pp.94-97.

- 35- Cui, H., Chen, Z., Zhong, S., Wooley, K. and Pochan, D. (2007). Block Copolymer Assembly via Kinetic Control. *Science*, 317(5838), pp.647-650.
- 36- Zhong, S., Cui, H., Chen, Z., Wooley, K. and Pochan, D. (2008). Helix self-assembly through the coiling of cylindrical micelles. *Soft Matter*, 4(1), pp.90-93.
- 37- Zhu, J., Liao, Y. and Jiang, W. (2004). Ring-Shaped Morphology of “Crew-Cut” Aggregates from ABA Amphiphilic Triblock Copolymer in a Dilute Solution. *Langmuir*, 20(9), pp.3809-3812.
- 38- Li, Z., Hillmyer, M.A. and Lodge, T.P. (2006). Control of Structure in Multicompartment Micelles by Blending μ -ABC Star Terpolymers with AB Diblock Copolymers. *Macromolecules*, 39(2), pp.765–771.
- 39- Yu, K. and Eisenberg, A. (1998). Bilayer Morphologies of Self-Assembled Crew-Cut Aggregates of Amphiphilic PS-b-PEO Diblock Copolymers in Solution. *Macromolecules*, 31(11), pp.3509–3518.
- 40- Battaglia, G. and Ryan, A. (2006). Neuron-Like Tubular Membranes Made of Diblock Copolymer Amphiphiles. *Angewandte Chemie*, 118(13), pp.2106-2110.
- 41- Reinecke, A. and Döbereiner, H. (2003). Slow Relaxation Dynamics of Tubular Polymersomes after Thermal Quench. *Langmuir*, 19(3), pp.605-608.
- 42- Liu, B., Wang, J., Zhang, Y., Wu, S., Ru, G. and Feng, J. (2017). Inhomogeneous-collapse driven micelle-vesicle transition of amphiphilic block copolymers. *Soft Matter*, 13(39), pp.7106-7111.
- 43- Lovett, J., Warren, N., Armes, S., Smallridge, M. and Cracknell, R. (2016). Order-Order Morphological Transitions for Dual Stimulus Responsive Diblock Copolymer Vesicles. *Macromolecules*, 49(3), pp.1016-1025.

- 44- Lovett, J., Warren, N., Ratcliffe, L., Kocik, M. and Armes, S. (2014). pH-Responsive Non-Ionic Diblock Copolymers: Ionization of Carboxylic Acid End-Groups Induces an Order-Order Morphological Transition. *Angewandte Chemie*, 127(4), pp.1295-1299.
- 45- Yoshida, E. (2014). Hydrophobic energy estimation for giant vesicle formation by amphiphilic poly (methacrylic acid)-block-poly(alkyl methacrylate-random-methacrylic acid) random block copolymers. *Colloid and Polymer Science*, 292(10), pp.2555-2561.
- 46- Zhang, H. and Dubin, P.L. (1997). Analysis of Polydispersity of Mixed Micelles of TX-100/SDS and C12E8/SDS by Capillary Electrophoresis. *Journal of Colloid and Interface Science*, [online] 186(2), pp.264–270.
- 47- Gilroy, J., Gädt, T., Whittell, G., Chabanne, L., Mitchels, J., Richardson, R., Winnik, M. and Manners, I. (2010). Monodisperse cylindrical micelles by crystallization-driven living self-assembly. *Nature Chemistry*, 2(7), pp.566-570.
- 48- Jennings, J., He, G., Howdle, S.M. and Zetterlund, P.B. (2016). Block copolymer synthesis by controlled/living radical polymerisation in heterogeneous systems. *Chemical Society Reviews*, 45(18), pp.5055–5084.
- 49- Plesch, P. (1982). *Advances in polymer science vol. 34/35 1980 Cationic polymerisation — Initiation processes with alkenyl monomers*. *Polymer*, 23(5), p.787.
- 50- Finch, C. (1969). *Theory of free radical polymerisation*. Kh. S. Bagdasar'yan (translated by J. Schmorak), *British Polymer Journal*, 1(5), pp.240-240.
- 51- Kamigaito, M., Ando, T. and Sawamoto, M. (2001). Metal-Catalyzed Living Radical Polymerization. *Chemical Reviews*, 101(12), pp.3689-3746.
- 52- Braunecker, W. and Matyjaszewski, K. (2007). Controlled/living radical polymerization: Features, developments, and perspectives. *Progress in Polymer Science*, 32(1), pp.93-146.

- 53- Barner-Kowollik, C. and Perrier, S. (2008). The future of reversible addition fragmentation chain transfer polymerization. *Journal of Polymer Science Part A: Polymer Chemistry*, 46(17), pp.5715-5723.
- 54- Halasa, A. (1981). Recent Advances in Anionic Polymerization. *Rubber Chemistry and Technology*, 54(3), pp.627-640.
- 55- Szwarc, M., Levy, M. and Milkovich, R. (1956). Polymerization Initiated By Electron Transfer to Monomer. A New Method of Formation of Block Polymers. *Journal of the American Chemical Society*, 78(11), pp.2656-2657.
- 56- Stridsberg .M, Ryner, M., Albertsson C. (2002) Controlled Ring-Opening Polymerization: Polymers with designed Macromolecular Architecture. In: *Degradable Aliphatic Polyesters*. *Advances in Polymer Science*, vol 157. pp 41-65.
- 57- Matyjaszewski, K. (2000). Comparison and classification of controlled/living radical polymerizations. *American Chemical Society*, 768, pp.2-26
- 58- Aoshima, S. and Kanaoka, S. (2009). A Renaissance in Living Cationic Polymerization. *Chemical Reviews*, 109(11), pp.5245-5287.
- 59- Yokozawa, T. and Yokoyama, A. (2004). Chain-Growth Polycondensation: Living Polymerization Nature in Polycondensation and Approach to Condensation Polymer Architecture. *ChemInform*, 35(30).
- 60- Khodaverdi, E., Golmohammadian, A., Mohajeri, S., Zohuri, G., Mirzazadeh Tekie, F. and Hadizadeh, F. (2012). Biodegradable In Situ Gel-Forming Controlled Drug Delivery System Based on Thermosensitive Poly(ϵ -caprolactone)-Poly(ethylene glycol)-Poly(ϵ -caprolactone) Hydrogel. *ISRN Pharmaceutics*, 2012, pp.1-7.
- 61- Zhao, L., Qu, R., Li, A., Ma, R. and Shi, L. (2016). Cooperative self-assembly of porphyrins with polymers possessing bioactive functions. *Chemical Communications*, 52(93), pp.13543-13555.

- 62- Zhao, Y., Sakai, F., Su, L., Liu, Y., Wei, K., Chen, G. and Jiang, M. (2013). Progressive Macromolecular Self-Assembly: From Biomimetic Chemistry to Bio-Inspired Materials. *Advanced Materials*, 25(37), pp.5215-5256.
- 63- Movassaghian, S., Merkel, O. and Torchilin, V. (2015). Applications of polymer micelles for imaging and drug delivery. *Wiley Interdisciplinary Reviews: Nanomedicine and Nanobiotechnology*, 7(5), pp.691-707.
- 64- Mourya, V., Inamdar, N., Nawale, B., Kulthe, S. (2011). Polymeric micelles: general considerations and their applications. *Indian J Pharm Educ Res*, 2(45), pp.128-38.
- 65- Jeong, Y., Kim, S., Jung, T., Kim, I., Kang, S., Jin, Y., Ryu, H., Sun, H., Jin, S., Kim, K., Ahn, K. and Jung, S. (2006). Polyion Complex Micelles Composed of All-Trans Retinoic Acid and Poly (Ethylene Glycol)-Grafted-Chitosan. *Journal of Pharmaceutical Sciences*, 95(11), pp.2348-2360.
- 66- Wang, R., Qu, R., Jing, C., Zhai, Y., An, Y. and Shi, L. (2017). Zinc porphyrin/fullerene/block copolymer micelle for enhanced electron transfer ability and stability. *RSC Advances*, 7(17), pp.10100-10107.
- 67- Wang, R., Qu, R., Zhai, Y., Jing, C., Li, A., An, Y. and Shi, L. (2017). Enhanced electron transfer ability via coordination in block copolymer/porphyrin/fullerene micelle. *Chinese Journal of Polymer Science*, 35(11), pp.1328-1341.
- 68- Bonar-Law, R.P. (1996). Porphyrin Synthesis in Surfactant Solution: Multicomponent Assembly in Micelles. *The Journal of Organic Chemistry*, 61(11), pp.3623–3634.
- 69- Gunathilagan, S. (n.d.). Metalloporphyrin-catalysed epoxidation using hydrogen peroxide. University of Surrey, phd thesis. pp.16–189.
- 70- Qu, R., Shen, L., Chai, Z., Jing, C., Zhang, Y., An, Y. and Shi, L. (2014). Hemin-Block Copolymer Micelle as an Artificial Peroxidase and Its Applications in Chromogenic

- Detection and Biocatalysis. *ACS Applied Materials & Interfaces*, 6(21), pp.19207-19216.
- 71- Kataoka, K., Harada, A. and Nagasaki, Y. (2001). Block copolymer micelles for drug delivery: design, characterization and biological significance. *Advanced Drug Delivery Reviews*, 47(1), pp.113-131.
- 72- Nishiyama, N., Bae, Y., Miyata, K., Fukushima, S. and Kataoka, K. (2005). Smart polymeric micelles for gene and drug delivery. *Drug Discovery Today: Technologies*, 2(1), pp.21-26.
- 73- Fukushima, S., Miyata, K., Nishiyama, N., Kanayama, N., Yamasaki, Y. and Kataoka, K. (2005). PEGylated Polyplex Micelles from Triblock Cationomers with Spatially Ordered Layering of Condensed pDNA and Buffering Units for Enhanced Intracellular Gene Delivery. *Journal of the American Chemical Society*, 127(9), pp.2810-2811.
- 74- Boeckle, S., von Gersdorff, K., van der Piepen, S., Culmsee, C., Wagner, E. and Ogris, M. (2004). Purification of polyethylenimine polyplexes highlights the role of free polycations in gene transfer. *The Journal of Gene Medicine*, 6(10), pp.1102-1111.
- 75- Ward, C. (2001). Systemic circulation of poly (L-lysine)/DNA vectors is influenced by polycation molecular weight and type of DNA: differential circulation in mice and rats and the implications for human gene therapy. *Blood*, 97(8), pp.2221-2229.
- 76- van Grondelle, R., Dekker, J., Gillbro, T. and Sundstrom, V. (1994). Energy transfer and trapping in photosynthesis. *Biochimica et Biophysica Acta (BBA) - Bioenergetics*, 1187(1), pp.1-65.
- 77- van Grondelle, R., Dekker, J., Gillbro, T. and Sundstrom, V. (1994). Energy transfer and trapping in photosynthesis. *Biochimica et Biophysica Acta (BBA) - Bioenergetics*, 1187(1), pp.1-65.

- 78- Noy, D., Moser, C. and Dutton, P. (2006). Design and engineering of photosynthetic light-harvesting and electron transfer using length, time, and energy scales. *Biochimica et Biophysica Acta (BBA) - Bioenergetics*, 1757(2), pp.90-105.
- 79- Photobiology.info. (2020). Bacterial Photosynthesis. [online] Available at: <http://photobiology.info/Jones.html> [Accessed 11 Jan. 2020].
- 80- FAN, L., Jones Jr, E. (2010). Energy Transfer and Electronic Energy Migration Processes. *Photochemistry and Photophysics of Polymeric Materials*, 1, pp.1-39.
- 81- Danila, E. and Lucache, D.D. (2016). Efficient lighting system for greenhouses. 2016 International Conference and Exposition on Electrical and Power Engineering (EPE). [online] Available at: <https://ieeexplore.ieee.org/document/7781379/> [Accessed 11 Jan. 2020].
- 82- Fan, L.-J. and Jones, W. (n.d.). Energy Transfer and Electronic Energy Migration Processes. [online] Available at: <https://catalogimages.wiley.com/images/db/pdf/9780470137963.excerpt.pdf>.
- 83- Andrews, D.L., Demidov, A.A.: *Resonance Energy Transfer*. Wiley, Chichester (1999)
- 84- Tran Thi, T., Desforge, C., Thiec, C. and Gaspard, S. (1989). Singlet-singlet and triplet-triplet intramolecular transfer processes in a covalently linked porphyrin-phthalocyanine heterodimer. *The Journal of Physical Chemistry*, 93(4), pp.1226-1233.
- 85- El-Khouly, M., Ito, O., Smith, P. and D'Souza, F. (2004). Intermolecular and supramolecular photoinduced electron transfer processes of fullerene-porphyrin/phthalocyanine systems. *Journal of Photochemistry and Photobiology C: Photochemistry Reviews*, 5(1), pp.79-104.
- 86- de la Escosura, A., Martínez-Díaz, M., Guldi, D. and Torres, T. (2006). Stabilization of Charge-Separated States in Phthalocyanine-Fullerene Ensembles through

- Supramolecular Donor–Acceptor Interactions. *Journal of the American Chemical Society*, 128(12), pp.4112-4118.
- 87- Lee, M., Dunietz, B. and Geva, E. (2014). Donor-to-Donor vs Donor-to-Acceptor Interfacial Charge Transfer States in the Phthalocyanine–Fullerene Organic Photovoltaic System. *The Journal of Physical Chemistry Letters*, 5(21), pp.3810-3816.
- 88- Sakata, Y., Tsue, H., O'Neil, M., Wiederrecht, G. and Wasielewski, M. (1994). Effect of Donor-Acceptor Orientation on Ultrafast Photoinduced Electron Transfer and Dark Charge Recombination in Porphyrin-Quinone Molecules. *Journal of the American Chemical Society*, 116(15), pp.6904-6909.
- 89- Wiehe, A., Senge, M., Schäfer, A., Speck, M., Tannert, S., Kurreck, H. and Röder, B. (2001). Electron donor–acceptor compounds: exploiting the triptycene geometry for the synthesis of porphyrin quinone diads, triads, and a tetrad. *Tetrahedron*, 57(51), pp.10089-10110.
- 90- Rodríguez-Morgade, M., Torres, T., Atienza-Castellanos, C. and Guldi, D. (2006). Supramolecular Bis(rutheniumphthalocyanine)–Perylenediimide Ensembles: Simple Complexation as a Powerful Tool toward Long-Lived Radical Ion Pair States. *Journal of the American Chemical Society*, 128(47), pp.15145-15154.
- 91- Tannert, S., Ermilov, E., Vogel, J., Choi, M., Ng, D. and Röder, B. (2007). The Influence of Solvent Polarity and Metalation on Energy and Electron Transfer in Porphyrin–Phthalocyanine Heterotrimers. *The Journal of Physical Chemistry B*, 111(28), pp.8053-8062.
- 92- LO, P., LENG, X. and NG, D. (2007). Hetero-arrays of porphyrins and phthalocyanines. *Coordination Chemistry Reviews*, 251(17-20), pp.2334-2353.

- 93- Nyokong, T. (2007). Effects of substituents on the photochemical and photophysical properties of main group metal phthalocyanines. *Coordination Chemistry Reviews*, 251(13-14), pp.1707-1722.
- 94- Li, X., He, X., Ng, A., Wu, C. and Ng, D. (2000). Influence of Surfactants on the Aggregation Behavior of Water-Soluble Dendritic Phthalocyanines. *Macromolecules*, 33(6), pp.2119-2123.
- 95- Romeo, A., Angela Castriciano, M. and Scolaro, L. (2010). Spectroscopic and kinetic investigations on porphyrin J-aggregates induced by polyamines. *Journal of Porphyrins and Phthalocyanines*, 14(08), pp.713-721.
- 96- Phillips, D. (1995). The photochemistry of sensitisers for photodynamic therapy. *Pure and Applied Chemistry*, 67(1), pp.117-126.
- 97- Dhimi, S. and Phillips, D. (1996). Comparison of the photophysics of an aggregating and non-aggregating aluminium phthalocyanine system incorporated into unilamellar vesicles. *Journal of Photochemistry and Photobiology A: Chemistry*, 100(1-3), pp.77-84.
- 98- Ball, D., Wood, S., Vernon, D., Griffiths, J., Dubbelman, T. and Brown, S. (1998). The characterisation of three substituted zinc phthalocyanines of differing charge for use in photodynamic therapy. A comparative study of their aggregation and photosensitising ability in relation to mTHPC and polyhaematoporphyrin. *Journal of Photochemistry and Photobiology B: Biology*, 45(1), pp.28-35.
- 99- Qu, R., Shen, L., Qu, A., Wang, R., An, Y. and Shi, L. (2015). Artificial Peroxidase/Oxidase Multiple Enzyme System Based on Supramolecular Hydrogel and Its Application as a Biocatalyst for Cascade Reactions. *ACS Applied Materials & Interfaces*, 7(30), pp.16694-16705.

- 100- KC, C., Lim, G. and D'Souza, F. (2015). Multi-modular, tris(triphenylamine) zinc porphyrin–zinc phthalocyanine–fullerene conjugate as a broadband capturing, charge stabilizing, photosynthetic ‘antenna-reaction center’ mimic. *Nanoscale*, 7(15), pp.6813-6826.
- 101- Hill, J., Shrestha, L., Ishihara, S., Ji, Q. and Ariga, K. (2014). Self-Assembly: From Amphiphiles to Chromophores and Beyond. *Molecules*, 19(6), pp.8589-8609.
- 102- Kratz, F. and Elsadek, B. (2012). Clinical impact of serum proteins on drug delivery. *Journal of Controlled Release*, 161(2), pp.429-445.
- 103- Peng, H., Chen, Y., Zhao, Y., Yang, Q., Wu, L., Tung, C., Zhang, L. and Tong, Q. (2012). Artificial Light-Harvesting System Based on Multifunctional Surface-Cross-Linked Micelles. *Angewandte Chemie*, 124(9), pp.2130-2134.
- 104- Qu, R., Shen, L., Chai, Z., Jing, C., Zhang, Y., An, Y. and Shi, L. (2014). Hemin-Block Copolymer Micelle as an Artificial Peroxidase and Its Applications in Chromogenic Detection and Biocatalysis. *ACS Applied Materials & Interfaces*, 6(21), pp.19207-19216.
- 105- Miller, R., Presley, A. and Francis, M. (2007). Self-Assembling Light-Harvesting Systems from Synthetically Modified Tobacco Mosaic Virus Coat Proteins. *Journal of the American Chemical Society*, 129(11), pp.3104-3109.
- 106- Zhang, S. (2003). Fabrication of novel biomaterials through molecular self-assembly. *Nature Biotechnology*, 21(10), pp.1171-1178.
- 107- Reedy, C. and Gibney, B. (2004). Heme Protein Assemblies. *ChemInform*, 35(20).
- 108- Lin, V., DiMagno, S. and Therien, M. (1994). Highly conjugated, acetylenyl bridged porphyrins: new models for light-harvesting antenna systems. *Science*, 264(5162), pp.1105-1111.

- 109- Yella, A., Lee, H., Tsao, H., Yi, C., Chandiran, A., Nazeeruddin, M., Diao, E., Yeh, C., Zakeeruddin, S. and Gratzel, M. (2011). Porphyrin-Sensitized Solar Cells with Cobalt (II/III)-Based Redox Electrolyte Exceed 12 Percent Efficiency. *Science*, 334(6056), pp.629-634.
- 110- Ajayaghosh, A., Praveen, V. and Vijayakumar, C. (2008). Organogels as scaffolds for excitation energy transfer and light harvesting. *Chem. Soc. Rev.*, 37(1), pp.109-122.
- 111- Kumar, C. and Duff, M. (2009). DNA-Based Supramolecular Artificial Light Harvesting Complexes. *Journal of the American Chemical Society*, 131(44), pp.16024-16026.
- 112- Lee, J., Govorov, A. and Kotov, N. (2005). Bioconjugated Superstructures of CdTe Nanowires and Nanoparticles: Multistep Cascade Förster Resonance Energy Transfer and Energy Channeling. *Nano Letters*, 5(10), pp.2063-2069.
- 113- Zeng, Y., Li, Y., Chen, J., Yang, G. and Li, Y. (2010). Dendrimers: A Mimic Natural Light-Harvesting System. *Chemistry - An Asian Journal*, 5(5), pp.992-1005.
- 114- Adronov, A., Gilat, S., Fréchet, J., Ohta, K., Neuwahl, F. and Fleming, G. (2000). Light Harvesting and Energy Transfer in Laser-Dye-Labeled Poly(aryl ether) Dendrimers. *Journal of the American Chemical Society*, 122(6), pp.1175-1185.
- 115- Lu, A. and O'Reilly, R. (2013). Advances in nanoreactor technology using polymeric nanostructures. *Current Opinion in Biotechnology*, 24(4), pp.639-645.
- 116- Adams, P., Collins, A., Sahin, T., Subramanian, V., Urban, V., Vairaprakash, P., Tian, Y., Evans, D., Shreve, A. and Montaña, G. (2015). Diblock Copolymer Micelles and Supported Films with Noncovalently Incorporated Chromophores: A Modular Platform for Efficient Energy Transfer. *Nano Letters*, 15(4), pp.2422-2428.

- 117- Peng, H.-Q., Chen, Y.-Z., Zhao, Y., Yang, Q.-Z., Wu, L.-Z., Tung, C.-H., Zhang, L.-P. and Tong, Q.-X. (2012). Artificial Light-Harvesting System Based on Multifunctional Surface-Cross-Linked Micelles. *Angewandte Chemie*, 124(9), pp.2130–2134.
- 118- Bansal, K. (2015). Amphiphilic polymers from renewable feedstock: synthesis, characterisation and applications. University of Nottingham. phd thesis. pp.27–308.
- 119- Du, J., Tang, L., Song, W., Shi, Y. and Wang, J. (2009). Evaluation of Polymeric Micelles from Brush Polymer with Poly(ϵ -caprolactone)-b-Poly (ethylene glycol) Side Chains as Drug Carrier. *Biomacromolecules*, 10(8), pp.2169-2174.
- 120- Maiti, N.C., Mazumdar, S. and Periasamy, N. (1998). J- and H-Aggregates of Porphyrin–Surfactant Complexes: Time-Resolved Fluorescence and Other Spectroscopic Studies†. *The Journal of Physical Chemistry B*, 102(9), pp.1528–1538.
- 121- Yang, J. (2006). Synthesis of novel red-shifted phthalocyanines, PhD thesis, Dublin City University.
- 122- Kuzmina, E., Dubinina, T. and Tomilova, L. (2019). Recent advances in chemistry of phthalocyanines bearing electron-withdrawing halogen, nitro and N-substituted imide functional groups and prospects for their practical application. *New Journal of Chemistry*, 43(24), pp.9314-9327.
- 123- de la Torre, G., Claessens, C.G. and Torres, T. (2007). Phthalocyanines: Old Dyes, New Materials. Putting Color in Nanotechnology. *ChemInform*, 38(35).
- 124- Taratula, O., Schumann, C., Naleway, M., Pang, A., Chon, K. and Taratula, O. (2013). A Multifunctional Theranostic Platform Based on Phthalocyanine-Loaded Dendrimer for Image-Guided Drug Delivery and Photodynamic Therapy. *Molecular Pharmaceutics*, 10(10), pp.3946-3958.

- 125- Jang, W., Nakagishi, Y., Nishiyama, N., Kawauchi, S., Morimoto, Y., Kikuchi, M. and Kataoka, K. (2006). Polyion complex micelles for photodynamic therapy: Incorporation of dendritic photosensitizer excitable at long wavelength relevant to improved tissue-penetrating property. *Journal of Controlled Release*, 113(1), pp.73-79.
- 126- Jeong, Y., Yoon, H. and Jang, W. (2012). Dendrimer porphyrin-based self-assembled nano-devices for biomedical applications. *Polymer Journal*, 44(6), pp.512-521.
- 127- Cotanda, P., Lu, A., Patterson, J., Petzetakis, N. and O'Reilly, R. (2012). Functionalized Organocatalytic Nanoreactors: Hydrophobic Pockets for Acylation Reactions in Water. *Macromolecules*, 45(5), pp.2377-2384.
- 128- Rideout, D. and Breslow, R. (1980). Hydrophobic acceleration of Diels-Alder reactions. *Journal of the American Chemical Society*, 102(26), pp.7816-7817.
- 129- Bosman, A., Vestberg, R., Heumann, A., Fréchet, J. and Hawker, C. (2003). A Modular Approach toward Functionalized Three-Dimensional Macromolecules: From Synthetic Concepts to Practical Applications. *Journal of the American Chemical Society*, 125(3), pp.715-728.
- 130- Yu, J., RajanBabu, T. and Parquette, J. (2008). Conformationally Driven Asymmetric Induction of a Catalytic Dendrimer. *Journal of the American Chemical Society*, 130(25), pp.7845-7847.
- 131- Zidane, Y., Ourari, A., Bataille, T., Hapiot, P. and Hauchard, D. (2010). Electrochemical study with cavity microelectrode containing clay-supported Mn(III)salen complex – Dioxygen activation with cytochrome P450 model. *Journal of Electroanalytical Chemistry*, 641(1-2), pp.64-70.

- 132- Saratale, R., Saratale, G., Chang, J. and Govindwar, S. (2011). Bacterial decolorization and degradation of azo dyes: A review. *Journal of the Taiwan Institute of Chemical Engineers*, 42(1), pp.138-157.
- 133- Pálfi, T., Wojnárovits, L. and Takács, E. (2011). Mechanism of azo dye degradation in Advanced Oxidation Processes: Degradation of Sulfanilic Acid Azochromotrop and its parent compounds in aqueous solution by ionizing radiation. *Radiation Physics and Chemistry*, 80(3), pp.462-470.
- 134- Hodges, S., J. (1997). Metalloporphyrin-catalysed oxidation of azonaphthol dyes: the mechanism of oxidative bleaching by oxoiron (IV) porphyrins in aqueous solution. *Studies in Surface Science and Catalysis*, 110, PP.653-662.
- 135- QUICI, S., BANFI, S. and POZZI, G. (2010). ChemInform Abstract: Simple Synthetic Models of Cytochrome P-450: Efficient Catalysts in Hydrocarbon Oxidations. *ChemInform*, 25(20), p.no-no.
- 136- Barros, V. and Assis, M. (2013). Iron Porphyrins as Biomimetical Models for Disperse Azo Dye Oxidation. *Journal of the Brazilian Chemical Society*.
- 137- Qu, R., Shen, L., Chai, Z., Jing, C., Zhang, Y., An, Y. and Shi, L. (2014). Hemin-Block Copolymer Micelle as an Artificial Peroxidase and Its Applications in Chromogenic Detection and Biocatalysis. *ACS Applied Materials & Interfaces*, 6(21), pp.19207-19216.
- 138- Heijnen, J., de Bruijn, V., van den Broeke, L. and Keurentjes, J. (2003). Micellar catalysis for selective epoxidations of linear alkenes. *Chemical Engineering and Processing: Process Intensification*, 42(3), pp.223-230.
- 139- Maldotti, A., Andreotti, L., Molinari, A., Varani, G., Cerichelli, G. and Chiarini, M. (2001). Photocatalytic properties of iron porphyrins revisited in aqueous micellar

environment: oxygenation of alkenes and reductive degradation of carbon tetrachloride. *Green Chemistry*, 3(1), pp.42-46.

- 140- Nam, W., Han, H.J., Oh, S.-Y., Lee, Y.J., Choi, M.-H., Han, S.-Y., Kim, C., Woo, S.K. and Shin, W. (2000). New Insights into the Mechanisms of O–O Bond Cleavage of Hydrogen Peroxide and tert-Alkyl Hydroperoxides by Iron (III) Porphyrin Complexes. *Journal of the American Chemical Society*, 122(36), pp.8677–8684.
- 141- Nango, M., Iwasaki, T., Takeuchi, Y., Kurono, Y., Tokuda, J. and Oura, R. (1998). Peroxide Decoloration of Azo Dyes Catalyzed by Polyethylene Glycol-Linked Manganese Halogenated Porphyrins. *Langmuir*, 14(12), pp.3272–3278.
- 142- Khandpur, A., Foerster, S., Bates, F., Hamley, I., Ryan, A., Bras, W., Almdal, K. and Mortensen, K. (1995). Polyisoprene-Polystyrene Diblock Copolymer Phase Diagram near the Order-Disorder Transition. *Macromolecules*, 28(26), pp.8796-8806.

